Small RNAs as Molecular Tools to Dissect Function of Glutathione S-Transferase Mu Type 1

Laura Graham BSc (Hons)

Submitted in fulfilment of the requirements for the degree of Doctor of Philosophy (Ph.D.)

BHF Glasgow Cardiovascular Research Centre
Division of Cardiovascular and Medical Sciences
Faculty of Medicine
University of Glasgow

Declaration

I declare that this thesis has been written entirely by myself and is a record of research performed by myself with the exception of home office licensed procedures (Dr. D Graham, Dr. W.H Miller, Dr. L Denby and Ms. N Britton), haematoxylin and eosin staining (Ms. M Duffy), HPLC (Mr. S Miller) and some of the methods involved in microRNA target prediction and analysis (Dr. J McClure and Dr. M.W McBride). This work has not been submitted previously for a higher degree. The research was performed at the BHF Glasgow Cardiovascular Research Centre, University of Glasgow under the supervision of Dr W.H Miller and Professor A.F Dominiczak.

Laura Graham

Acknowledgements

Firstly, I would like to acknowledge my supervisors, Professor Anna Dominiczak and Dr. William Miller for their advice and support during the course of my PhD. Thanks also to my advisor, Dr. Delyth Graham.

I would like to thank Dr. Laura Denby for all her help and guidance with the virus work and thanks also to Professor Andrew Baker and Dr. Martin McBride for their help with experimental design.

Many thanks to Wendy Crawford, Nicola Britton, Gregor Aitchison, Stephen Miller, Dr. James Polke and Dr. Caline Koh-Tan for their technical expertise and to Dr. John McClure for advice on statistical analysis.

Finally, special thanks to my family and friends for all their support and to my partner, Brian for constant support and encouragement.

Contents

List of Figures

List of Tables

List of Abbreviations and Acronyms

11ßHSD	11ß-hydroxysteroid dehydrogenase
8-OH-dG	8-hydroxy-2-deoxyguanosine
AAV	Adeno-associated virus
ACE	Angiotensin converting enzyme
ACTH	Adrenocorticotropic hormone
Ad5	Adenovirus serotype 5
Adamts1	ADAM metallopeptidase with thrombospondin type 1 motif, 1
AGT	Angiotensinogen
AMD	Age-related macular degeneration
AME	Apparent mineralocorticoid excess
Ang	Angiotensin
APS	Ammonium persulphate
ASO	Antisense oligonucleotide
BCA	Bicinchoninic acid
BH_4	Tetrahydrobiopterin
BMI	Body mass index
BN	Brown Norway rat
BRIGHT	British Genetics of Hypertension
CAR	Coxsackie virus and adenovirus receptor
CAT	Catalase
CDNB	1-Chloro-2,4-Dinitrobenzene
cGMP	Cyclic guanosine monophosphate
CHD	Coronary heart disease
CHS	Chalcone synthase
CNV	Choroidal neovascularisation
Comt	Catechol-O-methyltransferase
Ctsb	Cathepsin B
Cu/Zn SOD	Copper/Zinc SOD
CVD	Cardiovascular disease
CYP11B1	11 ß-hydroxylase gene
CYP11B2	Aldosterone synthase gene
DBP	Diastolic blood pressure
dH2O	Distilled water

DNA	Deoxyribonucleic acid
dsRNA	Double-stranded RNA
EC	Endothelial cell
EDTA	Ethylenediamine tetraacetic acid
ENaC	Epithelial sodium channel
eNOS	endothelial nitric oxide synthase
FAD	Flavin adenine dinucleotide
FBPP	Family Blood Pressure Program
FCS	Foetal calf serum
FMN	Flavin mononucleotide
FX	Coagulation factor X
GCS	Glutamylcysteine synthetase
GPx	Glutathione peroxidase
GRA	Glucocorticoid-remediable aldosteronism
GSH	Glutathione
GSSG	Glutathione disulphide
GST	Glutathione transferase
Gstm1	Glutathione s-transferase mu type 1
GS-X	Glutathione S-conjugate export
H_2O_2	Hydrogen peroxide
HD	Huntington's disease
HPLC	High performance liquid chromatography
IFN	Interferon
Igfbp3	Insulin like growth factor binding protein 3
Igsf11	Immunoglobulin superfamily, member 11
IPA	Ingenuity pathway analysis
MCS	Multiple cloning site
miRNA	MicroRNA
MLCK	Myosin light chain kinase
Mn SOD	Manganese SOD
MOI	Multiplicity of infection
MR	Mineralocorticoid receptor
MRP	Multi-drug resistance protein
NAD(P)H oxidase	Nicotinamide adenine (phosphate) dinucleotide oxidase
NO	Nitric oxide

NOS	Nitric oxide synthase
NRK-52E	Normal rat kidney epithelial cells
nt	Nucleotide
O_2^-	Superoxide anion
OAS	Oligoadenylate synthetase
OH	Hydroxyl radical
$ONOO^-$	Peroxynitrite
OPA	Ortho-phthalaldehyde
PBS	Phosphate-buffered saline
PCR	Polymerase chain reaction
PHAII	Pseudohypoaldosteronism type II
PKG	cGMP dependent protein kinase
pre-miRNA	Precursor miRNA
pri-miRNA	Primary miRNA
PTGS	Post-transcriptional gene silencing
qRT-PCR	Quantitative real-time PCR
QTL	Quantitative trait loci
RAAS	Renin angiotensin aldosterone system
RISC	RNA induced silencing complex
RLC	RISC loading complex
RNA	Ribonucleic acid
RNAi	RNA interference
ROS	Reactive oxygen species
RSV	Respiratory syncytial virus
SBP	Systolic blood pressure
Scly	Selenocysteine lyase
SDS-PAGE	Sodium dodecyl sulphate polyacrylamide gel electrophoresis
sGC	Soluble guanylate cyclase
SHR	Spontaneously hypertensive rat
shRNA	Short hairpin RNA
SHRSP	Stroke-prone spontaneously hypertensive rat
siRNA	Short interfering RNA
SNP	Single nucleotide polymorphism
SOD	Superoxide dismutase
TBE	Tris-Borate EDTA

TBS	Tris-buffered saline
Trim35	Tripartite motif-containing 35
UTR	Untranslated region
VEGF	Vascular endothelial growth factor
VEGFR1	VEGF receptor 1
VSMC	Vascular smooth muscle cell
WHO	World Health Organisation
WKY	Wistar Kyoto rat
WTCCC	Welcome Trust Case Control Consortium

Summary

Human essential hypertension is a substantial public health problem with greater than 25% of the adult population affected worldwide. It is a complex disorder and a major risk factor for various cardiovascular diseases such as heart disease, renal disease and stroke. The stroke-prone spontaneously hypertensive rat (SHRSP) is a commonly used model of human essential hypertension. Previous studies identified a quantitative trait locus (QTL) for blood pressure regulation on rat chromosome 2. To further enhance the investigation of this QTL, rat chromosome 2 congenic strains were generated by transferring regions of chromosome 2 from the normotensive WKY onto the genetic background of the SHRSP. Congenic strains exhibited significantly lower blood pressure than the SHRSP parental strain indicating that genes within the congenic region are important for blood pressure regulation. Renal microarray analysis of congenic 2c* and parental strains led to the identification of glutathione s-transferase mu type 1 (*Gstm1*) as a positional and possible functional candidate gene for hypertension in the SHRSP. Expression of *Gstm1* was significantly lower in the SHRSP kidney than in 2c* and WKY and renal oxidative stress was increased in SHRSP. Glutathione s-transferase mu type 1 is part of a large family of antioxidant enzymes and may play a role in hypertension by modulating levels of oxidative stress.

This study has utilised small RNAs to examine the role of *Gstm1* in cellular oxidative stress and also investigated microRNA (miRNA) expression in the rat congenic strains. RNA interference (RNAi) was utilised to knock-down expression of *Gstm1* in a rat kidney tubular epithelial cell line (NRK-52E). Three different short interfering RNA (siRNA) sequences designed to target *Gstm1* were evaluated. Each sequence significantly reduced expression of *Gstm1* and was confirmed at both mRNA and protein level. Off-target effects on other *Gstm* isoforms and the interferon response gene, oligoadenylate synthetase 1 were prevented by reducing the concentration of siRNA used. To take knock-down of *Gstm1* expression into an *in vivo* setting, local delivery to the kidney via the renal artery was assessed but was found to cause significant kidney damage. Instead, kidney targeted vectors that can be delivered systemically were evaluated in the SHRSP. Immunohistochemistry confirmed specific targeting of

kidney tubules. Plasmid vectors were then generated that express *Gstm1* specific short-hairpin RNA (shRNA) molecules based on the sequences that successfully knocked down *Gstm1* expression *in vitro*. Transfection of these plasmids into NRK-52E cells was poor and knock-down of *Gstm1* could not be confirmed.

The role of *Gstm1* in protection against cellular oxidative stress was evaluated in NRK-52E cells by measuring markers of oxidative stress following knock-down of *Gstm1* expression. Total GST activity was not reduced in cells transfected with *Gstm1* specific siRNA however activity was increased following over-expression of *Gstm1*. No change in the levels of reduced glutathione was observed in cells following knock-down of *Gstm1*. Oxidative stress was determined by measuring 8-isoprostane (a marker of lipid peroxidation), 8-hydroxy-2-deoxyguanosine (8-OH-dG) (a marker of oxidative DNA damage) and by the comet assay (DNA damage). No significant difference in the levels of 8-isoprostane or 8-OH-dG was observed in cells treated with *Gstm1* specific siRNA compared to control siRNA. However a small but significant increase in 'comet' tail length was observed in cells with reduced *Gstm1* expression indicating greater DNA damage in these cells.

Two miRNAs that map to the chromosome 2 congenic regions were investigated (miR-137 and miR-9-1). The expression of each miRNA was investigated in kidney from SHRSP, WKY and congenic rat strains at 5, 16 and 21 weeks of age. Expression of miR-9-1 was unchanged in the SHRSP but was significantly reduced in 16 week 2c* and WKY compared to 5 week. Expression of miR-137 was unchanged in both WKY and 2k but was significantly increased in 21 week old salt-loaded SHRSP compared to 21 week old SHRSP without salt. Successful over-expression of each miRNA was demonstrated in NRK-52E cells but inhibition of each miRNA could not be confirmed. MicroRNA target prediction methods were employed to identify potential gene targets for each miRNA. A list of predicted targets for each miRNA was generated and combined with gene expression datasets generated from 5 week, 16 week, 21 week and 21 week plus salt kidney microarray analysis carried out previously. Using Ingenuity Pathway Analysis software, predicted target genes were identified according to patterns of expression. Analysis of predicted miR-137 targets failed to find any genes

that followed the correct pattern of expression (down-regulated in SHRSP but unchanged in both WKY and 2k). Of the targets predicted for miR-9-1, seven were identified that were up-regulated in both WKY and 2c* but not SHRSP. The expression levels of each of the seven genes were assessed in kidney and NRK-52E cells over-expressing miR-9-1 however none of the predicted targets could be validated.

In summary, a wide range of techniques have been employed in an attempt to investigate the function of *Gstm1* and the possible role of miRNA that map to the congenic regions implicated in blood pressure regulation. Although a specific role for *Gstm1* in protection against oxidative stress has yet to be fully determined, the integration of targeted vectors and modulation of *Gstm1* expression will allow the role of *Gstm1* to be investigated more fully *in vivo*.

Chapter 1: Introduction

1.1 Cardiovascular Disease

The Global Burden of Disease Study carried out by the World Health Organisation (WHO) identified cardiovascular disease (CVD) as the leading cause of death in the world, accounting for ~32% of all deaths in women and ~27% in men in 2004 (1). Cardiovascular diseases are disorders of the heart and vascular system serving the heart, brain, kidney and other vital organs and include coronary heart disease, heart failure, stroke, peripheral vascular disease and renal disease. Of these disorders, ischaemic heart disease and cerebrovascular disease are responsible for the majority of deaths worldwide with 12.2% and 9.7% of total deaths attributed to each cardiovascular disorder respectively. In 2004, CVD was responsible for 17.1 million deaths globally and this has been projected to increase to 23.4 million by 2030 (1). According to the British Heart Foundation Statistics Website, CVD is responsible for ~40% of deaths in the UK with coronary heart disease (CHD) as the most common cause. In terms of economic costs, CVD is a substantial problem. It is estimated that CVD costs the UK economy ~£30.7 billion a year, with CHD alone costing ~£9 billion (2). It is clear that investigation into the causes of CVD is of great benefit to public health.

1.1.1 Risk Factors

There are various modifiable risk factors for CVD including being overweight or obese, smoking, dyslipidaemia, type 2 diabetes and hypertension. Mortality from CHD is approximately 60% higher in smokers than non-smokers and this is increased to 80% in heavy smokers. Passive smoking is also detrimental to CV health, with an approximate 25% increased risk of CHD in those regularly exposed to second hand smoke. Estimates from the INTER-HEART case control study suggest that smoking is responsible for ~30% of heart attacks in Western Europe. As well as smoking, abdominal obesity has also been identified as a major cause of heart attacks and is deemed to be a more significant risk factor than body mass index (BMI) (3). Studies on obesity and weight gain have demonstrated increased incidence of CV events. Being overweight or obese is also a risk factor for raised blood cholesterol, hypertension and type 2 diabetes,

further contributing to CVD risk (4). Increased total blood cholesterol is estimated to be responsible for ~60% of cases of CHD and ~40% of strokes in developed countries. Abnormal lipids have also been identified as a major contributing factor to heart attack risk (3). Cardiovascular disease is a major cause of death in people with type 2 diabetes accounting for approximately 50% of all diabetic fatalities. Those with type 2 diabetes are 2 times more likely to suffer a heart attack or stroke. Coronary heart disease risk is 2 to 4 fold greater in men and 3 to 5 fold greater in women with diabetes (5).

1.1.1.1 Hypertension

Hypertension is responsible for approximately 6% of adult deaths worldwide and is a major contributing factor to cardiovascular disease. Hypertensive patients present an increased risk of developing various cardiovascular complications such as stroke, heart disease, heart failure and end-stage renal disease (6-10). Many studies have been carried out that show that even mild increases in blood pressure can dramatically increase the risk of a cardiovascular event. For every 20mmHg increase in SBP and 10mmHg increase in DBP, the mortality rate from cardiovascular disease doubles (11). It has also been shown that having high normal blood pressure, defined as systolic BP 130-139mmHg and diastolic BP of 85-89mmHg (see Table 1.1), can result in an increased risk of developing cardiovascular disease in both men and women (12).

Table 1.1: Blood Pressure Classification

Blood Pressure Category	Systolic BP (mmHg)	Diastolic BP (mmHg)
NORMAL	<120	<80
HIGH NORMAL	130-139	85-89
HYPERTENSION	>140	>90
STAGE 1	140-159	90-99
STAGE 2	>160	>100

Adapted from (11)

Clinical trials investigating the efficacy of antihypertensive therapies demonstrate that even small reductions in blood pressure can quite considerably reduce incidence of stroke, heart disease and other CV events (13).

Hypertension is often found in conjunction with other cardiovascular risk factors such as, insulin resistance, dyslipidaemia and obesity (14). These features together comprise what is commonly described as the metabolic syndrome. Data collected from the Framingham Heart Study found that hypertension is present as a single CVD risk factor in less than 20% of cases (15). The presence of a single risk factor at age 50 is associated with increased risk of cardiovascular disease, this risk increases substantially when 2 or more risk factors are present. As well as a greater likelihood of developing CVD, risk factor clusters also substantially reduce survival.

1.1.1.2 Blood Pressure Regulation

Normal blood pressure is defined as systolic blood pressure less than 120mmHg and diastolic pressure less than 80mmHg and can be described as the product of cardiac output and total peripheral resistance (11). Blood pressure is determined by many, complex regulatory mechanisms including the sympathetic nervous system, various chemical and hormonal controls that affect vascular resistance (see Figure 1.1) and local controls such as flow auto-regulation with the kidneys playing a major role in blood pressure control by regulating sodium and fluid balance (Figure 1.2). The importance of the kidney in blood pressure regulation was demonstrated in rat kidney transplant studies. Young hypertensive rats receiving kidneys from a normotensive rat strain did not develop hypertension, conversely, when kidneys from young hypertensive rats (before the onset of hypertension) were transplanted into normotensive rats, blood pressure was found to increase (16;17).

The renin-angiotensin system (RAS) is an important regulator of blood pressure and fluid balance. This system comprises an enzymatic cascade that results in the production of the potent vasoconstrictor angiotensin II (Ang II) (18). The cascade begins with the synthesis and release of the enzyme renin from the juxtaglomerular cells in response to various stimuli.

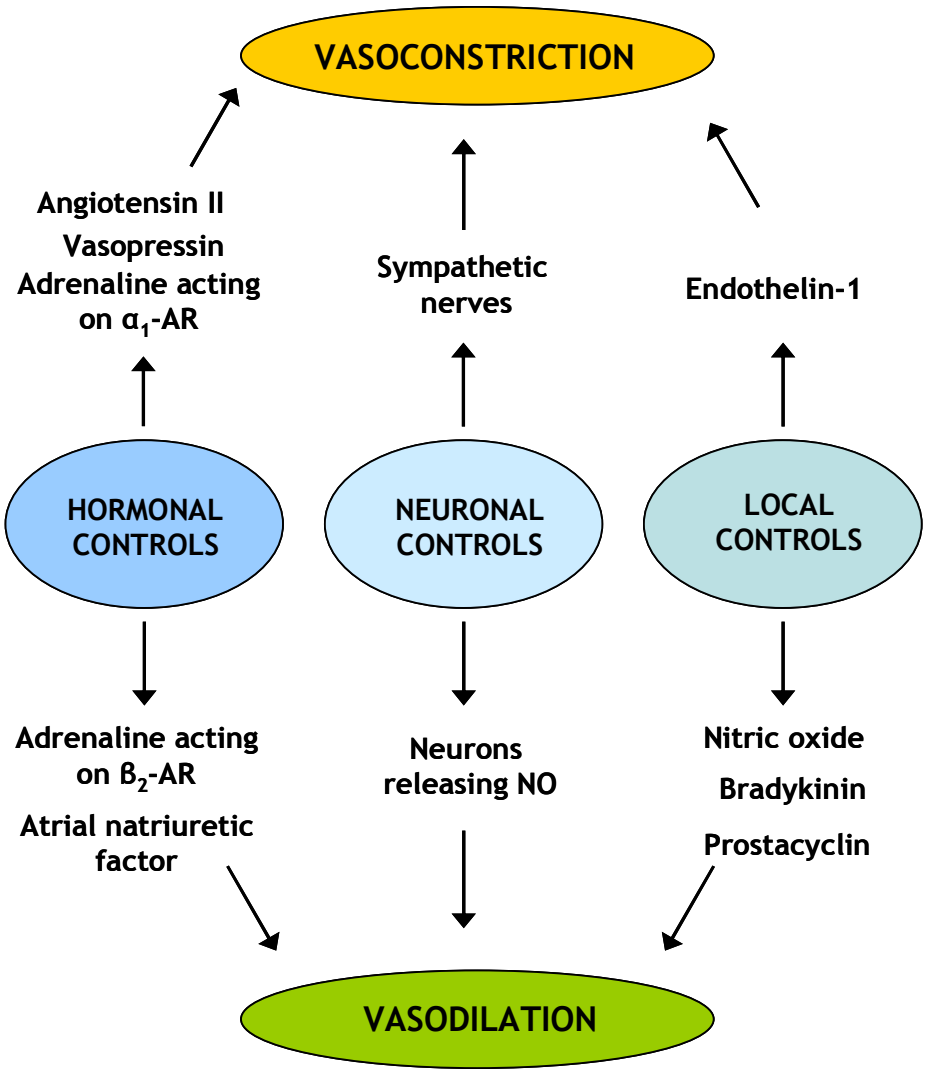

Figure 1.1 Factors regulating vascular tone

Vascular tone is subject to various hormonal, local and neuronal controls contributing to both vasoconstriction and vasodilation.

α1-AR: alpha 1-adrenergic receptor, ß2-AR: beta 2-adrenergic receptor, NO: nitric oxide

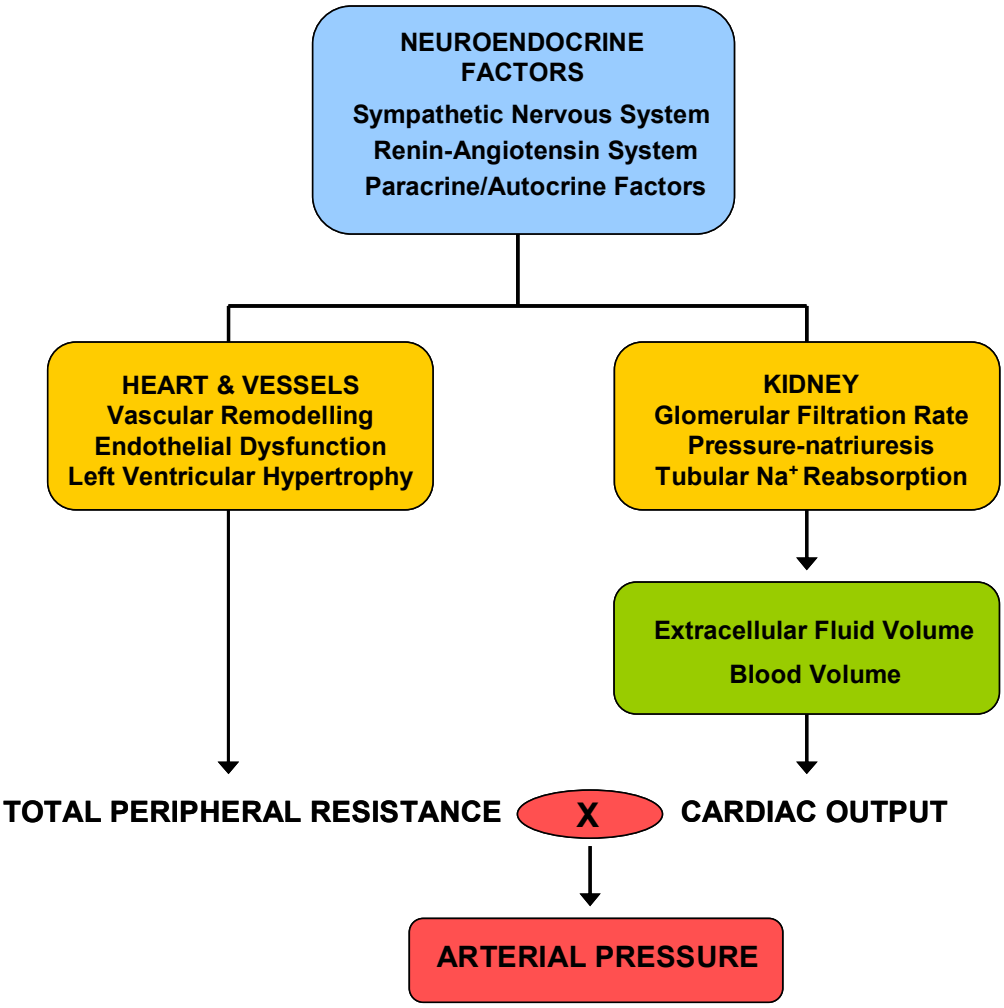

Figure 1.2 Factors contributing to blood pressure regulation

Arterial pressure can be defined as the product of cardiac output and total peripheral resistance and is affected by a range of complex regulatory mechanisms.

Adapted from (19)

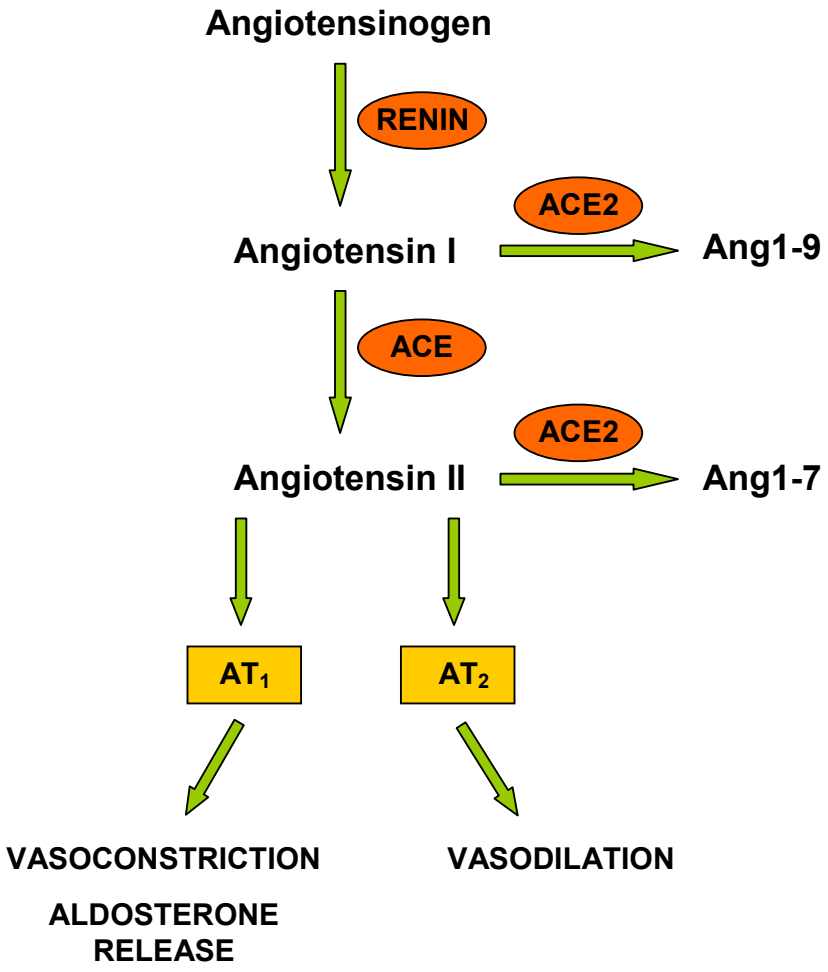

Figure 1.3 Renin-Angiotensin System

ACE: angiotensin converting enzyme, ACE2: ACE-related carboxypeptidase, AT_1: angiotensin II type 1 receptor, AT_2: angtiotensin II type 2 receptor

Angiotensinogen, produced in the liver, is the substrate for renin and is converted to the inactive angiotensin I. Angiotensin I is then cleaved to produce the active angiotensin II by angiotensin converting enzyme (ACE). Angiotensin converting enzyme can also cleave bradykinin, a vasodilator and in doing so, further contributes to vasoconstriction. Angiotensin II mediates its actions through two receptors; AT_1 and AT_2 (20). Binding of Ang II to the AT_1 receptor leads to vasoconstriction and increased retention of sodium in the kidneys. Ang II also stimulates secretion of aldosterone leading to further re-absorption in the kidney resulting in increased blood pressure. The AT_2 receptor when bound by Ang II counteracts the effects produced via the AT_1 receptor by stimulating vasodilation. More recently, a human homologue of ACE has been discovered. This ACE-related carboxypeptidase (ACE2) acts on Ang I and catalyses its cleavage to produce angiotensin 1-9 (Ang 1-9) and subsequent generation of angiotensin 1-7 (Ang 1-7) (21). Ang 1-7 has also been shown to interact with the G protein coupled receptor Mas. Deletion of this receptor in mouse kidney completely abolished Ang 1-7 binding and receptor deficiency in aortas resulted in diminished dilatory response, indicating that Ang 1-7 interacts with the Mas receptor and in doing so induces vasodilation (22) (Figure 1.3).

1.2 Essential Hypertension

Human essential hypertension is a substantial public health problem, with greater than 25% of the adult population affected (23). It is commonly defined as systolic pressure greater than 140mmHg and diastolic pressure greater than 90mmHg (11). Most cases of hypertension (>90%) are of unknown cause with many possible contributing factors. Hypertension is a complex disorder that is subject to both environmental and genetic factors. Non-modifiable risk factors such as gender, age and race have been shown to influence blood pressure. Blood pressure is sexually dimorphic where men tend to have higher blood pressure than women and systolic pressure is found to increase with age (24). Diastolic pressure also increases progressively in both men and women until approximately sixty years of age, after which time it begins to decrease.

1.2.1 Environmental Factors

Environmental factors such as diet, salt intake and weight all have an impact on blood pressure and it has been shown that by modifying diet or losing weight, blood pressure can be reduced (25-28). The DASH (Dietary Approaches to Stop Hypertension) trial investigated the blood pressure lowering effects of adopting a diet rich in fruits and vegetables and placed emphasis on low fat dairy products to help reduce total fat and saturated fat consumption. By modifying diet in this way a significant reduction in both systolic and diastolic pressure was observed (25). A minimal increase in age related blood pressure has been observed in populations where a very low sodium diet is consumed. However, in those populations consuming greater than 20g of salt per day, there is a much higher prevalence of hypertension (17). Alcohol consumption has also been associated with hypertension and studies have shown that by decreasing alcohol intake, blood pressure can be reduced (29;30).

Within the general population being overweight (assessed by BMI) is a major contributor to the onset of hypertension with greater than 40% of new onset hypertension attributable to being overweight. Increased body fat has also been found to be associated with hypertension, particularly centrally located body fat (4;11).

1.2.2 Genetics and Hypertension

Genetics play an important role in hypertension with approximately 30% attributed to genetics in combination with the environmental issues mentioned. Population studies found that blood pressure varied less within families than between families (31) and the NHLBI twin study identified greater genetic heritability of blood pressure in monozygotic twins than dizygotic twins (32).

1.2.2.1 Mendelian Forms of Hypertension

Most genetic studies of hypertension have focused on the Mendelian forms of the disorder, which are characterised by altered renal salt handling. Glucocorticoid-remediable aldosteronism (GRA) is an autosomal dominant disorder that results

in hypertension due to aberrant aldosterone synthesis and can be inhibited by treatment with glucocorticoids. It is characterised by low plasma renin activity and normal or raised aldosterone levels (33). Those with GRA have a form of salt sensitive hypertension, often associated with metabolic alkalosis and hypokalaemia. The disorder is caused by unequal crossing over between two closely related genes. These genes are *CYP11B1*, which encodes 11 ß-hydroxylase and *CYP11B2*, which encodes aldosterone synthase. This crossing over results in the production of a chimeric gene where aldosterone synthase is under the control of an adrenocorticotropic hormone (ACTH) dependent promoter. Instead of responding to Ang II, which normally regulates aldosterone synthase, aldosterone synthesis is stimulated by ACTH and is continuously produced. This increase in aldosterone causes salt retention leading to increased plasma volume and suppression of renin excretion.

Liddle's syndrome is an autosomal dominant hypertensive disorder characterised by low renin levels and suppressed aldosterone secretion. It is caused by gain of function mutations in the ß or γ subunits of the epithelial Na^+ channel (ENaC) so that the channel remains activated allowing for continued sodium re-absorption (34). This increase in salt retention leads to hypertension.

Pseudohypoaldosteronism type II (PHAII) or Gordon's syndrome is caused by mutations in two genes belonging to the WNK family of kinases. These genes are *WNK1* and *WNK4* and are expressed in the distal part of the nephron (35). Gordon's syndrome is associated with increased renal salt absorption, hyperkalaemia and low plasma renin and aldosterone levels.

Apparent mineralocorticoid excess (AME) is an autosomal recessive disorder that is associated with hypokalaemia, metabolic alkalosis and suppressed plasma renin activity with almost no circulating aldosterone present. It is caused by the absence of 11ß-hydroxysteroid dehydrogenase (11ßHSD), the enzyme responsible for conversion of cortisol to cortisone. Studies involving the use of antagonists of the mineralocorticoid receptor (MR) resulted in reduced blood pressure in patients with AME suggesting that a mineralocorticoid other than aldosterone can activate MR (36). Further investigation did not indentify another circulating mineralocorticoid but instead found that patients with AME do not produce

11ßHSD thereby reducing their ability to convert cortisol to cortisone. Subsequent *in vitro* studies and cloning of MR found that cortisol can bind and activate MR to a similar degree as aldosterone so that in the absence of aldosterone in these patients, MR can still be activated and result in increased ENaC activity.

1.2.2.2 Genetics of Essential Hypertension

These studies have identified various mechanisms by which hypertension can occur but do not provide the answer to the problems posed by the more complex and polygenic nature of essential hypertension. Monogenic forms of hypertension are very rare and account for less than 1% of all human hypertension.

1.2.2.3 Candidate Gene Analysis

Many candidate gene studies have been carried out to assess the association of genes that are implicated in BP variation with essential hypertension. Such genes fall into five broad categories: renin angiotensin aldosterone system (RAAS), adrenergic, vascular, metabolic and those with miscellaneous roles. However results within each category are conflicting and no candidate gene has shown consistent association with hypertension. This lack of reproducibility demonstrates the difficulty of trying to identify the genetic causes of complex disease.

The angiotensinogen gene (*AGT*) has been extensively studied in an attempt to identify an association with essential hypertension. Sib-pair linkage analysis identified significant linkage of the *AGT* gene locus to hypertension in two separate populations. However, in one of these populations, only a subset of participants with more severe hypertension demonstrated linkage. A common variant in this gene (M235T) was identified and found to be significantly more frequent in hypertensive subjects than controls (37). This variant has been shown to associate with hypertension in several but not all populations studied (38;39). A meta-analysis of combined case-control studies found that the T

allele associated with risk of hypertension in Caucasians but not Blacks or Asians (40). However this association found in Caucasians may be due to a publication bias with a lack of studies with negative results present in the meta-analysis.

Another candidate gene related to RAAS is the gene encoding angiotensin converting enzyme (*ACE*). Much work has been done to identify an association between *ACE* and essential hypertension but again the results have been conflicting. Jeunemaitre *et al* reported that there is no linkage between the *ACE* locus and essential hypertension following sib-pair linkage analysis of a marker linked to the *ACE* locus. The total population was then split into sub-groups to try and reduce heterogeneity in the population, but still no linkage with hypertension was found (41). However, a further two population studies identified association of *ACE* with hypertension in men but not women suggesting that *ACE* may be a sex specific candidate gene for hypertension (42;43). Again, no definitive conclusion can be drawn as results are not consistent (44).

The cytoskeletal protein adducin has also been implicated in hypertension. Adducin is composed of three subunits; α, ß and γ encoded by *ADD1*, *ADD2* and *ADD3* respectively and may play a role in sodium re-absorption in the renal tubule. Studies in the Milan hypertensive rat strain identified point mutations in α and ß-adducin coding sequence resulting in amino acid substitutions. The *Add1* gene mutation was found to associate with blood pressure and when a region encompassing the *Add1* locus was transferred from a hypertensive donor to a normotensive rat strain, blood pressure in the recipient increased (45-47). Several human studies have sought to establish a relationship between the α-adducin gene (*ADD1*) and blood pressure (17;45). A case control study performed in 190 hypertensive patients and 126 control subjects found significant linkage of markers surrounding the *ADD1* locus to hypertension. The greatest association was found with the marker closest to the adducin locus however this does not exclude the possibility that another gene in this region contributes to the blood pressure variation observed (48). Linkage of hypertension to the *ADD1* locus was confirmed in another population and cDNA analysis identified a mutation causing an amino acid substitution (G460W). This polymorphism was found to significantly associate with hypertension in both

populations used in this study (49). However, a more recent study found no association of the G460W polymorphism with hypertension (50). The *ADD2* gene encoding the ß-adducin subunit has also been investigated for its association with hypertension, with conflicting results. A study of the C1797T polymorphism in three European populations found that presence of the T allele was associated with increased blood pressure in two out of the three populations (51).

1.2.2.4 Genetic Linkage and Association Studies

Various genome wide linkage and association studies have been undertaken to attempt to identify genetic regions that are responsible for blood pressure phenotype in essential hypertension. One advantage of such studies is that no prior information of genetic function is required.

1.2.2.5 Linkage Analysis

Genome wide linkage studies are possible due to the vast number of microsatellite and single nucleotide polymorphism (SNP) markers spread throughout the genome. This combined with recent technological advances allow the location of chromosomal regions or quantitative trait loci (QTLs) linked to hypertension to be identified. By finding markers that associate with blood pressure phenotype, the location of a QTL can be determined. Using this approach, numerous QTLs relating to hypertension or blood pressure have been found throughout the human genome. However these studies have been poorly replicated due to the polygenic and multi-factorial nature of hypertension. Multiple loci have been found on some chromosomes suggesting that it is unlikely that a single genomic region is responsible for predisposition to hypertension (19;52).

In an attempt to improve the likelihood of detecting QTLs for essential hypertension, the MRC British Genetics of Hypertension (BRIGHT) study was performed on sibling pairs from families with severe early onset hypertension. Individuals were only selected for the study if non-diabetic, non-obese with no history of secondary hypertension and with blood pressure in the top 5% of the

blood pressure distribution in the UK. Linkage analysis identified a locus on chromosome 6 and 3 further regions that have suggested linkage on chromosomes 2, 5 and 9 (53). Further analysis of this data with additional microsatellite markers reinforced support for linkage of essential hypertension with chromosome 5 (54). However, analysis supporting linkage to chromosome 6 should be regarded with care as the locus is present near the end of the chromosome. Analysis of such regions by linkage computer programs can produce misleading results (55). The Family Blood Pressure Program (FBPP) study was a meta-analysis of four separate family studies designed to identify linkage to hypertension through genome wide linkage scans. The study involved over 6000 individuals but failed to identify any hypertension related QTLs, indicating that blood pressure is not subject to control by single genomic regions but by many loci imparting small effects on phenotype (56).

1.2.2.6 Genome Wide Association Studies

Genome wide association studies utilise the availability of SNP markers to carry out large scale association mapping and involve comparisons of allele frequency throughout the genome in a case-control design. This approach is unbiased as no assumptions are made regarding the genomic location of genetic variants that may have an affect on phenotype. Such studies have been made possible due to the availability of high throughput technologies and genome wide determination of genetic variation by the HapMap project (52;57).

The Welcome Trust Case Control Consortium (WTCCC) carried out a large scale genome wide association study in an attempt to identify genes involved in 7 common human diseases, including hypertension (58). For each disease 2000 individuals were examined with a shared set of 3000 controls all of whom identified themselves as white Europeans. Following analysis, 24 independent association signals were identified at $p<5x10^{-7}$, the genome wide significance level set for this experiment. The association signals included 1 in bipolar disorder, 1 in coronary artery disease, 9 in Crohn's disease, 3 in rheumatoid arthritis, 7 in type 1 diabetes and 3 in type 2 diabetes. For hypertension, none of the previously suggested associated variants were identified and no further SNPs were discovered with significance below the set threshold level. There are

many reasons that may explain why no significant associations were detected for hypertension, such as poor gene coverage in the Affymetrix chip used in the study. For example, *WNK1*, which has been previously identified as a candidate gene for hypertension but is poorly tagged on the Affymetrix chip. Another issue with this study is the use of a shared set of common controls, as this increases the likelihood that a proportion of controls may have hypertension or may go on to develop it in the future. This could significantly reduce the power of the study for identifying associations with hypertension. It has been estimated that "if 5% of controls would meet the definition of cases at the same age, the loss of power is approximately the same as that due to a reduction of sample size by 10%" (58).

1.3 Animal Models

In order to better understand the mechanisms contributing to complex human disease, such as hypertension, animal models can be studied. The rat is the most commonly used model for investigating hypertension. There are various non genetic models of hypertension that are useful for investigation of secondary hypertension. These include the 2 kidney, 1 clip rat and DOCA salt rats for investigating renovascular and endocrine causes of hypertension.

1.3.1 Genetic Models of Hypertension

The spontaneously hypertensive rat or SHR is an example of a selectively bred animal model that can be utilised for the genetic analysis of hypertension. Other genetic models of hypertension include the stroke-prone SHR, the genetically hypertensive rat, Sabra model, Lyon hypertensive rat, Milan hypertensive rat and Dahl salt sensitive rats. The SHR was generated from the Wistar rat strain. Male Wistar rats exhibiting spontaneous hypertension (SBP >150mmHg) were mated with female rats with above average blood pressure (SBP >130mmHg). Pairs of rats from the F_1 generation with spontaneous hypertension were then mated. This process was repeated so that in subsequent generations, spontaneous hypertension was observed approximately 100% of the time. In this strain, blood pressure increases with age, as is the case in human

hypertension. Blood pressure rises steadily from ~140mmHg SBP at about 5 weeks of age to ~200mmHg at 25 weeks (59). The stroke prone spontaneously hypertensive rat (SHRSP) is a sub-strain of the SHR that displays extremely high blood pressure and has a high incidence of stroke. Both strains are excellent genetic models of human hypertension as they exhibit many features that are common to the human disorder, such as endothelial dysfunction, cardiac hypertrophy, renal dysfunction and heart failure (60;61). The high blood pressure phenotype observed in the SHR and SHRSP models is independent of dietary salt or other environmental influence unlike Dahl salt sensitive rats which develop high blood pressure following a high salt diet. However, when fed a 1% salt solution, spontaneously hypertensive rats do have increased blood pressure (62). Both SHR and SHRSP exhibit salt sensitivity.

1.3.2 Congenic Strains

Genetic linkage studies carried out in rat models of hypertension have led to the identification of numerous QTLs for blood pressure regulation across many chromosomes. However QTLs usually encompass regions that are too large to yield a small number of genes that can easily be investigated. To overcome this, congenic strains can be generated to narrow down the region for investigation. This involves the transfer of one chromosomal region from one rat strain to another. A donor and recipient strain are crossed and the progeny containing the region of interest are then backcrossed to the recipient strain. Backcrossing is carried out until the progeny are entirely of recipient genetic background with the exception of the region transferred (63). It is estimated that following eight generations of back-crossing that more than 99% will be from the recipient. This process can be accelerated by using a speed congenic strategy, where back-crossed male rats are screened for genetic markers allowing for rats with the least donor genetic background to be selected for future crosses (Figure 1.4). By narrowing down the congenic region, the possibility of identifying causative genes is increased.

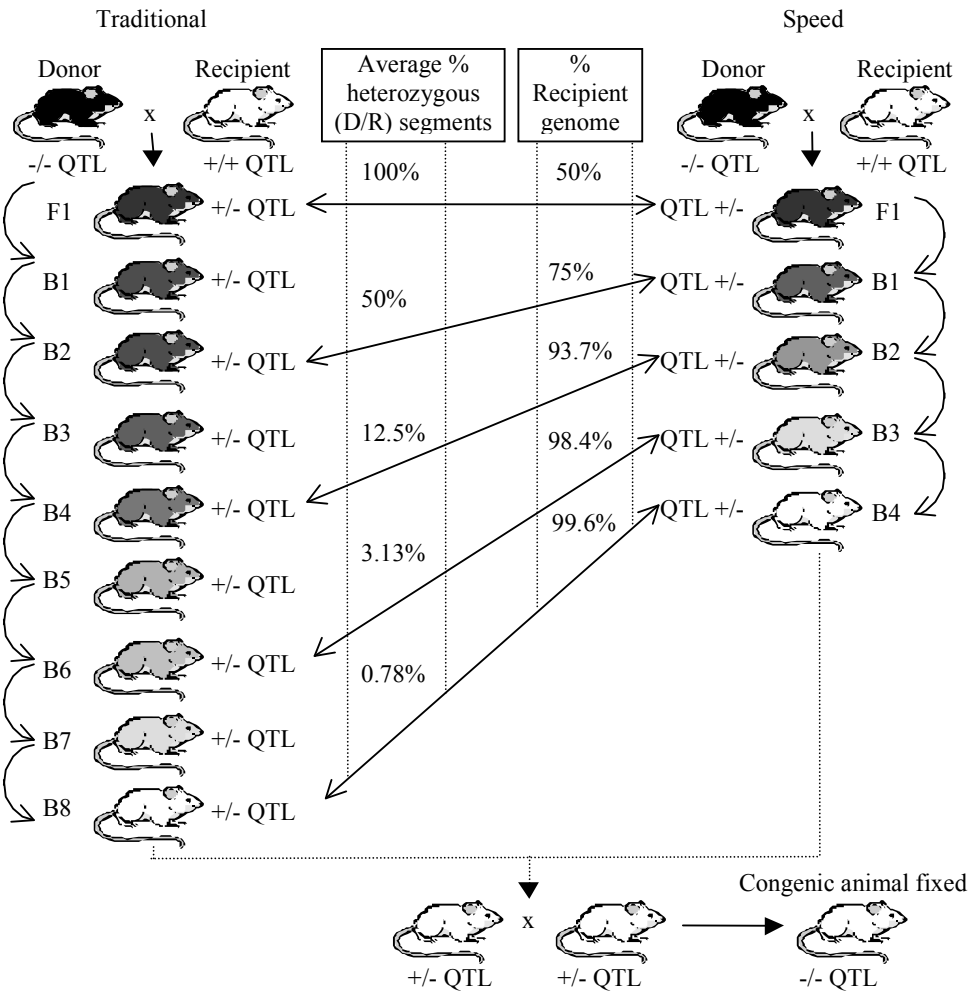

Figure 1.4 Traditional and speed congenic breeding

Construction of congenic strains demonstrating the differences between traditional and marker-assisted speed congenic breeding. Decreasing shades of grey represent dilution of the donor genome. D: donor strain alleles, R: recipient strain alleles, B: backcross, F1: first filial generation

Taken from (60). Permission to reproduce this figure has been granted by John Wiley & Sons, Inc.

The congenic strategy to discover candidate genes as described above was successfully utilised by Aitman *et al* to identify *Cd36* as an insulin resistance gene. Previous studies identified a QTL on chromosome 4 in spontaneously hypertensive rats for defective glucose and fatty acid metabolism in adipocytes (64). In order to further investigate the QTL region, Aitman and colleagues generated a congenic strain where the SHR QTL on chromosome 4 was replaced with the equivalent region from the Brown Norway (BN) rat. The congenic strain showed improved insulin mediated glucose uptake and complete restoration of the normal lipid metabolism phenotype, thus confirming that genes with the QTL are responsible. To further dissect which genes may be responsible, cDNA microarray analysis was performed to identify genes that are differentially expressed across strains. In this way *Cd36* was identified and pursued as a candidate gene. This gene maps to the chromosome 4 QTL region and encodes a fatty acid translocase with expression in adipose tissue and in skeletal and cardiac muscle. However, in the SHR, Cd36 protein was undetectable in adipocyte plasma membrane. A transgenic mouse over-expressing *Cd36* in heart and skeletal muscle was found to have lower blood triglycerides. This investigation identified that *Cd36* deficiency is responsible for insulin resistance and defects in fatty acid metabolism in the SHR (65). Further studies involving transgenic overexpression of *Cd36* in the SHR found that *Cd36* decreases serum fatty acid levels, increases sensitivity to insulin and improves glucose tolerance but has no effect on mean arterial blood pressure (66). More recently, renal expression of *Cd36* has been shown to have an inverse correlation with blood pressure. Renal transplantation experiments have demonstrated that rats receiving kidneys expressing wild type *Cd36* result in reduced blood pressure compared to those receiving kidneys lacking *Cd36* (67).

A similar congenic strategy has been utilised in our own laboratory to identify candidate genes for hypertension. Genome wide linkage analysis of the SHRSP led to the identification of 2 QTL for blood pressure regulation within rat chromosome 2 (68). In order to further dissect the contribution of the QTL region of rat chromosome 2 to blood pressure regulation, congenic strains were generated.

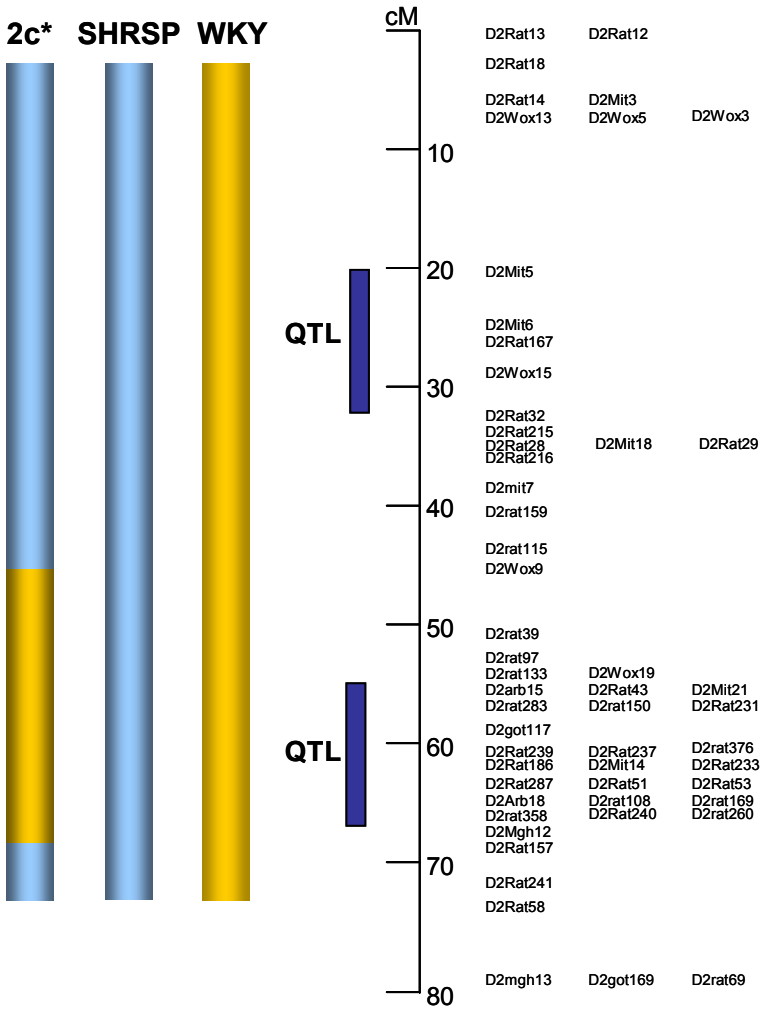

Figure 1.5 Rat chromosome 2 congenic strain SP.WKYGla2c*

The 2c* congenic strain was generated by transferring a chromosomal region from WKY onto the SHRSP background. This region, between markers D2Wox9 and D2Mgh12, encompasses a blood pressure quantitative trait locus (QTL).

Adapted from (69)

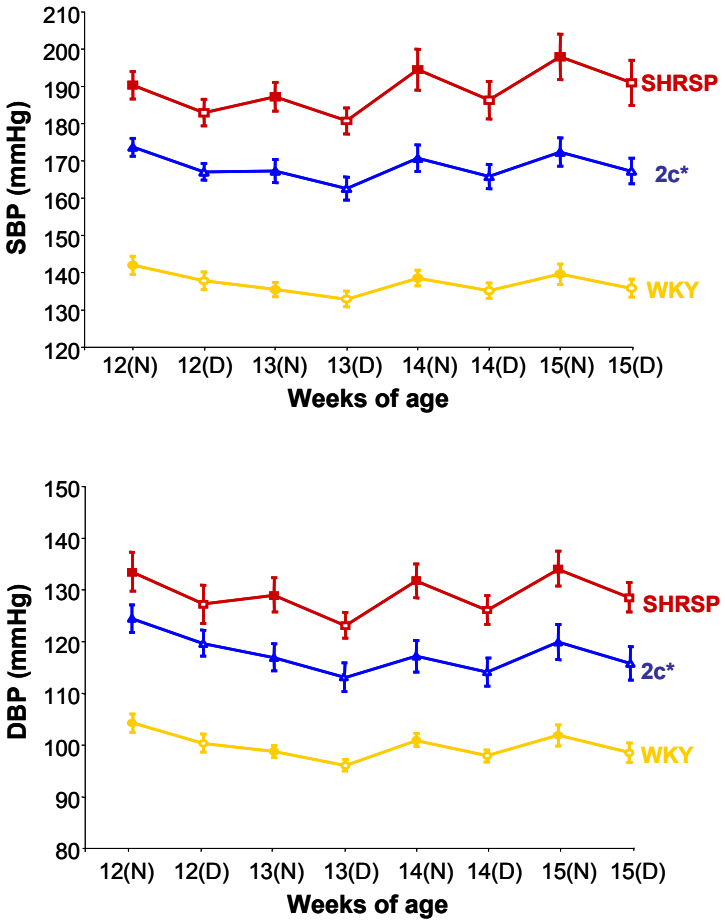

Figure 1.6 Day and night-time average systolic and diastolic blood pressure

Blood pressure measured by radiotelemetry in SHRSP, WKY and congenic 2c*. SBP: systolic pressure (top panel), DBP: diastolic pressure (bottom panel)

Adapted from (69)

In this case, a region encompassing the lower QTL on chromosome 2 from a normotensive strain (WKY) was transferred onto the genetic background of the SHRSP using a marker assisted breeding strategy (70) to generate the SP.WKYGla2c* (2c*) (Figure 1.5). Initial studies with the congenic SP.WKYGla2c* found that blood pressure was significantly lower in the congenic when compared to the SHRSP (Figure 1.6). This indicates that genes found within the congenic region are indeed responsible for blood pressure regulation. To further examine which genes may be playing a role, microarray analysis was carried out on the congenic strains. Of the many probe sets that were found to be differentially expressed, three mapped to the congenic region. All three probes corresponded to the gene encoding glutathione S-transferase mu type 1 (*Gstm1*) (69). *Gstm1* was found to have significantly lower expression in the SHRSP compared to the congenic and WKY. As the congenic strain has lower blood pressure than the SHRSP, genes within the congenic region appear to be important and due to its position and differential expression, *Gstm1* has been identified as a positional candidate gene for rat and possibly human hypertension.

The microarray analysis that led to identification of *Gstm1* was performed in kidney tissue from SHRSP, WKY and 2c* congenic strains. The kidney was chosen for investigation of candidate genes in hypertension as it is the major organ responsible for long term blood pressure control and evidence from kidney transplant studies in rats have shown that blood pressure phenotype follows the kidney (71). In experimental models of hypertension, the induction of hypertension involves some reduction of renal function (72). It has been well documented that the kidney plays an important role in blood pressure regulation where control of sodium and water excretion has been suggested as the main mechanism contributing to pressure control (73). As described in section 1.1.1.2, the renin-angiotensin system contributes to blood pressure control and in the kidney stimulates retention of sodium and water, thereby raising blood volume and consequently raising blood pressure. The activation of AT_1 receptors by angiotensin II leads to vasoconstriction and a study has shown that the absence of kidney AT_1 receptors in mice was enough to enable a blood pressure reduction of almost 20 mmHg even with normal expression of the receptor in other tissues (74). Another action of angiotensin II is to stimulate release of

aldosterone from the adrenal cortex. Aldosterone promotes sodium and water retention in the kidney via the epithelial sodium channel (ENaC). Elevated levels of circulating aldosterone in Sprague Dawley rats led to an increased abundance of the α subunit of ENaC and caused redistribution of ENaC subunits to the apical region of principal cells of the collecting duct (75).

The absorption of sodium and water by the collecting duct is important as it is here that sodium and water excretion is subjected to 'fine tuning' by the kidney (76). Studies performed to identify where *Gstm1* was expressed found that *Gstm1* expression was present in kidney tubular epithelium and in particular was found in the principal cells of the collecting duct (77). Due to the localisation of *Gstm1* expression to kidney tubules and its reduced expression in renal tissue from hypertensive rats, the focus of the work presented in this thesis has been the kidney and in particular has utilised a rat kidney tubular epithelial cell line (NRK-52E).

At present very little is known about the specific role of *Gstm1* in the rat however a gene mapping study in the mouse identified *Gstm1* as a positional candidate gene for susceptibility to renal vascular injury. A study of a genetic model of angiotensin II type 1A receptor deficiency found that the genetic background of these mice could modify their susceptibility to renal vascular hypertrophy (78). Those with a C57BL/6 genetic background were found to be more susceptible to renal vascular hypertrophy and linkage analysis identified a locus on chromosome 3 with significant linkage to the vascular phenotype. Screening for candidate genes found that *Gstm1* mapped to this region and was differentially expressed between C57BL/6 susceptible and 129 resistant strains suggesting that *Gstm1* may play a role in vascular homeostasis (79). Expression of *Gstm1* was significantly lower in aortic VSMCs isolated from C57BL/6 compared to VSMCs from 129 mice. The C57BL/6 VSMCs also exhibited a higher cell proliferation rate and increased reactive oxygen species when compared to 129 VSMCs. Transfection of VSMCs with *Gstm1* siRNA to reduce *Gstm1* expression resulted in a significant increase in VSMC proliferation, migration and superoxide levels. It may be that *Gstm1* modulates VSMC proliferation and migration by protecting cells from products of oxidative stress which could influence VSMC proliferation, although the exact mechanism is not yet known (79).

1.4 Oxidative Stress

The term oxidative stress refers to a state where cellular antioxidants are overwhelmed by pro-oxidants resulting in an increased production of reactive oxygen species (ROS). Reactive oxygen species are produced by all cells of the vasculature and play an important role in cellular homeostasis and signalling. Reactive oxygen species include non-radical molecules such as hydrogen peroxide (H_2O_2) and peroxynitrite ($ONOO^-$) and free radicals such as superoxide (O_2^-), nitric oxide (NO) and hydroxyl radical (OH^-).

There is much evidence available that suggests a role for oxidative stress in the development of hypertension (80). Increased levels of ROS can cause remodelling of the vasculature due to inflammation and cellular damage (Figure 1.7). This leads to an increase in total peripheral resistance thus causing blood pressure to become elevated (81). Oxidative stress, induced by depletion of glutathione, has been shown to cause normotensive Sprague-Dawley rats to become hypertensive (82). Treating pre-hypertensive spontaneously hypertensive rats (SHR) with Tempol, a SOD mimetic, prevents rats from becoming hypertensive. This indicates that by lowering levels of oxidative stress, hypertension can be prevented (83).

1.4.1 Superoxide and Vascular NAD(P)H Oxidase

Superoxide is a key molecule in the production of oxidative stress as it is a precursor for various other reactive oxygen species. Superoxide is produced from the one electron reduction of molecular oxygen. There are many sources of superoxide such as xanthine oxidase and the mitochondrial respiratory chain but within the vasculature, the principal source is NAD(P)H (nicotinamide adenine dinucleotide phosphate) oxidase (84). Vascular NAD(P)H oxidase is similar in structure to the phagocytic type oxidase but instead of producing superoxide in short bursts, it is generated at a much lower level over a longer period of time. NAD(P)H oxidase is a multi-subunit enzyme comprising 2 membrane associated and 3 cytosolic components, see Figure 1.8.

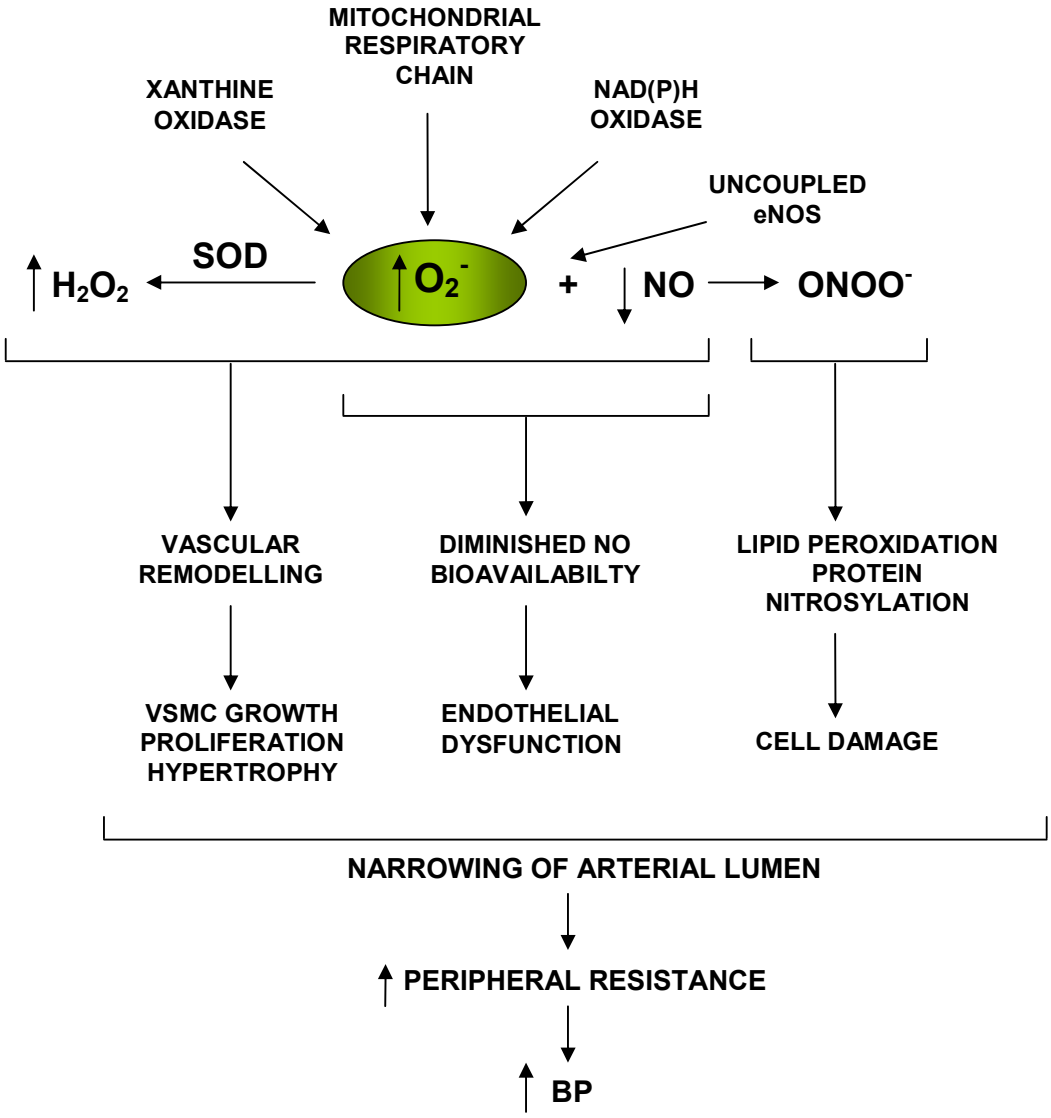

Figure 1.7 Oxidative stress

Increased production of superoxide can lead to endothelial dysfunction by diminishing nitric oxide bioavailability. Superoxide also results in the generation of various other reactive oxygen and nitrogen species that can inflict cellular damage and vascular remodelling contributing to increased peripheral resistance and blood pressure.

O_2^-: superoxide, H_2O_2: hydrogen peroxide, NO: nitric oxide, $ONOO^-$: peroxynitrite, SOD: superoxide dismutase, eNOS: endothelial nitric oxide synthase, BP: blood pressure

Adapted from (81)

The membrane associated subunits are $p22^{phox}$ and Nox, a homologue of the $gp91^{phox}$ found in phagocytic NAD(P)H oxidase. Together, the 2 subunits form the cytochrome b_{558}. Studies carried out in vascular smooth muscle cells identified $p22^{phox}$ as a critical factor in NAD(P)H oxidase mediated superoxide production. Cells transfected with $p22^{phox}$ antisense cDNA have reduced Ang II stimulated NAD(P)H oxidase activity, producing less superoxide thus indicating the importance of $p22^{phox}$ for enzyme function (85). The 3 cytosolic components are $p40^{phox}$, $p47^{phox}$ and $p67^{phox}$ all of which reside in the cytosol and translocate to the membrane upon activation. When cells are stimulated, $p47^{phox}$ becomes phosphorylated allowing interaction with the cytochrome b_{558} complex. The G protein, Rac1, is also required for enzyme activation through its interaction with $p67^{phox}$. When all of the components assemble at the cell membrane, the active enzyme complex is formed (86). Evidence from studies in endothelial and vascular smooth muscle cells suggests that NADH is the preferred substrate for superoxide generation with NADPH used to a lesser degree (87).

Increased NAD(P)H oxidase activity has been implicated in the development of hypertension (86;88). Chabrashvili *et al* reported that expression of $p47^{phox}$ was greater in SHR kidney than kidneys from WKY rats; this increased expression was also found in younger, pre-hypertensive rats (89). NAD(P)H oxidase activation has been observed in Sprague Dawley rats infused with Ang II to induce hypertension. Following Ang II infusion, superoxide production and SBP increase but when infused with NE, only SBP increases indicating that Ang II activates NAD(P)H oxidase and is associated with the onset of hypertension (90). In mice treated with an NAD(P)H oxidase inhibitor that prevents assembly of the enzyme complex, superoxide production was attenuated and SBP was significantly lower further adding support to a role for increase NAD(P)H oxidase activity and subsequent superoxide production in the development of hypertension (91).

1.4.2 Nitric Oxide

Superoxide readily reacts with the free radical nitric oxide (NO). First described as endothelium derived relaxing factor, NO is a potent vasodilatory signalling molecule that plays an important role in the regulation of platelet aggregation and vascular tone.

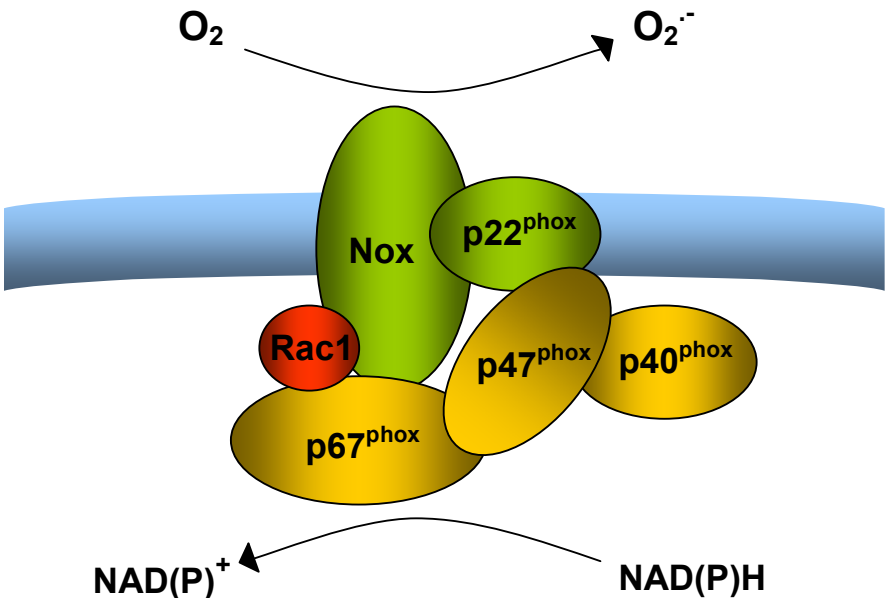

Figure 1.8 Active NAD(P)H oxidase complex structure

NAD(P)H oxidase is composed of 5 subunits, comprising 2 membrane bound (Nox and $p22^{phox}$) and 3 cytosolic subunits ($p40^{phox}$, $p47^{phox}$ and $p67^{phox}$). The activation of the enzyme complex is regulated by Rac1.

NAD(P)H: nicotinamide adenine dinucleotide phosphate, O_2: oxygen, $O_2^{\cdot-}$: superoxide, Phox: phagocytic oxidase, Nox: NAD(P)H oxidase ($gp91^{phox}$ homologue)

Adapted from (92)

Nitric oxide is produced by nitric oxide synthase of which there are three isoforms; neuronal, inducible and endothelial (NOSI, NOSII and NOSIII respectively). Endothelial nitric oxide synthase (eNOS) produces nitric oxide during the conversion of L-arginine to L-citrulline and requires various co-factors. Enzyme activity is Ca^{2+}/calmodulin dependent and also requires NADPH, flavin adenine dinucleotide (FAD), flavin mononucleotide (FMN) and tetrahydrobiopterin (BH_4).

Endothelial NOS is activated in response to increased intracellular Ca^{2+} resulting in NO generation. Nitric oxide can then diffuse from the endothelium and exert its vasodilatory effects on nearby smooth muscle cells via cyclic guanosine monophosphate (cGMP). Nitric oxide activates soluble guanylate cyclase (sGC) by binding to its haem group which in turn converts GTP to cGMP. Accumulation of cGMP leads to activation of cGMP dependent protein kinase (PKG) triggering a decrease in $[Ca^{2+}]_i$ through various mechanisms (93). PKG mediated phosphorylation of K^+ ion channels results in membrane hyperpolarisation and inhibition of Ca^{2+} influx (94). PKG can also inhibit Ca^{2+} channels directly to reduce $[Ca^{2+}]_i$. Reduced Ca^{2+} levels result in diminished myosin light chain kinase (MLCK) activity and subsequent reduction of myosin light chain phosphorylation leading to smooth muscle relaxation (Figure 1.9).

1.4.2.1 eNOS Uncoupling and Endothelial Dysfunction

As well as producing NO, eNOS can also generate superoxide. Elevated levels of superoxide are present in SHRSP aorta but can be attenuated by removing the endothelium or by adding NOS inhibitors, indicating that in the aortas of these animals superoxide is being produced by eNOS (95). This phenomenon, known as eNOS uncoupling occurs when L-arginine or BH_4 levels are depleted. The production of superoxide by uncoupled eNOS leads to diminished bioavailability of nitric oxide, which has been associated with endothelial dysfunction in the vasculature.

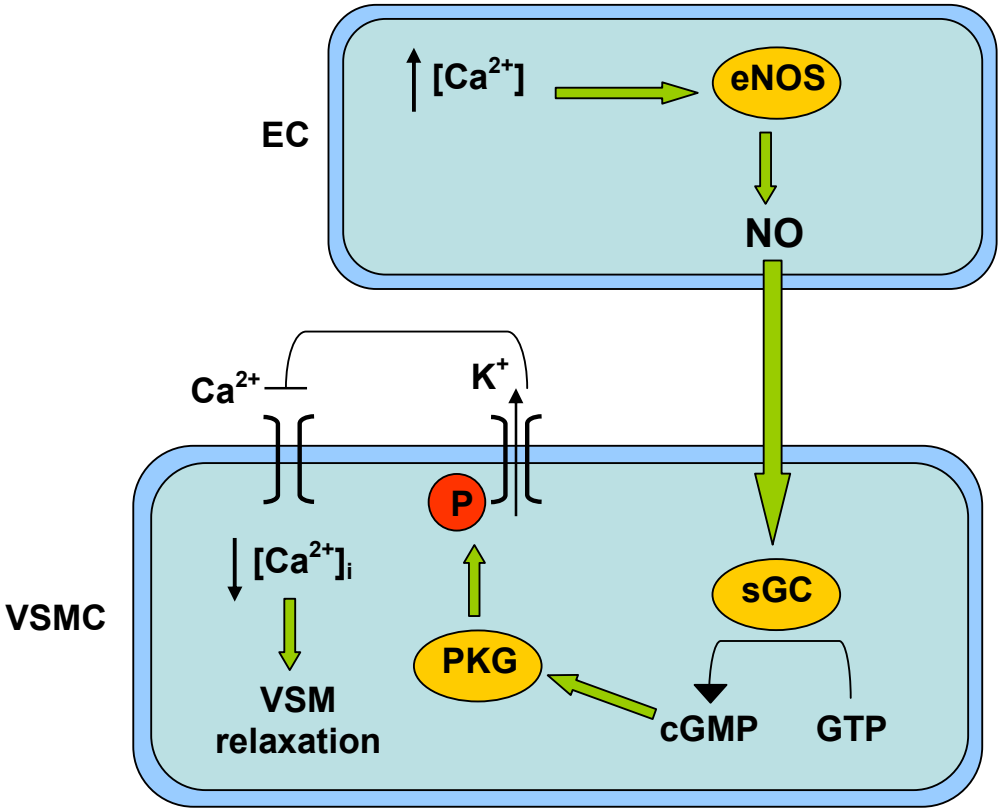

Figure 1.9 Nitric oxide signalling in vascular smooth muscle

Nitric oxide regulates vascular smooth muscle relaxation through activation of soluble guanylate cyclase and accumulation of cGMP resulting in decreased intracellular calcium concentration.

VSMC: vascular smooth muscle cell, EC: endothelial cell, eNOS: endothelial nitric oxide synthase, NO: nitric oxide, sGC: soluble guanylate cyclase, cGMP: cyclic guanosine monophosphate, guanosine triphosphate, PKG: cGMP dependent protein kinase, P: phosphorylation

Endothelial dysfunction is characterised by impaired endothelium dependent vasorelaxation due to reduced bioavailability of nitric oxide and is a feature of many cardiovascular risk factors such as hypertension and atherosclerosis. Coronary endothelial dysfunction has been associated with atherosclerosis progression and subsequent coronary artery disease (96). Impaired vasorelaxation is also found in rat models of hypertension (97) and hypertensive patients (98). In rat models of hypertension, superoxide levels are elevated and this contributes to the reduced NO bioavailability observed. Nitric oxide rapidly interacts with superoxide resulting in the production of the highly reactive peroxynitrite ($ONOO^-$). Peroxynitrite can cause damage to DNA, protein and lipids and can also oxidise the co-factors required by eNOS, contributing further to eNOS uncoupling.

1.4.3 Antioxidant Systems

In order to counteract the production of ROS there are many antioxidant systems in place to help prevent oxidative damage (99;100). These defences include small non-protein antioxidants such as vitamins and glutathione and enzymes such as superoxide dismutase (SOD), catalase (CAT), glutathione transferases (GST) and glutathione peroxidase (GPx).

1.4.3.1 Antioxidant Vitamins

Vitamin E (α-tocopherol) effectively scavenges lipid peroxides but in doing so can become a radical itself. Data from epidemiological studies suggests an inverse association between vitamin E intake and risk of cardiovascular disease (101). However, studies designed to test the effect of vitamin E supplementation on cardiovascular risk have shown no significant decrease in the number of CV events and in some cases increased intake of vitamin E was associated with a greater risk of heart failure (102;103). Vitamin C (ascorbate) can reduce oxidative stress by scavenging ROS directly and by recycling α-tocopherol, preventing its radical formation thus helping to prevent lipid oxidation (104). It has also been shown to be effective in the reduction of endothelial dysfunction in patients with coronary artery disease (105;106) and

hypertension (107). Studies in endothelial cells show that treatment with ascorbate leads to increased production of nitric oxide and stabilisation of the eNOS co-factor BH_4, preventing eNOS uncoupling and maintaining bioavailability of NO (108;109).

1.4.3.2 Superoxide Dismutase

Superoxide can be scavenged by SOD by catalysing the conversion of superoxide to oxygen and H_2O_2. The reaction involves the binding of two superoxide anions and two protons by SOD leading to the production of hydrogen peroxide and oxygen. Three SOD isoforms have been identified in mammals, encoded by three distinct genes. *SOD1* encodes a dimeric copper-zinc (Cu/Zn) SOD that is located in the cytoplasm. The second isoform, manganese (Mn) SOD, is found in the mitochondria as a tetrameric enzyme and is encoded by *SOD2*. *SOD3* encodes a tetrameric Cu/Zn SOD isoform that is found mainly in extracellular spaces and is commonly described as ecSOD.

Superoxide dismutase helps to increase NO bioavailability and improve endothelium dependent vasodilatation in a rabbit model of diabetes. In afferent arterioles from diabetic rabbits, acetylcholine induced vasodilatation is inhibited but when treated with the SOD mimetic Tempol, the dilatory response is restored (110). Gene transfer studies have shown that ecSOD can cause a decrease in arterial blood pressure in SHR and improve carotid artery relaxation in response to acetylcholine (111). The benefits of SOD activity are clear, superoxide mediated cytotoxicity is reduced and NO bioavailability is increased. However, SOD generates H_2O_2, a stable molecule with oxidising properties that in turn can lead to production of the highly reactive OH^-.

Hydrogen peroxide has been shown to function in vascular smooth muscle cell (VSMC) proliferation and hypertrophy, features that are common to vascular disease. Upon stimulation with phenylephrine, the level of H_2O_2 in VSMC is increased and proliferation is induced. However, when H_2O_2 is inhibited by catalase, phenylephrine induced proliferation is also inhibited (112). Hydrogen peroxide itself can be scavenged by enzymes such as catalase and glutathione peroxidase. In the presence of metal containing molecules, H_2O_2 can be reduced

to form hydroxyl (OH^-) radical another reactive species that can inflict local damage (113).

1.4.3.3 Catalase

Catalase is a tetrameric enzyme that reacts with H_2O_2 and generates water and molecular oxygen. The protective benefit of catalase has been demonstrated in the cardiovascular system. Catalase transgenic mice were generated to investigate the role of H_2O_2 in vascular hypertrophy. Angiotensin II induced aortic wall hypertrophy was attenuated by the increased expression and activity of catalase specifically in vascular smooth muscle (114). Over-expression of catalase in *ApoE*$^{-/-}$ mice has also been shown to have protective properties by inhibiting the development of atherosclerosis and reducing markers of oxidative stress (115).

1.4.3.4 Glutathione

Glutathione is a small tripeptide molecule (γ-glutamyl-cysteinyl-glycine) that is used by various detoxifying enzymes such as GPx and GST and plays an important role in antioxidant defence. Glutathione exists in a reduced state and acts as an electron donor. It can be oxidised to produce glutathione disulphide (GSSG) by various electrophilic substances including ROS leading to lower levels of reduced glutathione. The GSH:GSSG ratio is often used as an indicator of cellular oxidative stress status. Upon stimulation by oxidative stress glutathione reductase is stimulated and converts glutathione back to its reduced form.

The liver is a major producer of GSH, the most abundant low molecular weight thiol. Glutathione is synthesised in a two step reaction in the presence of ATP by two cytosolic enzymes; γ-glutamylcysteine synthetase (γGCS) and GSH synthetase, see Figure 1.10.

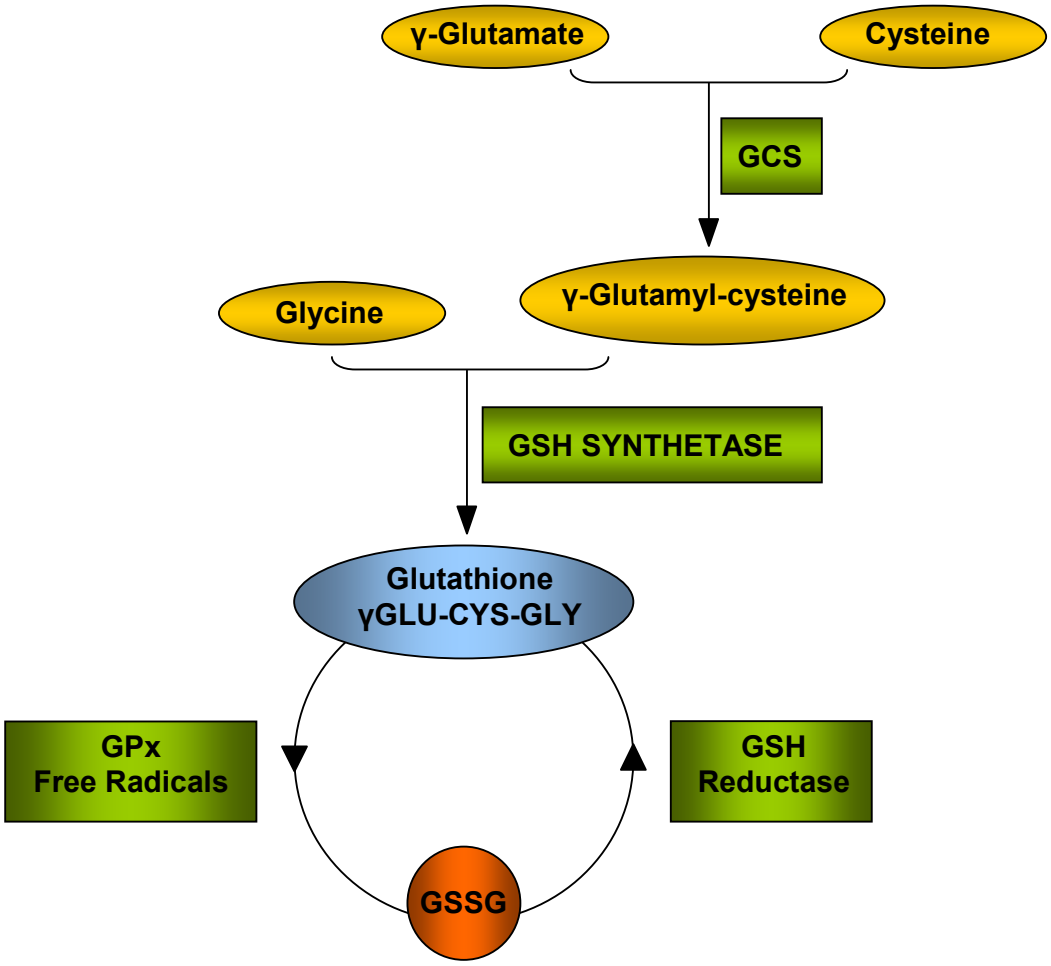

Figure 1.10 Glutathione synthesis

Glutathione is synthesised in a 2 step reaction by GCS and GSH synthetase. It can be oxidised to GSSG by various electrophilic substrates and reduced by GSH reductase.

GSH: glutathione, GCS: glutamyl-cysteine synthetase, GSSG: glutathione disulphide, GPx: glutathione peroxidase

Firstly, γ-glutamyl-cysteine is produced by γGCS which catalyses the reaction of the γ carboxyl of glutamate with the amino group of cysteine. This first step is rate limiting for GSH synthesis as is the availability of L-cysteine. The second step involves the interaction of glycine with γ-glutamyl-cysteine to produce GSH which is catalysed by GSH synthetase.

Glutathione can exert its antioxidant effect either independently or through enzymatic activity such as GPx or GST. Glutathione can non-enzymatically interact with and detoxify OH^- and can also detoxify products of nitrosative stress such as peroxynitrite.

1.4.3.5 Glutathione Peroxidase

Glutathione peroxidases are able to catalyse the reduction of hydroperoxides including H_2O_2 by utilising glutathione as a reducing agent. In mammals, there are 4 known selenocysteine containing isoforms of GPx. GPx-1 and GPx-2 are both tetrameric proteins and share similar activities. Each is capable of metabolising H_2O_2 but cannot reduce phospholipid hydroperoxides. GPx-1 was discovered first and is also known as classic or cytosolic GPx (cGPx). GPx-2 is found predominantly in the epithelium of the gastrointestinal tract and is also known as GPx-GI. GPx-3 is a tetrameric glycoprotein that is present in plasma. The main source of this enzyme is the kidney, with mRNA expression found particularly in epithelial cells of the proximal tubules. GPx-4 is a monomeric enzyme that is able to metabolise phospholipid hydroperoxides.

The effect of adenosine mediated over-expression of GPx-1 on human primary endothelial cell sensitivity to H_2O_2 was assessed by Zhang *et al*. Increased expression of GPx-1 reduced H_2O_2 cellular toxicity, confirming its protective role against oxidative stress (116). GPx-1 deficiency in mice has been associated with endothelial dysfunction and structural abnormalities in the vasculature and has been shown to increase levels of isoprostanes, indicating increased oxidative stress in these animals (117).

1.4.3.6 Glutathione Transferases

Glutathione S-transferase mu type 1, identified as a positional and functional candidate gene for hypertension in the rat, is one of a large family of phase II detoxifying enzymes that play a role in the cellular defence against oxidative stress, by catalysing the conjugation of glutathione to various electrophilic substrates (118). The effectiveness of glutathione transferases (GST) as antioxidant enzymes is limited by the enzymes responsible for GSH synthesis and those responsible for transporting the GSH conjugates out of the cell. Once conjugated to GSH, substrates can be removed from the cell by various ATP dependent transport mechanisms including multi-drug resistance associated proteins (MRP) (119) and glutathione S-conjugate export pumps (GS-X) (120).

The GSTs are dimeric enzymes and can exist as homodimers or heterodimers but can only be formed from subunits from the same class. Members of the same class share greater than 40% identity and between classes share less than 25%. Each GST subunit is composed of two distinct domains. The N-terminal domain 1 or G site is highly conserved between classes and is responsible for binding glutathione through its interaction with cysteine. It is connected to domain 2 or the H site by a short linker sequence. Domain 2 is less well conserved and is responsible for binding hydrophobic substrates. The diversity in the H site between classes may account for the broad substrate specificities of the various GSTs. Once bound to the G site, GSH is activated and becomes deprotonated. By doing so, GSH becomes a strong nucleophile and facilitates its interaction with an electrophilic substrate (121).

GSTs have been shown to detoxify the breakdown products of oxidative damage to protein, DNA and lipids such as base propenals and 4-hydroxyalkenals (118). Oxidative stress can lead to oxidation of nucleotides and DNA degradation and subsequently generate base propenals. GSTs have been shown to protect cells against cytotoxicity mediated by adenine and thymine propenal generation, particularly Pi class GSTs (122). Peroxynitrite induced protein nitrotyrosine production can be inhibited by incubation with GST, leading to denitration of proteins (123). .

Alpha class GSTs also demonstrate glutathione peroxidase activity against lipid hydroperoxides generated from damage to cell membranes. Although endogenous systems are in place to counteract ROS, if superoxide production is increased, these systems can be overwhelmed causing damage to DNA, proteins and lipids.

In mammals there are at least seven classes of cytosolic GST including, alpha, mu, pi, theta, sigma, omega and zeta. There are eight possible members of the mu class in the rat that have been reported to date. The rat mu family includes, *Gstm1, 2, 3, 4, 5* and *6*. A further 2 genes are designated *Gstm6l* (Gstm6-like) and *Gstm7* (GSTM7-7 like). All eight genes map to chromosome 2q34 and form a cluster in the order m7-m1-m2-m4-m6l-m3-m6 followed by m5 (inverted). There are five members of the mu class in humans (*GSTM1*-5) all of which map to chromosome 1p13.3 (124). The genes are arranged in the following order: M4-M2-M1-M5 and M3 (inverted).

1.4.3.7 Glutathione S-Transferase Mu Type 1

Polymorphisms in various genes encoding glutathione transferases have been implicated in carcinogenesis (125). In humans, 50% of the population is *GSTM1* null and as such do not express GSTM1 protein. The *GSTM1* null allele has been associated with an increased risk of developing various cancers, particularly lung cancer (126). At present, little work has been done to investigate the role of GSTM1 in cardiovascular disease. A recent study aimed to assess the association between various *GSTM* variants and hypertension. Individuals with and without hypertension were screened for SNPs in *GSTM1*, *2*, *3*, *4* and *5*. In the initial screen a SNP in the 3' region of *GSTM5* was found to be associated with hypertension. However this result was not replicated in a second cohort and suggests that *GSTM* gene variants are not associated with hypertension (127). Although an association between human *GSTM1* and hypertension could not be confirmed, it is not yet known which human *GSTM* is the true orthologue of rat *Gstm1*.

The reduced expression of *Gstm1* in 16 week old SHRSP kidneys was found in parallel with increased renal oxidative stress and blood pressure compared to the 2c* and WKY strains (69;77). Expression of *Gstm1* was found to be significantly lower in 5 week old SHRSP before the onset of severe hypertension indicating that the differential expression of renal *Gstm1* may be a contributing factor to the development of hypertension and is not an adaptive response to long term increased blood pressure (77). It may be that increased renal oxidative stress in the SHRSP is contributing to the development of hypertension. Increased renal oxidative stress has been demonstrated to contribute to hypertension in various rat models. In Sprague Dawley rats, oxidative stress was induced in the renal medulla by infusion of the CuZn-SOD inhibitor diethyldithiocarbamic acid (DETC). Following infusion of DETC, increased superoxide levels were found in the renal medulla and blood pressure was significantly increased (128). The addition of TEMPOL prevented the DETC-induced increase in superoxide but did not prevent the DETC-induced hypertension. However, when catalase was co-infused with TEMPOL, DETC-induced hypertension was blocked. This suggested that removal of superoxide from the renal medulla alone was not sufficient to prevent the development of hypertension but by limiting TEMPOL induced H_2O_2 production, hypertension could be prevented. Direct renal infusion of H_2O_2 alone was also found to produce hypertension, possibly as a result of oxidative injury to renal medullary cells (129). Hypertensive Dahl S rats on a high salt diet exhibited significantly lower SOD activity levels and increased excretion of urinary isoprostanes (a marker of lipid peroxidation), indicating increased oxidative stress in the kidneys of these rats (130). The reduction of *Gstm1* expression in kidney tubular epithelium may result in reduced protection against the products of oxidative stress and subsequently lead to oxidative DNA, protein or lipid damage in these cells. This is in turn may contribute to the development of hypertension due to an impaired ability of tubular cells to properly regulate the sodium-fluid balance.

1.5 RNA Interference

RNA interference (RNAi) is a naturally occurring mechanism that results in post-transcriptional gene silencing (PTGS) in response to double stranded RNA (dsRNA) molecules that are homologous to a target gene. By exploiting this mechanism experimentally it is possible to reduce the expression of a particular gene of interest to further investigate its function. Post-transcriptional gene silencing was first observed by Napoli *et al*. during transgenic experiments in plants. They found that introducing a chimeric chalcone synthase (CHS) gene (responsible for petunia petal pigmentation) generated white flowers lacking pigmentation resulting from suppression of both the endogenous and introduced CHS genes. This unexpected effect was described as co-suppression (131;132). Experiments carried out in *Neurospora crassa* identified a related mechanism for gene inactivation, termed quelling (133;134). Both of these mechanisms are related to RNAi which was first described in *C.elegans* by Fire *et al*. Investigations into the role of RNA structure in genetic silencing found that dsRNA mediates RNAi, as dsRNA directed against a luciferase reporter gene had a much stronger silencing effect than either sense or antisense strand alone (135). Tushl and colleagues then reported that the strong silencing observed in response to dsRNA is not just due to the longer half life of dsRNA as single stranded RNA modified with a 7-methyl guanosine cap to increase stability is still unable to inhibit gene expression (136).

1.5.1 RNA Interference: Mechanism

The mechanism by which RNAi works has been elucidated through various studies with *C.elegans* and *Drosophila* (137). This mechanism is outlined in Figure 1.11. RNA interference is induced by dsRNA sequences that are 21-22 nucleotides (nt) long and have 2nt 3'overhangs. The 5' end of the sequence contains a phosphate group and the 3' end contains a hydroxyl group (138). These short interfering RNAs (siRNAs) are generated from long dsRNA molecules by Dicer, an ATP dependent RNase III like enzyme that is specific for dsRNA (139).

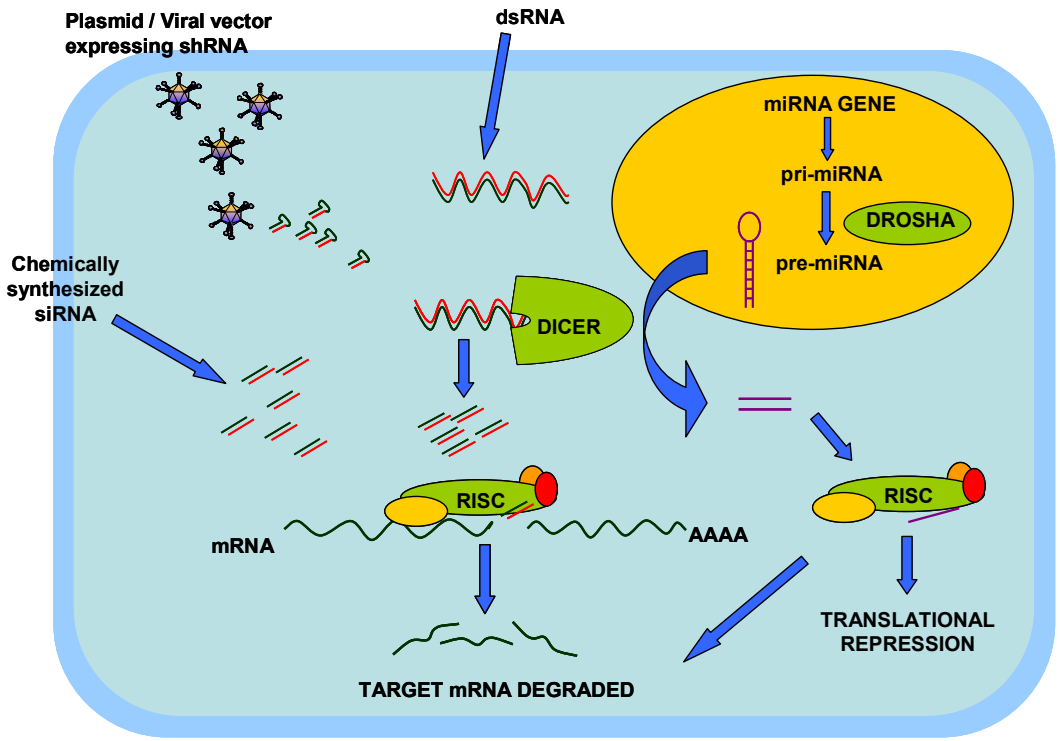

Figure 1.11 Mechanism of RNA interference

Double stranded interfering RNA molecules (siRNA/shRNA) are introduced to the cell. Duplex RNA dissociates and one strand is incorporated into the RNA induced silencing complex. The target mRNA and siRNA strand anneal and the target is then degraded via nuclease activity. Part of this RNAi pathway is also utilised by microRNAs.

RISC: RNA induced silencing complex, siRNA: short interfering RNA, shRNA: short hairpin RNA, mRNA: messenger RNA, miRNA: microRNA, pri-miRNA: primary miRNA, pre-miRNA: precursor miRNA

Dicer is found in complex with R2D2, a dsRNA binding protein that facilitates siRNA binding. Although R2D2 is involved in binding the siRNA duplex it is not required for production of siRNA as R2D2 mutant flies are no different to wild type in their ability to generate siRNAs (140). However, R2D2 is necessary for siRNA incorporation into the RNA induced silencing complex (RISC), the effector complex responsible for sequence specific degradation of the mRNA (141;142). R2D2 has been found to bind to the more stable end of the siRNA duplex whereas Dicer binds to the less stable end; this binding of siRNA by Dicer/R2D2 produces the RISC loading complex (RLC) (143). It is RISC that is responsible for mRNA cleavage and for this to take place; RISC must associate with the siRNA duplex and incorporate the guide strand. Active RISC is composed of the Argonaute family of proteins and siRNA. Argonaute proteins are composed of 4 domains: an N-terminal, PAZ domain (also found in Dicer), Mid domain and PIWI domain (144). Prior to incorporation of siRNA, RISC is inactive and is termed holo-RISC. To become active, the Argonaute complex interacts with the RISC loading complex allowing association with the siRNA duplex. The duplex is cleaved by the Argonaute protein allowing it to unwind and the guide strand becomes part of the now active RISC (145). RISC can now interact with the target mRNA through complementary base pairing with the siRNA. The endonuclease activity provided by RISC results in cleavage of mRNA every 21-23 nucleotides, reflecting the size of the siRNA (146).

1.5.2 MicroRNAs

MicroRNAs (miRNAs) are another class of small RNA that regulate gene expression, in part, through the RNAi pathway (147). Unlike siRNAs that are generated via viral replication or through introduction of chemically synthesised molecules or expression vectors, miRNAs are produced from endogenously expressed transcripts. Genes encoding miRNAs generate primary miRNAs (pri-miRNAs) that form long stem loop structures. The hairpin region is then cut out by the RNase III family enzyme Drosha to generate a stem loop precursor miRNA (pre-miRNA) of ~70nt long (148;149). The pre-miRNA is then exported from the nucleus to the cytoplasm where Dicer cleaves the stem loop structure to form the 21-25nt long mature miRNA (150;151). The mature miRNA associates with

RISC and binds to the target 3'UTR and in doing so results in translational repression.

1.5.3 *In Vitro* RNAi

Elbashir *et al*. were the first to demonstrate siRNA induced RNA interference in cultured mammalian cells. They found that transfecting cells with 21nt siRNA duplexes resulted in knock-down of genes expressed endogenously and from reporter constructs (152). To utilise RNAi for *in vitro* experimental purposes, double stranded RNA molecules first have to gain access to cells expressing the gene of interest. This can be achieved in a variety of ways. Chemically synthesised short interfering RNA (siRNA) molecules of 21 nucleotides in length can be incorporated into lipid or amine based complexes and introduced using various transfection methods. As well as transfection, siRNA can be introduced via electroporation (153). By using synthetically generated siRNA, the need for processing by Dicer is avoided. As described previously, Dicer is responsible for cleaving long dsRNA into short sequences that can initiate RNAi. However, introduction of dsRNA molecules greater than 30nt can result in activation of the interferon response in mammalian cells (152). Therefore, using short sequences, the possibility of adverse activation of interferon response genes can be limited. Alternatively, plasmid or viral vectors can be used that are engineered to express short hairpin RNAs (shRNA) that are complementary to the target mRNA. Once in the cytoplasm, the siRNA/shRNA molecules can then associate with RISC. Once incorporated into RISC the siRNA associates with the target mRNA, leading to its degradation and subsequent knockdown of gene expression.

1.5.4 *In Vivo* RNAi

As previously mentioned, RNAi requires the introduction of dsRNA molecules directly to those cells expressing the gene that is to be silenced. This can be readily achieved *in vitro* (136;152) however; *in vivo* RNAi poses a greater challenge. It is possible to introduce naked siRNA molecules *in vivo*. McCaffrey *et al* was able to demonstrate luciferase reporter gene silencing in the livers of adult mice following the delivery of naked siRNA via hydrodynamic tail vein

injection (154). Hydrodynamic delivery involves the rapid injection of nucleic acid in a large volume of fluid (155). This method of delivery can elicit a quick silencing response, as the molecule need only gain access to the cytoplasm where it can interact with RISC and carry out its function. However, the stability of these 21nt sequences within an *in vivo* environment is an issue, as well as factors such as the half-life of the target protein (156;157). By introducing siRNA in this way the silencing effect would be short lived and although introducing large concentrations of siRNA may help to prolong the effect, excess siRNA could result in off-target effects. While siRNA is designed to be specific to a target mRNA, excess molecules could cause aberrant silencing of unintended genes (158). High specificity will also help to ensure that no non-specific binding occurs, thus helping to prevent off-target effects.

To further facilitate *in vivo* delivery, siRNA molecules can be introduced in complex with cationic lipids. A liposome-based method was utilised by Sorensen *et al*, to induce gene silencing in adult mice (159). More recently, Santel *et al* have demonstrated the use of lipoplexes for *in vivo* delivery of siRNA molecules targeted against genes expressed in the vascular endothelium of mice. Following intravenous injection of the lipoplex (cationic lipid, helper lipid and siRNA), reduced expression of endothelial specific genes was observed (160). This method of liposomal delivery has since been utilised to silence gene expression in the liver of cynomolgus monkeys (161).

Alternatively, interfering RNA fragments can be introduced via expression vectors, such as plasmids or viral vectors. Viral vectors such as adeno-associated viral (AAV) vectors can be manipulated to express short-hairpin RNA molecules (shRNA), that can target host cell mRNA for destruction. For this method to be effective the virus must gain entry to the nucleus, thus enabling the expression of the shRNA molecule and although this may take more time to produce an effect, the silencing obtained would be more stable. Once expressed, the shRNA is processed and exported to the cytoplasm where it can associate with RISC, thereby allowing its interaction with the target mRNA. Wang *et al* have demonstrated gene silencing in rats following intravenous delivery of AAV vectors engineered to express shRNA (162).

1.5.5 Therapeutic Potential

RNA interference has more recently shown promise as a potential therapeutic for the treatment of disease. Synthetically generated siRNAs have been shown to inhibit hepatitis C virus production in cultured cells (163). Mice treated with siRNA targeted to the Fas receptor gene are shown to have greater resistance to liver disease. Following intravenous injection of siRNA, hepatocytes isolated from treated mice were resistant to apoptosis (164). DiFuglia et al demonstrated the potential use of RNAi as a treatment for the neurological disorder Huntington's disease (HD). A virus mediated transgenic model of HD was utilised to test the efficacy of anti-htt (HD gene) siRNA. Striatal neurons in siRNA treated mice had a prolonged survival and presented fewer abnormalities that are associated with HD.

RNA interference has also been evaluated as a potential antiviral therapy for respiratory syncytial virus (RSV) infection. Bitko et al demonstrated inhibition of RSV following nasal administration of anti-RSV siRNA in mice. Antiviral effects were observed before and after RSV infection indicating the potential of siRNA as a therapy that can be delivered locally to combat RSV infection (165). This siRNA has since gone on to be tested in a phase II clinical trial to evaluate its safety as an antiviral therapeutic. The siRNA was delivered to the respiratory tract via a nasal spray and was found to be well tolerated with few side effects (166). Another disorder where clinical trials are underway for a therapeutic siRNA is age-related macular degeneration (AMD). Studies have shown that siRNAs targeted against vascular endothelial growth factor (VEGF) or VEGF receptor 1 (VEGFR1) have beneficial effects in mouse models of AMD. In these models, reducing expression of VEGF or VEGFR1 inhibited choroidal neovascularisation (CNV), a common cause of vision loss in people suffering with AMD (167;168). Following on from these and other studies, siRNA targeting VEGFR1 (siRNA-027) has since been taken forward to phase II clinical trials (169). Another siRNA (REDD14NP) is also being evaluated for AMD in a phase I clinical trial (170).

RNA interference provides an excellent tool for elucidating gene function both *in vitro* and *in vivo*. Using various means of delivery it is possible to reduce

expression in animal models of human disease and as such may prove beneficial in the identification of the function of glutathione S-transferase mu type 1 in both oxidative stress and hypertension. *In vivo* delivery of *Gstm1* specific interfering RNA molecules would allow for a more accurate investigation into the role of *Gstm1* in rat hypertension, with a view to finding similar blood pressure regulatory mechanisms in human.

1.6 Hypothesis

Due to the role of GSTs in defence against oxidative stress and the involvement of oxidative stress in the development of hypertension, we hypothesise that depleted renal expression of *Gstm1* may contribute to development of hypertension by reducing the capacity of renal cells to protect themselves against the damaging products of oxidative stress. In addition to the differential expression of *Gstm1* observed between the parental and congenic strains, it may be that microRNAs mapping to the chromosome 2 congenic region are responsible for regulating the expression of genes which could contribute to the blood pressure phenotypes observed in these strains.

1.6.1 Aims

A combination of congenic breeding and microarray analysis has identified *Gstm1* as a positional and functional candidate gene for hypertension in the stroke-prone spontaneously hypertensive rat (SHRSP). This aims of this study are to investigate the role of *Gstm1* using an RNAi mediated approach and develop molecular tools that could be used for targeted modulation of gene expression *in vivo*. In addition to this, another aim is to investigate microRNAs that map to the chromosome 2 congenic regions.

The specific aims of this study are:

1. To assess the ability to knock-down *Gstm1* expression specifically with siRNA and develop tools for *in vivo* kidney targeted knock-down
2. To assess the contribution of reduced *Gstm1* expression to markers of oxidative stress
3. To investigate expression of microRNAs in kidney from parental and chromosome 2 congenic strains and assess expression levels of potential microRNAs targets

Chapter 2: Materials and Methods

2.1 General Laboratory Practice

This chapter outlines general materials and methods that are common to more than one chapter. Where necessary, more details are given in the appropriate chapters.

All laboratory equipment and reagents used throughout the project were of the highest available grades. A laboratory coat and latex powder-free gloves were worn during all procedures. Handling of hazardous reagents was carried out in accordance with Control of Substances Hazardous to Health regulations.

Laboratory glassware was cleaned in Decon 75 detergent, rinsed with distilled water and dried in a 37°C cabinet. Sterile, disposable plastic-ware was also used, including 0.5 ml, 1.5 ml and 2 ml microcentrifuge tubes (Greiner Bio-One), 15 ml and 50 ml Corning centrifuge tubes and 5 ml and 20 ml Universal containers (Sterilin). Glass-ware and reagents requiring sterilisation were autoclaved in a Priorclave Tactrol 2.

To weigh out reagents an Ohaus Portable Advanced balance (sensitive to 0.01 g) or a Mettler HK160 balance (sensitive to 0.0001 g was used). To dispense volumes from 0.1 µl to 1000 µl, Gilson pipettes were used (Gilson Medical Instruments. For larger volumes from 1 ml to 25 ml, sterile disposable pipettes (Corning) were used with a Gilson battery-powered pipetting aid. When preparing solutions, distilled water (dH_20) was used unless otherwise stated and to aid dissolving and mixing a Jenway 1000 hotplate and stirrer was used. The pH of solutions was determined using a Mettler Toledo digital pH meter. The meter was calibrated before use with solutions of pH 4, 7 and 10 prepared from buffer tablets (Sigma-Aldrich). Vortexing was carried out using an FSA Laboratory Supplies WhirliMixer. For experiments requiring incubations between 37°C and 90°C, a Julabo TW8 water bath utilised and for temperatures up to 100°C a Grant SBB14 boiling water bath was used. For centrifugation of samples up to 2 ml, an Eppendorf 4515 microcentrifuge was used. Larger volume samples were centrifuged in a Sigma 4K15, compatible with 15 ml and 50 ml centrifuge tubes, 20 ml Universal containers and carriers for standard reaction plates.

For all experiments involving RNA, certified nuclease-free reagents and plastic-ware were used, including nuclease-free water, 0.5 ml, 1.5 ml and 2 ml RNase-free microcentrifuge tubes (Ambion) and nuclease-free pipette tips for volumes between 0.2 µl and 1 ml (RAININ). Prior to beginning RNA work, all pipettes and bench space were wiped with RNaseZap (Ambion) and rinsed with nuclease-free water.

2.2 Cell Culture

All i*n vitro* RNA interference experiments were carried out in the rat renal tubular epithelial cell line NRK-52E. Cells were obtained from the European Collection of Cell Culture (ECACC). The details of other cell lines used are described in the methods section of the relevant chapters. NRK-52E cells were grown in 150 cm^2 flasks containing Dulbecco's modified Eagle's medium plus GlutaMAX supplemented with 10% (v/v) foetal calf serum (FCS), 100 U/ml penicillin and 100 mg/ml streptomycin. Cells were maintained at 37°C in a 5% CO_2/95% air atmosphere incubator.

2.2.1 Cell Passage

Cell culture medium, sterile PBS (Lonza) and 1X TE (0.05% trypsin; 0.2% ethylenediamine tetraacetic acid (EDTA)) were warmed to 37°C in a water bath. Culture medium was removed from the flask and cells were rinsed twice with 10 ml sterile PBS. To detach cells, 5 ml 1X TE was added to the flask and incubated at 37°C for 5 minutes. Once cells had detached from the flask, 15 ml of culture medium containing 10% (v/v) FCS (to inactivate trypsin) was added and the cell mixture was transferred to a 50 ml centrifuge tube (Corning). Cells were centrifuged at 1500 rpm for 5 minutes to pellet cells. The supernatant was removed and cells were re-suspended in fresh culture medium. Of this suspension, 1/20-1/10 was transferred to a fresh 150 cm^2 flask containing 25 ml culture medium.

2.2.2 Cell Counting

Cells were counted using a haemocytometer (Hausser Scientific). A cell suspension was prepared by detaching cells with 1X TE as described in section 2.3. A cover-slip was placed on the haemocytometer counting surface and 10 µl of the cell suspension was applied to the grid under the coverslip. The number of cells in a 1 mm square was determined by counting the number of cells in each quadrant. The average number of cells in each 1mm square was determined and multiplied by 10^4 to give the number of cells per ml.

2.3 Transfection of NRK-52E Cells with siRNA

Cells were cultured in 6 well plates until ~70% confluent and then transfected with 30 to 100nM *Silencer*® Pre-designed *Gstm1* specific siRNA (Applied Biosystems). Three different sequences were evaluated, designated A (ID# 200597), B (ID# 200598) and C (ID# 200599). The siRNA sequences were as follows:

Sequence A: GCUCAUCAUGCUUUGUUACtt (sense)
GUAACAAAGCAUGAUGAGCtg (antisense)

Sequence B: CCUAUAUUUUCGAAGUUGGtt (sense)
CCAACUUCGAAAAUAUAGGtg (antisense)

Sequence C: CCUCACAGUCCUUUUCUGUtt (sense)
ACAGAAAAGGACUGUGAGGtt (antisense)

Each sequence was 19nt long with 2nt 3'overhangs. A *Silencer*® Cy™ 3 labelled control siRNA that has no known homology to any expressed genes was also used, allowing for an assessment of transfection efficiency by fluorescence microscopy. In each experiment, three controls were used: untransfected cells (UTF), cells with transfection reagent only (TFC) and cells transfected with labelled control siRNA (siCTL). RNase free micro-centrifuge tubes and pipette tips were used throughout. Each transfection was carried out in triplicate using

siPORT™ *Amine* transfection reagent (Applied Biosystems) according to manufacturer's instructions. Briefly, 12 µl of siPORT™ *Amine* was diluted to a final volume of 197 µl (per well) in Opti-MEM® Reduced Serum Medium (Invitrogen) and incubated at room temperature for 15 minutes. The volume of growth medium in each well was reduced to 800 µl. Chemically synthesised siRNA was added to the transfection reagent mix (to give a final concentration of 30 or 100nM siRNA) and incubated at room temperature for 15 minutes. The transfection reagent and siRNA complexes were added drop-wise to each well. Plates were gently rocked back and forth to disperse the transfection complex and incubated at 37°C for 5 hours. The medium in each well was then topped up with 2 ml of normal growth medium and incubated at 37°C for a further 48 hours. After 48 hours, cells or medium were collected for further analysis.

2.4 Protein Extraction

Protein was collected from cells cultured in tissue culture plates. Culture medium was removed and cells were rinsed twice with sterile PBS. Adherent cells were made permeable with 0.2% Triton X-100/PBS and samples were collected by scraping the cells with a pipette tip. Protein samples were then passed through a 25 gauge needle 5 times and briefly centrifuged to remove cell debris. The supernatant containing protein was then transferred to a fresh 1.5 ml centrifuge tube and stored at -20°C.

2.4.1 Measuring Protein Concentration

The total protein concentration of each lysate was determined using a bicinchoninic acid (BCA) assay kit (Pierce) according to the manufacturer's instructions. A set of 9 albumin protein standards ranging from zero to 2000 µg/ml were prepared by diluting each standard in PBS and used to generate a standard curve. The BCA working reagent (WR) was prepared by mixing BCA Reagent A with BCA Reagent B at a ratio of 50:1 (A:B). The total volume of working reagent required was calculated as follows: (no. of standards + no. of unknown samples) x (no. of replicates) x (volume of WR per sample). Each standard and sample (25 µl) was assayed in duplicate in a 96 well plate and 200 µl of the WR was added to each well. The plate was then covered to protect

from light and incubated at 37°C for 30 minutes. Following incubation the plate was cooled to room temperature and the absorbance from each well was read at 560nm using a Wallac Victor^2 plate reader. Each standard and sample was measured in duplicate and average readings were taken. A standard curve was generated and the protein concentration in each sample was determined from the curve using 'Work-Out' software (Wallac).

2.5 Western Blot

Western blotting was performed to assess levels of protein expression.

2.5.1 Gel Electrophoresis

Proteins were resolved by SDS PAGE (sodium dodecyl sulphate polyacrylamide gel electrophoresis) in a Hoefer SE 600 gel electrophoresis tank. A 12% resolving gel was prepared and poured between 18 cm x 16 cm glass plates followed by a 4% stacking gel poured on top. The 12% resolving gel consisted of 40% (v/v) polyacrylamide (30%) (BIORAD), 0.375M Tris pH 8.8, 0.1% (v/v) SDS, 300 µl ammonium persulphate (APS) and 30 µl TEMED (N,N,N',N'-tetramethylethylenediamine). The 4% stacking gel consisted of 13.3% (v/v) polyacrylamide (30%), 0.125M Tris pH 8.8, 0.1% (v/v) SDS, 300 µl APS and 30 µl TEMED.

Protein samples and controls were added to 2X Laemmli sample buffer (Sigma Aldrich) in a 1:1 ratio to a maximum volume of 60 µl and heated to 100°C for 10 minutes. Amersham low range rainbow molecular weight markers (GE Healthcare Life Sciences) were loaded (15 µl) to allow for determination of protein size. Samples were loaded into the wells of the gel and subjected to electrophoresis at 100V for 1 hour in running buffer (0.025M Tris-HCl, 0.2M glycine and 0.001M SDS). Once through the stacking gel, the voltage was increased to 200V for approximately 3 hours until proteins were sufficiently resolved as determined by the separation of the rainbow markers.

After electrophoresis the gel and six sheets of Whatman 3 mm chromatography blotting paper were prepared for transfer by placing in transfer buffer (0.025 M Tris, 0.2 M glycine, 20% (v/v) methanol and 0.01% (v/v) SDS) for 20 minutes. Hybond™-P nitrocellulose membrane (Amersham) was prepared by wetting with methanol for 5 seconds and then soaking in distilled water for 5 minutes followed by 10 minutes in transfer buffer. A transfer cassette was then set up (cathode to anode) as follows: 3 sheets of blotting paper, gel, membrane and another 3 sheets of blotting paper Resolved proteins were transferred onto the nitrocellulose membrane overnight at 90mA in transfer buffer in a Hoefer TE 50X transfer tank.

2.5.2 Antibody Probing

Following transfer, the membrane was blocked for at least 6 hours (with shaking) in a 10% (w/v) milk solution (blocking buffer) prepared in Tris-buffered saline Tween buffer (TBS-T) (0.025 M Tris pH7.4, 0.14 M NaCl, 0.0027 M KCl, 0.1% (v/v) Tween 20 (Sigma)). After blocking, the membrane was incubated in primary antibody solution at 4°C overnight, with shaking. The membrane was then washed 6 times for 5 minutes with TBS-T and then incubated with a secondary antibody conjugated to horseradish peroxidase (Dako) for 1 hour at room temperature. All antibodies were diluted to the required concentration in blocking buffer. The membrane was washed again as described previously.

2.5.3 Enhanced Chemiluminescence and Detection

Bands were detected using Amersham ECL (enhanced chemiluminescence) western blotting detection reagents (GE Healthcare). Equal quantities of the two reagents were mixed and poured over the membrane, ensuring the membrane was completely covered. After 3 minutes at room temperature, the membrane was removed from the ECL reagents and any excess was drained off. The membrane was then wrapped in Saran wrap and placed in an autoradiography cassette. Film exposure and development was carried out in a dark room. Kodak general purpose medical X-ray film was used and films were

exposed for varying lengths of time from 5 seconds to overnight. Films were developed in a Kodak X-Omat 1000 developer.

2.5.4 Densitometry

To ensure that any change in protein level was not due to unequal loading, membranes were stripped and re-probed for ß-actin. The membrane was incubated with stripping buffer (0.2 M glycine and 1% (v/v) SDS at pH 2.2) for 30 minutes at room temperature then washed twice for 10 minutes in TBS-T. The membrane was blocked as before and incubated at 4°C overnight with a mouse ß-actin antibody (Abcam) used at a dilution of 1/1000. Bands were detected on X-ray film as before.

To normalise each band, the X-ray films were scanned using the BIORAD Fluor-S Multi-imager and bands were quantified using 'Quantity One' software (BIORAD). The intensity of each band was determined by the software using the global background subtraction method and expressed in units of optical density per mm_2 (ODU/mm^2). The adjusted volume value for each band was divided by the equivalent value obtained for the ß-actin band to give a final value corrected for loading.

2.6 RNA Extraction

RNA was extracted from NRK-52E cells using an RNeasy Mini Kit (Qiagen), according to the manufacturer's guidelines. Cell culture medium was removed and cells were rinsed twice with PBS. Cells were lysed by scraping with a pipette tip in 350 µl buffer RLT containing guanidine isothiocyanate with the addition ß-mercaptoethanol (10µl/ml). The lysates were transferred to RNase free 1.5 ml centrifuge tubes and mixed with 350 µl 70% ethanol by pipetting. The samples were transferred to RNeasy mini columns allowing RNA to bind to the membrane and then centrifuged at 8000 g for 15 seconds and the flow-through discarded. The columns were washed with 700 µl Buffer RW1 and centrifuged at 8000 g for 15 seconds. The columns were then washed with 500 µl Buffer RPE and centrifuged at 8000 g for 15 seconds. This wash step was

repeated but centrifuged at 8000 g for 2 minutes. The flow-through was discarded and the column was centrifuged again for 1 minute at full speed to remove any residual buffer. RNA was eluted in 40 µl nuclease free water, put through the column twice and centrifuged at 8000 g for 1 minute. RNA samples were stored at -80°C.

2.6.1 DNase Treatment of Extracted RNA

To remove any contaminating DNA from RNA preparations, samples were subjected to TURBO DNA-free DNase treatment (Applied Biosystems). Samples were transferred to 0.5 ml RNase free centrifuge tubes. To each sample, 0.1 volumes of 10X TURBO DNase buffer and 1 µl TURBO DNase were added and mixed gently followed by incubation at 37°C for 30 minutes. Re-suspended DNase inactivation reagent was then added to each sample (0.1 volumes) and incubated for 2 minutes at room temperature with occasional mixing. To remove the DNase inactivation reagent, samples were centrifuged at 10,000 g for 1.5 minutes. This step pellets the DNase inactivation reagent and the supernatant containing the RNA can be transferred to a fresh RNase free tube.

2.6.2 Nucleic Acid Quantification

Total RNA or DNA concentrations were quantified using the NanoDrop ND-1000 Spectrophotometer and ND-1000 v3.1.0 programme. For each sample, 1.5 µl of either DNA or RNA was quantified. An absorbance ratio (260nm/280nm) of approximately 2 for RNA and 1.8 for DNA indicated nucleic acid samples of high purity.

2.7 Reverse Transcription

TaqMan® Reverse Transcription Reagents (Applied Biosystems) were used to generate 1st strand cDNA from 1 µg of total RNA using random hexamer primers. Nuclease free water was added to 1 µg of total RNA to give a volume of 7.7 µl. The reverse transcription reaction mix was prepared as follows:

- 2 µl 10X TaqMan RT buffer

- 4.4 µl 25mM magnesium chloride
- 4 µl deoxyNTPs mixture
- 1 µl random hexamer primers
- 0.4 µl RNase inhibitor
- 0.5 µl MultiScribe reverse transcriptase (50U/µl).

This was added to the RNA sample to give a final reaction volume of 20 µl. Two control samples were also run; 1 blank (no RNA in sample) and 1 no RT control (nuclease free water was added instead of reverse transcriptase). Reverse transcription was carried out using the following thermal cycling parameters:

- 10 minutes at 25°C
- 30 minutes at 48°C
- 5 minutes at 95°C

cDNA samples were stored at -20°C until ready for use.

2.7.1 TaqMan® Quantitative Real-Time Polymerase Chain Reaction

Quantitative real-time PCR (qRT-PCR) was performed on cDNA using Applied Biosystems Gene Expression Assays and the ABI PRISM 7900ht Sequence Detection System. The comparative C_T method ($2^{-\Delta\Delta Ct}$)(171) was used to determine expression of the gene of interest relative to a *β-actin* house-keeping control gene. Efficiency tests were performed for each gene of interest to determine whether the assays for both the control gene (*β-actin*) and gene of interest could be performed in the same well (duplex) or separate wells (simplex). If the gene of interest amplified with equal efficiency to the control gene then both assays could be run in duplex, if not then they were run separately. Serial dilutions of a cDNA template were prepared and set up in simplex and duplex reactions for each gene of interest and the *β-actin* control gene. Efficiencies were calculated according to the manufacturer's instructions (ABI PRISM 7700 Sequence Detection System User Bulletin #2). The Ct values were plotted against log (dilution) for the gene of interest and *β-actin* and the gradient of each slope was compared. If the absolute value of the slope was <0.1 then the efficiencies were considered to be equal.

For each gene of interest a 5µl duplex reaction was set up in a 384 well plate consisting of:

- 0.25µl FAM labelled probe
- 0.25µl VIC labelled probe
- 2µl of template cDNA
- 2.5µl of TaqMan® Universal PCR master mix

The probes for the gene of interest were tagged to FAM labelled fluorescent dyes and ß-actin probes were tagged to VIC labelled fluorescent dyes. If the efficiency of the gene of interest was not equal to ß-actin, then a simplex reaction was prepared with nuclease free water added in place of the second probe. All samples were assayed in duplicate or triplicate and subjected to the following temperature cycling:

- 50°C for 2 minutes
- 95°C for 10 minutes
- 35 cycles of 95°C for 15 seconds followed by 60°C for 1 minute

2.8 Production of Short Hairpin RNA Expressing Plasmids

The pShuttle-CMV vector (Stratagene) was used to generate *Gstm1* targeting and control short-hairpin RNA (shRNA) expressing vectors (pShuttle-CMV-shRNA), see Figure 2.1.

2.8.1 pShuttle-CMV Plasmid DNA Purification

The pShuttle-CMV vector (Figure 2.1) was grown from a glycerol stock by streaking onto Luria agar (Sigma) plates containing kanamycin at 50 µg/ml. Plates were inverted and incubated at 37°C overnight. A single colony was picked and added to 10 ml Luria broth (LB) plus kanamycin and incubated with shaking at 37°C for approximately 8 hours. After this time, cells were transferred to 2 litre flasks containing 500 ml of LB and left to incubate at 37°C overnight with shaking.

The following day, the culture was transferred to sterile bug pots and bacteria were harvested by centrifugation at 6000 g for 15 minutes at 4°C in a Beckman Coulter Avanti J-26XP. Plasmid DNA was extracted using the Qiagen Plasmid Maxi Kit, according to kit instructions. The bacteria pellet was re-suspended in 10 ml buffer P1 (lysis buffer) until no clumps were visible and 10 ml buffer P2 was added. The pot was inverted 4-6 times to mix and then 10 ml chilled buffer P3 was added. The pot was inverted again and then kept on ice for 20 minutes. The lysates were then subjected to centrifugation at 20,000 g for 30 minutes at 4°C. The supernatant was retained and transferred to equilibrated columns (equilibrated with 10 ml buffer QBT). The supernatant was allowed to completely run through the column before the column was washed twice with 30 ml buffer QC. Plasmid DNA was eluted with 15 ml buffer QF into polypropylene centrifuge tubes and DNA was precipitated by the addition of 10.5 ml isopropanol and centrifuged at 15,000 g for 30 minutes at 4°C. The supernatant was carefully poured off and the pellet was re-suspended in 5 ml 70% ethanol and centrifuged at 15,000 g for 10 minutes at room temperature. The ethanol was carefully removed by pipette and the DNA pellets were left to air dry for approximately 10 minutes before being re-suspended in 200 µl nuclease free water. The plasmid DNA concentration was quantified as described in section 2.5.2 and stored at -20°C

2.8.2 Restriction Digest

To enable cloning of the shRNA sequences into the pShuttle-CMV backbone, plasmid DNA was digested with restriction enzymes. A total of 3 µg of DNA was digested in a reaction containing 4-CORE SYSTEM reaction buffer (Promega) and a 10-fold excess of enzyme over DNA, as per manufacturer's instructions. Typically a 20 µl reaction was carried out, including 1.5 µg plasmid DNA, 2 µl 10X restriction buffer, 0.2 µl BSA and 1.5 µl of each restriction enzyme (10U/µl) so that there was a 10-fold excess of each enzyme per reaction. The reagents were mixed gently, then centrifuged briefly and incubated in a water bath at 37°C overnight.

A

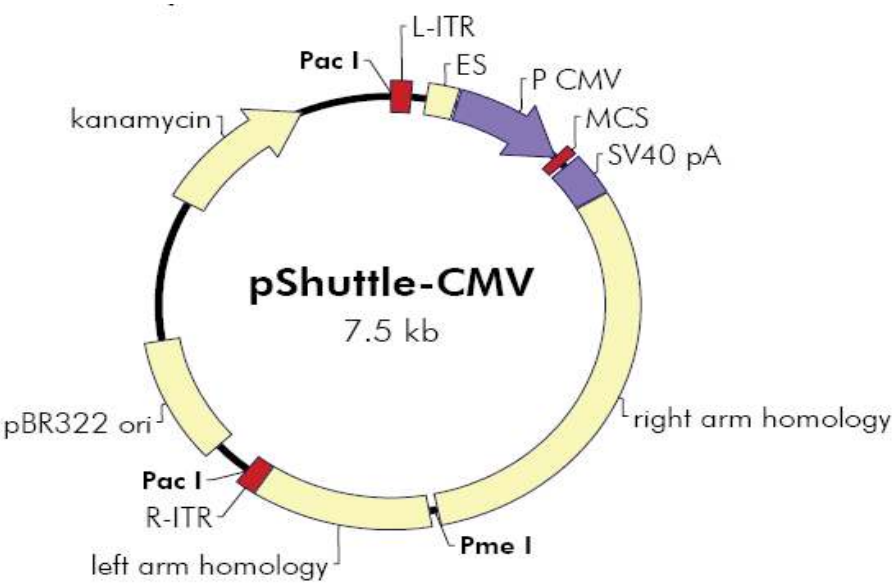

B

shRNA B
CCTATATTTTCGAAGTTG
GTGGATATAAAAGCTTCAAC

shRNA C
CCTCACAGTCCTTTTCTG
TTGGAGTGTCAGGAAAAGAC

shRNA SCR
ACTACCGTTGTTATAGGT
TTTGATGGCAACAATATCCA

Figure 2.1 pShuttle-CMV vector and shRNA sequences

A: Outline of the pShuttle-CMV vector map used to generate shRNA expressing plasmids (172). B: Oligonucleotides encoding each shRNA as shown above were cloned into the pShuttle-CMV vector backbone.

2.8.3 Agarose Gel Purification

The digested plasmid DNA fragments were separated by agarose gel electrophoresis. A 1% agarose gel (Eurogentec) was prepared in 1X Tris-Borate EDTA (TBE) (Fisher Bioreagents) containing 1µl ethidium bromide (Sigma) per 100 ml of molten agarose. Loading dye (6X) (50% glycerol and 0.05% bromophenol blue) was added to the DNA sample and to a control sample (linearised pShuttle-CMV DNA). Samples and a 1kb DNA ladder were subjected to electrophoresis at 6 volts per cm length of gel. Gels were visualised by UV transillumination on a BIO-RAD Fluor-S Multi-Imager. Electrophoresis was stopped after clear resolution of bands was observed. The band containing digested pShuttle-CMV DNA was cut out of the gel and DNA was extracted using the Wizard SV gel and PCR clean up system (Promega). The gel band was weighed and stored in a 1.5 ml tube. Membrane binding solution was then added (10 µl per 10 mg of gel) and incubated at 65°C for 10 minutes until agarose had melted. DNA was then extracted using the kit protocol provided and then eluted into 50 µl of nuclease free water.

2.8.4 Annealing and Ligation

Oligonucleotides encoding shRNA based on the siRNA sequences already evaluated were designed to include ends that were compatible with restriction sites present in the multiple cloning site of pShuttle-CMV (Figure 2.1). The oligonucleotide concentration required for annealing was 1 µg/µl. To achieve this, oligonucleotides were first diluted with nuclease free water to 2 µg/µl and then diluted to 1 µg/µl in 1X TE. Oligonucleotides were annealed in a reaction containing 46 µl 1X DNA Annealing Solution (Ambion) and 2 µl of each oligonucleotide (top and bottom). The reaction was incubated at 90°C for 3 minutes followed by 1 hour at 37°C. Annealed oligonucleotides were stored at -20°C.

The NEB Quick Ligation kit was used to ligate the different *Gstm1* shRNA inserts into the pShuttle-CMV vector backbone. A 100:1 insert to vector ratio was used

with 100 ng of vector in each ligation. The following equation was used to calculate how much insert to add to each ligation reaction:

((ng of vector x kb size of insert) / kb size of vector) x (molar ratio of insert to vector)

The ligation reaction was then carried out according to the manufacturer's instructions. A reaction mix was prepared containing 100 ng vector and a 100-fold molar excess of insert adjusted to 10 µl with water, 10 µl 2X Quick Ligation Buffer and 1 µl T4 DNA Ligase, this was mixed gently, centrifuged briefly and incubated at room temperature for 5 minutes. After ligation, samples were kept on ice until required for transformation.

2.8.5 Transformation of DH5α Cells

MAX Efficiency DH5α competent cells (Invitrogen) were thawed gently on ice for approximately 5 minutes. Once thawed, 50 µl of competent cells were transferred into pre-chilled 1.5 ml tubes and kept on ice. Ligation reactions were diluted 5-fold in 10 mM Tris-HCL, 1 mM EDTA and then 1 µl of the dilution was added to one 50 µl aliquot of cells. To determine transformation efficiency, a control transformation was carried out with 50 pg of control plasmid DNA (ampicillin resistant pUC19). The cells were kept on ice for 30 minutes, heat shocked at 42°C for 45 seconds and then returned to ice for a further 2 minutes. Cells were removed from the ice and 0.9 ml of room temperature SOC media was added to each aliquot followed by 1 hour incubation at 37°C with shaking. The control plasmid transformation was diluted 1:100 and 100 µl was plated onto an agar plate containing ampicillin. For all other transformations, 200 µl was spread onto agar plates with kanamycin (50 µg/ml). The plates were kept in a 37°C incubator overnight.

2.8.6 Polymerase Chain Reaction (PCR)

After overnight incubation, plates were removed from the incubator and the number of colonies on each plate was determined. Single colonies were picked

and added to nuclease free water in a 96 well PCR plate. A PCR master mix was then prepared containing:

- 10X PCR buffer (plus 20mM $MgCl_2$)
- 2.5 µl forward primer (2µM)
- 2.5 µl reverse primer (2µM)
- 4 µl dNTPs (1mM)
- 0.2 µl Taq (5U/µl).

This was added to each well to give a final reaction volume of 20 µl. Each sample was then subjected to:

- 4 minutes at 95°C
- 34 cycles of 30 seconds at 94°C
- 30 seconds at 58°C
- 1 minute at 72°C
- 7 minutes at 72°C.

A 1.5% agarose gel was prepared in 1X TBE containing 2µl ethidium bromide. Loading dye (6X) was added to 10 µl of each PCR reaction and subjected to electrophoresis at 150V for 1½ hours alongside a 50bp DNA ladder (Promega). Reactions that generated a band at the correct size were purified and sequenced.

2.8.6.1 PCR Purification

PCR samples were purified using an AMPure PCR purification kit (Agencourt) according to manufacturer's instructions. Briefly, 18 µl of AMPure reagent was added to each PCR reaction in a 96 well plate. Reagents were mixed, centrifuged at 1000 rpm for 1 second and incubated for 4 minutes at room temperature. The plate was then placed on a SPRI magnet plate for 8 minutes. With the plate on the magnet, the plate was inverted and the cleared solution was discarded. Fresh 70% ethanol was prepared and 200 µl was added to each well and incubated for 30 seconds. The plate was inverted onto tissue and centrifuged at 600 rpm for 1 second then left to air dry for 20 minutes. Once dry, 40 µl of nuclease free water was added to each well, mixed and centrifuged

at 1000 rpm for 1 second. Cleaned products were then transferred to a 96 well plate and stored at -20°C until required for sequencing.

2.8.7 Sequencing

Forward and reverse strand sequencing was carried out on each PCR sample using the BigDye Terminator v3.1 Cycle Sequencing Kit (Applied Biosystems). The sequencing reaction was carried out in a 96 well plate and prepared as follows:

- 10 µl of each PCR sample
- 1 µl Ready Reaction Mix
- 4µl of BigDye Terminator Sequencing Buffer (5X)
- 2µl of forward or reverse primer (2µM)
- Nuclease free water to a final volume of 20 µl

Each reaction was then subjected to:

- 25 cycles of 45 seconds at 96°C
- 25 seconds at 50°C
- 4 minutes at 60°C
- 5 minutes at 12°C.

2.8.7.1 Sequencing Clean-up

Dye terminator removal was carried out on each sequencing reaction using the Agencourt CleanSeq Dye Terminator Removal Kit. Briefly, 10 µl of room temperature CleanSeq was added to each sequencing reaction, followed by the addition of 62 µl of 85% ethanol. The reagents were mixed and centrifuged to 1000 rpm for 1 second. The plate was then placed on a SPRI magnet plate for 3 minutes. With the plate on the magnet, the plate was inverted and the cleared solution discarded. Then 150 µl of 85% ethanol was added to each well and incubated at room temperature for 30 seconds. The plate was inverted on tissue paper, centrifuged to 600 rpm and then left to air dry for 20 minutes. Once dry, 40 µl of nuclease free water was added to each well and centrifuged to 1000

rpm. The cleaned sequencing product (20 µl) was then transferred to a bar-coded 96 well plate and analysed with the Applied Biosystems 3730 DNA Analyzer and SeqScape v2.5 software.

2.9 Immunohistochemistry

2.9.1 Rat Tissue Preparation

Tissues were rinsed in PBS and cut into sections. Each section was fixed in 10% formalin solution at 4°C overnight. After overnight fixing, the formalin solution was removed and replaced with PBS. The fixed tissues were then embedded into paraffin. Using a microtome, 3 µm paraffin kidney sections were cut and baked onto microscope slides at 60°C for 3 hours followed by overnight incubation at 40°C to ensure that the tissue section adhered to the slide.

2.9.2 Deparaffinisation and Rehydration of Sections

Slides were placed in racks then sections were deparaffinised and rehydrated through an alcohol gradient consisting of Histoclear, twice for 3 minutes, Histoclear and 100% ethanol (1:1 ratio) for 3 minutes, 100% ethanol, twice for 3 minutes, 95% ethanol for 3 minutes, 70% ethanol for 3 minutes, 50% ethanol for 3 minutes and a final rinse in running cold tap water.

2.9.3 Primary Antibody

Sections were washed twice for 5 minutes in TBS plus 0.025% Triton X-100. The slides were then transferred onto humidified trays and a wax pen was used to draw around each section. The sections were then blocked in 10% (v/v) normal goat serum in TBS for 2 hours at room temperature. The blocking solution was drained off and sections were incubated with primary antibody or negative control IgG diluted in 1% goat serum in TBS overnight at room temperature.

2.9.4 Secondary Antibody

Sections were washed twice for 5 minutes in TBS plus 0.025% Triton X-100, then incubated for 30 minutes in 0.03% H_2O_2 diluted in methanol to quench endogenous peroxidase activity. The slides were returned to humidified trays and sections were incubated with biotinylated secondary antibody from the Vectastain ABC kit, for 30 minutes at room temperature. Sections were washed with TBS, 3 times for 5 minutes and then ABC complex (pre-incubated for 30 minutes) was added to each section and incubated at room temperature for 30 minutes (according to manufacturer's instructions).

2.9.5 Staining

Sections were washed 3 times for 5 minutes in TBS. Sections were then incubated with DAB chromogen (3, 3'-diamionbenzidine, Vector Lab DAB Substrate Kit) plus nickel solution to produce black staining, for 5 minutes at room temperature in humidified trays. Sections were washed for 5 minutes in distilled water and counter-stained with haematoxylin for 10 seconds followed by 5 minutes in running tap water. The sections were then dehydrated by putting through an alcohol gradient as described before, in reverse. Sections were cover-slip mounted using Histomount (National Diagnostics).

2.10 Haematoxylin and Eosin Staining

Following the removal of paraffin and rehydration of sections as described in section 2.9.2, sections were stained with haematoxylin for 2 minutes. Slides were then washed in running tap water for 5 minutes and then transferred to eosin for 2 minutes. Slides were washed again for 5 minutes in running tap water. Sections were dehydrated through an alcohol gradient and cover-slip mounted using Histomount.

2.11 Statistical Analysis

Analysis of results for multiple groups was performed by one way analysis of variance (ANOVA) and Dunnet's post-hoc test, comparing all results to a designated control group. For comparisons between two groups, 2 sample t-

tests were applied. Statistical analysis was performed using Prism 4.0 Graph Pad Software. Significance was determined as $p<0.05$.

Chapter 3: Development of Molecular Tools for Modulation of *Gstm1* Expression

3.1 Introduction

Glutathione S-transferase mu type 1 (*Gstm1*) has been identified as a positional and functional candidate gene for hypertension in the SHRSP (69). At present there are no selective pharmacological inhibitors of *Gstm1* making further investigation of its function difficult. To overcome this, an approach involving RNA interference (RNAi) has been adopted. RNA interference is an endogenous gene silencing mechanism that can be exploited to experimentally reduce the expression of a particular gene of interest (137). *In vitro* knock-down of gene expression has been successfully achieved through the introduction of chemically synthesised gene specific siRNA (152). To assess siRNA mediated silencing of *Gstm1* expression *in vitro* an appropriate cell line had to be chosen. Previous work carried out by our group found that *Gstm1* expression was localised to the tubular epithelium of the kidney, particularly the collecting ducts (77). For this reason, *in vitro* RNAi experiments have been carried out in the rat cell line NRK-52E, a renal tubular cell line.

3.1.1 Adenoviral Vectors

To utilise RNAi for *in vivo* gene knock-down, adenoviral vectors have been used to drive the expression of short hairpin RNA molecules that mediate gene silencing (173). Recombinant adenovirus serotype 5 (Ad5) vectors have been commonly used for delivery as they are able to infect both dividing and non-dividing cells and have a broad cellular tropism. However, Ad5 vectors have a high hepatic tropism so that when delivered systemically most vectors end up in the liver (174;175). This characteristic means that Ad5 vectors are not practical for site specific delivery via systemic administration.

The adenoviral capsid is composed of three main structural proteins; hexon, fiber and penton base. The fiber is a major determinant of virus tropism and is composed of an N-terminal tail, a central shaft and a C-terminal knob domain (176). The fiber knob domain interacts with the coxsackie virus and adenovirus receptor (CAR) to mediate cell binding and infection. As mentioned previously, Ad5 vectors have a high hepatic tropism but recent studies have shown that following intravascular administration, CAR is not involved in liver transduction.

Following intravascular injection of mutant Ad5 vectors that are unable to bind CAR, liver transduction is the same as unmodified vectors that are able to bind CAR, indicating that another pathway is involved (177). Ad5 vectors have been shown to bind blood coagulation factors and when mutations were introduced into the fiber domain to ablate blood factor binding, reduced liver cell transduction was observed (178). It has since been shown that the Ad5 hexon protein interacts with the vitamin K dependent coagulation factor X (FX) and in doing so mediates liver transduction (179-181).

3.1.1.1 Adenoviral Vector Tropism

High hepatic tropism is problematic for site specific delivery but it has been shown that it is possible to modify tropism by pseudotyping Ad5 vectors with a fiber from another serotype. To aid the re-targeting of Ad5 gene therapy vectors, a helper independent adenovirus vector expressing the ß-galactosidase reporter gene and with E1, E3 and fiber genes deleted (Ad5.ßgal.ΔF) was developed (182). This vector in combination with packaging cell lines that express the fiber gene of choice would allow for easier modification of virus tropism (183). Previous work carried out by our group found that pseudotyping Ad5 with the fiber from serotype Ad19p (Ad5/19p) reduced hepatic tropism (184). The ability of Ad5/19p to infect cultured rat, mouse and human hepatocyte cells was significantly reduced compared to unmodified Ad5 and following systemic administration *in vivo* a similar reduction in liver transduction was observed (184). This Ad5/19p pseudotyped vector was further developed to enable it to target the kidney specifically. *In vivo* phage display was utilised to identify the peptides HTTHREP (HTT) and HITSLLS (HIT) both of which selectively target the kidneys in rats. The Ad19p fiber gene was genetically modified to allow peptide insertion and oligonucleotides encoding HTT and HIT were cloned into modified fiber expressing plasmids. The plasmids were used to generate peptide modified vectors that when systemically delivered to WKY rats were found to localise to kidney tubular epithelium (Ad19p-HTT) and glomeruli (Ad19p-HIT) (185). The use of such targeted vectors provides a powerful tool for site specific knock-down of *Gstm1*. It has previously been shown that Gstm1 expression is localised to the tubular epithelium, specifically in the collecting ducts (77). Therefore Ad19p-HTT would be an appropriate choice of vector for

expression of *Gstm1* shRNA to allow for the role of *Gstm1* to be investigated more fully *in vivo*.

3.1.2 RNA Interference and Immune System Activation

The use of targeted adenoviral vectors for knock-down of gene expression may overcome the transduction issues associated with systemic delivery but there is still the possibility that delivery of dsRNA could activate the innate immune response (186). Double stranded RNA is recognized by cells as a by-product of viral replication and so to counteract this, the interferon (IFN) system is induced and protein synthesis is inhibited. Double stranded RNA longer than 30 bp has been found to stimulate the IFN response (152).

3.1.2.1 Oligoadenylate Synthetase

The 2'-5'-oligoadenylate synthetases (2'-5'OAS) have been characterised as IFN induced enzymes activated by dsRNA molecules longer than 15bp (187). Oligoadenylate synthetase 1 (OAS1) is one of four members of the mammalian 2'-5'OAS family (186). The enzyme is composed of two domains that when assembled form a dsRNA binding site and when bound by dsRNA result in enzyme activation (188). Once activated, 2'-5'OAS uses ATP to form 2'-5' linked oligomers of adenosine (2'-5'oligoadenylates or 2-5A) which in turn bind and activate the endoribonuclease, RNase L. This leads to degradation of both foreign and cellular RNA and a subsequent reduction in protein synthesis (189).

Early studies carried out to investigate *in vitro* silencing of gene expression by dsRNA found that the introduction of long dsRNA (>30 bp) to rabbit reticulocyte lysates caused substantial non-specific mRNA degradation (136). This was likely due to the activation of RNase L by the presence of long dsRNA as previously observed by Williams and colleagues (190). However, it has been proposed that short dsRNAs would not activate 2'-5'OAS and it has been observed that dsRNA between 21 and 27 bp long are poor inducers of 2'-5'OAS *in vitro* (186;191).

3.2 Aims

- To evaluate 3 different siRNA sequences designed to be specific for *Gstm1* for their ability to knock-down *Gstm1* expression *in vitro* and quantify expression at both mRNA and protein level

- To investigate non-specific effects on other members of the *Gstm* family in response to *Gstm1* specific siRNA

- To determine if introduction of *Gstm1* specific siRNA into renal cells leads to induction of an interferon response

- To generate plasmids expressing *Gstm1* specific and control shRNAs and evaluate their function

- To assess targeting of kidney tubules by modified adenoviral vectors

- To assess methods for local delivery of siRNA/shRNA to renal cells *in vivo*

3.3 Methods

3.3.1 Transfection of NRK-52E Cells with siRNA

Short interfering RNA sequences targeted against *Gstm1* were evaluated for their ability to knockdown gene expression in NRK-52E cells. Transfections were carried out as described in section 2.3. Transfected cells were incubated at 37°C for 48 hours and then protein or RNA was extracted for analysis by western blot or quantitative real-time PCR.

3.3.2 Transfection of NRK-52E Cells with Plasmid DNA

Each transfection experiment was performed in triplicate and included an untransfected control (UTF) and a mock transfection control (cells treated with

transfection reagent only) (TFC). In experiments involving transfection of pShuttle-CMV-shRNA vectors, a control vector (SCR) that expresses a scrambled shRNA sequence (based on the negative siRNA control used previously that has no known homology to any expressed genes) was also used.

3.3.2.1 FuGENE® 6 Transfection

FuGENE® 6 (Roche) is a proprietary mix of lipids in 80% ethanol that facilitates the transfer of plasmid DNA across cell membranes. NRK-52E cells were cultured in 6 well tissue culture plates until 70% confluent. Transfection complexes were prepared at a ratio of 6:3 (µl FuGENE® reagent : µg of plasmid DNA). Per well, 6 µl FuGENE® reagent was added directly to 94 µl OptiMEM® Reduced Serum Medium in a 1.5 ml tube, mixed gently and incubated at room temperature for 5 minutes. To the transfection reagent mix, 3 µg of plasmid DNA was added and incubated for 25 minutes at room temperature. The transfection reagent/DNA complex was added drop-wise to each well containing 2 ml normal growth medium. Plates were gently rocked back and forth to disperse the transfection complex and then incubated at 37°C for 48 hours.

3.3.2.2 Lipofectamine™ 2000 Transfection

NRK-52E cells were cultured in 6 well tissue culture plates until 80%-90% confluent. Lipofectamine™ 2000 (Invitrogen) is a proprietary cationic lipid formulation. Transfection complexes were prepared at a ratio of 3:1 (µl Lipofectamine™ 2000 : µg plasmid DNA). Per well, 5 µl Lipofectamine™ 2000 reagent was added to 245 µl OptiMEM® Reduced Serum Medium, mixed gently and incubated for 5 minutes at room temperature. A volume of plasmid DNA (2 µg) was diluted to 250 µl with OptiMEM® Reduced Serum Medium. The diluted DNA was then combined with the diluted Lipofectamine™ 2000 reagent and incubated for 20 minutes at room temperature. The culture medium was removed from each well and cells were washed twice with 2 ml sterile PBS. To each well, 500 µl OptiMEM® Reduced Serum Medium was added followed by 500 µl of the Lipofectamine™ 2000/DNA complex, added drop-wise. Plates were gently rocked back and forth to disperse the transfection complex and incubated

for 5 hours at 37°C. After this time, 2 ml of normal growth medium containing 20% (v/v) FCS was added to each well. Cells were incubated at 37° for a further 48 hours.

3.3.3 ß-galactosidase Expression Staining

NRK-52E cells with transfected with the p-Shuttle-CMV-*LacZ* vector (Stratagene) to assess transfection efficiency. Following transfection, cell culture medium was removed from each well and cells were washed twice with 2 ml sterile PBS. To fix cells, 2 ml 2% paraformaldehyde in 0.1M sodium phosphate (72 mM Na_2HPO_4, 23 mM NaH_2PO_4) was added to each well and cells were kept on ice for 15 minutes. The paraformaldehyde was removed and cells were washed again with PBS. To each well, 2 ml X-Gal (5-bromo-4-chloro-3-indolyl ß-D-galactopyranoside) stain (77mM Na_2HPO_4, 23mM NaH_2PO_4, 1.3mM $MgCl_2$, 3mM $K_4Fe(CN)_6$, 0.05% (v/v) 20 mg/ml X-Gal dissolved in dimethyl formamide) was added and cells were incubated at 37°C overnight. After overnight incubation, cells were examined under a microscope for blue staining.

3.3.4 Gstm1 Western Blot Analysis

Protein samples were prepared and quantified as described in sections 2.4 and 2.4.1. Gel electrophoresis and blotting were carried out on these samples as described in section 2.5.1 Into each lane, 30µg of protein sample prepared in an equal volume of 2x sample reducing buffer was loaded and a low range rainbow marker was used to determine band size. A rat GSTM1 purified protein standard (Yb1) was also loaded as a positive control (Oxford Biomedical). For immuno-detection the membrane was incubated at 4°C overnight with a rabbit anti-rat GSTM1 polyclonal antibody (gift from Prof. John Hayes, University of Dundee) used at a dilution of 1/2000 followed by a goat anti-rabbit IgG secondary antibody conjugated to horseradish peroxidase (Dako) at 1/2000 for one hour at room temperature. Bands were visualised using enhanced chemiluminescence, as described in section 2.5.3.

3.3.5 *Gstm* Family mRNA Expression

RNA was extracted from NRK-52E cells and 1st strand cDNA was generated as described in sections 2.6 and 2.7. Quantitative RT-PCR was performed on cDNA using TaqMan Gene Expression Assays (Applied Biosystems) for *Gstm1* (Assay ID: Rn00755117_m1), *Gstm2* (Rn00598597_m1), *Gstm3* (Rn00579867_m1), *Gstm5* (Rn00597012_m1) and *Gstm7* (Rn00579867_m1) (FAM labelled probes) in duplex with *β-actin* (Assay ID: 4352340E) (VIC labelled probe). Efficiency tests were carried out (section 2.7.1) to ensure that the *β-actin* housekeeper was compatible with each of the *Gstm* probes allowing each reaction to be carried out in duplex.

3.3.6 OAS-1 mRNA Expression

RNA and cDNA from transfected NRK-52E cells was prepared as before. Samples were assayed separately for OAS-1 (Assay ID: Rn00594390_m1) and *β-actin* expression. A 5µl reaction was set up in a 384 well plate consisting of:

- 0.25µl OAS-1 FAM labelled probe or 0.25µl *β-actin* VIC labelled probe
- 0.25µl nuclease free water
- 2µl of template cDNA
- 2.5µl of TaqMan Universal PCR master mix

Each sample was analysed with the ABI PRISM 7900ht Sequence Detection System and results generated as before.

3.3.7 Fiber-modified Adenovirus Vector Production

Vector production was carried out in human embryonic kidney 293T cells that express the adenovirus E1A gene necessary for viral replication.

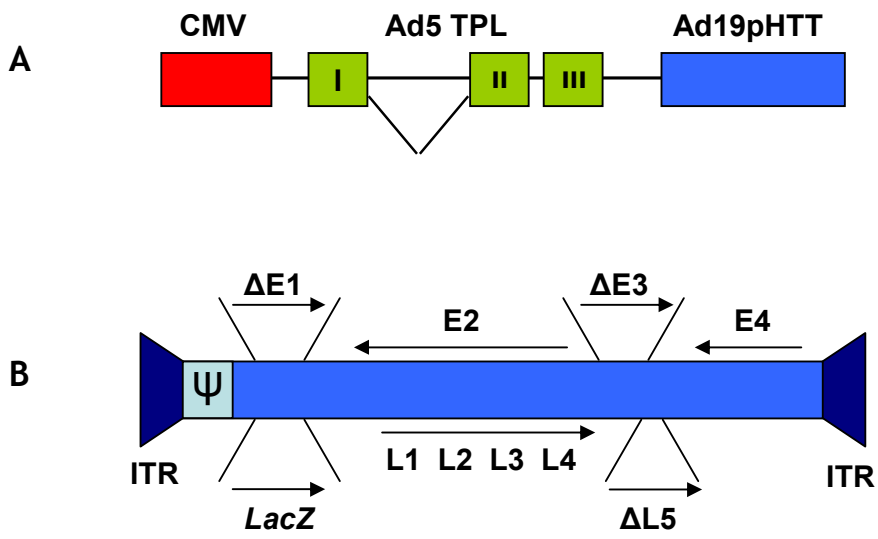

Figure 3.1 Ad19p-HTT plasmid construct and genome structure of the Ad5.ßgal.ΔF vector

A: The plasmid for the expression of the modified Ad19p-HTT fiber protein (185). The plasmid contains the CMV promoter, Ad5 tripartite leader (to improve fiber gene expression) and the modified Ad19p-HTT fiber sequence (for renal selectivity).

B: The genome structure of the Ad5.ßgal.ΔF vector. This vector has E1, E3 and L5 (fiber gene) regions deleted with a ß-galacotsidase reporter gene (*LacZ*) inserted in place of the E1 region (182). Arrows indicate direction of transcription. Adapted from (192)

TPL: tripartite leader, ITR: inverted terminal repeat, ψ: packaging signal, E1-E4: adenoviral early genes, L1-L5: adenoviral late genes

Cells were maintained in Eagle's modified medium (MEM) supplemented with 10% (v/v) FCS, 2mM L-Glutamine, 1mM sodium pyruvate, 100 U/ml penicillin and 0.1 mg/ml streptomycin. To passage cells, citric saline (0.13M KCl, 0.017M sodium citrate in PBS) was used instead of trypsin. Transfections were carried out in 70% confluent 293T cells cultured in 10cm^2 tissue culture plates (Nunc).

293T cells were transfected with HTT modified fiber expressing plasmid (Figure 3.1) using a calcium chloride ($CaCl_2$) differential pH method. Culture medium was removed from each plate and cells were washed twice in sterile PBS. To each plate, 4.5 ml of low glucose (1000 mg/L) DMEM supplemented with 10% (v/v) FCS and 25mM HEPES, pH 7.9 was added. A solution containing 960 µl low glucose DMEM (supplemented with 25mM HEPES pH 7.1), 48 µl $CaCl_2$ and 21 µg plasmid DNA was prepared and added drop-wise to each plate and gently mixed. Cells were incubated at 37°C overnight.

Following overnight incubation, cells were washed in sterile PBS and infected with Ad5.ßgal.ΔF (a fiber gene deleted vector that expresses the reporter gene *LacZ*, see Figure 3.1) at 2000 virus particles per cell. The volume of virus required was calculated and added to the standard 293T culture medium and 15 ml of this mix was added to each plate. After the cytopathic effect was observed (the majority of cells will have detached from the plate) cells were harvested in sterile PBS and centrifuged at 850 g for 10 minutes. The supernatant was discarded and the cell pellet was re-suspended in 6 ml of sterile PBS. Cells were lysed by freeze/thawing four times and cell debris was removed by centrifugation at 850 g for 10 minutes. The adenovirus containing supernatant was stored at -80°C until purification by caesium chloride (CsCl) density gradient centrifugation.

3.3.7.1 Adenovirus Purification

Virus particles were purified by CsCl density gradient centrifugation. Fourteen ml ultra clear centrifuge tubes (Beckman Coulter) were sterilised by rinsing with 70% ethanol followed by sterile water. A CsCl gradient was prepared in the centrifuge tube by adding 2 ml 1.45 g/cm^3 CsCl followed by a layer of 1.32

g/cm^3 CsCl added drop-wise then a layer of 2 ml 40% glycerol. To the top of this gradient, the adenovirus supernatant was added and the rest of the tube was filled with sterile water. The tube was loaded into a Sorvall Discovery 90 rotor container and centrifuged at 90000 g for 1.5 hours with maximum acceleration and free deceleration. Following centrifugation a white band containing virus could be seen. The virus was removed by piercing the centrifuge tube just below the virus layer with a syringe and a 22 gauge needle. The virus was carefully drawn up into the syringe without disturbing any of the other layers.

A 10000 molecular weight cut-off Slide-A-Lyzer dialysis cassette (Pierce) was prepared by soaking in 0.01M Tris pH 8, 0.001M EDTA (TE buffer) for 30 minutes. Extracted virus was then transferred to the cassette and any excess air was removed. The virus was dialysed against 2 L 0.01M TE buffer pH 8 for 2 hours then the TE buffer was replaced and dialysis was continued overnight. The next day, the TE buffer was changed and supplemented with 10% (v/v) glycerol and dialysis was continued for a further 2 hours. After this time, the virus was carefully removed from the cassette and stored in 50 µl aliquots at -80°C.

3.3.7.2 Calculating Virus Particle Titres

Virus particle titres were calculated using a Micro-BCA assay kit (Pierce). Eight BSA standards (from 0.5 µg/ml to 200 µg/ml) and PBS blanks were prepared and 150 µl of each was added, in duplicate, to a 96 well plate. Three volumes of virus preparation (1 µl, 3 µl and 5 µl) were diluted to 150 µl with PBS and assayed in duplicate. The BCA working reagent was prepared by mixing 25 parts Solution A, 24 parts Solution B and 1 part Solution C and 150 µl of the working reagent was added to each well. The plate was covered to protect it from the light and incubated at 37°C for 2 hours. The absorbance at 570nm was measured for each standard and sample and duplicate readings were averaged and the blank measurements were subtracted. A standard curve was generated and used to calculate the protein concentration in each virus sample. The virus particle titre was then calculated using the formula: 1 µg protein = 1×10^9 virus particles.

3.3.8 Animal Models

Inbred colonies of SHRSP and WKY rat strains have been maintained by our group since 1991. Animals were housed in a temperature and humidity controlled environment with 12 hour light/dark cycles. Rats were fed standard rat chow and water provided *ad libitum*. All experimental animal procedures were performed in accordance with the UK Home Office Animals (Scientific Procedures) Act 1986 under the project licence number 60/3618.

3.3.9 Local Delivery to a Single Kidney

WKY rats were anaesthetised by inhalation of isofluorane. A laparotomy was performed and the intestines were exteriorised and wrapped carefully in moistened swabs. The left kidney and renal artery/vein were exposed by blunt dissection. Ties were placed on the renal artery and vein to control blood flow to and from the kidney. The artery was clamped briefly during administration (injection into artery) of Ad5/19p virus ($1x10^{11}$ virus particles). A maximum volume of 500 µl was infused over a maximum of 20 seconds. The blood flow was re-established and haemorrhage from the injection site was prevented by cauterisation. The intestines were returned to the abdominal cavity and the laparotomy incision was closed. Kidneys were removed and used for histological analysis.

3.3.10 *In Vivo* Virus Administration

To investigate targeting of Ad19pHTT 8-week old male SHRSP rats were infused with $3.5x10^{11}$ virus particles per rat, via the femoral vein. After 5 days rats were sacrificed and organs removed. Expression of *LacZ* in the kidney was determined by IHC as described in section 2.9.

3.4 Results

3.4.1 Transfection Efficiency of NRK-52E Cells

In order to carry out *in vitro* RNAi experiments in NRK-52E cells, it was important to evaluate the transfection efficiency of these cells. To do this, NRK-52E cells were transfected with a Cy3 labelled scrambled siRNA control. This siRNA has no known homology to any expressed genes and as such should not generate a silencing effect. Figure 3.2 shows a representative transfection experiment. Panel C demonstrates that there was no background fluorescence generated when cells were subjected to a mock transfection (treated with transfection reagent only). However when cells were transfected with 100nM Cy3 labelled siRNA, fluorescence was detectable throughout indicating successful transfection of these cells (panel B). This control transfection was carried out in all subsequent *Gstm1* RNAi experiments and in each experiment, greater than 70% transfection efficiency was achieved.

3.4.2 Glutathione S-Transferase Mu Type 1 mRNA Expression

TaqMan quantitative real-time PCR was carried out to investigate silencing of *Gstm1* mRNA expression following transfection of NRK-52E cells with 100nM siRNA. The ability of each siRNA to knock-down *Gstm1* is shown in Figure 3.3. Figure 3.3 is representative of 8 individual experiments carried out in triplicate. All 3 siRNA sequences resulted in significantly reduced *Gstm1* mRNA expression. At 100nM, siRNA A produced knock-down of between 65 and 79%, siRNA B between 78 and 93% and siRNA C achieved between 63 and 69% knock-down when compared to the scrambled siRNA control. In each experiment, siRNA B appeared to be the most effective as knock-down from this sequence was consistently higher as illustrated in Figure 3.3 (85% knock-down, $p<0.01$ v siCTL compared to 79% and 68% knock-down with siRNA A and C respectively, $p<0.01$ v siCTL).

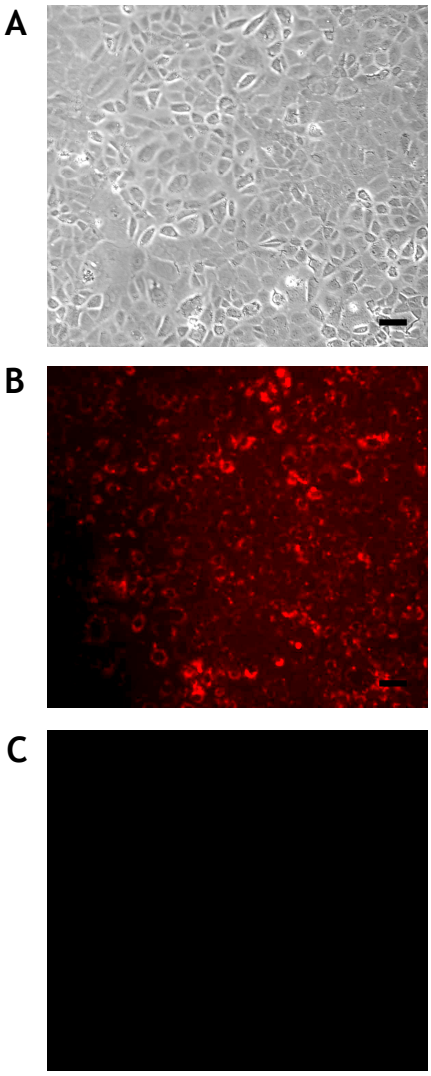

Figure 3.2 Transfection efficiency of NRK-52E cells with 100nM siRNA

A: Transmitted light image of NRK-52E cells. B: Cells transfected with 100nM Cy3 labelled siRNA. Comparison with transmitted light image of the same field (A) suggests high transfection efficiency. C: Mock transfected cells showing no background fluorescence. Scale bar: 50μm

3.4.2.1 Glutathione S-Transferase Mu Family mRNA Expression

The mu family of glutathione transferases is highly homologous and as such, a sequence designed to target *Gstm1* may inadvertently have a non-specific effect on other *Gstm* isoforms. To check the specificity of each siRNA sequence, NRK-52E cells were transfected as before and RNA extracted for TaqMan analysis of *Gstm2, 3, 5* and *7*. The mRNA expression levels of each isoform following knock-down of *Gstm1* are shown in Figure 3.4. Figure 3.4 is representative of 6 individual experiments carried out in triplicate. Both siRNA A and C were found to be specific for *Gstm1* as no significant effect on the mRNA levels of other isoforms was detected. Table 3.1 shows the range of knock-down of each isoform in response to each siRNA at 100nM. However, siRNA B was found to be less specific, resulting in reduced expression of all four isoforms as shown in Figure 3.4. Expression of *Gstm2, 3, 5* and *7* was reduced by 63, 93, 31 and 49% in this example (*Gstm2, 3* and 7, $p<0.01$ and *Gstm5*, $p<0.05$ when compared to siRNA control).

To investigate if the non-specific effect of siRNA B on the other *Gstm* family members was possibly due to transfection of an excess of siRNA into cells, transfections were repeated using a reduced concentration of siRNA. Following transfection of NRK-52E cells with 30nM siRNA, RNA and protein were extracted for TaqMan and western analysis respectively. Firstly *Gstm1* expression levels were evaluated to ensure that by reducing the concentration of siRNA, the silencing potency was not diminished. Figure 3.5 is representative of 4 individual experiments carried out in triplicate and shows that each siRNA, at 30nM, was still capable of significantly reducing *Gstm1* expression. In the example shown in Figure 3.5, *Gstm1* expression was reduced by 71% by siRNA A, 61% by siRNA B and 66% by siRNA C when compared to control siRNA, $p<0.05$. Across the 4 experiments, levels of knock-down varied between 56 and 71% (siRNA A), 61 and 76% (siRNA B) and 46 and 66% (siRNA C). As before with siRNA used at 100nM, siRNAs A and C did not significantly knock-down expression of *Gstm2, 3, 5* and *7* and by reducing the concentration to 30nM, siRNA B no longer had a non-specific effect on any other *Gstm* isoform (Figure 3.6).

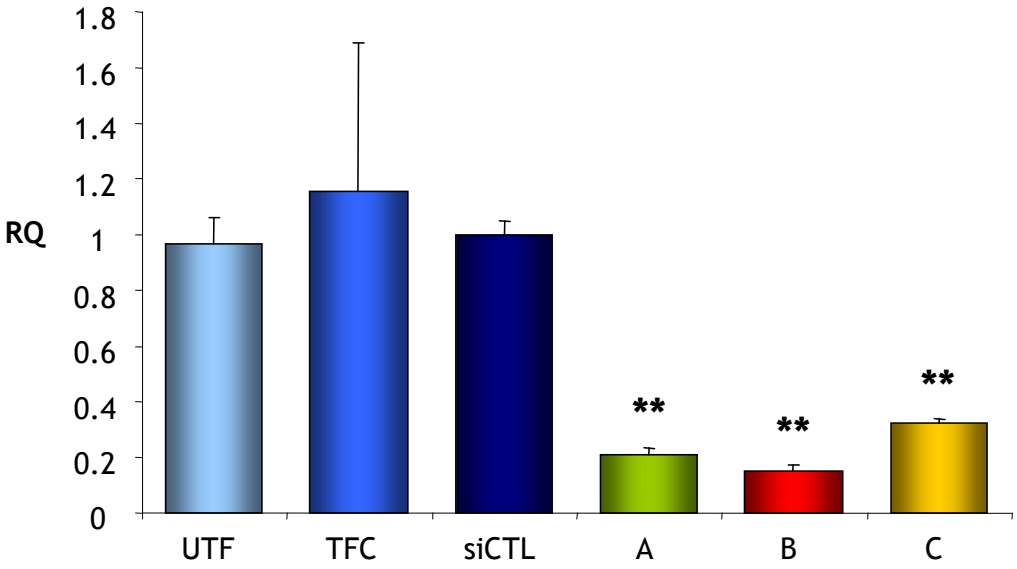

Figure 3.3 *Gstm1* mRNA expression following *Gstm1* RNA interference in NRK-52E cells

NRK-52E cells were transfected with 100nM control (siCTL) or *Gstm1* specific siRNA (A, B or C). TaqMan qRT-PCR was performed to assess *Gstm1* expression. In this example, 79% knock-down was achieved by siRNA A, sequence B achieved 85% and sequence C achieved 68% compared to siCTL (n=1 experiment performed in triplicate and is representative of 8 experiments in total) ** $p<0.01$ vs siCTL (ANOVA + Dunnett's post-hoc test).

UTF: untransfected cells, TFC: mock transfection, siCTL: siRNA control transfected cells

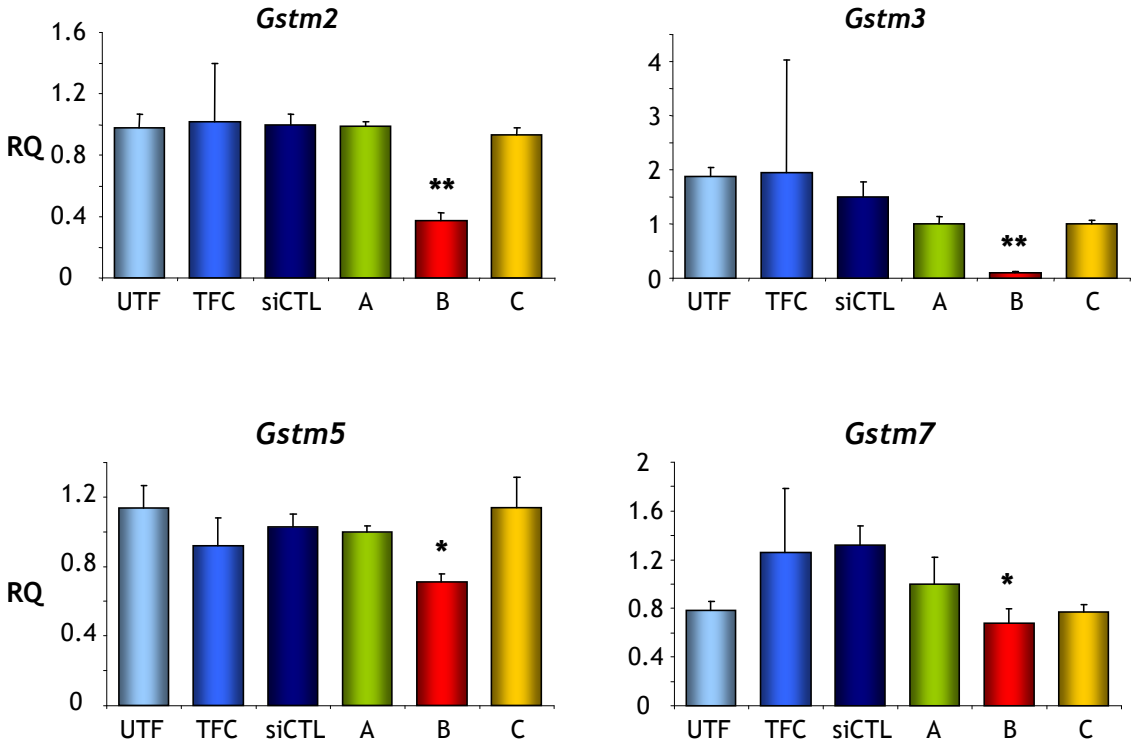

Figure 3.4 *Gstm* family mRNA expression following *Gstm1* RNA interference in NRK-52E cells

NRK-52E cells were transfected with 100nM control (siCTL) or *Gstm1* specific siRNA (A, B or C). TaqMan qRT-PCR was performed to assess expression levels of *Gstm2, 3, 5* & 7. No significant knock-down of any *Gstm* isoforms was observed with siRNA A and C. However, siRNA B significantly reduced each of the 4 isoforms. In this example, *Gstm2* and *Gstm3* were reduced by 63% and 93% respectively compared to siCTL (n=1 experiment performed in triplicate and is representative of 6 experiments in total), ** $p<0.01$ vs siCTL (ANOVA + Dunnett's post-hoc test). *Gstm5* and *Gstm7* were reduced by 31% and 49% respectively compared to siCTL (n=1 experiment performed in triplicate and is representative of 6 experiments in total) *$p<0.05$ vs siCTL (ANOVA + Dunnett's post-hoc test).
UTF: untransfected cells, TFC: mock transfection, siCTL: siRNA control transfected cells

Gene	RANGE OF KNOCK-DOWN (%)		
	siRNA A	siRNA B	siRNA C
Gstm2	1 to 30	48 to 87	7 to 42
Gstm3	7 to 33	77 to 93	2 to 49
Gstm5	3 to 36	31 to 56	7 to 43
Gstm7	24	21 to 55	21 to 42

Table 3.1 Percentage knock-down of expression of Gstm isoforms in response to each siRNA at 100nM

3.4.3 Glutathione S-Transferase Mu Type 1 Western Blot Analysis

The sensitivity of the anti-rat GSTM1 antibody was initially evaluated against a range of NRK-52E protein dilutions. It was important that the antibody could detect different levels of GSTM1 protein in order to determine if effective knock-down of GSTM1 had taken place. Figure 3.7 indicates that the antibody was sensitive to a range of concentrations of GSTM1 (Panel A). Due to the homologous nature of GSTM1 and other members of the GSTM family, detecting GSTM1 selectively can be problematic. To ensure GSTM1 specificity, the antibody was evaluated against GSTM1 (M1) and GSTM2 (M2) protein standards. The antibody was found to be specific to GSTM1 and did not detect GSTM2 (Panel A in Figure 3.7).

To determine whether transfection with any of the three siRNA sequences resulted in efficient knock-down of GSTM1, western blot analysis was performed. A representative blot following transfection of NRK-52E cells with 100nM siRNA is shown in Figure 3.7 (Panel B). Each band (~26kD) corresponds with the purified GSTM1 protein standard. Each siRNA sequence caused a reduction in GSTM1 protein (bands A, B and C) when compared with the scrambled siRNA control (siCTL). This was confirmed by normalising each band to the housekeeper ß-actin by densitometry. A representative ß-actin blot and the corresponding densitometry results are shown in Figure 3.7 (Panels B and C). The densitometry results show a 93% reduction in GSTM1 protein by siRNA A and knock-down of 87 and 88% with siRNA B and C respectively. Western blot analysis and densitometry was also performed to assess the ability of each siRNA to knock-down GSTM1 protein levels when used at 30nM, as shown in Figure 3.8. As before, GSTM1 protein was lower in siRNA treated samples. At 30nM siRNA, protein expression was reduced by 60% with siRNA A and by 59 and 77% with siRNA B and C respectively.

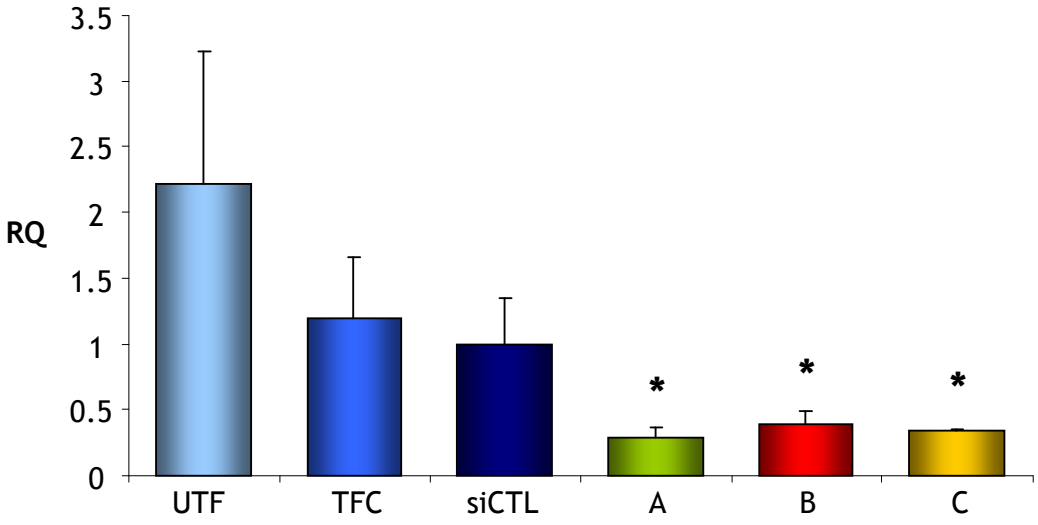

Figure 3.5 Knock-down of Gstm1 expression is preserved with reduced concentrations of siRNA

NRK-52E cells were transfected with 30nM control (siCTL) or *Gstm1* specific siRNA (A, B or C). TaqMan qRT-PCR was performed to assess *Gstm1* expression. In this example, 71% knock-down was achieved by siRNA A, sequence B achieved 61% and sequence C achieved 66% compared to siCTL (n=1 experiment performed in triplicate and is representative of 4 experiments in total) * $p<0.05$ vs siCTL (ANOVA + Dunnett's post-hoc test)

UTF: untransfected cells, TFC: mock transfection, siCTL: siRNA control transfected cells

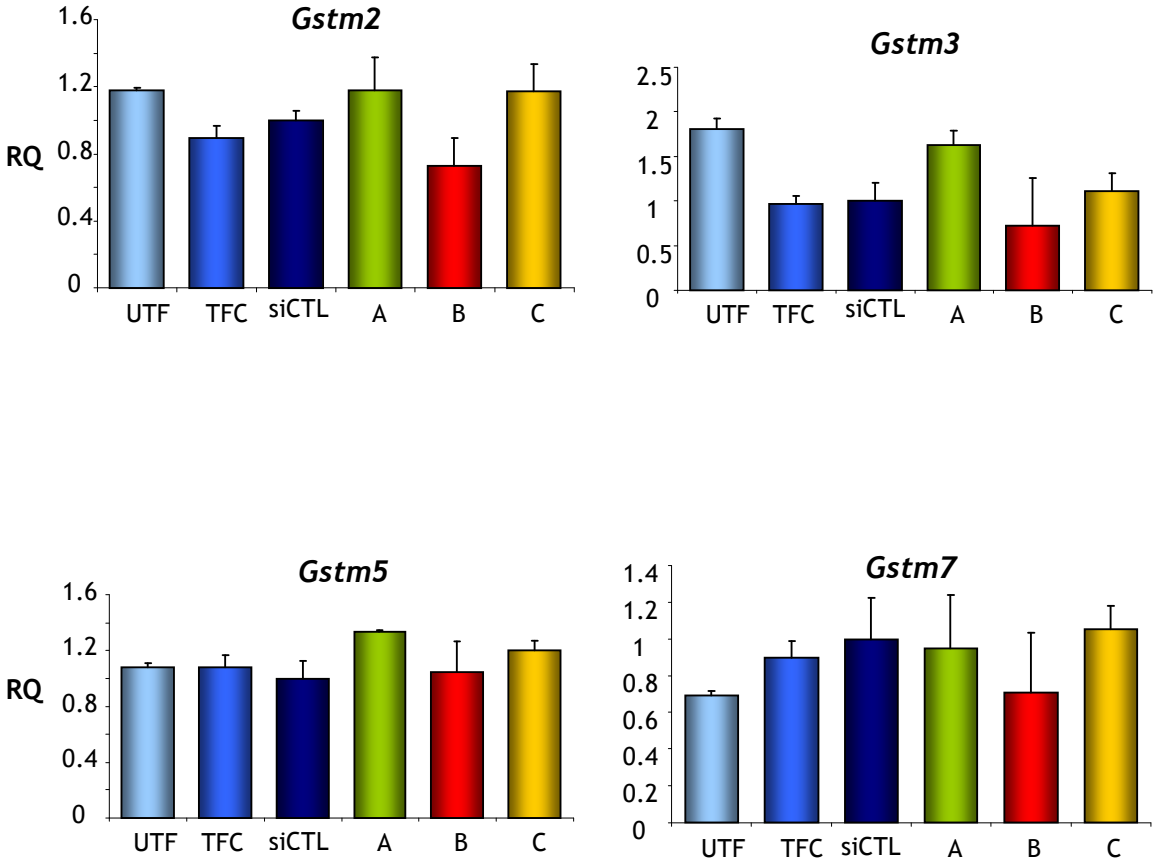

Figure 3.6 *Gstm* family mRNA expression is unaffected by reduced concentrations of *Gstm1* siRNA

NRK-52E cells were transfected with 30nM control (siCTL) or *Gstm1* specific siRNA (A, B or C). TaqMan qRT-PCR was performed to assess expression of *Gstm2, 3, 5* & 7. No significant reduction of mRNA expression was observed for any of the other *Gstm* isoforms following transfection with 30nM siRNA (n=1 experiment performed in triplicate and is representative of 4 experiments in total).

UTF: untransfected cells, TFC: mock transfection, siCTL: siRNA control transfected cells

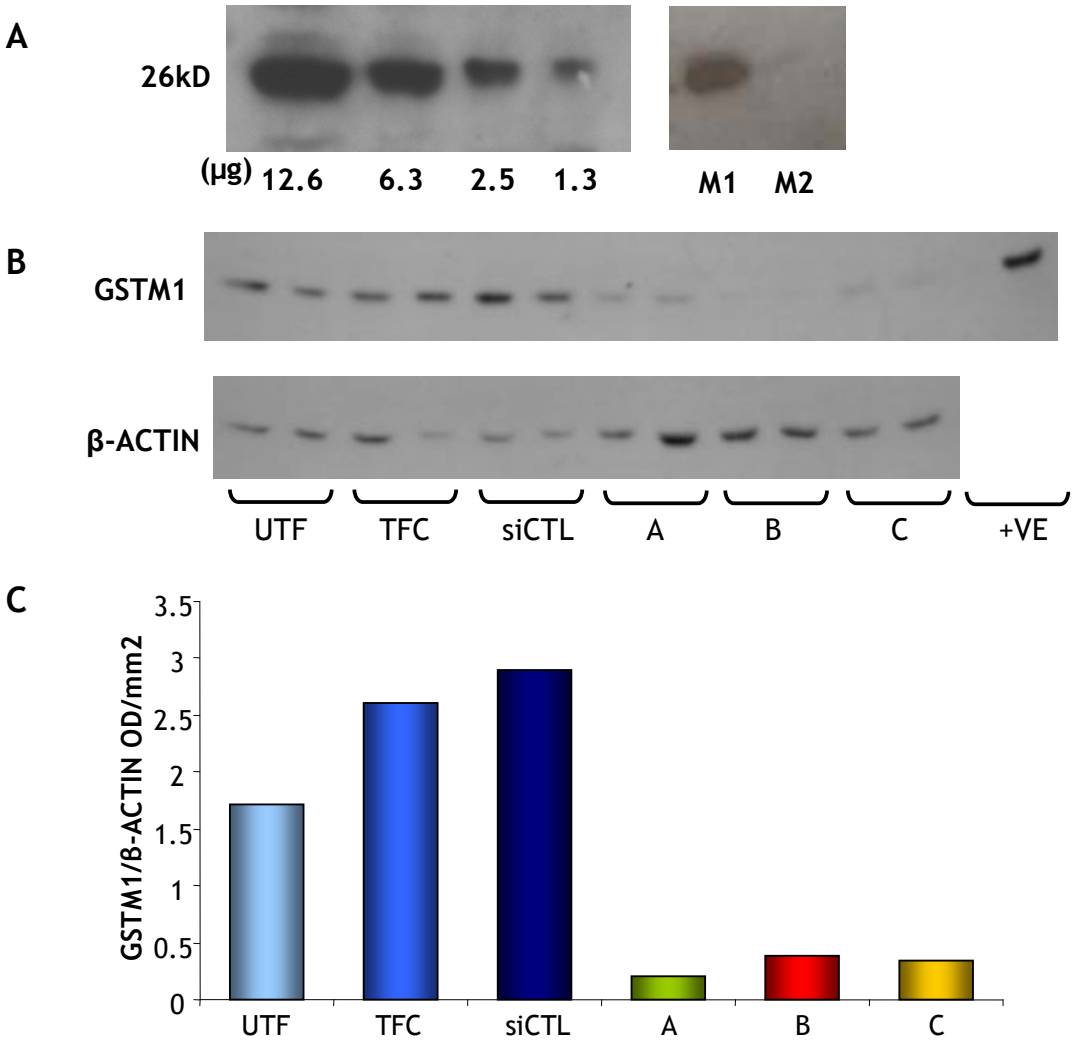

Figure 3.7 Western blot analysis of GSTM1 protein expression

A: Total protein was extracted from NRK-52E cells and resolved by gel electrophoresis. Western blotting confirmed the anti-rat GSTM1 antibody was sensitive to a range of GSTM1 concentrations. Anti-rat GSTM1 was tested against GSTM1 (M1) and GSTM2 (M2) protein standards and was found to be specific for GSTM1. B: NRK-52E cells were transfected with 100nM control (siCTL) or *Gstm1* specific siRNA (A, B or C). Western blotting indicated GSTM1 protein levels were lower in cells transfected with *Gstm1* specific siRNA compared to siCTL. C: Reduced GSTM1 was confirmed by densitometry with each band normalised to ß-actin (n=1 experiment performed in duplicate and is representative of 8 experiments in total).

UTF: untransfected cells, TFC: mock transfection, siCTL: siRNA control transfected cells

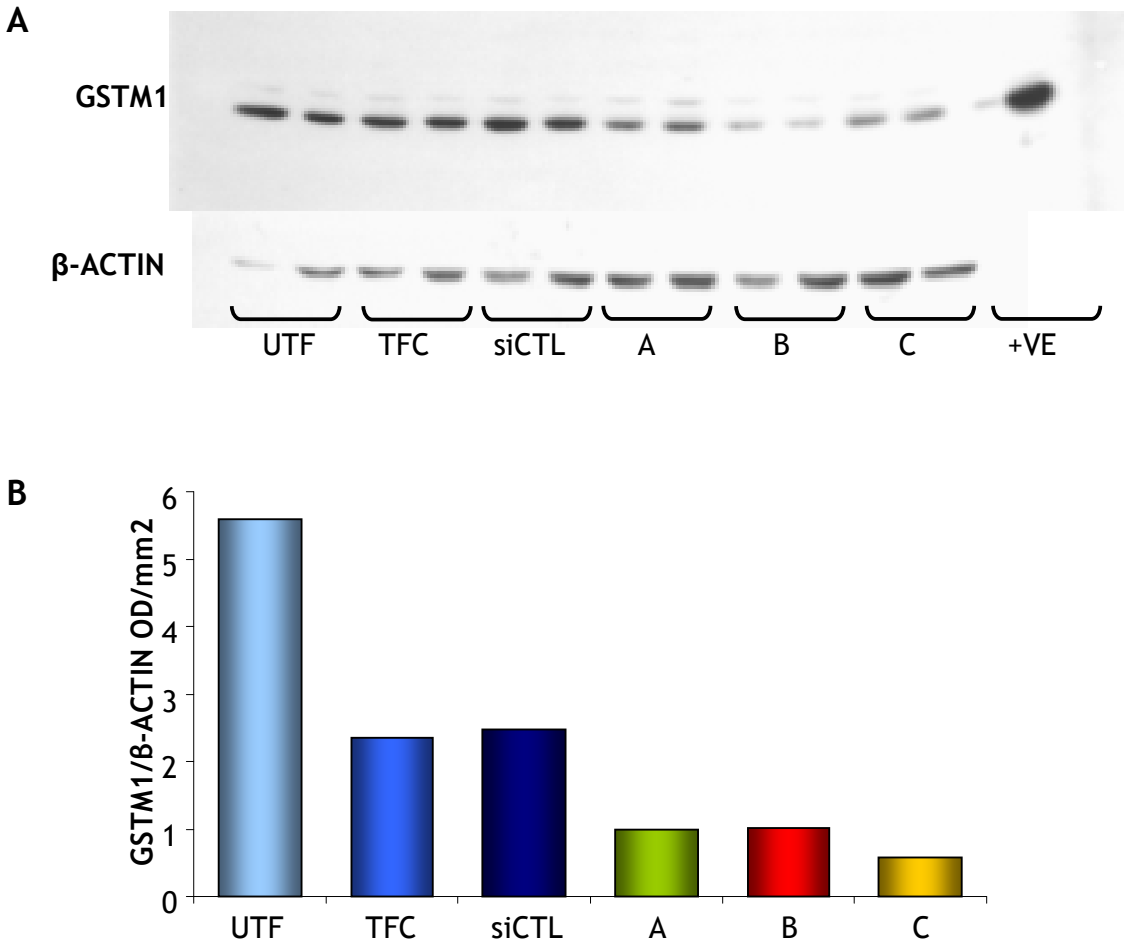

Figure 3.8 Western blot analysis of GSTM1 protein expression (30nM siRNA)

A: NRK-52E cells were transfected with 30nM control (siCTL) or *Gstm1* specific siRNA (A, B or C). Total protein was extracted and resolved by gel electrophoresis. Western blotting was performed and bands indicated GSTM1 protein levels were lower in cells transfected with *Gstm1* specific siRNA compared to siRNA control. B: Reduced GSTM1 was confirmed by densitometry with each band normalised to ß-actin (n=1 experiment performed in duplicate and is representative of 3 experiments in total).

UTF: untransfected cells, TFC: mock transfection, siCTL: siRNA control transfected cells

3.4.4 Interferon Response

As well as the potential for non-specific silencing of other genes by siRNAs, it was also possible that introduction of siRNA to cells may induce off target effects through induction of an interferon response. To investigate the likelihood of each *Gstm1* specific siRNA to induce an interferon response in NRK-52E cells, the expression level of oligoadenylate synthetase-1 was quantified. Following transfection with 100nM siRNA, OAS-1 expression was significantly increased with the greatest increase observed in response to siRNA sequences A and B, as shown in the top panel of Figure 3.9. In this example, siRNA A induced OAS-1 expression 245.8 fold when compared to siCTL and siRNA resulted in 489.5 fold induction of OAS-1, $p<0.01$. The induction of OAS-1 by siRNA C was much less, with only a 4.6 fold increase. Expression of OAS-1 varied between experiments; siRNA A caused a 17.5 to 245.8 fold increase, siRNA B caused a 330.5 to 628.3 fold increase and siRNA C caused a 4.2 to 14.3 fold increase in OAS-1 expression. This effect was diminished by reducing siRNA concentration to 30nM, as shown in the bottom panel of Figure 3.9. When reduced to 30nM, no significant induction of OAS-1 expression was observed.

3.4.5 Assessment of Local Delivery to Kidney

Local delivery to the kidney was assessed by injecting modified Ad5/19p into the renal artery. Haematoxylin and eosin staining was performed on kidney sections to assess what effect direct administration through the renal artery had on kidney structure. Figure 3.10 shows sections from infused and contralateral kidney. Extensive damage was observed in kidney infused with virus. In the contralateral kidney, the tubules can be observed as discrete structures but in the infused kidney, these defined structures are lost indicating tubular necrosis.

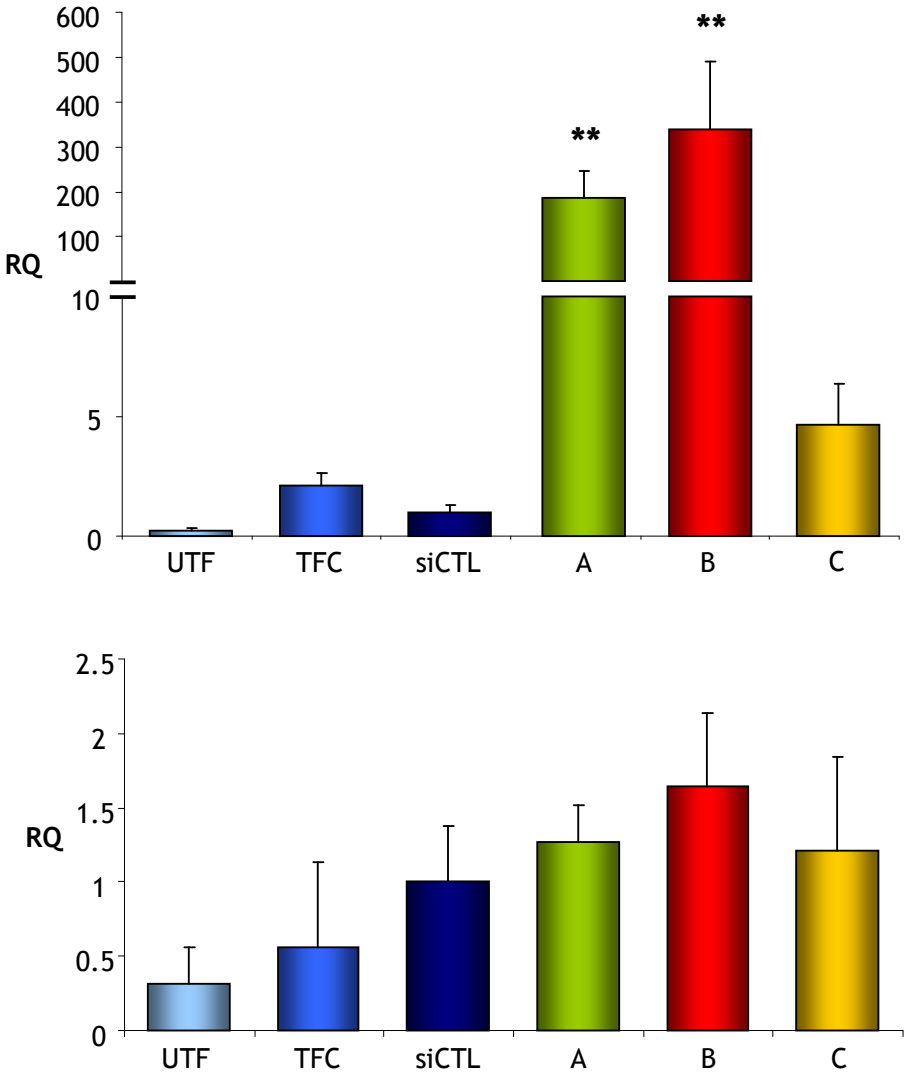

Figure 3.9 Oligoadenylate synthetase expression levels

Top panel: NRK-52E cells were transfected with 100nM control (siCTL) or *Gstm1* specific siRNA (A, B or C). TaqMan qRT-PCR was performed to assess expression levels of oligoadenylate synthetase (OAS-1). A large, significant increase in oligoadenylate synthetase expression was observed in response to siRNA A and B (n=1 experiment performed in triplicate and is representative of 6 experiments in total) **p<0.01 vs siCTL. Bottom panel: NRK-52E cells were transfected with 30nM control (siCTL) or *Gstm1* specific siRNA (A, B or C). Induction of OAS-1 expression was diminished by reducing siRNA concentration to 30nM (n=1 experiment performed in triplicate and is representative of 4 experiments in total). UTF: untransfected cells, TFC: mock transfection, siCTL: siRNA control transfected cells

3.4.6 Ad19pHTT Targeting in SHRSP Kidney

The adenoviral vector Ad19pHTT has been shown to target the kidney tubular epithelium of WKY rats following peripheral intravenous injection. To be able to use this vector for *in vivo* modulation of *Gstm1* expression in the congenic 2c* (entirely SHRSP apart from region of chromosome 2 which is from WKY) targeting in SHRSP had to be determined. Figure 3.11 shows representative images of the staining observed in sections of the same kidney region treated with either negative control IgG antibody (right panel) or ß-galactosidase antibody (left panel). ß-galactosidase staining was observed specifically in tubules, as had been shown previously in WKY with little or no staining in control sections.

3.4.7 Evaluation of shRNA Expressing Plasmids

Gstm1 targeting shRNA expression vectors were generated by cloning oligonucleotides encoding shRNA into the multiple cloning site (MCS) of the pShuttle-CMV vector backbone. The shRNA sequences used were based on the *Gstm1* siRNA and scrambled siRNA control sequences tested previously. An outline of the pShuttle-CMV vector map and shRNA sequences are shown in Figure 2.1. The plasmid region encompassing the MCS was amplified and subjected to gel electrophoresis to check if the shRNA insert was present. Plasmid vector containing insert generated a band of ~200 bp and vector without insert generated a band of ~150 bp. Samples that generated a band at 200 bp were then sequenced to check that the orientation and sequence of the shRNA insert was correct. An example gel and sequencing results are shown in Figure 3.12.

To assess the transfection efficiency of NRK-52E cells for transfection of plasmid DNA, cells were transfected with a pShuttle-CMV vector that expresses the ß-galactosidase reporter gene, *LacZ* (pShuttle-CMV-*LacZ*).

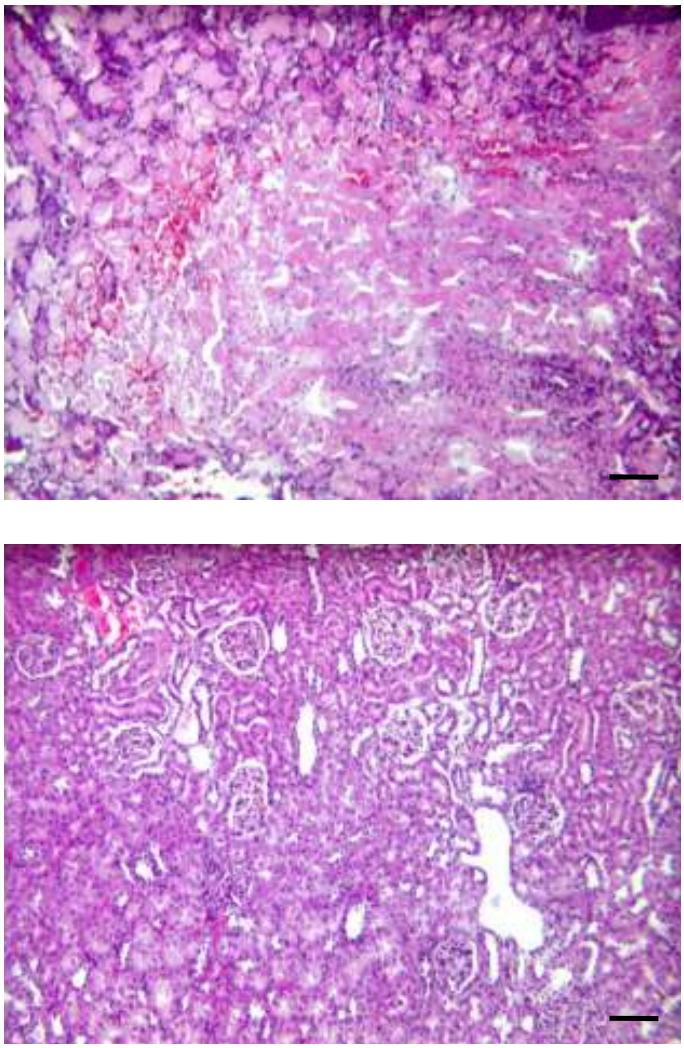

Figure 3.10 Haematoxylin and eosin staining of WKY kidney sections

Top panel: Ad5/19p virus (1 x 10^{11} virus particles) was administered directly to male WKY rat kidney via the renal artery. Renal artery infusion leads to significant kidney damage. Bottom panel: Undamaged contralateral kidney with normal appearance. Scale bar = 100μm.

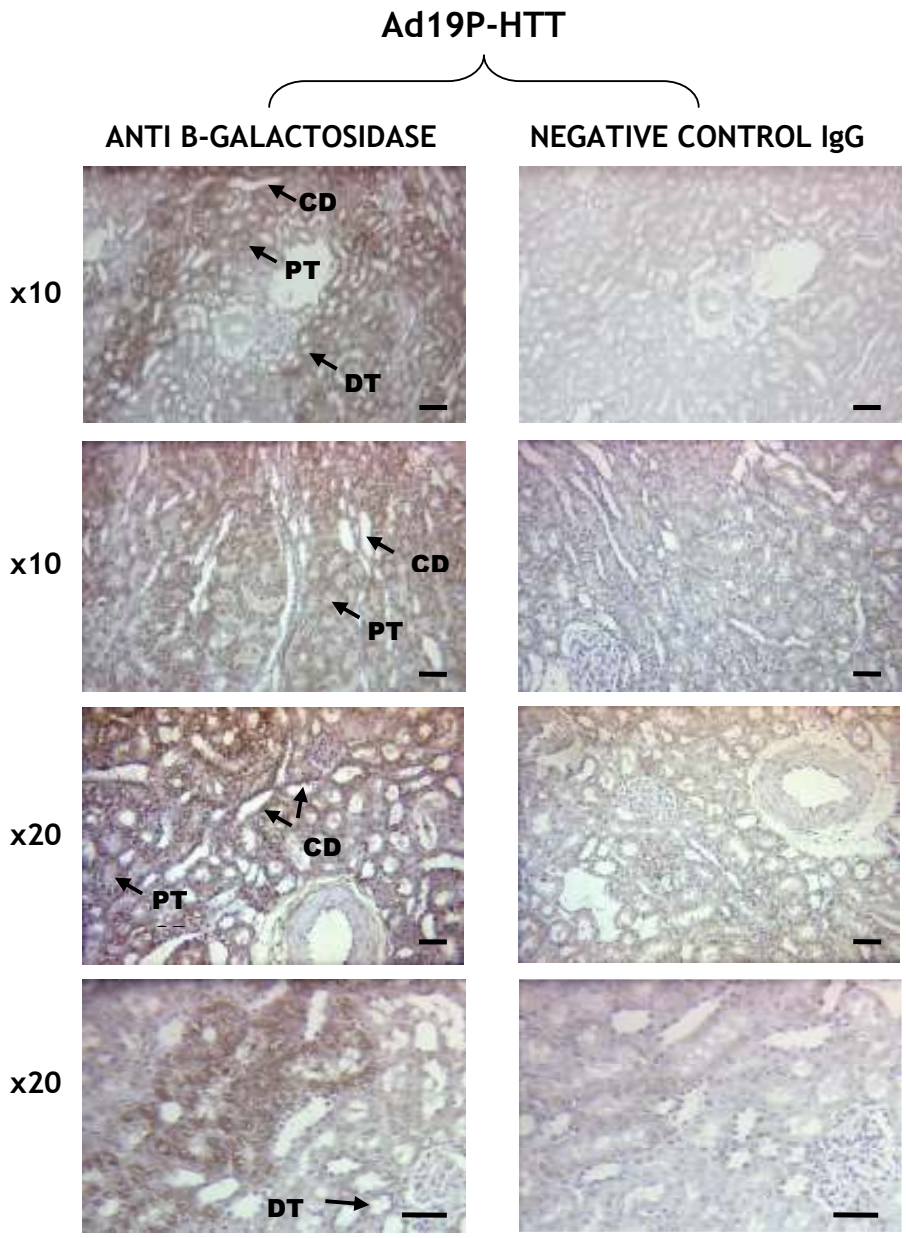

Figure 3.11 Analysis of kidney targeting in SHRSP

Eight week old male SHRSP were infused with Ad19pHTT ($3.5x10^{11}$ virus particles per rat) via the femoral vein. Immunohistochemistry performed on kidney sections confirmed ß-galactosidase expression (grey-black staining) in the tubules with no non-specific staining in the control sections treated with a negative control IgG antibody. Sections were counter-stained with haematoxylin to stain nuclei blue. Representative sections are shown (n=3). Scale bar = 100 µm (x10 magnification). Scale bar = 50 µm (x20 magnification).

CD: collecting ducts, PT: proximal tubules, DT: distal tubules

Plasmid DNA transfection of NRK-52E cells was optimised using two different transfection reagents and by altering the ratio of DNA to transfection reagent used. Using 2 µg of plasmid DNA was found to be most effective in combination with 5 µl of transfection reagent (Lipofectamine™ 2000). However, transfection of NRK-52E cells with plasmid DNA was very low as shown by the low level of blue stained cells (Figure 3.12). Approximately 5-10% transfection efficiency was achieved.

The ability of the pShuttle-CMV-shRNA plasmids to knock-down *Gstm1* expression *in vitro* was assessed by transfecting the plasmids into NRK-52E cells. TaqMan RT-PCR was carried out to assess changes in expression. The top panel in Figure 3.13 indicates that *Gstm1* mRNA expression is reduced in cells transfected with a plasmid expressing *Gstm1* shRNA. When compared to cells transfected with a scrambled control shRNA (SCR), *Gstm1* expression was 58% lower, $p<0.05$. However this result was not reproducible, of 8 experiments only 1 demonstrated successful knock-down of *Gstm1*. The remaining 7 experiments did not show any significant knock-down as demonstrated in the bottom panel of Figure 3.13.

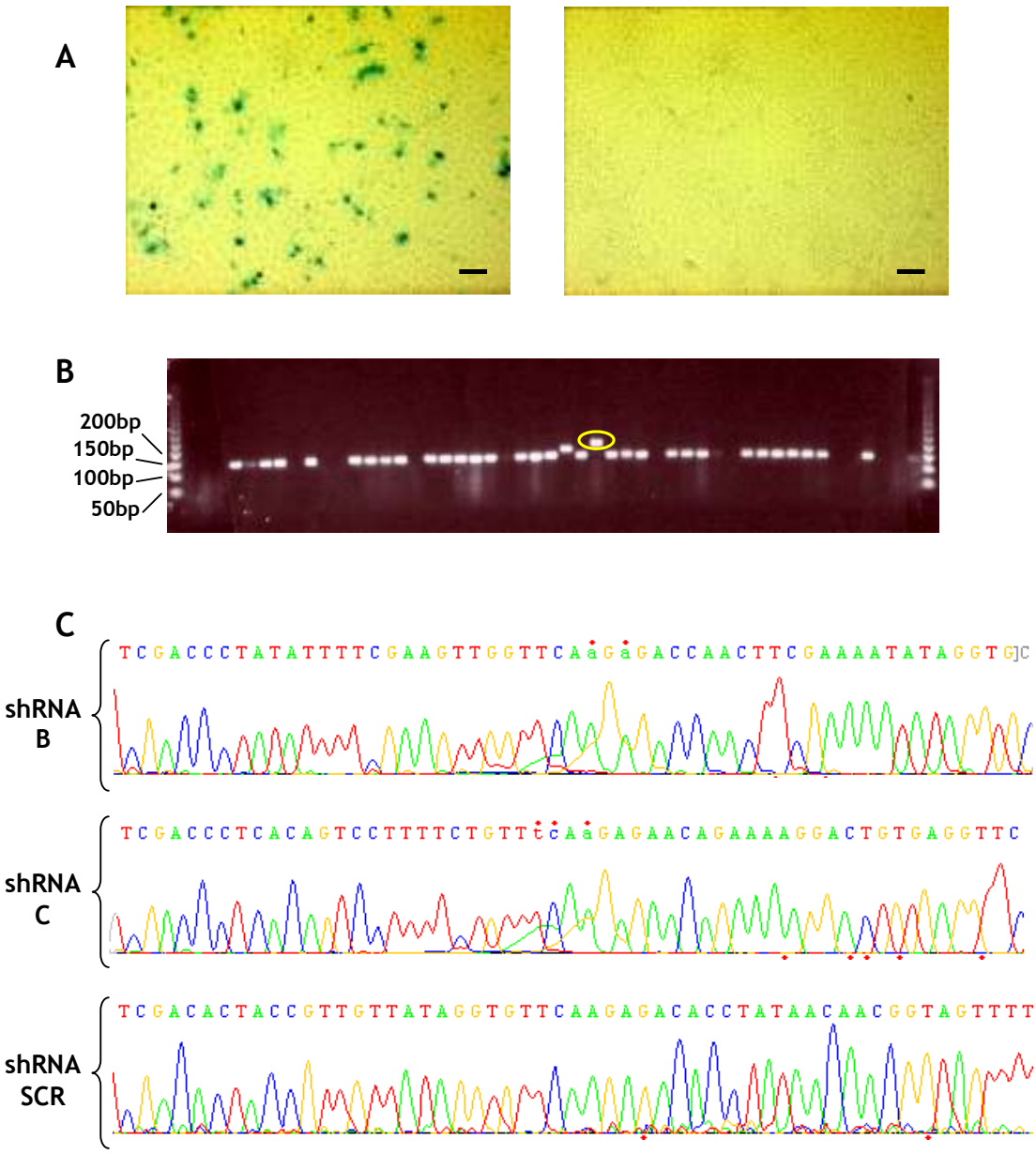

Figure 3.12 Transfection efficiency of NRK-52E cells and shRNA vector sequencing analysis

A: NRK-52E cells were transfected with pShuttle-CMV at Lipofectamine:DNA ratio of 5:2 (µl:µg). ß-galactosidase staining demonstrated 5-10% transfection efficiency. Scale bar = 100µm. B: PCR gel of amplified vector to check for insert. Samples that generated a band at ~200bp were selected for sequencing (circled in yellow). C: DNA sequencing electropherogram showing correct insertion of each shRNA sequence.

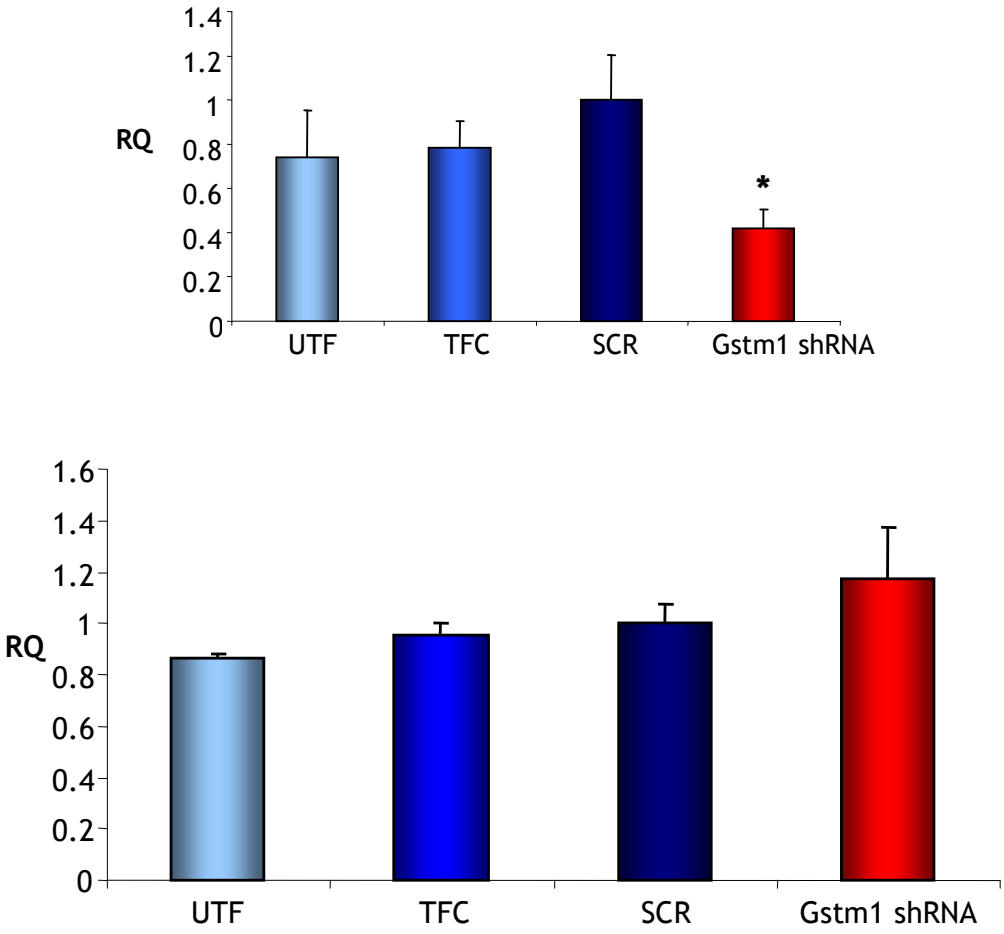

Figure 3.13 *Gstm1* mRNA expression levels in cells transfected with *Gstm1* shRNA expressing vector

TaqMan qRT-PCR analysis of *Gstm1* mRNA expression following transfection of NRK-52E cells with *Gstm1* shRNA expressing pShuttle-CMV. Top panel: *Gstm1* mRNA expression was reduced by 58% in cells transfected with *Gstm1* shRNA compared to scrambled shRNA control (SCR) (n=1 experiment performed in triplicate) *$p<0.05$ vs SCR (ANOVA + Dunnett's post-hoc test). Bottom panel: no change in *Gstm1* expression was observed in shRNA treated cells (n=1 experiment performed in triplicate and is representative of 7 experiments in total).

UTF: untransfected, TFC: mock transfection, SCR: control vector transfection

3.5 Discussion

The *in vitro* experiments described so far indicate that NRK-52E cells are amenable to transfection with siRNA allowing for accurate measurement of reduced gene expression. Using available RNA interference technology, three siRNA sequences have been identified that can successfully and reproducibly knock-down *Gstm1* expression *in vitro*. The level of knock-down achievable can be quantified at both protein and mRNA expression level by western blot and quantitative real-time PCR analysis respectively. Although significant silencing could be achieved with each siRNA, sequence B was consistently more effective at reducing *Gstm1* mRNA expression than either siRNA A or C. As well as measuring *Gstm1* expression, levels of *Gstm2, 3, 5* and *7* were also quantified to ensure that no non-specific silencing occurred. The genes that encode the *Gstm* family are all highly homologous and because of this, a sequence targeted against *Gstm1* may result in non-specific knock-down of other members of the family, especially at high siRNA concentrations. *Gstm1* shares 84% homology with *Gstm2,* 85% with *Gstm3,* 71% with *Gstm5* and 82% homology with *Gstm7*. At 100nM siRNA, all isoforms were affected by siRNA B but not siRNA A or siRNA C. To minimise this effect, the concentration of siRNA was reduced to 30nM. Lowering the concentration of siRNA used from 100nM to 30nM still resulted in significant reduction of *Gstm1* expression but the level of knock-down achievable from each siRNA was slightly reduced. At 30nM, the non-specific effect on other *Gstm* isoforms was lost. This demonstrates that by reducing siRNA concentration the selectivity of the siRNA for *Gstm1* can be increased.

This is also the case when trying to limit the risk of inducing an interferon response following the introduction of double stranded RNA (dsRNA) molecules. Double stranded RNA of greater than 30bp has been shown to induce an interferon response in mammalian cells (152). By using shorter RNA molecules it is thought that this effect can be avoided as it has been suggested that at least 40 to 60 bp of dsRNA are required for the activation of 2'-5'OAS (191). However, OAS-1 expression was significantly increased in NRK-52E cells following the introduction of short (21 nt) siRNA molecules against *Gstm1*. This effect was removed by lowering the siRNA concentration from 100nM to 30nM, indicating that as well as dsRNA length, concentration is also important. This was found to

be the case in studies with IFN treated HeLa cells, where higher concentrations of dsRNA were able to activate 2'-5'OAS more effectively (193). Therefore, to achieve successful and specific RNA interference, the lowest effective concentration of siRNA should be used to limit off-target effects.

To be able to take investigation of the function of *Gstm1* into an *in vivo* setting, local delivery to the kidney was evaluated as a potential means of introducing *Gstm1* targeting siRNA directly to the kidney. Direct administration of siRNA would maintain a high concentration of siRNA at the target site without having to deliver a large dose and so would also help to limit systemic side effects. Local delivery of siRNA has proved successful for delivery to the eye in mouse models of ocular neovascularisation (167;168). However, delivery of siRNA throughout the kidney has been found to be more difficult (194). Various methods have been employed to deliver siRNA/shRNA to the kidney. An adeno-associated virus vector expressing shRNA targeted against the mineralocorticoid receptor (MR) was introduced to Sprague Dawley rats by IV injection to the jugular vein. Renal MR expression was reduced and cold induced hypertension and renal damage were subsequently inhibited (162). The jugular vein was also used as a delivery route for a liposomal siRNA complex targeting V2 receptors in mouse kidney (195). The method investigated in this study for potential *in vivo* knock-down of *Gstm1* involved direct delivery to the kidney via the renal artery. However, following injection of Ad5/19p to the kidney, extensive damage was observed. Successful kidney delivery via renal artery injection has been described previously. Renal artery injection of a shRNA expression plasmid effectively inhibited TGF-β1 expression in mouse kidney (196). Direct delivery to rat kidney has also been shown using an electroporation mediated gene transfer system (197). Synthetic siRNA was introduced to the kidney by injection via the renal artery, the renal vein was then clamped and the kidney was subjected to electrical pulses. This method resulted in efficient transduction of glomeruli and significant silencing of gene expression (198). The silencing effect was restricted to the glomeruli with limited transduction of tubules observed. This method would not be appropriate for investigation of *Gstm1* silencing as expression of *Gstm1* has been found in kidney tubular epithelium. Neither study mentioned kidney damage sustained as a result of renal artery infusion.

To overcome the damage induced by direct kidney injection, a kidney targeting adenoviral vector that can be delivered systemically was evaluated. Kidney targeted Ad5 vectors have been generated as described previously (185) and targeting was evaluated in SHRSP. This testing in SHRSP was necessary as previous work had been carried out in WKY animals. The 2c* congenic strain is entirely SHRSP apart from a region of chromosome 2 encompassing *Gstm1* which has been transferred from WKY. The 2c* was found to have a greater level of *Gstm1* expression than SHRSP. Knocking down expression of *Gstm1* in the kidney of 2c* may re-establish the SHRSP phenotype and a greater understanding of the role of reduced expression observed in the SHRSP would be gained. Selective staining of the tubules has been shown which is important for *in vivo Gstm1* studies as differential expression of *Gstm1* was previously localised to kidney tubular epithelium (77).

Plasmid vectors that express short hairpin forms of the siRNA sequences already tested *in vitro* have been generated and could be incorporated into the kidney targeted Ad5 vector system. However, when assessing the activity of *Gstm1* shRNA *in vitro*, knock-down of *Gstm1* expression could not be achieved. Various studies have investigated optimal shRNA design for efficient knock-down of gene expression. In a study performed by Siolas *et al*, shRNAs with a 29 nt long stem and 3' nt overhang were found to be more efficient inducers of RNAi than shRNAs with 19 nt long stems. It has been suggested that Dicer substrates are incorporated into RISC more effectively. The 29-mer shRNAs with 3' overhangs were efficiently converted to 22 nt products (mediators of RNAi) by incubation with Dicer however, this was not the case for 19-mer shRNAs suggesting that Dicer requires a minimum stem length for successful cleavage. The presence of 3' overhangs was also found to be important for Dicer activity as 29-mer shRNAs without the overhang generated very little 22 nt product. Both 29-mer and 19-mer stems were connected by a 4 nt loop in this study (199). This would suggest that for efficient Dicer activity and subsequent incorporation into RISC, shRNAs should be designed with 29-mer stems and a 3' nt overhang. The shRNAs designed for knock-down of *Gstm1* in this study are composed of 19 nt stems with a 3' nt overhang and a 9 nt loop sequence. However, experiments carried out by Li and colleagues found that only when a 4 nt loop was incorporated into the shRNA design were 29-mer stem shRNAs more effective than 19-mer shRNA.

When combined with a 9 nt loop, shRNA with 19-mer stems were more efficient than 29-mer shRNA (200). They also found that 19 nt stems with a 9 nt loop provide an appropriate substrate for Dicer. This would suggest that the shRNA design used in our study should be processed by Dicer and result in the production of small RNAs capable of knocking down *Gstm1*.

Another factor that could affect the production of shRNA is the promoter used to drive shRNA expression. The p-Shuttle vector used to generate the *Gstm1* specific shRNA in this study utilises a CMV promoter. Many viral vectors use CMV to drive shRNA expression and a recent study involving plasmid generated shRNA found no significant differences in the silencing response generated from H1, U6 and CMV promoters (201). However, another group found that CMV was not suitable for expression of shRNA and that CMV-driven shRNA constructs were far less efficient than other promoter driven constructs (200). It may be that the pShuttle-CMV vector is not suitable for efficient production of shRNA and that perhaps another vector should be used in the future. As well as the various hairpin RNA design and expression considerations, a major factor contributing to *in vitro* gene silencing is transfection efficiency. It seems most likely that the reason the pShuttle-CMV-shRNA constructs failed to successfully knock-down *Gstm1* was due to the poor transfection efficiency of NRK-52E cells with plasmid DNA. At most, 20% of cells were successfully transfected with the *Gstm1* pShuttle-CMV-shRNA expression vectors as determined by *LacZ* expression. NRK-52E cells have proved to be very difficult to transfect with plasmid DNA as observed in this study and by other colleagues in the laboratory. Even if the cells that have taken up the shRNA constructs can generate a complete knockout of *Gstm1* expression, still only 20% knock-down would be observed for the entire cell population. Thus, the pShuttle-CMV-shRNA construct may generate effective *Gstm1* targeting shRNA but to fully evaluate their potency, a cell line more amenable to plasmid transfection would need to be used in any future studies.

Chapter 4: Investigating the Impact of Altered Gstm1 Expression on Markers of Oxidative Stress

4.1. Introduction

As described in detail in Chapter 1, Gstm1 is part of a large family of antioxidant enzymes involved in the detoxification of the by-products of oxidative stress such as the break-down products of lipid peroxidation and oxidative DNA damage (118). The results of Chapter 3 demonstrated that expression of *Gstm1* can be successfully and consistently knocked down at both protein and mRNA level by siRNA mediated RNA interference. The effect of reduced *Gstm1* expression on markers of oxidative stress was investigated to assess the antioxidant role of Gstm1.

4.1.1. Lipid Peroxidation

Lipid peroxidation is a common feature of free radical induced damage to membranes (202). Cell membranes containing polyunsaturated fatty acids are highly susceptible to peroxidation and the lipid radicals produced lead to propagation of free radical reactions, further contributing to lipid damage. Increased lipid peroxidation has been described as a significant contributor to the development of atherosclerosis (203). The production of lipid radicals and their intermediates can affect cell function, lead to inflammation and vascular damage and may contribute to endothelial dysfunction (204).

Isoprostanes are commonly used markers of lipid peroxidation and oxidative stress. The prostaglandin like F_2 isoprostanes are derived from the peroxidation of arachidonic acid and can be measured in blood and urine to assess lipid peroxidation *in vivo* (204;205). The most commonly used biomarker of lipid peroxidation is 8-isoprostane (204). Levels of 8-isoprostane have been shown to be higher in subjects with cardiovascular risk factors than in healthy subjects and were also found to be elevated in smokers (206;207). Studies in hypertensive individuals have shown that plasma 8-isoprostane concentration is higher in salt sensitive subjects during salt loading (208) and that angiotensin II infusion also leads to increased 8-isoprostane in plasma of hypertensive subjects with high salt intake (209). Measurement of 8-isoprostane has also been performed *in vitro* (210) and was used as an indicator of oxidative stress in NRK-52E cells (211).

4.1.2. DNA Damage

Increased levels of oxidative stress can also lead to DNA modification and damage. Free radicals, such as the hydroxyl radical can cause DNA base oxidation (212). 8-hydroxy-2-deoxyguanosine (8-OH-dG) is a product of such free radical induced damage resulting from hydroxylation of the guanosine base. It is frequently measured as an indicator of oxidative stress *in vivo* (213). Studies measuring 8-OH-dG have shown that increased DNA damage is present in patients with type 2 diabetes compared to non-diabetic subjects (214) and plasma levels of 8-OH-dG are higher in hypertensive patients compared to normotensive subjects (215).

The comet assay or single cell gel electrophoresis is commonly used to assess levels of DNA damage in response to oxidative stress (216). It is frequently used to measure and analyse DNA breakage in individual cells and is sensitive to low levels of DNA damage (217). Damaged DNA when subjected to an electric current, following unwinding under alkaline conditions, will migrate out of the nucleoid and when stained can be visualised as a comet (218). The length of the comet tail generated is proportional to the level of damage, so that a longer comet tail indicates greater damage to DNA. The comet assay has been used to investigate the protective effects of antioxidant treatment in various intervention studies and to assess oxidative stress both *in vitro* and *in vivo* (219).

4.2 Aims

- To assess GST activity following modification of *Gstm1* expression
- To measure levels of reduced glutathione, by high performance liquid chromatography (HPLC)
- To assess the contribution of *Gstm1* to oxidative stress, using 8-isoprostane and 8-OH-dG assays and the comet assay

4.3 Methods

4.3.1 Transfection of NRK52E Cells with siRNA

NRK-52E cells were transfected with anti-*Gstm1* siRNA (30 to 100nM) as outlined in section 2.3.

4.3.2 Cell Culture

HeLa cells were cultured in Eagle's minimum essential medium supplemented with 10% FCS, 100 I.U/ml of penicillin and 100 µg/ml of streptomycin. A10 and H9C2 cells were cultured in Dulbecco's modified Eagle's medium plus GlutaMAX supplemented with 10% FCS, 100 I.U/ml of penicillin and 100 µg/ml of streptomycin. All cells were maintained in a 5% CO_2 atmosphere at 37°C.

4.3.3 HeLa Cell Infection

To examine the effect of over-expression of *Gstm1* on GST activity, HeLa cells were infected with an adenovirus engineered to express the WKY version of *Gstm1* (RAd WKY Gstm1) (220). As a negative control, cells were also infected with a non-expressing vector (RAd60). Twenty four hours prior to infection, HeLa cells were plated out in 6 well plates and infected once approximately 90% confluent. The number of cells in each well was determined by collecting and counting the cells from a control well as described in section 2.2. The number of cells/well was then used to calculate the number of virus particles required for a multiplicity of infection (MOI) of 10, 50 and 100 and the volume of virus required per well was determined by virus titre. The virus stocks were diluted in sterile PBS and added to cell culture medium in each well. Following overnight incubation at 37°C, the virus containing medium was removed and replaced with fresh medium. Forty eight hours after infection, protein was harvested from cells as described in section 2.4.

4.3.4 Total GST Activity

Total GST activity was determined by the rate at which glutathione is conjugated to 1-Chloro-2,4-Dinitrobenzene (CDNB) by glutathione transferases present in each sample (GST Activity kit from Sigma). Protein samples were prepared as described in section 2.4. Assays were carried out in 96 well plates as per manufacturer instructions. The substrate solution was prepared as follows: 2µl of 100mM CDNB, 2µl of 200mM reduced GSH and 196µl of DPBS (per well). Control GST was diluted to a final concentration of 25µg/ml. 20µl of each sample and 4µl of diluted control GST was added to substrate solution to a final volume of 200µl per well and run in duplicate. Immediately after preparing reaction samples, the absorbance from each well was read at 340nm and then at 1 minute intervals until 10 readings had been obtained. The increase in absorbance is directly proportional to total GST activity in the sample. The change in absorbance per minute was used to calculate specific GST activity.

4.3.5 Glutathione Measurement

High performance liquid chromatography (HPLC) (221) was utilised to measure levels of reduced GSH in NRK-52E cells following knock-down of *Gstm1* expression.

4.3.5.1 Cell Culture

NRK-52E cells were cultured in 100mm plates until 70% confluent and then transfected with 30nM siRNA, as described before.

4.3.5.2 Sample Preparation

Culture medium was removed from each plate and cells were rinsed twice with PBS. To detach cells, 3ml of 1X Trypsin-EDTA was added to each plate and incubated at 37°C for 5 minutes. Once detached, 10ml of medium containing 10% FCS was added to inactivate trypsin and cells were transferred to a 50ml falcon tube. Cells were centrifuged at 1000rpm for 5 minutes to pellet cells and medium was removed. 200µl of cold 10% metaphosphoric acid was added to

each NRK-52E sample and incubated for 10 minutes at 4°C. Samples were transferred to 1.5ml centrifuge tubes and centrifuged at 16,000g for 25 minutes at 4°C. The supernatants were transferred into fresh 1.5ml tubes and immediately stored at -80°C.

4.3.5.3 Derivatisation of GSH

To 50µl of each sample, 1ml of 0.1% EDTA in 0.1M sodium hydrogenphosphate (pH 8.0) was added. After mixing well, a 20µl aliquot was removed and to this, 300µl of 0.1% EDTA in 0.1M sodium hydrogenphosphate and 20µl of 0.1% ortho-phthalaldehyde (OPA) in methanol was added. Each sample was briefly vortexed to mix and incubated, in the dark, for 25 minutes at 25°C. Glutathione standards were prepared in the same way and used to generate a calibration curve.

4.3.5.4 Chromatography

Following derivatisation of GSH with OPA, chromatography was performed using a Shimadzu LC-10AT HPLC pump with a SIL-9A auto-injector and a reverse phase column. The mobile phase consisted of 12% methanol in 25mM sodium hydrogenphosphate, pH 6.0 and the flow rate was held at a constant 0.8ml/minute. Fluorescence was detected using the Perkin Elmer Series 200 fluorescence detector and excitation and emission wavelengths were set to 350 and 420nm respectively. Data was collected and analysed using the JCL6000 for Windows 2.0 Chromatography Data System. The concentration of GSH in each sample was determined from the calibration curve.

4.3.6 Lipid Peroxidation: 8-Isoprostane Assay

Levels of 8-isoprostane in the culture medium of cells transfected with *Gstm1* specific siRNA were measured using an 8-isoprostane ELISA kit according to manufacturer's instructions (Cayman Chemical).

4.3.6.1 Sample Preparation

Culture medium samples were collected from cells 48 hours post transfection with siRNA (as described before) and assayed immediately. Each sample was run in duplicate alongside 8-isoprostane standards in a 96 well plate. All standard dilutions were prepared with fresh culture medium. All assay reagents were prepared with UltraPure water (Cayman Chemical). The EIA buffer used in the assay was diluted by adding 90ml of UltraPure water to the buffer concentrate supplied with the kit. The 8-isoprostane tracer and 8-isoprostane antiserum were reconstituted with 6ml EIA buffer. Wash buffer was prepared by diluting the Wash Buffer concentrate 1:400 and adding Tween 20 (0.5 ml/litre of wash buffer).

4.3.6.2 8-isoprostane Assay

Each 96 well plate was set up to include 2 blanks, 2 non-specific binding (NSB) wells, 2 maximum binding (Bmax) wells and an 8 point standard curve run in duplicate. To each NSB well, 50µl of culture medium, 50µl EIA buffer and 50µl of tracer was added. To each Bmax well, 50µl of culture medium, 50µl of tracer and 50µl of antiserum was added. Antiserum and tracer (50µl) was also added to each well containing standard or sample (50µl). Once all reagents were added, the plate was covered with plastic film and incubated for 18 hours at 4°C. To develop the plate, Ellman's reagent was reconstituted with 20ml UltraPure water and kept in the dark until ready to use. Each well was emptied and rinsed 5 times with wash buffer then 200µl of Ellman's reagent was added to each well. The plate was left in the dark on a shaker for at least 90 minutes to allow the plate to develop. The absorbance was measured at 405nm and readings were taken when the Bmax wells reached 0.3 A.U. after the blank wells had been subtracted.

4.3.6.3 Analysis

Each absorbance reading was blank corrected and then the average reading from the NSB wells was subtracted from the average reading from the Bmax wells to

give the corrected maximum binding. The % sample or standard bound / maximum bound (%B/Bmax) was calculated by subtracting the average NSB absorbance from the average standard or sample absorbance and dividing this by the corrected Bmax absorbance. This was then multiplied by 100 to give the %B/Bmax. A standard curve was generated by plotting the %B/Bmax of each of the standards against 8-isoprostane concentration and used to calculate the concentration of 8-isoprostane in each sample.

4.3.7 DNA Damage: Comet Assay

The Trevigen comet assay kit was used to assess damage to DNA following knock-down of *Gstm1* expression. This assay works on the basis of single cell gel electrophoresis on a pre-treated slide provided with the kit.

4.3.7.1 Cell Preparation

NRK52E cells were transfected with 100nM siRNA as before and cells were examined for DNA damage. As a control, cells were treated with 100μM H_2O_2 in normal cell culture medium for 20 minutes at 4°C. Cells were collected using a cell scraper and centrifuged at 1500 rpm for 5 minutes to form a pellet. The cell pellet was washed in ice cold PBS, centrifuged again and then re-suspended in ice cold PBS to 1 x 10^5 cells/ml.

4.3.7.2 Single Cell Gel Electrophoresis

The electrophoresis step was carried out according to kit instructions. Briefly, 50μl of each cell suspension was combined with 500μl agarose (pre-warmed to 37°C) and spread evenly over the CometSlide™ area. Slides were kept in the dark at 4°C for 10 minutes and then placed in lysis solution at 4°C for 40 minutes. The slides were then placed in alkaline solution and incubated in the dark at room temperature for 40 minutes. Slides were washed twice for 5 minutes in 1X TBE buffer and then placed in the middle an electrophoresis tank containing 1X TBE, so that the slides were just covered with buffer. Electrophoresis was carried out at 14 volts for 10 minutes. After

electrophoresis, slides were removed from the tank and placed in 70% ethanol for 5 minutes. The samples were then left to air dry.

4.3.7.3 Staining

To visualise the DNA, samples were stained with 50µl of diluted SYBR® Green I nucleic acid gel stain (supplied with comet assay kit) and examined under a fluorescence microscope. To evaluate DNA damage, comet tail length was measured. For each slide, up to 60 measurements were taken resulting in a maximum of 180 measurements per triplicate group.

4.3.8 DNA Damage: 8-hydroxy-2-deoxy Guanosine Assay

Levels of 8-hydroxy-2-deoxy guanosine (8-OH-dG) were measured in NRK-52E cells following transfection with *Gstm1* specific siRNA using an 8-OH-dG ELISA kit (Cayman Chemical) according to the manufacturer's instructions.

4.3.8.1 Sample Preparation

NRK-52E cells were cultured and transfected using serum free medium as foetal calf serum. Cell culture medium was collected from NRK-52E cells 48 hours after transfection with siRNA (as described before) and immediately stored at -80°C until ready to be assayed. All assay reagents were prepared in UltraPure water (Cayman Chemical). The EIA Buffer was prepared by adding 90ml of UltraPure water to the buffer concentrate supplied. The 8-OH-dG tracer and antiserum were reconstituted with 6ml EIA buffer. The wash buffer was prepared by diluting the Wash Buffer concentrate 1:400 and adding Tween 20 (0.5ml/litre of wash buffer). All standard dilutions were prepared in fresh, serum free culture medium.

4.3.8.2 8-hydroxy-2-deoxy Guanosine Assay

Each sample was run in duplicate alongside 8-OH-dG standards in a 96 well plate. Each plate also contained 2 NSB wells and 2 Bmax wells. The plate was

set up and assayed as described in section 4.3.5.2 using 8-OH-dG tracer and antiserum. The 8-OH-2dG concentration was calculated as described for 8-isoprostane in section 4.3.5.3.

4.4 Results

4.4.1 GST Activity Assay

Prior to investigating the effect of *Gstm1* silencing in NRK-52E cells on total GST activity, protein samples were extracted from 3 different rat cell lines and tested for their basal levels of GST activity. The following cell lines were used: A10 cells (aortic smooth muscle) H9C2 cells (cardiomyocytes) and NRK-52E cells (renal tubular). Figure 4.1 demonstrates that a measureable level of GST activity was present in NRK-52E cells (n=1 experiment performed in duplicate and is representative of 3 experiments in total). In this example, the highest level of total GST activity was measured in NRK-52E cells.

Following confirmation that total GST activity was readily detectable in NRK-52E cells, the assay was repeated with protein from cells transfected with 100nM siRNA to knock-down *Gstm1*. From the initial experiment carried out it seemed that lowering *Gstm1* expression resulted in reduced total GST activity as shown in the top panel of Figure 4.2. In this experiment, total GST activity was reduced by 53% in siRNA A treated cells when compared to control siRNA treated cells (siCTL) ($p<0.05$). In cells transfected with siRNA B, activity was reduced by 72% compared to siCTL ($p<0.05$) but no significant change was observed in siRNA C treated cells. However, this result was not reproducible. Instead, upon repeated experiments (n=6), total GST activity levels were unaffected by reduced *Gstm1* expression, with no significant difference between cells transfected with *Gstm1* siRNA and those transfected with control siRNA as shown in the bottom panel of Figure 4.2.

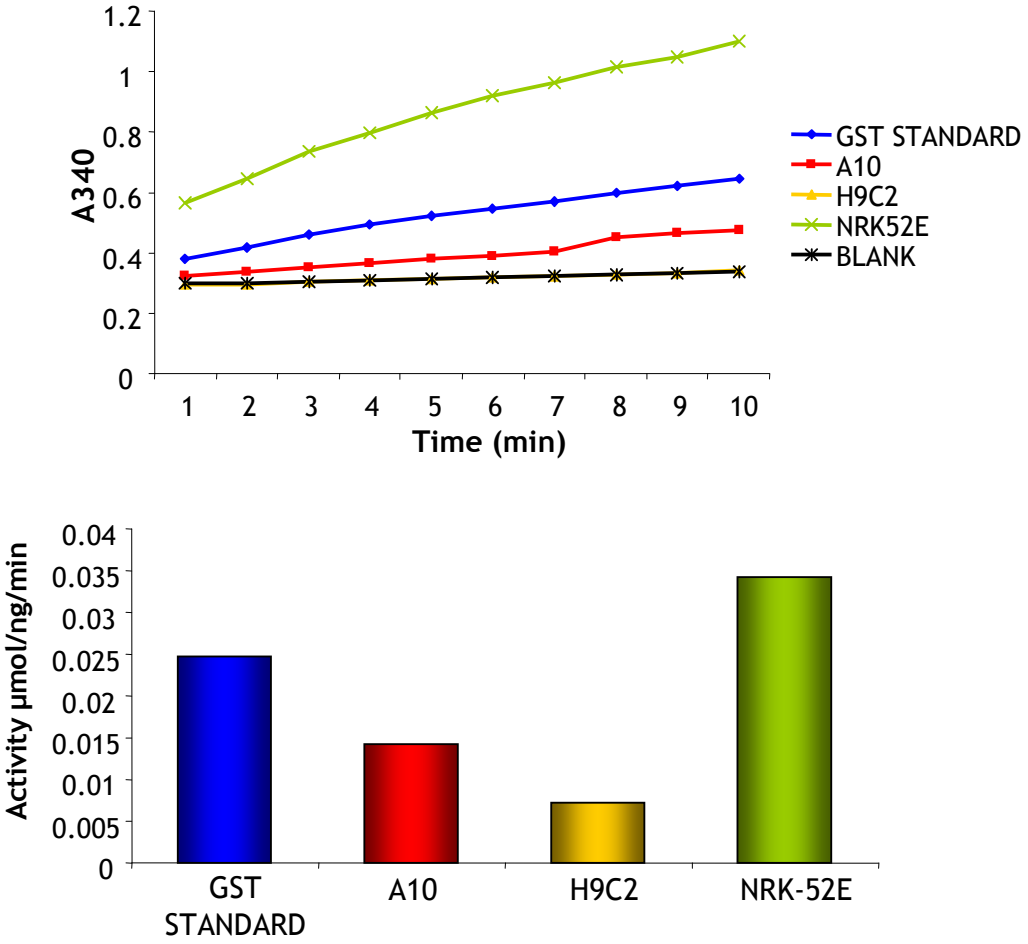

Figure 4.1 Total GST activity in rat cell lines

Top panel: GST activity increases over time. Bottom panel: Total GST activity observed in 3 rat cell lines. Basal activity was highest in NRK-52E cells and lowest in H9C2 cells (n=1 experiment performed in duplicate and is representative of 3 experiments in total).

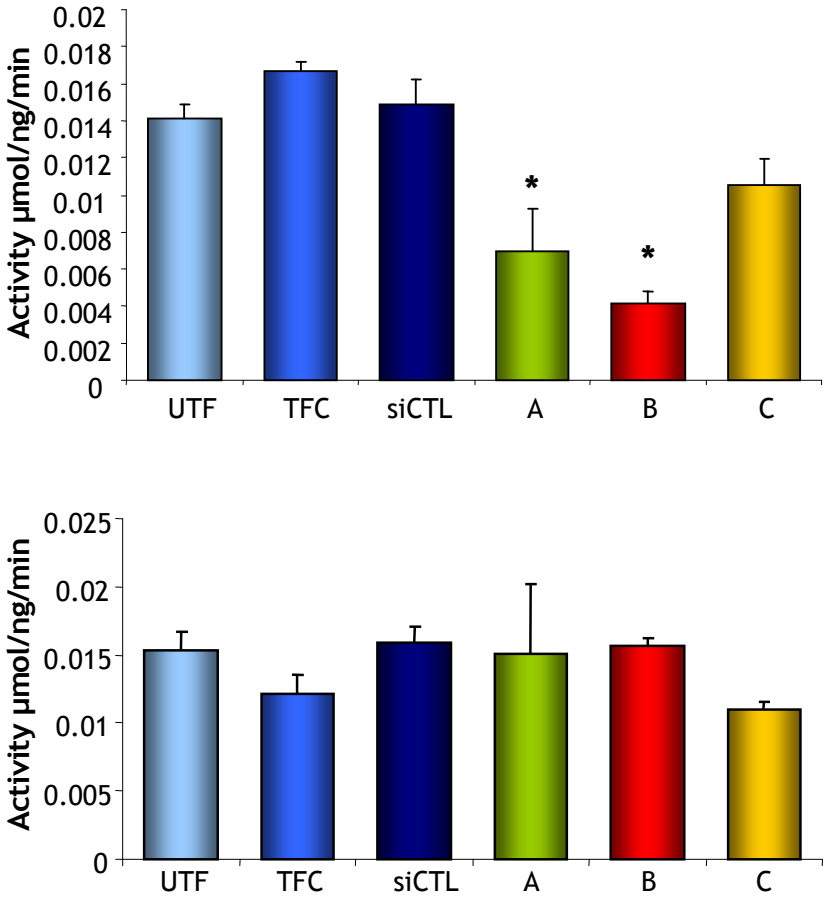

Figure 4.2 GST activity following *Gstm1* RNAi

NRK-52E cells were transfected with 100nM control (siCTL) or *Gstm1* specific siRNA (A, B or C). Total protein was extracted and GST activity was measured. Top panel: Reduced GST activity was observed in response to siRNA A and B (n=1 experiment performed in triplicate) *p<0.05 vs siCTL (ANOVA + Dunnett's post-hoc test). Bottom panel: No change in GST activity was observed following knock-down of *Gstm1* in NRK-52E cells (n=1 experiment performed in triplicate and is representative of 6 experiments in total).

UTF: untransfected cells, TFC: mock transfection, siCTL: control siRNA transfected cells

As total activity could not be modulated by reducing *Gstm1* expression, it was then investigated if over-expression of *Gstm1* could alter GST activity levels. For the purposes of this experiment, HeLa cells were used instead of NRK-52E cells. Previous experiments carried out in the laboratory found that NRK-52E cells were not amenable to infection with a recombinant adenoviral vector engineered to express *Gstm1*. HeLa cells were infected with the empty vector RAd60 as a negative control and a recombinant Ad vector expressing *Gstm1* (RAd_*Gstm1*) at MOI of 10, 50 and 100. Figure 4.3 shows a dose dependent increase in total GST activity following the over-expression of *Gstm1*, compared to cells infected with an empty vector (n=3). The RAd60 control vector had no significant effect on GST activity. No significant increase in GST activity was observed between RAd_*Gstm1* infected cells and RAd60 infected cells at MOI 10. At MOI 50, a significant 30% increase in activity was observed between control cells and *Gstm1* over-expressing cells, $p<0.05$ and at MOI 100, activity in RAd_*Gstm1* infected cells was 63% higher than control cells, $p<0.01$.

4.4.2 Glutathione Measurement

High performance liquid chromatography (HPLC) was performed to measure reduced glutathione concentration in NRK-52E cells to assess whether levels were affected by reduced *Gstm1* expression. A representative trace is shown in Figure 4.4. The top panel is a representative HPLC chromatogram generated from the samples assayed and the bottom panel is a blank control chromatogram where only 10% metaphosphoric acid was assayed. The top panel shows a peak representing GSH at a retention time of 2.36 minutes and this was the same for all samples, no peak was observed in the blank trace (bottom panel). A calibration curve was generated using GSH standards from 2 to 10 μM (Figure 4.5, top panel). The relative fluorescence generated from each standard was plotted against concentration and this was used to calculate the concentration of GSH in each unknown sample. The bottom panel in Figure 4.5 shows the GSH concentration measured in each NRK-52E sample. No significant difference in GSH concentration was observed between control and siRNA treated groups. The concentration of glutathione was found to be similar in all groups; 13.36μM in the untransfected group, 9.98μM in the mock transfected group, 11.98μM in the control siRNA group and 13.68μM in the siRNA B treated group.

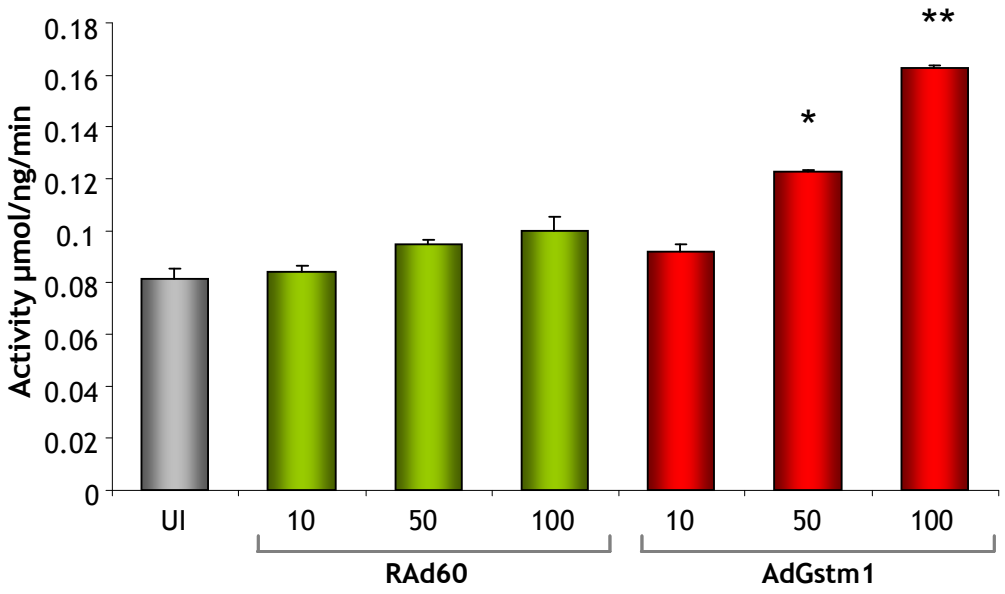

Figure 4.3 Total GST activity following over-expression of Gstm1 in HeLa cells Total GST activity in uninfected (UI) HeLa cells and following infection with a non-expressing vector (RAd60) or vector expressing *Gstm1* (AdGstm1) at MOI of 10, 50 and 100. GST activity shows a dose dependent increase in response to over-expression of *Gstm1* compared to RAd 60 infected cells at equivalent MOI (n=1 experiment performed in triplicate and is representative of 3 experiments in total) *$p<0.05$ vs Rad60, **$p<0.01$ vs Rad60 (ANOVA + Dunnett's post-hoc test).

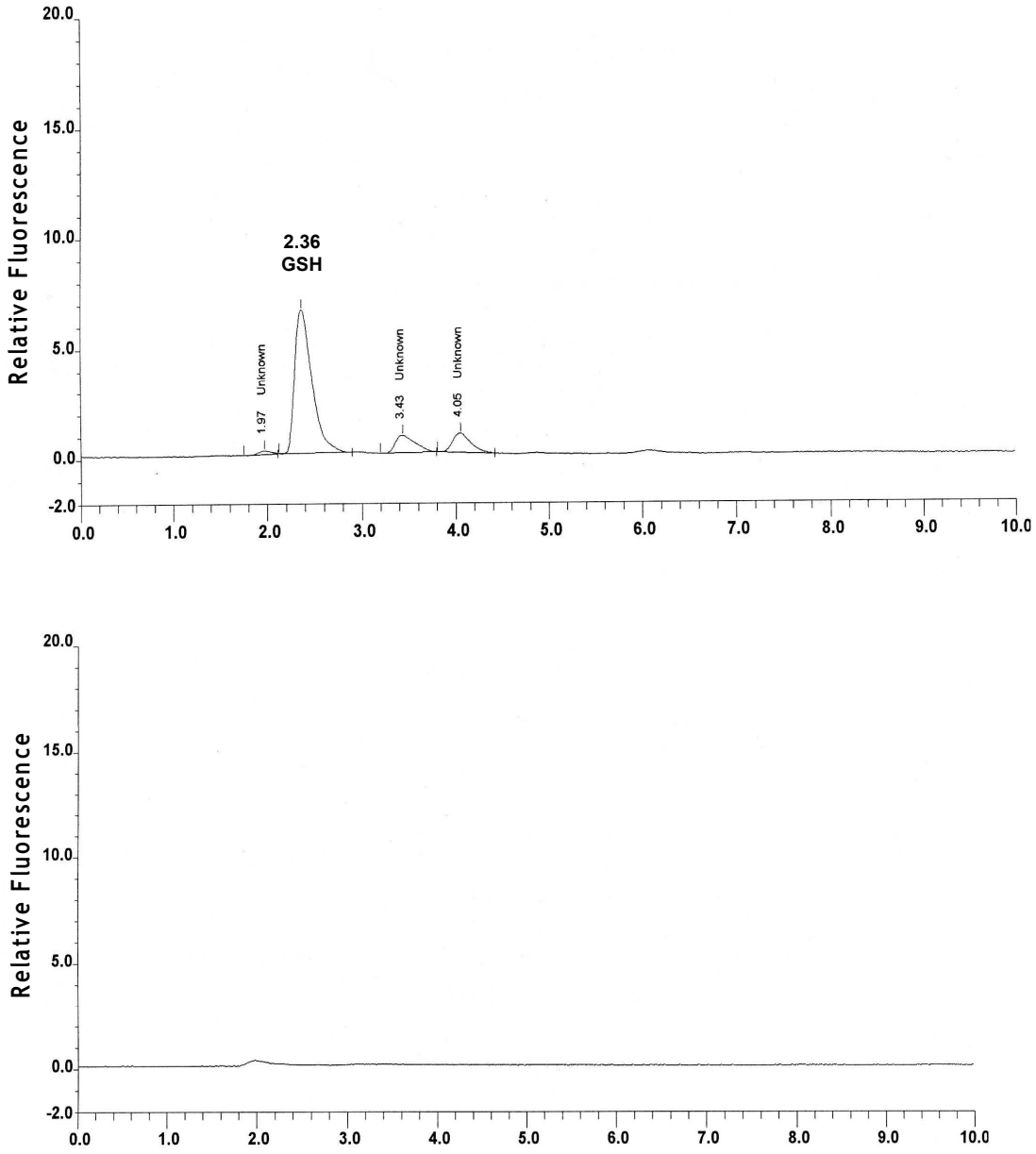

Figure 4.4 HPLC analysis of glutathione

Top panel: Representative HPLC chromatogram of glutathione present in NRK-52E cells. Bottom panel: Blank control HPLC chromatogram with no peak detected.

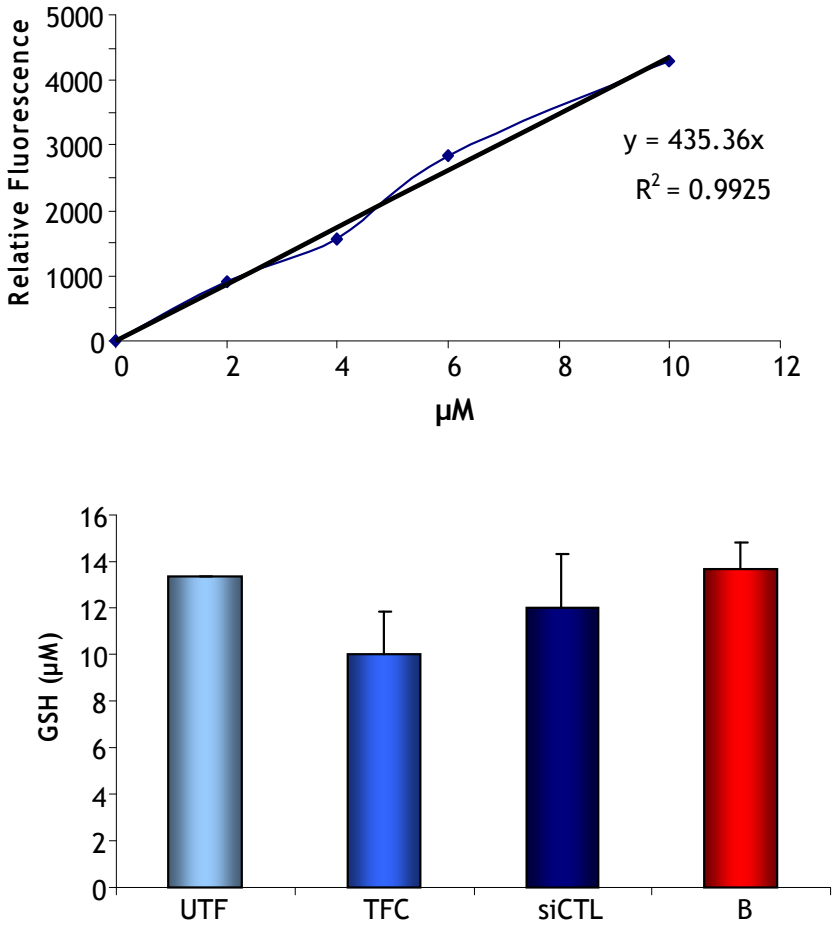

Figure 4.5 Glutathione measurement

Top panel: Glutathione calibration curve showing linear relationship in low µM range. Bottom panel: Glutathione concentration in NRK-52E cells transfected with 30 nM control (siCTL) or *Gstm1* specific siRNA (B). No difference in GSH concentration was observed in cells transfected with *Gstm1* specific siRNA B when compared to control groups (n=1 experiment performed in triplicate).

UTF: untransfected cells, TFC: mock transfection, siCTL: control siRNA transfected cells

4.4.3 Lipid Peroxidation

In an attempt to examine what affect reducing *Gstm1* expression would have on oxidative stress, an ELISA based assay that measures levels of 8-isoprostane was used. Initially the assay was tested on the culture medium from NRK-52E cells treated with H_2O_2 to ensure that a change in 8-isoprostane could be detected following induction of oxidative stress. As indicated in Figure 4.6 (Panel B), 8-isoprostane levels show a dose and time dependent increase in response to H_2O_2 (n=1 experiment performed in duplicate and is representative of 3 experiments in total). This indicates that 8-isprostane can be measured in the culture medium from NRK-52E cells.

The assay was then performed with culture medium from NRK-52E cells transfected with each of the *Gstm1* specific siRNA sequences. In the initial experiment, 8-isoprostane concentration appeared to be significantly increased in response to knock-down of *Gstm1* as shown in the bottom panel of Figure 4.6. In this experiment, treatment of NRK-52E cells with siRNA A and C had no significant effect on 8-isoprostane concentration but transfection of NRK-52E cells with siRNA B resulted in a 96% increase in 8-isoprostane concentration and was significant, $p<0.05$. However, no significant change in 8-isoprostane was observed following knock-down of *Gstm1* in any other experiments (n=6) as shown in Figure 4.7. Western blot analysis was performed to ensure that GSTM1 was still being effectively knocked down in each experiment and this is shown in a representative blot in Figure 4.7. Each band was normalised to ß-actin and the densitometry results indicated that GSTM1 was successfully knocked down by 65%, 79% and 40% by siRNA A, B and C respectively when compared to the scrambled siRNA control bands.

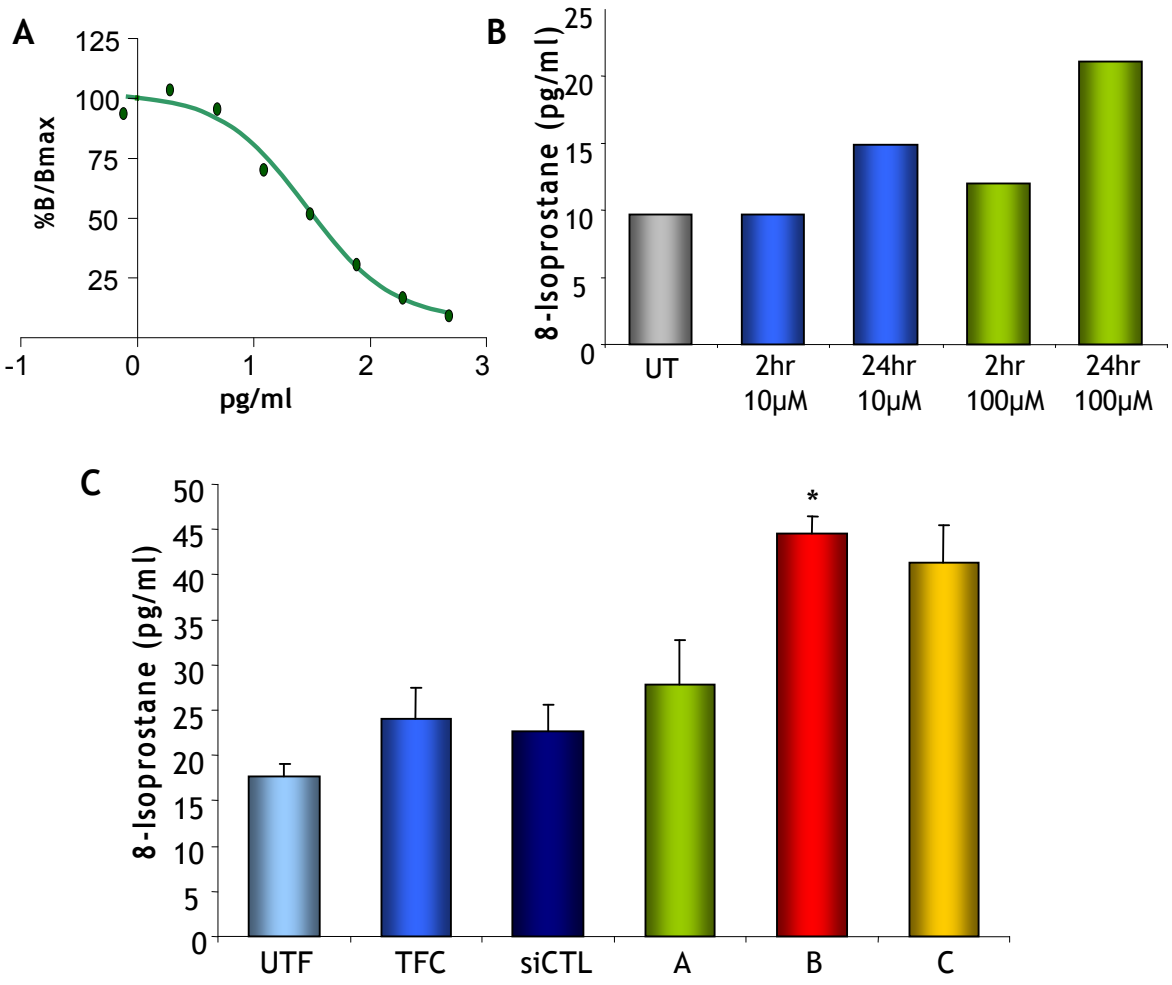

Figure 4.6 8-Isoprostane measurement

A: 8-isoprostane standard curve. B: 8-isoprostane concentration in NRK-52E cells following treatment with H_2O_2. 8-isoprostane concentration is increased in response to increasing concentrations of H_2O_2 (n=1 experiment performed in duplicate and is representative of 3 experiments in total). C: NRK-52E cells were transfected with 30nM control (siCTL) or *Gstm1* specific siRNA (A, B or C). 8-isoprostane concentration was significantly increased in NRK-52E cells transfected with siRNA B compared to control siRNA transfected cells (n=1 experiment performed in triplicate) *$p<0.05$ vs siCTL (ANOVA + Dunnett's post-hoc test).

UTF: untransfected cells, TFC: mock transfection, siCTL: control siRNA transfected cells

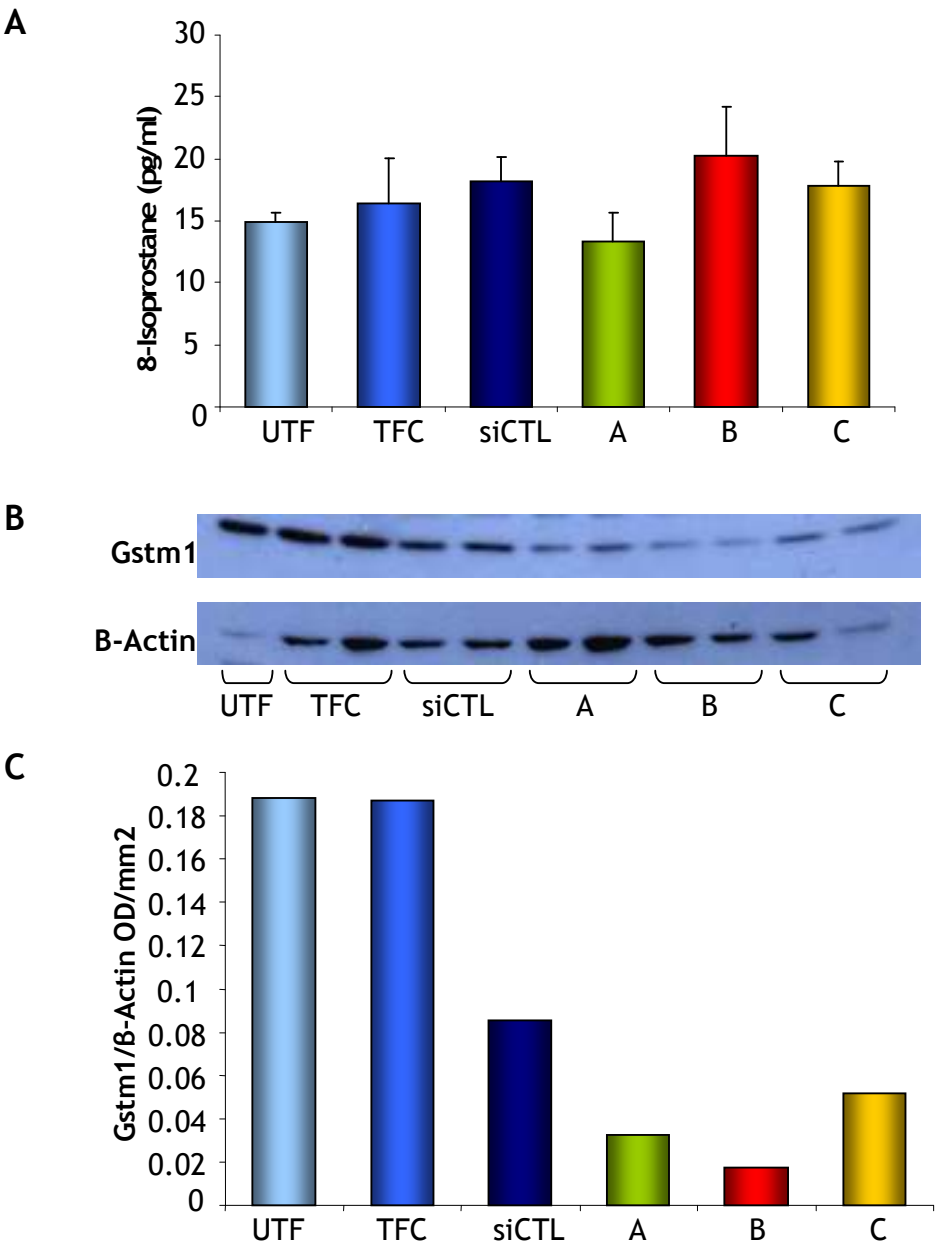

Figure 4.7 8-Isoprostane measurement and Gstm1 western blot analysis

NRK-52E cells were transfected with 30nM control (siCTL) or *Gstm1* specific siRNA (A, B or C). A: No significant change in 8-isoprostane concentration was observed in cells transfected any *Gstm1* specific siRNA (n=1 experiment performed in triplicate and is representative of 6 experiments in total). B: GSTM1 and ß-actin western blots indicating that GSTM1 protein levels were reduced in cells transfected with *Gstm1* siRNA. C: Reduced GSTM1 protein was confirmed by densitometry with each band normalised to ß-actin (n=1 experiment performed in duplicate).

UTF: untransfected cells, TFC: mock transfection, siCTL: control siRNA transfected cells

4.4.4 DNA Damage

To examine whether reduced *Gstm1* contributes to increased DNA damage, single cell gel electrophoresis was carried out using a comet assay kit.

To ensure that comet tails could be easily detected using our available resources, NRK-52E cells were treated with increasing concentrations of H_2O_2 to induce oxidative stress before being assessed. Representative images of the cells examined are shown in Figure 4.8. As shown in the top panel of Figure 4.8 no visible tail was detected in untreated control cells or those that had been treated with 10μM H_2O_2. However, when the concentration of H_2O_2 was increased to 100μM, a pronounced tail was clearly visible indicating that an increased level of DNA damage was present in this cell. At 300μM, a similar level of DNA damage was observed.

Following knock-down of *Gstm1*, a significant increase in tail length was observed in cells transfected with either siRNA B or C indicating increased DNA damage in these cells (n=3). Tail length measurements are shown in the chart in Figure 4.8. In this example, when compared to cells transfected with control siRNA, tail length increased by 20% in response to siRNA B and 33% in response to siRNA C, $p<0.05$. No significant increase in tail length was observed in response to siRNA A in this example. Representative comet images obtained from each of the groups are shown in Figure 4.9. As demonstrated in this Figure, no substantial comet tails were detected in any of the control groups when compared to the H_2O_2 induced tails as a reference. In each of the siRNA treated groups, comet tails were readily detectable but with variation in length between cells and groups.

4.4.5. 8-Hydroxy-2-Deoxyguanosine Measurement

Levels of 8-OH-dG were measured in the culture medium of NRK-52E cells following knock-down of *Gstm1* expression. Figure 4.10 is representative of 4 experiments. As shown in Figure 4.10, no significant difference in 8-OH-dG concentration was observed between NRK-52E cells treated with *Gstm1* specific siRNA B and control siRNA.

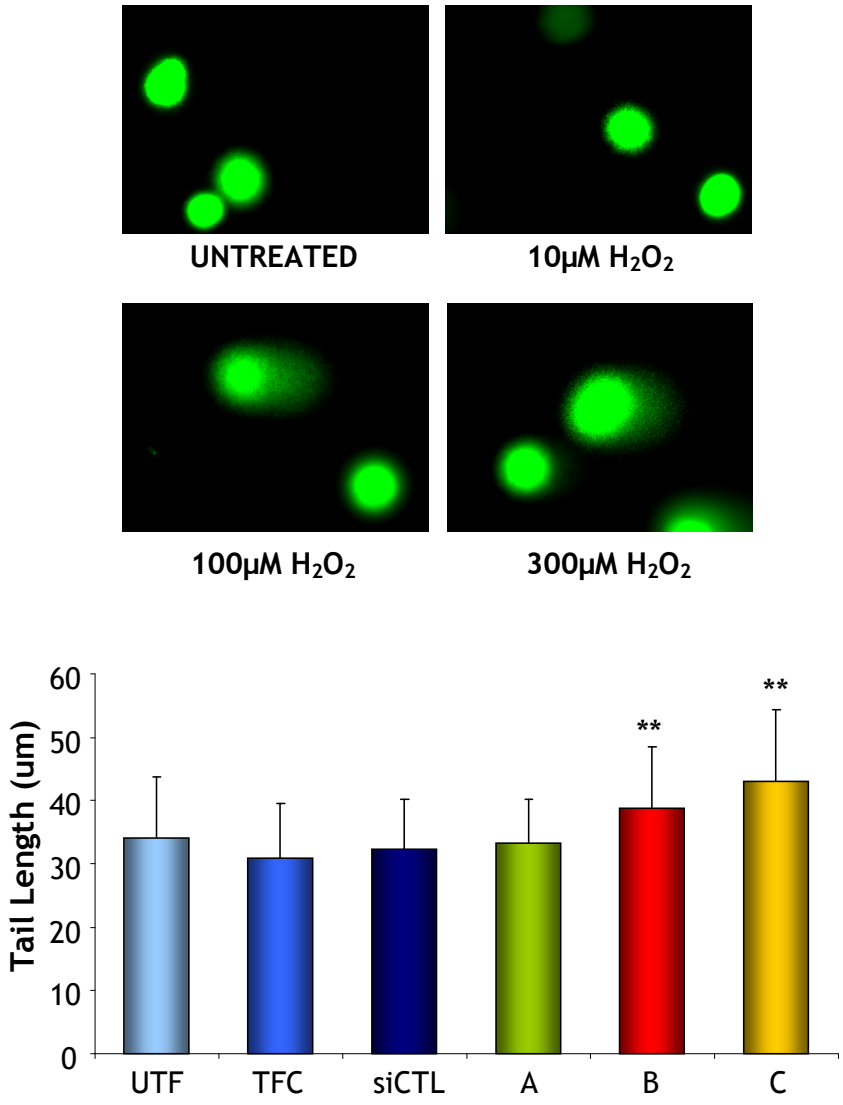

Figure 4.8 Analysis of DNA damage by comet assay

Top panel: Representative comet images from NRK-52E cells stimulated with increasing concentrations of H_2O_2. Bottom panel: NRK-52E cells were transfected with 30nM control (siCTL) or *Gstm1* specific siRNA (A, B or C). Following knock-down of *Gstm1* expression by RNAi, increased comet tail length was observed compared to the siRNA control indicating increased damage to DNA (n=1 experiment performed in triplicate and is representative of 3 experiments in total) **p<0.01 vs siCTL (ANOVA + Dunnett's post-hoc test).

UTF: untransfected cells, TFC: mock transfection, siCTL: control siRNA transfected cells

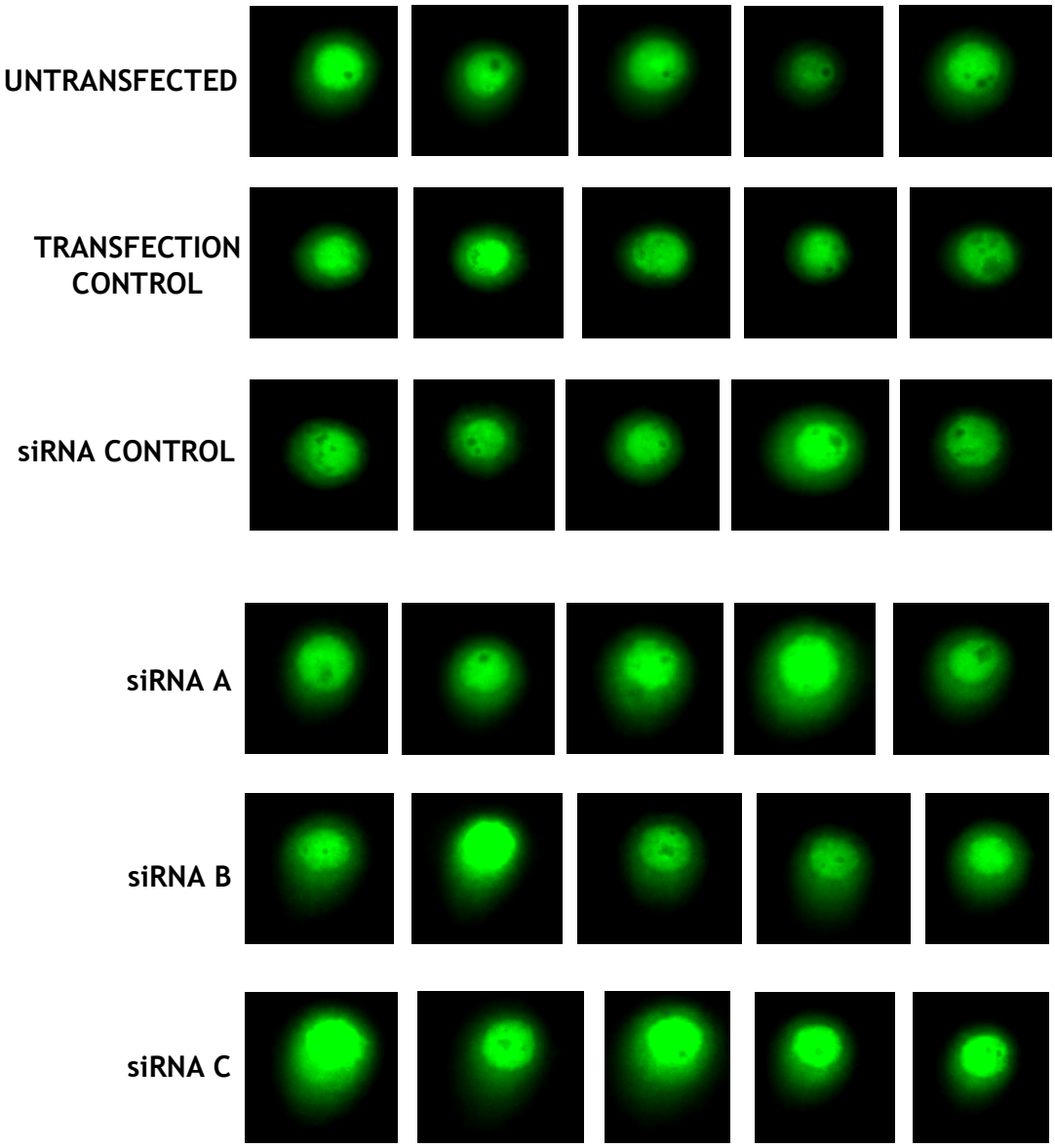

Figure 4.9 Comet assay analysis

Representative images obtained from NRK-52E cells transfected with 30nM control (siRNA CONTROL) or *Gstm1* specific siRNA (A, B or C). No clearly visible tails were present in any of the control groups (top 3 panels). Comet tails of varying lengths were observed in cells treated with *Gstm1* specific siRNA.

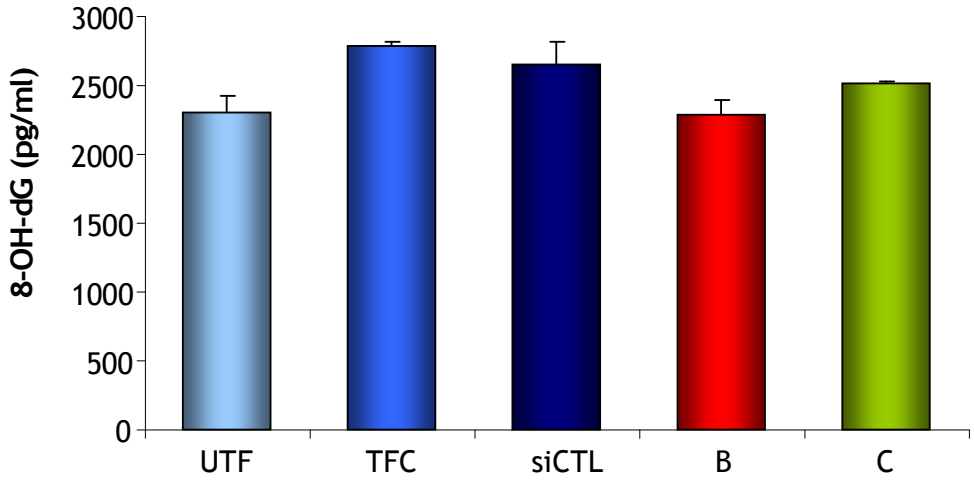

Figure 4.10 Measurement of 8-hydroxy-2-deoxyguanosine

8-OH-dG was measured in NRK-52E cells following transfection with 30nM control (siCTL) or *Gstm1* specific siRNA (B and C). No significant change in concentration was observed in response to knock-down of *Gstm1* expression (n=1 experiment performed in triplicate and is representative of 4 experiments in total).

UTF: untransfected cells, TFC: mock transfection, siCTL: control siRNA transfected cells

4.5 Discussion

The results of the previous chapter show that *Gstm1* expression can be selectively knocked down using RNA interference. In an attempt to translate the expression data into a change in Gstm1 activity, a GST assay kit was evaluated. At present, there are no selective substrates for Gstm1; instead the kit used measures total GST activity by measuring the rate at which glutathione is conjugated to CDNB, a substrate for a broad range of GST isozymes. After a number of attempts, no significant change in GST activity could be measured in response to reduced *Gstm1* expression. Therefore, one obvious conclusion from these experiments is that a kit measuring total GST activity is not sensitive enough to detect changes when only one member of a large class of enzymes is reduced, as reduction of Gstm1 enzyme activity may be masked by other GSTs in the sample. In contrast, total GST activity was increased when *Gstm1* was over-expressed. This suggests that total GST activity can indeed be modulated when a single GST (*Gstm1* in this case) is over-expressed to a high enough level.

Glutathione transferases detoxify the products of oxidative stress by catalysing the conjugation of reduced glutathione (GSH) to such products. Therefore, lower levels of GST expression may lead to increased levels of GSH. The concentration of GSH in NRK-52E cells with lower expression of *Gstm1* was evaluated but no difference in GSH concentration was found. Again, this is likely due to the presence and activity of other GST in the sample. It is unlikely that total GSH levels would be greatly affected by the reduction of one GST when other GST isozymes and other enzyme systems such as glutathione peroxidase utilise glutathione as a substrate.

As previously mentioned, oxidative stress has been implicated in development of hypertension. Following knock-down of *Gstm1* by RNA interference, DNA damage and lipid peroxidation were investigated as both are markers of oxidative stress. Lipid peroxidation showed no change in any of the siRNA treated cells demonstrated by the levels of 8-isoprostane in the culture medium. This data suggests that *Gstm1* does not play a role in protection from lipid peroxides; however, it could be that other members of the GST super-family are compensating for reduced *Gstm1* expression. Treatment of primary cultured rat

cerebral cortical cells with valproate (a mood stabilising drug) inhibited lipid peroxidation and also increased Gstm1 and Gsta4 levels (222;223). This may suggest a role for *Gstm1* in lipid peroxidation protection. Previous studies have shown a role for alpha class GSTs in reduction of lipid hydroperoxides (224). Therefore, the increase in Gsta4 may have contributed more to lipid peroxidation inhibition. Although 8-isoprostane is a commonly used biomarker for lipid peroxidation *in vivo*, it may not be the best way to assess oxidative stress as such products are quite often only minor end products of peroxidation and may not give a reliable indication of oxidative stress status (225).

As well as lipid peroxidation, DNA damage was investigated using the comet assay and by assessing levels of the oxidative DNA damage marker 8-OH-dG. The data collected from comet assay analysis show that reduced *Gstm1* expression was associated with a small but significant increase in comet tail length, suggesting greater DNA damage in these cells compared to cells transfected with control siRNA. However, this result did not correlate with the results from the 8-OH-dG assay. No change in 8-OH-dG concentration was observed when *Gstm1* expression was reduced, suggesting that lowering *Gstm1* expression does not contribute to oxidative stress mediated DNA damage. The comet assay detects strand breaks and as such may not represent damage resulting solely from oxidative stress. In order to enhance evaluation of oxidative DNA damage in NRK-52E cells, the comet assay could be used in combination with formamidopyrimidine DNA glycosylase (FPG). This enzyme recognizes and removes oxidative DNA base modifications including 8-OH-dG and generates a strand break. By measuring comet tails after incubation with FPG and then subtracting the score obtained from cells without enzyme an indication of oxidative damage could be obtained (216;226). However, it has been suggested that 8-OH-dG may not be a particularly reliable marker of oxidative damage to DNA. The initial products generated from free radical attack on DNA bases are converted into end products such as 8-OH-dG and relative amounts will depend on various reaction rates and conditions leading to variation between samples (213). This may be important when measuring 8-OH-dG *in vivo* but in the current study, all assays were performed in medium from cultured cells where sample to sample variation is less likely. It has also been suggested that it is

unreliable to measure one single reaction product and use this alone as an indicator of oxidative stress (227).

The current study has assessed various markers of oxidative stress and results demonstrated that reduction of *Gstm1* alone was not sufficient to cause increased oxidative damage. It may be that expression of other GSTs in NRK-52E cells compensate for reduced *Gstm1* expression and in doing so, mask any functional significance resulting from *Gstm1* knock-down. However, it could be the case that *Gstm1* is not important for protection against oxidative stress in NRK-52E cells. Previous studies have shown that *Gstm1* expression is localised to kidney tubular epithelium, particularly the collecting ducts (77). Perhaps investigating *Gstm1* in primary cells isolated from the collecting ducts of SHRSP and WKY rats would provide a better model for assessment of the role of *Gstm1* in oxidative stress. However, it may be that the only way to actually assess the function of *Gstm1* is to modulate expression in specific cells of interest *in vivo.*

Chapter 5: MicroRNA Analysis in Rat Congenic Strains

5.1 Introduction

The previous chapters have demonstrated knock-down of gene expression via siRNA mediated RNAi. Analogous to siRNA, microRNAs (miRNA) are a class of *endogenous* short RNA that drive post-transcriptional inhibition of gene expression. These short regulatory RNAs were first described in *C.elegans* with the discovery of *lin-4* and *let-7,* short transcripts that were found to be complementary to regions in the 3' UTR of genes involved in larval development (228;229). MicroRNA induced gene silencing can result from translational repression like that observed in studies with *C.elegans* or from mRNA degradation (230;231). Unlike siRNAs, miRNAs are generated from endogenous transcripts that produce long hairpin structures. These hairpins are further processed to generate 21-22 nt mature miRNAs (147-149). For efficient siRNA mediated gene knock-down, near perfect complementary base pairing is required between the siRNA and target mRNA. However for efficient miRNA activity, it has been suggested that complementary base pairing is most important between the miRNA seed region (6-7nt consecutive nucleotides at 5' end of miRNA) and the 3' UTR of the target gene, with binding at multiple sites (232;233).

5.1.1 MicroRNA Target Prediction

Various computational programs have been developed to improve miRNA target gene identification, including TargetScan, MiRanda and PicTar. Each program uses specific base pairing rules to identify miRNA targets and also take into account cross species conservation of the target site (234). Target sites can be classified according to miRNA interaction. Those target sites that have perfect complementarity with at least the miRNA seed region and substantial pairing at the 3' end can be described as 5' dominant canonical sites. Where perfect base pairing is limited to the 5' seed region, target sites are described as 5' dominant seed only. Targets where there is imperfect pairing to the seed region but considerable pairing to the 3' end of the miRNA are described as 3' compensatory target sites (234;235). Following on from target identification it is important then to try and validate the miRNA/mRNA target pair (236).

5.1.2 Microarray Analysis of Gene Expression

It may be possible to further enhance miRNA target identification by combining the computational systems described with microarray analysis of gene expression. Microarray analysis of rat parental and congenic strains was utilised previously by our group, leading to the identification of *Gstm1* as a positional and potentially functional target in blood pressure regulation (69). This work was performed in 16 week old animals, since then microarrays have been carried out in kidney tissue from SHRSP, WKY and congenic animals at 5 weeks and 21 weeks of age, allowing for examination of changes in gene expression over time.

As well as the 2c* congenic strain, other chromosome 2 congenic strains have been generated. The SP.WKYGla2a (2a) strain is of SHRSP background with a region of chromosome 2 incorporating 2 BP QTLs transferred from WKY (70). The SP.WKYGla2k (2k) strain is of SHRSP background with a 10 cM region of chromosome 2 transferred from WKY (237). The 2a congenic encompasses both 2c* and 2k congenic regions and the 2c* and 2k regions partially overlap as shown in Figure 5.1. The 2a and 2k strains demonstrate significantly lower baseline and salt-loaded blood pressure, however the 2c* retains salt sensitivity (237). Thus the region that differs between the 2c* and 2k likely contains genes responsible for salt sensitivity. The genes encoding miR-9-1 (rno-miR-9-1) and miR-137 (rno-miR-137) map to the 2c* and 2k congenic regions respectively and may play a role in baseline blood pressure regulation (miR-9-1) and salt-sensitive hypertension (miR-137).

Ingenuity Pathway Analysis (IPA) is a web-based data analysis tool and knowledge database that can be used to investigate relationships between gene expression data generated from microarray and other high throughput analyses.

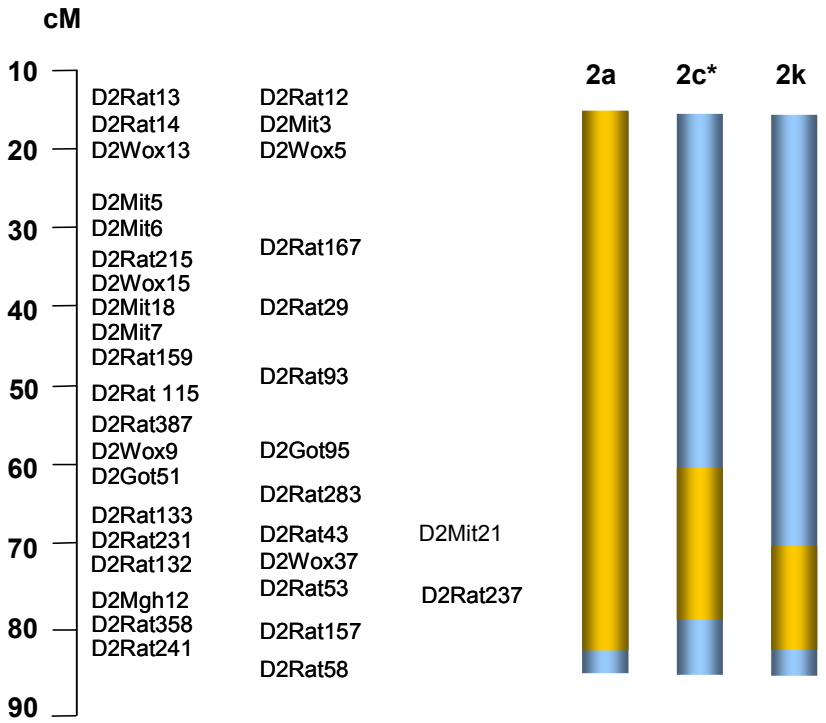

Figure 5.1 Rat chromosome 2 congenic sub-strains

Chromosome 2 congenic strains were generated by transferring chromosomal regions from WKY onto the SHRSP background. Yellow bars represent regions of WKY homozygosity. Blue bars represent regions of SHRSP homozygosity.

Adapted from (237).

Ingenuity Pathway Analysis was combined with microarray analysis of salt-loaded 21 week SHRSP, WKY and 2a strains to identify genes involved in salt sensitivity (237). Using IPA, microarray data can potentially be integrated with results from miRNA target prediction to identify genes which may be differentially expressed as a result of miRNA targeting.

5.2 Aims

- To investigate the expression of miR-9-1 and miR-137 in kidneys from SHRSP, WKY and congenic rat strains at 5 weeks (post weaning), 16 weeks (adult) and 21 weeks (post salt challenge)

- To identify potential miRNA gene targets and assess differential expression of these targets in the microarray datasets previously generated

- To evaluate the ability of precursor miRNA molecules and miRNA inhibitors to drive up and knock-down miRNA expression in NRK-52E cells

- To assess expression of predicted miRNA gene targets in rat kidney tissue and in NRK-52E cells following modulation of miRNA expression

5.3 Materials and Methods

5.3.1 Transfection of NRK-52E Cells

NRK-52E cells were transfected with Pre-miR™ miRNA precursors and Anti-miR™ miRNA inhibitors for rno-miR-9 and rno-miR-137 (Applied Biosystems) using the siPORT™ *Amine* transfection protocol outlined in section 2.3. All reagent volumes and incubation times were the same as those described in section 2.3, replacing siRNA with 30nM to 50nM of Pre-miR™ or Anti-miR™. To assess transfection efficiency, cells were transfected with Cy™3 dye-labelled Pre-miR™

or Anti-miR™ negative control sequences and transfection levels were assessed by fluorescence microscopy. All transfection experiments were performed in triplicate and included the following controls: untransfected cells (UTF), cells treated with transfection reagent only (TFC) and cells treated with either Pre-miR™ negative control (Pre-CTL) or Anti-miR™ negative control (Anti-CTL).

5.3.2 MicroRNA Extraction

The miRNeasy Mini Kit (Qiagen) was used for the purification of total RNA (including miRNA) from NRK-52E cells and frozen rat kidney tissue. Cultured cells and tissues were first homogenized in QIAzol® lysis reagent (phenol and guanidine thiocyanate solution). Each frozen kidney section was transferred into 5 ml of cold QIAzol® lysis reagent and homogenised with a Polytron 2100 rotor homogeniser at full speed. The homogenate was split into 700 µl aliquots. NRK-52E cells (cultured in 6 well plates) were rinsed twice with PBS and then 700 µl QIAzol® lysis reagent was added to each well. Cells were homogenized by scraping with a pipette tip, transferred to a 1.5 ml centrifuge tube and vortexed briefly.

Cell/tissue homogenates were incubated at room temperature for 5 minutes, followed by the addition of 140 µl chloroform to each sample. Samples were mixed by shaking vigorously for 15 seconds and incubated at room temperature for 2-3 minutes. This was followed by centrifugation at 12000 g for 15 minutes at 4°C to separate the homogenate into aqueous and organic phases. The upper aqueous layer was transferred to a fresh 1.5 ml centrifuge tube and 1.5 volumes of 100% ethanol was added and mixed by pipetting. A maximum of 700 µl was then applied to the RNeasy Mini spin column and centrifuged at 8000 g for 15 seconds. The flow-through was discarded and the remaining sample was applied to the column and centrifuged as before. The column was washed with 700 µl buffer RWT, centrifuged at 8000 g for 15 seconds and the flow-through discarded. The column was then washed with 500 µl buffer RPE and centrifuged at 8000 g for 15 seconds. This wash step was repeated but with centrifugation at 8000 g for 2 minutes. The flow-through was discarded and columns were centrifuged again for 1 minute to dry the column membrane.

To elute RNA, nuclease-free water was added to the column membrane. For tissue RNA samples, 40 µl of nuclease-free water was added to the column membrane and centrifuged for 1 minute at 8000 g. This elution step was repeated with 40 µl nuclease-free water and centrifuged again at 8000 g for 1 minute. For cell RNA samples, 40 µl of nuclease-free water was added to the column membrane and centrifuged at 8000 g for 1 minute. The flow-through (containing RNA) was applied to the column membrane again and centrifuged at 8000 g for 1 minute. All RNA samples were subjected to DNase treatment as described in section 2.6.1 and quantified as described in section 2.6.2.

5.3.3 MicroRNA Reverse Transcription

The TaqMan® MicroRNA Reverse Transcription Kit (Applied Biosystems) was used to generate cDNA for analysis of miRNA expression with miRNA specific primers and TaqMan® MicroRNA Assays. Each RNA sample was diluted in nuclease-free water to 2 ng/µl and 5 µl of this was used in each reverse transcription reaction. The reverse transcription reaction mix was prepared as follows:

- 1.5 µl 10X RT Buffer
- 0.15 µl dNTP mix
- 1 µl MultiScribe reverse transcriptase (50 U/µl)
- 0.19 µl RNase inhibitor (20 U/µl)
- 4.16 µl nuclease-free water

This was added to 5 µl of the diluted RNA sample and 3 µl of the specific miRNA primer (supplied with the TaqMan® MicroRNA Assay, Applied Biosystems) to give a final reaction volume of 15 µl. Reverse transcription was carried out in a 96 well plate using the following thermal cycling parameters:

- 30 minutes at 16°C
- 30 minutes at 42°C
- 5 minutes at 85°C

cDNA samples were stored at -20°C.

5.3.3.1 TaqMan® MicroRNA Assays

Quantitative real-time PCR was performed using TaqMan® MicroRNA Assays (Applied Biosystems) for quantification of rat miR-9-1 (Assay ID: 000583, hsa-miR-9) and rat miR-137 (Assay ID: 001129, mmu-miR-137). Expression of each miRNA was normalised to U87 (control miRNA, Assay ID: 001712) and expression levels were determined using the comparative C_T method ($2^{-\Delta\Delta Ct}$) (171). For each miRNA assay, a 20 µl simplex reaction was prepared in a 96 well plate as follows:

- 10 µl 2X TaqMan® Universal PCR master mix
- 1 µl 20X TaqMan® MicroRNA Assay
- 7.6 µl nuclease-free water
- 1.2 µl RT product

Each reaction was performed in duplicate and subjected to the thermal cycling parameters described in section 2.7.1.

5.3.4 miR-9 Target Genes: mRNA Expression

Quantitative RT-PCR was performed on cDNA using TaqMan Gene Expression Assays (Applied Biosystems) for the following genes:

Gene ID	Gene Name	Assay ID
Adamts1	ADAM metallopeptidase with thrombospondin type 1 motif, 1	Rn01646120_m1
Comt	Catechol-O-methyltransferase	Rn00561037_m1
Ctsb	Cathepsin B	Rn00575030_m1
Igfbp3	Insulin-like growth factor binding protein 3	Rn01401281_m1
Igsf11	Immunoglobulin superfamily, member 11	Rn01439426_m1
Scly	Selenocysteine lyase	Rn01427211_m1
Trim35	Tripartite motif-containing 35	Rn01534954_m1

The expression of each gene of interest was normalised to *β-actin* expression and all assays were performed in simplex as described in section 2.7.1.

5.4 Results

5.4.1 Rat Kidney Expression of miR-9-1 and miR-137

The expression levels of miR-9-1 and miR-137 were examined in kidney tissue from SHRSP, WKY and congenic strains at various time-points to assess whether miRNA expression differs between strains. Figure 5.2 shows the levels of miR-9 expression in SHRSP, 2c* and WKY kidney at 5, 16 and 21 weeks of age (n=4). No significant change in miR-9 levels was observed at any time-point in SHRSP. However, a significant decrease in miR-9 expression was observed between 5 and 16 weeks of age in 2c* and WKY animals, $p<0.05$. Figure 5.3 shows the levels of miR-137 expression in SHRSP, WKY and 2k kidney at 5, 16 and 21 weeks of age and at 21 weeks with salt (n=4). No significant change in miR-137 expression was observed in 2k or WKY strains regardless of time-point or salt loading. However, a significant increase in miR-137 expression was observed in 21 week old salt loaded SHRSP compared to 21 week old SHRSP animals without salt, $p<0.05$.

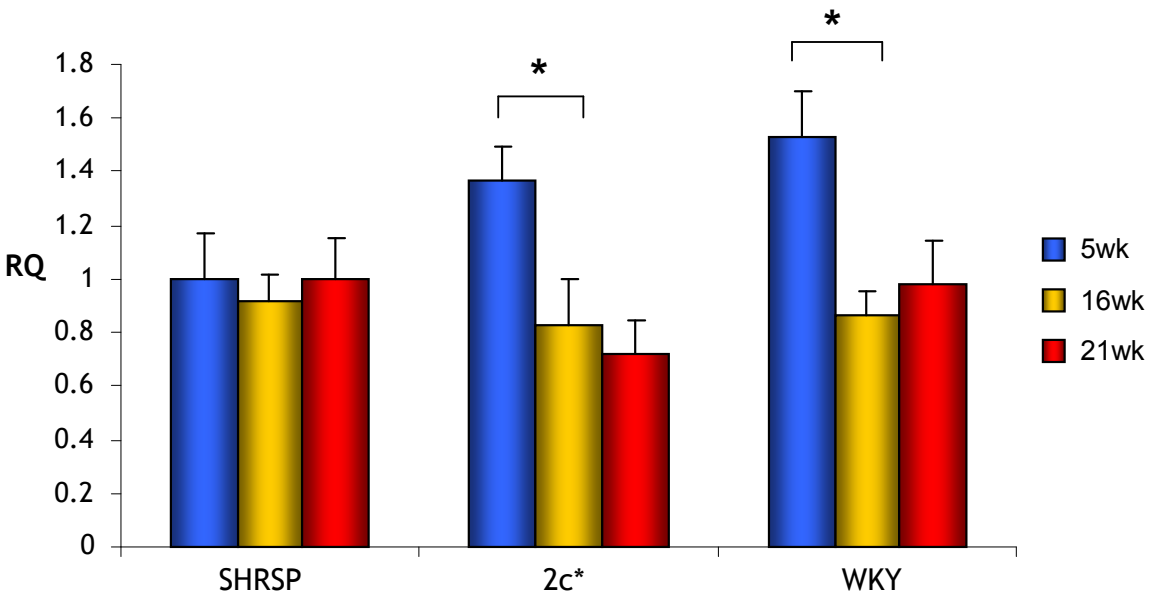

Figure 5.2 Kidney miR-9-1 expression levels

TaqMan® qRT-PCR analysis of miR-9-1 expression in rat kidney shows that expression of miR-9-1 was unchanged across all time-points in SHRSP. Expression of miR-9-1 was significantly reduced in 16 week 2c* and WKY kidney compared to 5 week, n=4, *$p<0.05$.

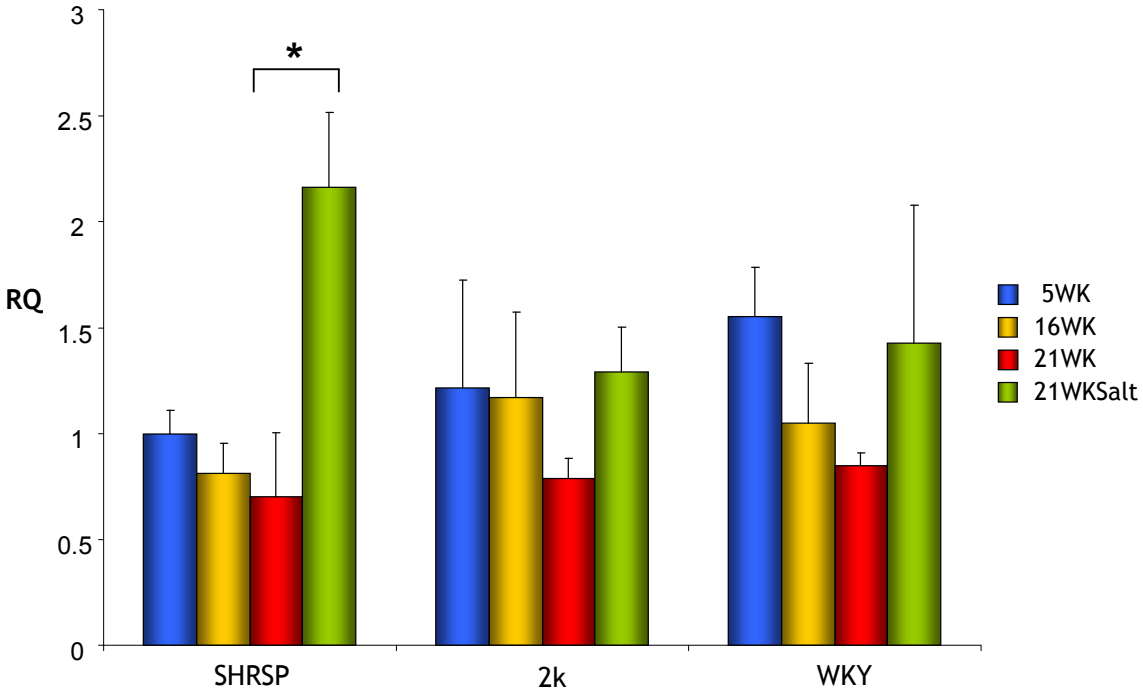

Figure 5.3 Kidney miR-137 expression levels

TaqMan® qRT-PCR analysis of miR-137 expression in rat kidney shows that expression of miR-137 was unchanged across all time-points in 2k and WKY kidney. Expression of miR-137 was significantly increased in 21 week salt loaded SHRSP compared to 21 week SHRSP without salt, n=4, *$p<0.05$.

5.4.2 *In Vitro* Modulation of miR-9-1 and miR-137 Expression

To modulate expression of miR-9-1 and miR-137 *in vitro*, Pre-miR™ miRNA precursors or Anti-miR™ miRNA inhibitors were used. The transfection efficiency of NRK-52E cells for transfection of Pre-miR™ and Anti-miR™ molecules was assessed using Cy™3 labelled control versions of both. Figure 5.4 shows a representative Cy™3 labelled control Pre-miR™ transfection experiment. Panel B demonstrates that no fluorescence is generated when NRK-52E cells are subjected to a mock transfection (treated with transfection reagent only). However, when cells are treated with 30nM Cy™3 labelled control Pre-miR™, fluorescence is detected throughout (panel C). The level of fluorescence observed indicates that at least 70% transfection efficiency was achieved. Figure 5.5 shows a representative Cy™3 labelled control Anti-miR™ transfection experiment. As before, cells subjected to a mock transfection do not generate fluorescence (Figure 5.5, panel B). Initial experiments performed with 30nM Cy™3 labelled control Anti-miR™ did not achieve the levels of transfection observed with the Pre-miR™. However, when increased to 50nM, similar levels of transfection efficiency were achieved, as shown in Figure 5.5, panel C.

Following confirmation of efficient transfection of NRK-52E cells with control Pre-miR™ and Anti-miR™, transfections were repeated with miR-9-1 and miR-137 Pre-miR™ and Anti-miR™ molecules. The ability to over-express each miRNA was evaluated first. Figure 5.6 is representative of 4 individual experiments performed in triplicate. The top panel of Figure 5.6 shows the results obtained from transfection of NRK-52E cells with 30nM Pre-miR-9. In this example, transfection with Pre-miR-9 resulted in a 1928 fold increase in miR-9-1 expression compared to cells transfected with control Pre-miR (Pre-CTL), $p<0.0001$. Across the 4 experiments, expression of miR-9 was increased up to 2629 fold. The bottom panel of Figure 5.6 shows the results obtained from transfection of NRK-52E cells with 30nM Pre-miR-137. In this example, miR-137 expression was increased 2278 fold in cells transfected with Pre-miR-137 compared to Pre-CTL cells, $p<0.0001$.

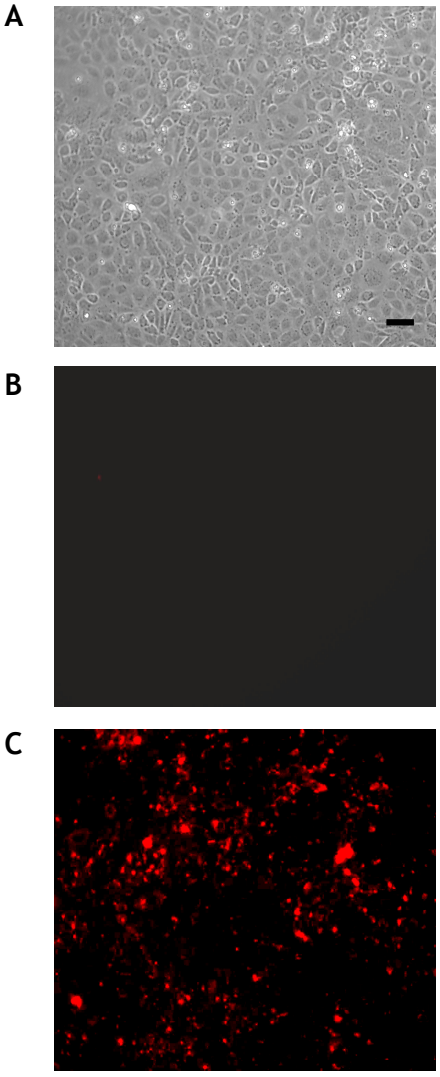

Figure 5.4 Pre-miR transfection efficiency of NRK-52E cells

Panel A: Transmitted light image of NRK-52E cells. B: Mock transfected cells showing no background fluorescence. C: Cells transfected with 30nM Cy™3 labelled Pre-miR. Comparison with transmitted light image of the same field (A) suggests high transfection efficiency. Scale bar: 50μm

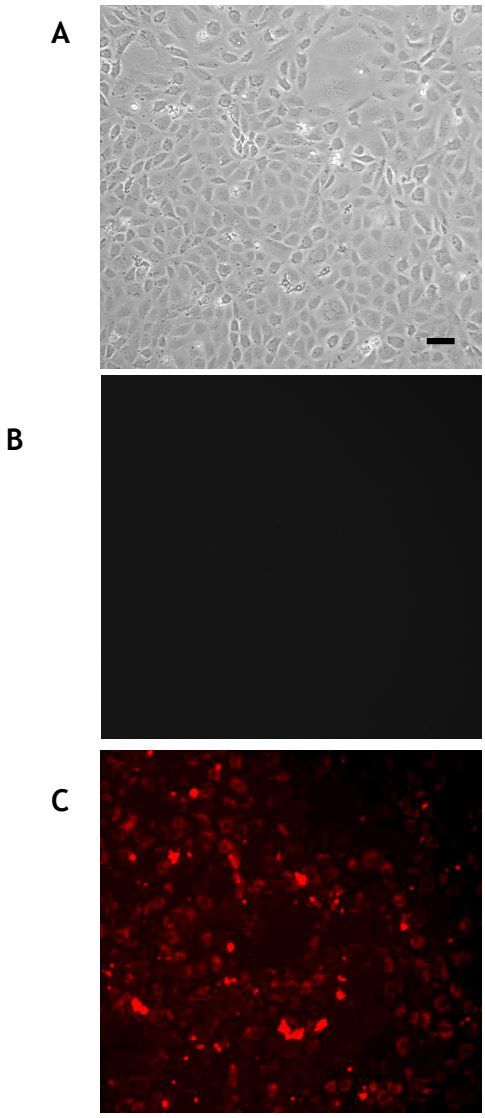

Figure 5.5 Anti-miR transfection efficiency of NRK-52E cells

Panel A: Transmitted light image of NRK-52E cells. B: Mock transfected cells showing no background fluorescence. C: Cells transfected with 50nM Cy™3 labelled Anti-miR. Comparison with transmitted light image of the same field (A) suggests high transfection efficiency. Scale bar: 50µm

The ability to inhibit miR-9-1 and miR-137 expression was then assessed by transfecting NRK-52E cells with 50nM of each miRNA inhibitor. Figure 5.7 is representative of 4 individual experiments performed in triplicate. The top panel indicates that miR-9-1 expression was not reduced in cells transfected with Anti-miR-9 as no significant change in expression was detected. The bottom panel of Figure 5.7 shows the results obtained from transfection of NRK-52E cells with Anti-miR-137. Expression of miR-137 was not inhibited although expression levels were found to be highly variable.

5.4.3 Target Identification and Ingenuity Pathway Analysis

Target genes were identified by searching for perfect complementarity between miR seed regions (miR-9-1 and miR-137) and the 3' UTR of genes represented on the microarray chips used previously. The seed region was designated as a consecutive stretch of 6 nucleotides starting from the second nucleotide at the 5' end of the mature miRNA.

```
                    5' CCAAAG 3'
                       ||||||
3' AGUAUGUCGAUCUAUUGGUUUCU 5'  miR-9-1
```

```
                    5' GCAATA 3'
                       ||||||
3' GAUGCGCAUAAGAAUUCGUUAUU 5'  miR-137
```

The sequence marked in red was used to search through 3' UTRs for regions that would base pair with each miRNA. A list of predicted gene targets for miR-9-1 and miR-137 was generated (see Table A1 and A2 in the appendix for full list of genes) and uploaded to the Ingenuity Pathway Analysis (IPA) website.

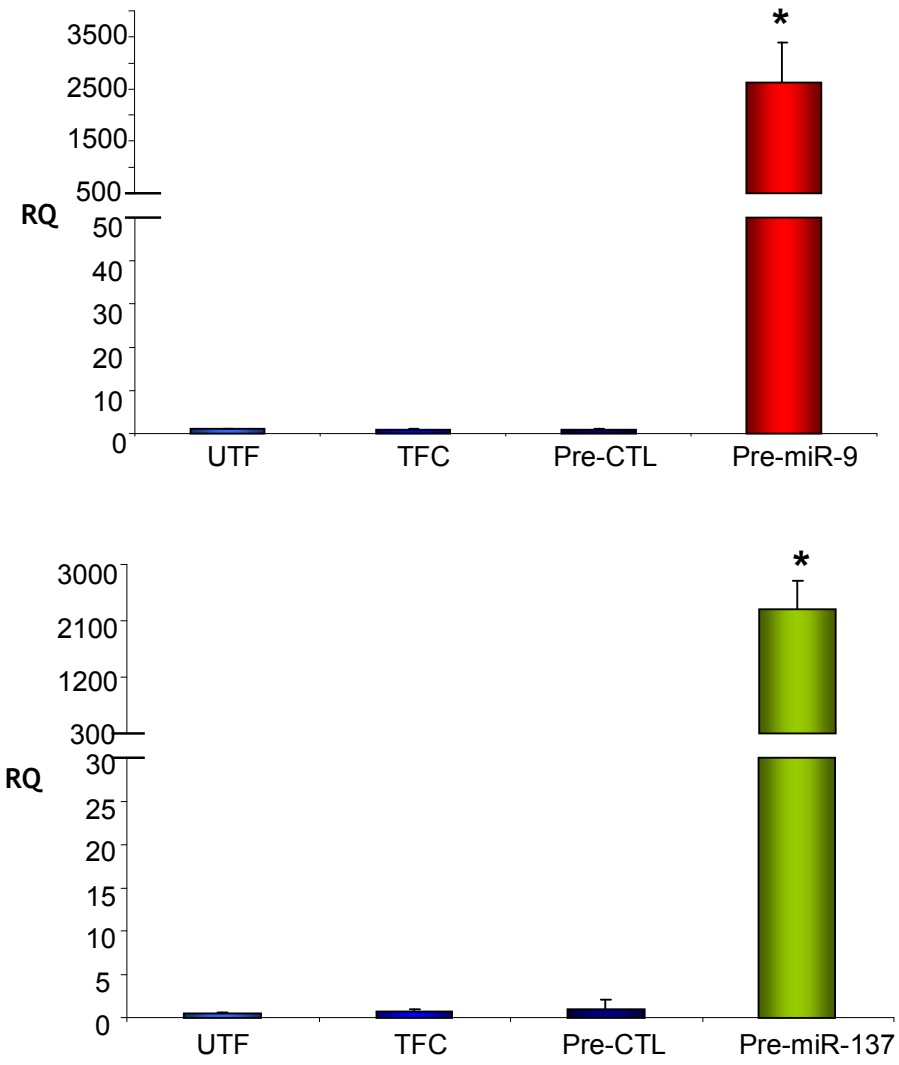

Figure 5.6 Over-expression of microRNAs in NRK-52E cells

TaqMan® qRT-PCR analysis of miRNA expression in NRK-52E cells following transfection with Pre-MiR. Top panel: Following transfection of cells with 30nM Pre-miR-9, miR-9-1 expression was significantly increased (~1900 fold) compared to Pre-CTL (n=1 experiment performed in triplicate and is representative of 4 experiments in total) *p<0.0001 vs Pre-CTL (ANOVA + Dunnett's post-hoc test). Bottom panel: Following transfection of cells with 30nM Pre-miR-137, miR-137 expression was significantly increased (~2000 fold) compared to Pre-CTL (n=1 experiment performed in triplicate and is representative of 4 experiments in total) *p<0.0001 vs Pre-CTL (ANOVA + Dunnett's post-hoc test).

UTF: untransfected cells, TFC: mock transfected cells, Pre-CTL: Control Pre-miR transfected cells

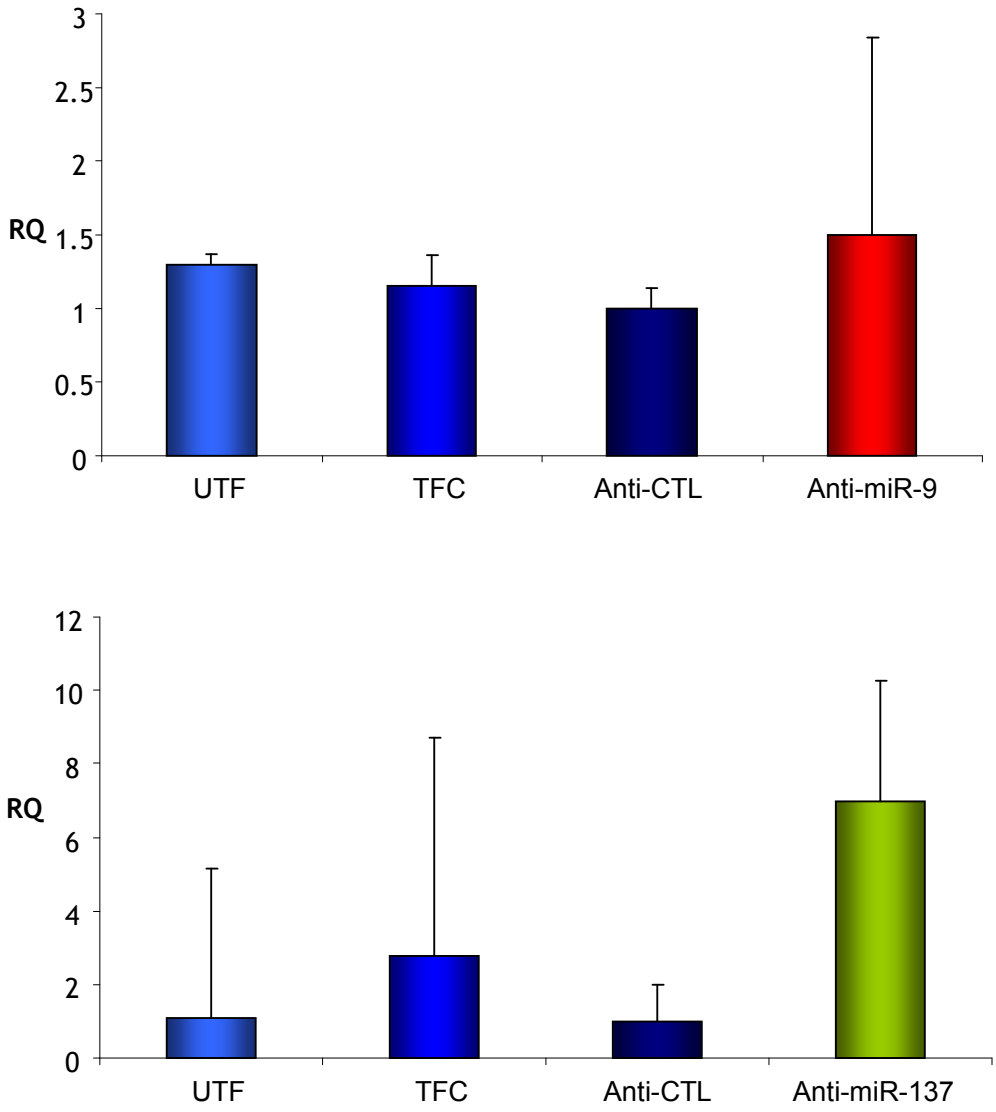

Figure 5.7 Effect of Anti-miR transfection on miRNA expression in NRK52E cells

TaqMan® qRT-PCR analysis of miRNA expression in NRK-52E cells following transfection with Anti-miR. Top panel: Following transfection of cells with 50nM Anti-miR-9, no significant change in miR-9-1 expression was observed compared to Anti-CTL (n=1 experiment performed in triplicate and is representative of 4 experiments in total). Bottom panel: Following transfection of cells with 50nM Anti-miR-137, no significant change in miR-137 expression was observed compared to Anti-CTL (n=1 experiment performed in triplicate and is representative of 4 experiments in total).

UTF: untransfected cells, TFC: mock transfected cells, Anti-CTL: Control Anti-miR transfected cells

Using IPA, the list of targets was combined with gene expression datasets generated from 5 week, 16 week, 21 week and 21 week plus salt kidney microarray analysis carried out previously. The predicted targets identified for miR-9-1 were combined with SHRSP, WKY and congenic microarray datasets (16 week versus 5 week) to identify genes that were up-regulated in both the congenic and WKY datasets but not in the SHRSP dataset (as kidney miR-9-1 expression was lower in 16 week WKY and congenic but was unchanged in SHRSP). The predicted targets identified for miR-137 were combined with SHRSP, WKY and congenic microarray datasets (21 week versus 21 week plus salt) to identify genes that were down-regulated in the SHRSP comparison but were unchanged in both WKY and congenic datasets (as SHRSP kidney miR-137 expression was greater in 21 week old animals with salt than in 21 week old animals without but was unchanged in the congenic and WKY). Table 5.1 contains information regarding miR-9-1 seed/target interactions of gene targets identified by IPA. Of the list of targets uploaded, 7 were found that were up-regulated and common to both the congenic and WKY (Figure 5.8) but were unchanged in the SHRSP (Figure 5.9). The following genes were identified: ADAM metallopeptidase with thrombospondin type 1 motif, 1 (*Adamts1*), Cathepsin B (*Ctsb*), Catechol-O-methyltransferase (*Comt*), Insulin like growth factor binding protein 3 (*Igfbp3*), Immunoglobulin superfamily, member 11 (*Igsf11*), Selenocysteine lyase (*Scly*) and Tripartite motif-containing 35 (*Trim35*). Table 5.2 outlines the miR-9-1 gene targets identified by IPA. However, analysis of the miR-137 targets failed to find any genes that were down-regulated in the SHRSP 21 week/21 week salt dataset and unchanged in both congenic and WKY datasets.

5.4.4 Expression of miR-9-1 Target Genes

The mRNA expression levels of the gene targets identified by IPA were examined in kidney tissue from SHRSP, WKY and congenic strains at 5 weeks and 16 weeks of age (n=4 for each target gene) and in NRK-52E cells transfected with Pre-miR-9-1 (each figure is representative of 4 individual experiments performed in triplicate).

RefSeq	Gene	No. of Seeds	Position in 3' UTR	A1	M8
NM_024400	*Adamts1*	1	230	T	C
NM_012531	*Comt*	1	212	G	G
NM_022597	*Ctsb*	1	337	G	T
NM_012588	*Igfbp3*	1	209	T	G
NM_001013120	*Igsf11*	1	1197	A	C
NM_001007755	*Scly*	2	601	T	G
			756	G	G
NM_001025142	*Trim35*	1	106	T	C

Table 5.1 Seed site information for predicted miR-9-1 targets
A1: nucleotide at first position downstream of the seed match, M8: nucleotide at first position upstream of the seed match

			Congenic (16wk V 5wk)		WKY (16wk V 5wk)		SHRSP (16wk V 5wk)	
RefSeq	Gene	Location	Mean Difference	p-value	Mean Difference	p-value	Mean Difference	p-value
NM_024400	*Adamts1*	11q11	1.031	0.0125	1.106	0.0054	1.695	0.2055
NM_012531	*Comt*	11q23	1.141	0.0025	1.907	$5.74E^{-6}$	1.056	0.0992
NM_022597	*Ctsb*	15p12	1.823	0.0173	1.591	$4.13E^{-6}$	1.474	0.1278
NM_012588	*Igfbp3*	14q21	1.310	0.0515	3.002	$7.63E^{-6}$	1.066	0.4538
NM_001013120	*Igsf11*	11q21	1.037	0.0218	1.802	$5.40E^{-6}$	0.751	0.2495
NM_001007755	*Scly*	9q36	0.775	0.0124	1.107	$2.10E^{-4}$	0.281	0.7195
NM_001025142	*Trim35*	15p12	1.552	0.0090	2.172	0.0011	1.893	0.0803

Table 5.2 Microarray expression data: predicted miR-9-1 targets

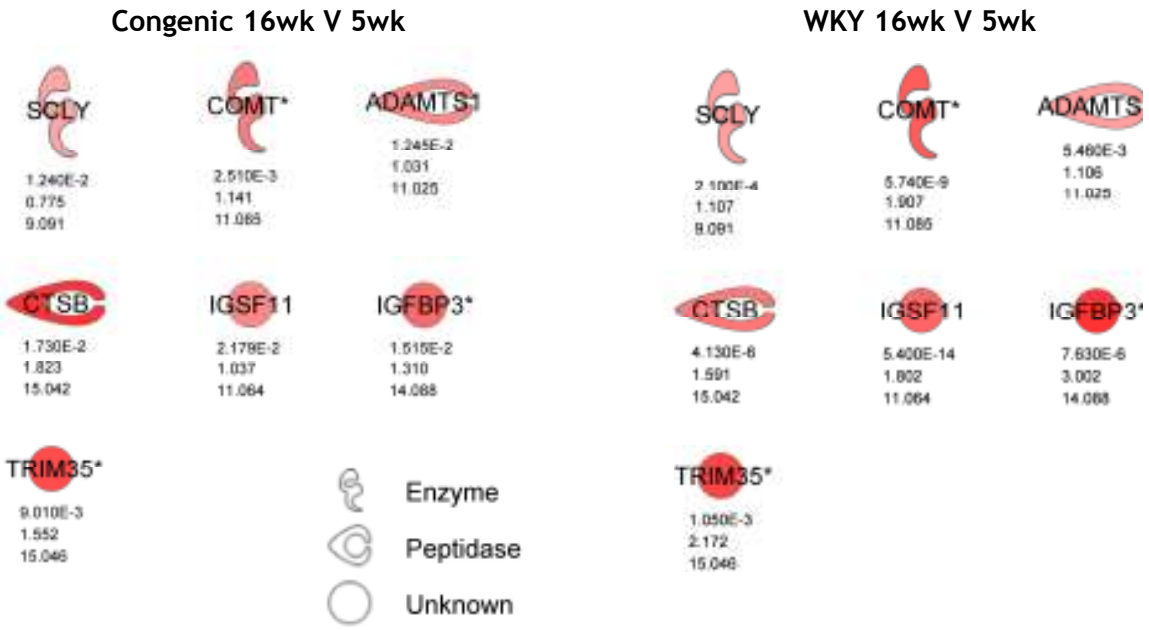

Figure 5.8 Ingenuity Pathway Analysis of congenic and WKY microarray datasets

Data output from Ingenuity Pathway Analysis of predicted miR-9-1 target genes. Seven targets were identified that were up-regulated in 16 week versus 5 week datasets and common to both congenic and WKY strains. Red represents up-regulation of genes and colour intensity represents the significance of up-regulation.

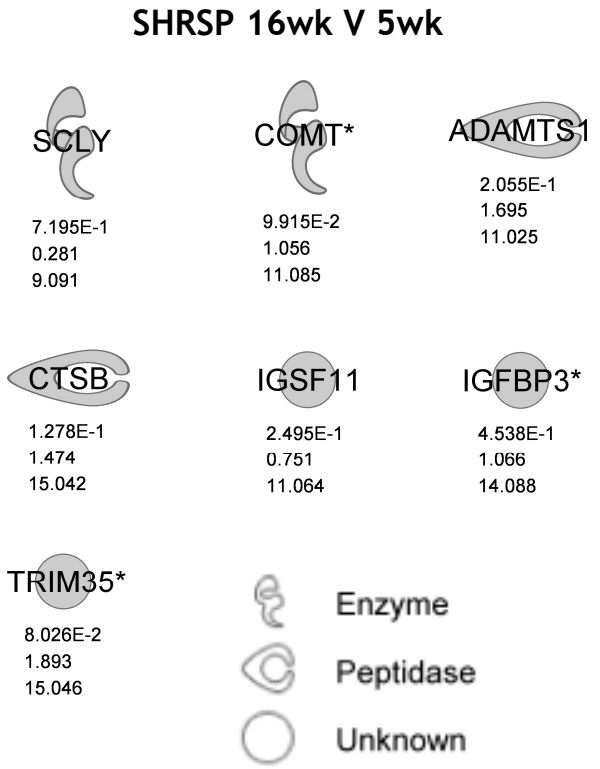

Figure 5.9 Ingenuity Pathway Analysis of SHRSP microarray datasets

Data output from Ingenuity Pathway Analysis of predicted miR-9-1 target genes. Data shows that predicted miR-9-1 targets are not differentially expressed in 16 week versus 5 week SHRSP microarray dataset.

As miR-9-1 expression was found to be down-regulated in 16 week compared to 5 week old 2c* and WKY strains, it would be expected that miR-9-1 target genes would be up-regulated in these strains at 16 weeks compared to 5 weeks. Conversely, target gene expression would be expected to go down in NRK-52E cells where miR-9-1 has been over-expressed. The functions of each gene target are summarised in Table 5.3.

5.4.4.1 Adamts1

Kidney mRNA expression of *Adamts1* showed no change between 5 and 16 week old 2c* but was significantly up-regulated by 6.5 fold in 16 week old WKY compared to 5 week, $p<0.05$ (Figure 5.10, top panel). No significant change in expression was observed between 5 and 16 week old SHRSP. The bottom panel of Figure 5.10 shows *Adamts1* expression in NRK-52E cells following over-expression of miR-9-1. No significant change in *Adamts1* expression was observed in NRK-52E cells treated with Pre-miR-9.

5.4.4.2 Comt

No significant difference in *Comt* expression was observed between 5 week and 16 week time-points in SHRSP and WKY strains (Figure 5.11, top panel). However a significant 1.3 fold increase in expression was detected in 16 week 2c* compared to 5 week, $p<0.05$. Over-expression of miR-9-1 in NRK-52E cells had no significant effect on *Comt* expression (Figure 5.11, bottom panel).

5.4.4.3 Ctsb

No significant difference in *Ctsb* mRNA expression was observed between 5 and 16 week time-points in any of the strains (Figure 5.12, top panel). Expression of *Ctsb* in NRK-52E cells showed no significant difference following transfection with Pre-miR-9 (Figure 5.12, bottom panel).

Gene	Function	Refs
Adamts1	Binds VEGF and inhibits VEGFR2 phosphorylation. Inhibits endothelial cell proliferation. Inhibits tumour growth and has anti-angiogenic function.	(238-240)
Comt	Catalyses the methylation and inactivation of catecholamine neurotransmitters. Possible role in BP regulation in SHR and Dahl S rats. Decreased levels have been shown to associate with pre-eclampsia	(241-243)
Ctsb	Role in cell proliferation, tumour development and tumour progression. Possible target for cancer therapy.	(244;245)
Igfbp3	Role in growth, proliferation and apoptosis. Shown to have anti-proliferative and pro-apoptotic functions	(246)
Igsf11	Preferentially expressed in brain and testes. Regulates cell growth and is elevated in various cancers.	(247;248)
Scly	Metabolism of L-selenocysteine	(249)
Trim35	Member of the tripartite motif containing family with roles in cell growth, proliferation and apoptosis	(250;251)

Table 5.3 Functional information of each miR-9-1 predicted target gene identified by IPA

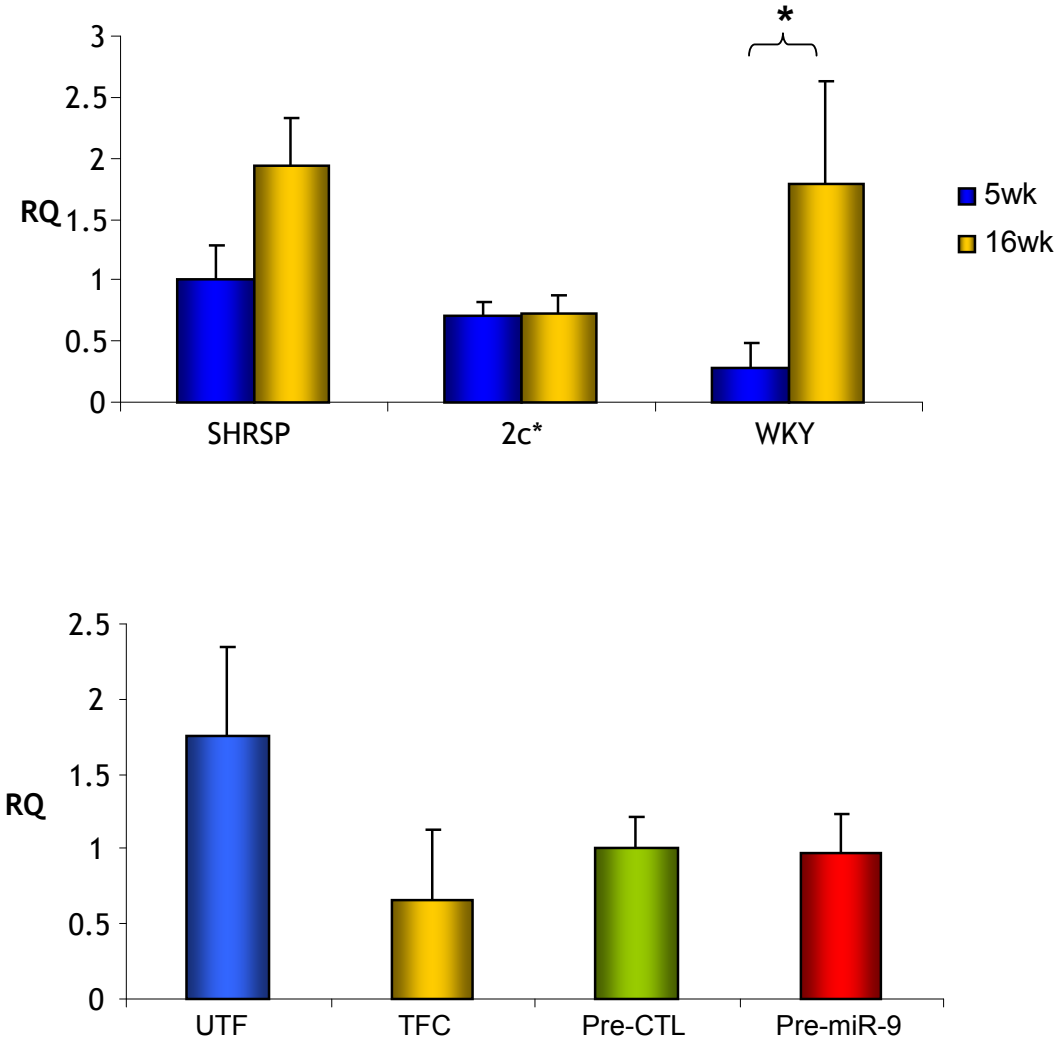

Figure 5.10 *Adamts1* mRNA expression

TaqMan® qRT-PCR analysis of *Adamts1* mRNA expression. Top panel: Expression of *Adamts1* in kidney of SHRSP, congenic and WKY strains at different time-points. No significant change in expression was observed in SHRSP or congenic but was significantly increased in 16 week WKY compared to 5 week (n=4) *p<0.05 vs 5wk WKY (2 sample t-test). Bottom panel: *Adamts1* expression following transfection of NRK-52E cells with 30nM control (Pre-CTL) or miR-9 precursor (Pre-miR-9). No significant change in expression was observed (n=1 experiment performed in triplicate and is representative of 4 experiments in total).

UTF: untransfected cells, TFC: mock transfected cells, Pre-CTL: Control Pre-miR transfected cells

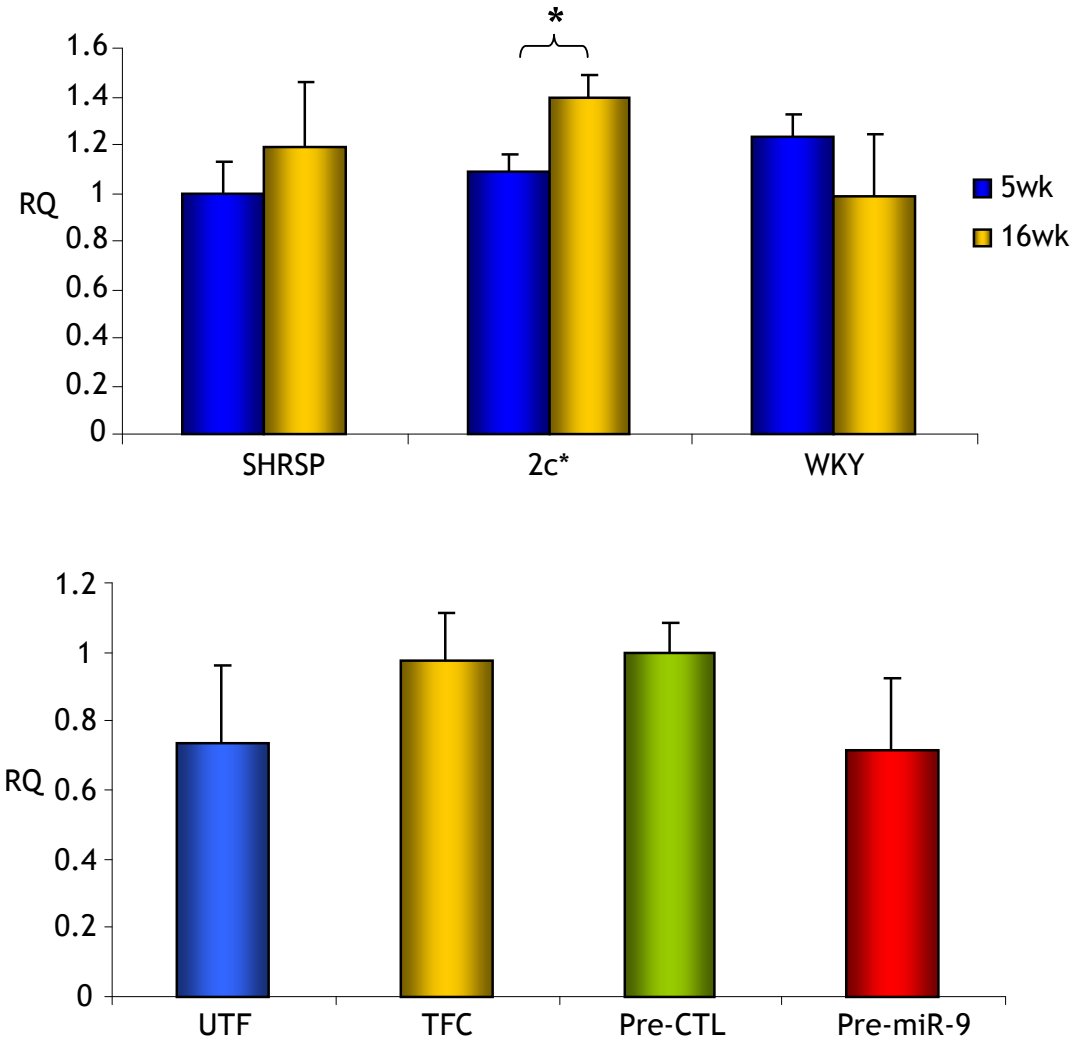

Figure 5.11 *Comt* mRNA expression

TaqMan® qRT-PCR analysis of *Comt* mRNA expression. Top panel: Expression of *Comt* in kidney of SHRSP, congenic and WKY strains at different time-points. No significant change in expression was observed in SHRSP or WKY but was significantly increased in 16 week congenic compared to 5 week (n=4) *$p<0.05$ vs 5wk 2c* (2 sample t-test). Bottom panel: *Comt* expression following transfection of NRK-52E cells with 30nM control (Pre-CTL) or miR-9 precursor (Pre-miR-9). No significant change in expression was observed (n=1 experiment performed in triplicate and is representative of 4 experiments in total).

UTF: untransfected cells, TFC: mock transfected cells, Pre-CTL: Control Pre-miR transfected cells

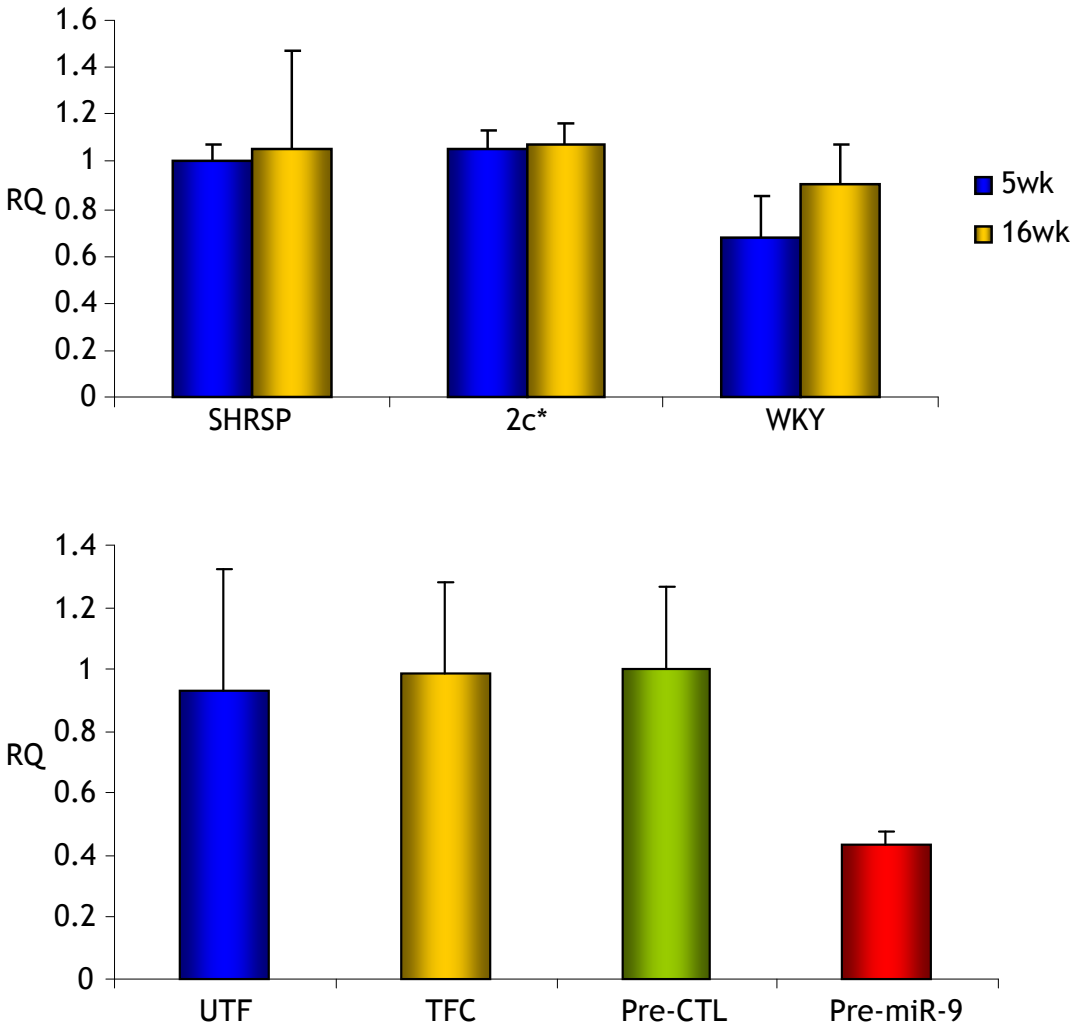

Figure 5.12 *Ctsb* mRNA expression

TaqMan® qRT-PCR analysis of *Ctsb* mRNA expression. Top panel: Expression of *Ctsb* in kidney of SHRSP, congenic and WKY strains at different time-points. No significant change in expression was observed in any of the strains, regardless of time-point (n=4). Bottom panel: *Ctsb* expression following transfection of NRK-52E cells with 30nM control (Pre-CTL) or miR-9 precursor (Pre-miR-9). No significant change in expression was observed (n=1 experiment performed in triplicate and is representative of 4 experiments in total).

UTF: untransfected cells, TFC: mock transfected cells, Pre-CTL: Control Pre-miR transfected cells

5.4.4.4 Igfbp3

No significant difference in *Igfbp3* expression was observed between 5 and 16 week time-points in any of the strains (Figure 5.13, top panel). No significant change in *Igfbp3* expression was observed in Pre-miR-9 transfected NRK-52E cells when compared to Pre-CTL transfected cells. However, expression was markedly reduced, by approximately 10 fold in all cell groups treated with transfection reagent compared to untransfected cells, $p<0.05$ (Figure 5.13, bottom panel).

5.4.4.5 Igsf11

No significant change in expression of *Igsf11* was observed in SP or WKY between 5 week and 16 week. A significant decrease in *Igsf11* expression of approximately 2 fold was observed in 16 week 2c* compared to 5 week, $p<0.05$ (Figure 5.14). No detectable level of *Igsf11* expression was found in NRK-52E cells.

5.4.4.6 Scly

No significant difference in *Scly* expression was observed between 5 and 16 week time-points in any of the strains (Figure 5.15, top panel). No change in expression was observed in NRK-52E cells transfected with Pre-miR-9 compared to Pre-CTL transfected cells (Figure 5.15, bottom panel).

5.4.4.7 Trim35

No significant change in *Trim35* expression was observed between 5 and 16 week time-points in any of the strains. (Figure 5.16, top panel).

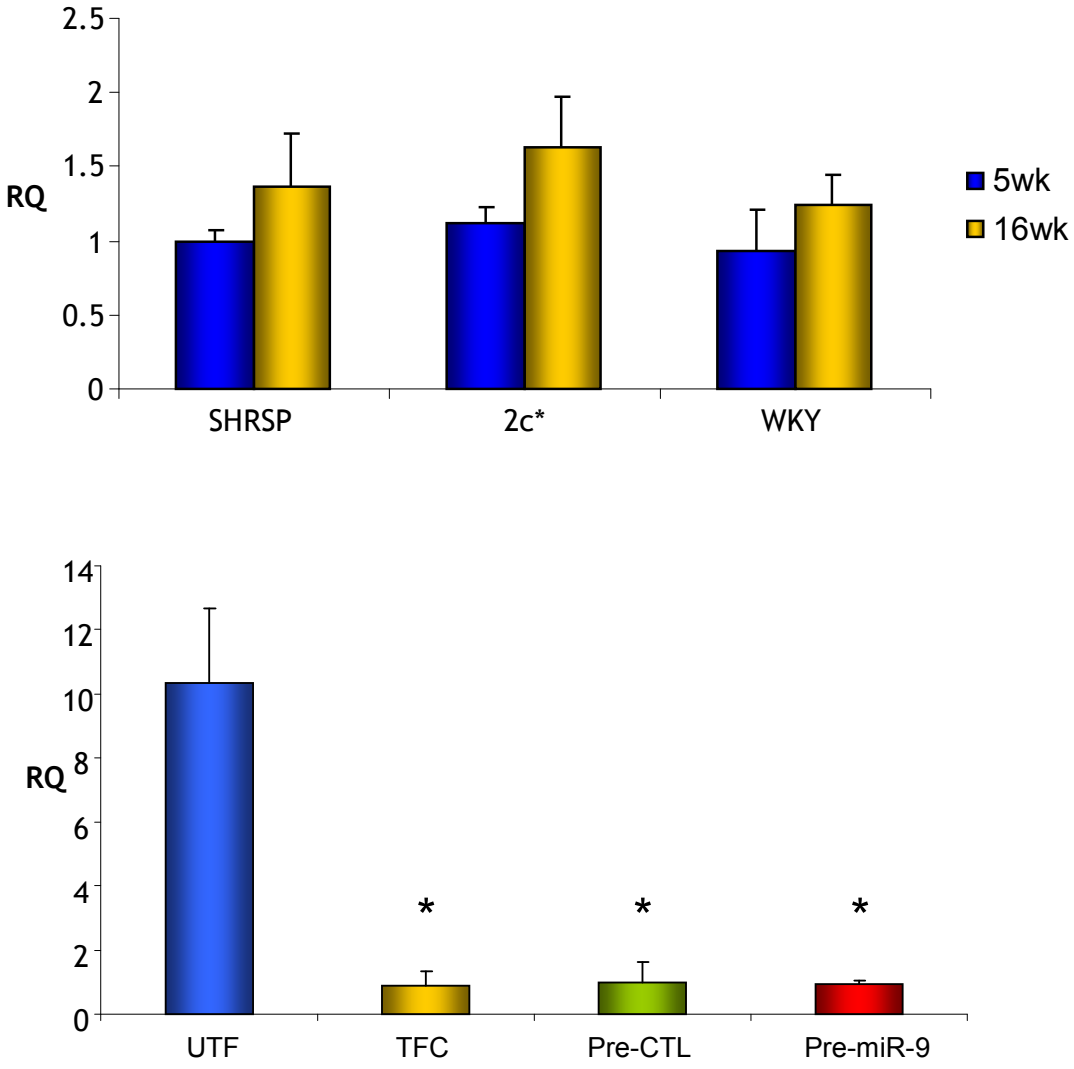

Figure 5.13 *Igfbp3* mRNA expression

TaqMan® qRT-PCR analysis of *Igfbp3* mRNA expression. Top panel: Expression of *Igfbp3* in kidney of SHRSP, congenic and WKY strains at different time-points. No significant change in expression was observed in any of the strains, regardless of time-point (n=4). Bottom panel: *Igfbp3* expression following transfection of NRK-52E cells with 30nM control (Pre-CTL) or miR-9 precursor (Pre-miR-9). No significant change in expression was observed compared to Pre-CTL, however when compared to UTF all other groups were significantly reduced (n=1 experiment performed in triplicate and is representative of 4 experiments in total) *$p<0.05$ vs UTF (ANOVA + Dunnett's post-hoc test).

UTF: untransfected cells, TFC: mock transfected cells, Pre-CTL: Control Pre-miR transfected cells

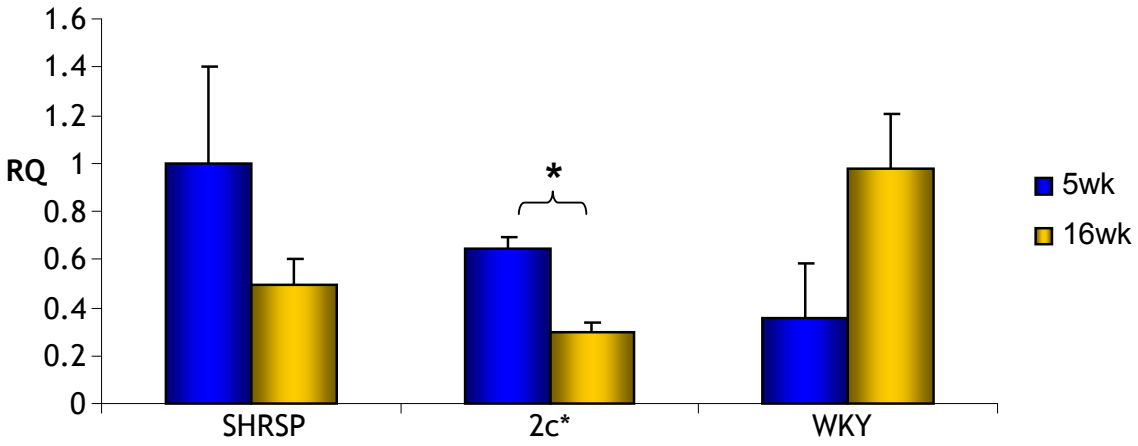

Figure 5.14 *Igsf11* mRNA expression

TaqMan® qRT-PCR analysis of *Igsf11* mRNA expression in kidney of SHRSP, congenic and WKY strains at different time-points. No significant change in expression was observed in SHRSP or WKY between 5 week and 16 week time points. *Igsf11* expression was significantly decreased in 16 week congenic compared to 5 week (n=4) *$p<0.05$ vs 16 wk 2c* (2 sample t-test).

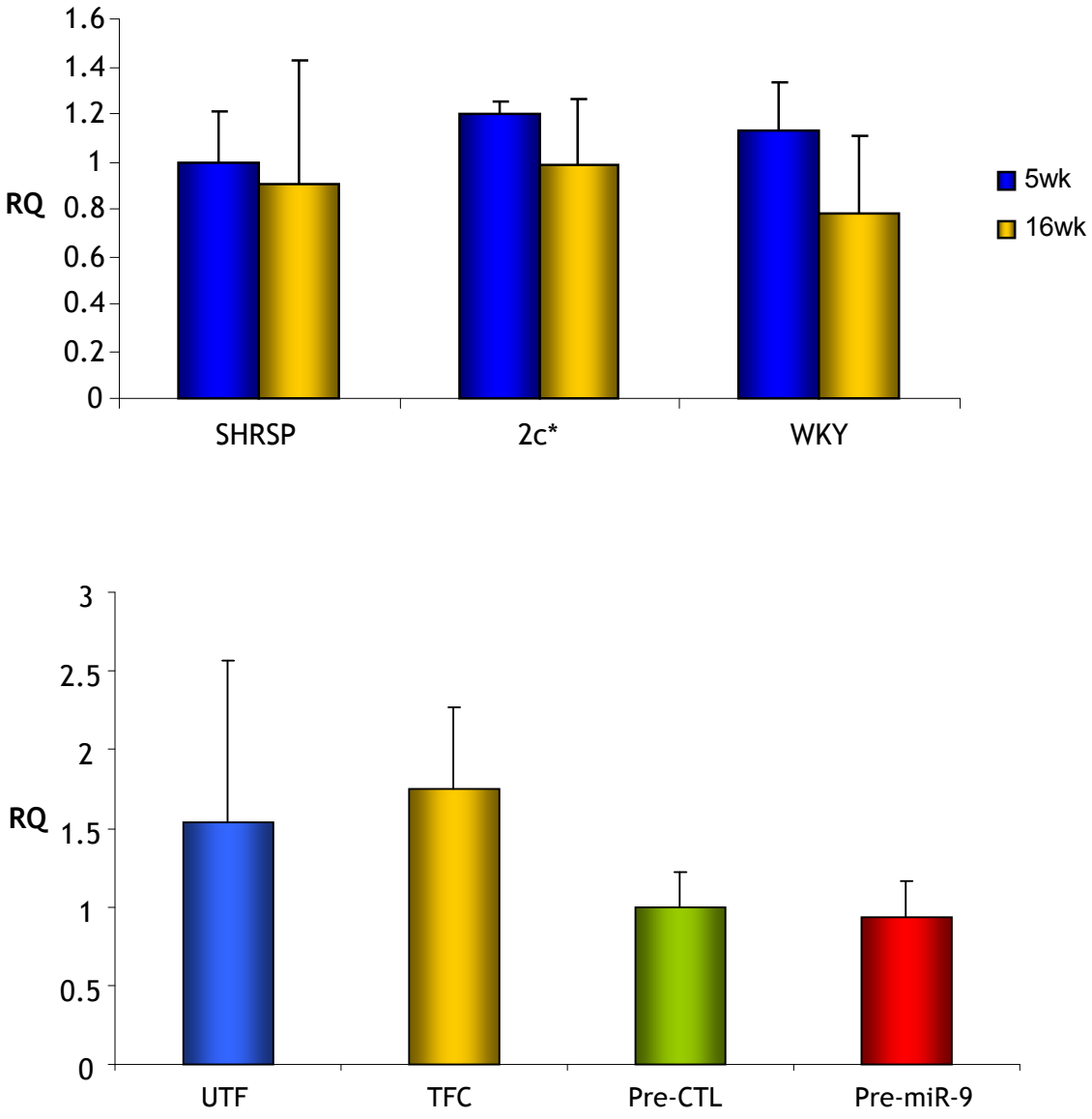

Figure 5.15 *Scly* mRNA expression

TaqMan® qRT-PCR analysis of *Scly* mRNA expression. Top panel: Expression of *Scly* in kidney of SHRSP, congenic and WKY strains at different time-points. No significant change in expression was observed in any of the strains, regardless of time-point (n=4). Bottom panel: *Scly* expression following transfection of NRK-52E cells with 30nM control (Pre-CTL) or miR-9 precursor (Pre-miR-9). No significant change in expression was observed (n=1 experiment performed in triplicate and is representative of 4 experiments in total).

UTF: untransfected cells, TFC: mock transfected cells, Pre-CTL: Control Pre-miR transfected cells

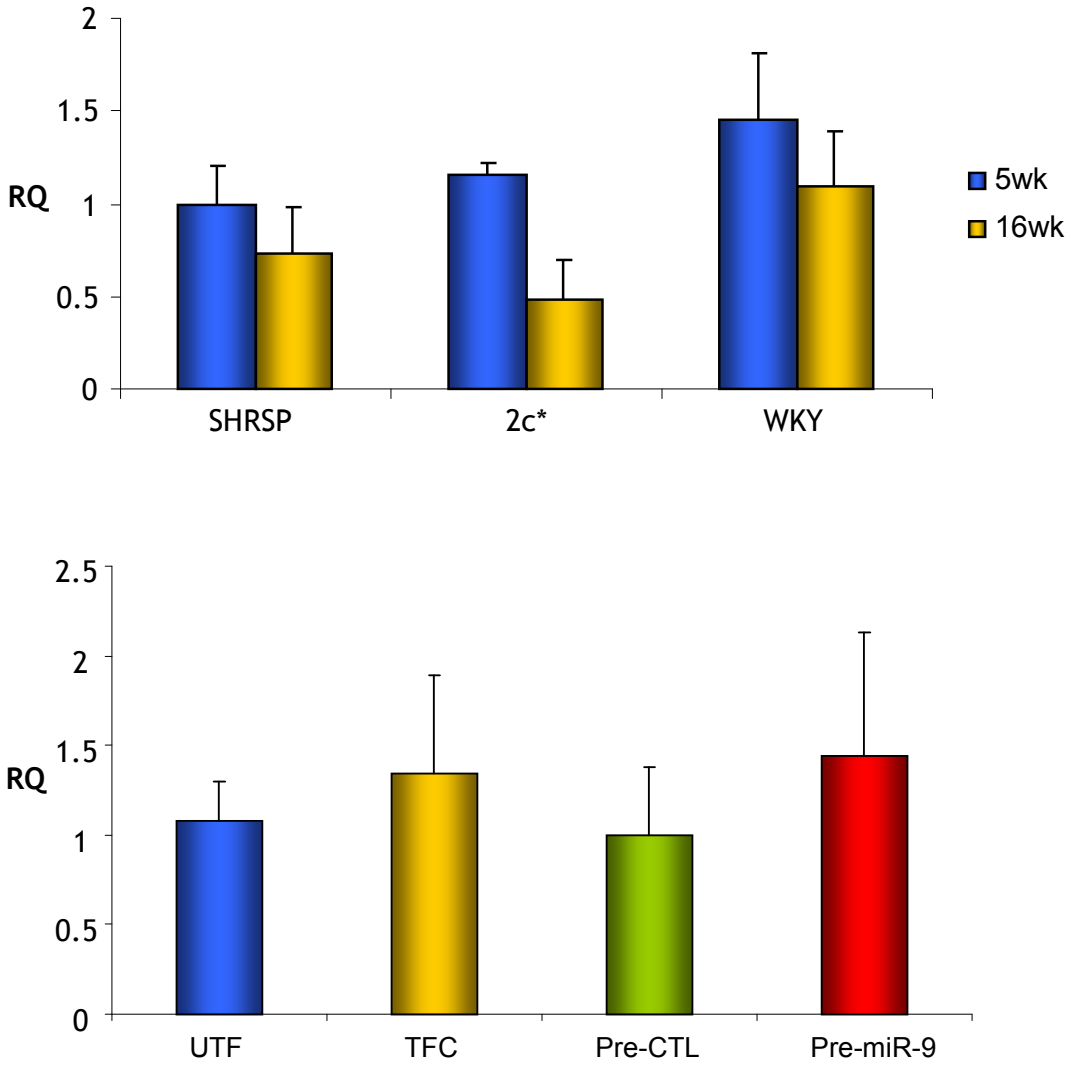

Figure 5.16 *Trim35* mRNA expression

TaqMan® qRT-PCR analysis of *Trim35* mRNA expression. Top panel: Expression of *Trim35* in kidney of SHRSP, congenic and WKY strains at different time-points. No significant change in expression was observed in any of the strains, regardless of time-point (n=4). Bottom panel: *Trim35* expression following transfection of NRK-52E cells with 30nM control (Pre-CTL) or miR-9 precursor (Pre-miR-9). No significant change in expression was observed (n=1 experiment performed in triplicate and is representative of 4 experiments performed in triplicate).

UTF: untransfected cells, TFC: mock transfected cells, Pre-CTL: Control Pre-miR transfected cells

No change in *Trim35* expression was observed in NRK-52E cells following over-expression of miR-9 (Figure 5.16, bottom panel).

5.5 Discussion

As previously mentioned, miR-9-1 and miR-137 map within the 2c* and 2k congenic regions. Using commercially available TaqMan® probes designed to detect and quantify mature miRNAs, it has been possible to investigate expression of miR-9-1 and miR-137 in kidney tissue from SHRSP, congenic and WKY animals. As the mature miRNA is the active species responsible for binding to the 3' UTR of target mRNA and subsequent inhibition of gene expression, quantification of mature miRNA is preferred (252). Kidney expression of mature miR-9-1 was found to be higher in 5 week old than 16 week old congenic and WKY strains. However, expression of miR-9-1 in SHRSP was unchanged over time. Kidney expression of mature miR-137 was found to be higher in salt-loaded 21 week old SHRSP than in 21 week old SHRSP without salt loading. No significant change in miR-137 expression was observed in kidney from congenic and WKY strains at any time-point. This suggests that miR-137 and its gene targets may be play a role in salt sensitivity in the SHRSP.

To aid in the validation of miRNA/mRNA target pairs, 'gain of function' and/or 'loss of function' experiments can be performed (236). If a predicted miRNA/mRNA is valid then over-expression of a miRNA mimic (gain of function) would result in reduced target expression and inhibition of a miRNA by antisense oligonucleotides (loss of function) would result in increased target expression. NRK-52E cells were transfected with miRNA precursor and inhibitor molecules for miR-9-1 and miR-137 and the ability of each miRNA to be up-regulated or down-regulated was assessed. Using precursor miRNA molecules (designed to mimic mature miRNAs); expression of miR-137 and miR-9-1 was significantly up-regulated. However, when NRK-52E cells were transfected with miRNA inhibitors, no down-regulation of either miRNA was observed. Anti-miRNA antisense oligonucleotides (ASO) have been used previously in attempts to modulate miRNA expression to improve target validation. Antisense oligonucleotides are chemically modified single stranded RNA molecules and

have been used to target and inhibit mature miRNA (253). However, measuring the level of miRNA inhibition can be difficult. Neither miR-9-1 nor miR-137 inhibition was detectable by qRT-PCR. Other studies investigating the efficacy of miRNA inhibition by ASO have utilised reporter constructs to demonstrate reduced miRNA activity. Cheng and colleagues used a luciferase reporter construct engineered so that the 3' UTR contained miRNA target sites. The reporter constructs and miRNA inhibitors were then co-transfected into HeLa cells. In those cells treated with miRNA inhibitor, luciferase activity was increased due to the inhibition of endogenous miRNA thus preventing miRNA mediated repression of reporter gene expression (254). A luciferase reporter system was also used to assess the effect of different ASO chemical modifications on ASO activity after attempts to measure target expression by RT-PCR were not sensitive enough to detect subtle changes following ASO treatment (255). An EGFP reporter construct containing a miR-21 complementary sequence in the 3' UTR was used to evaluate anti-miR-21 activity in HeLa cells. Expression of EGFP was restored when cells were transfected with anti-miR-21 (256). The expression data generated from TaqMan® analysis of miR-9-1 and miR-37 suggests that expression is quite low in NRK-52E cells and may explain why it was not possible to detect reduced miRNA expression by qRT-PCR. In future experiments involving analysis of miRNA activity a reporter construct method could be used in conjunction with qRT-PCR of mature miRNA to further enhance miRNA expression analysis.

It has been shown that over-expression of miR-9-1 and miR-137 can be readily achieved in NRK-52E cells. This over-expression was then used to try and validate predicted miRNA targets. Target validation has proved to be problematic. The targets of interest were identified using a computational method to find 3' UTR sequences complementary to the miRNA seed region combined with bioinformatic analysis to identify which targets were differentially expressed. Analysis found 7 predicted target genes for miR-9-1 but none for miR-137. The mRNA expression levels of each predicted target were assessed in kidney tissue and in NRK-52E cells over-expressing miR-9-1. None of the predicted targets followed the pattern of expression expected in kidney tissue and no significant changes in target expression were observed in NRK-52E cells following over-expression of miR-9-1.

The lack of miR-9-1 induced changes to gene expression may be because binding of just one miRNA to the 3' UTR of these targets is not sufficient and that binding of multiple miRNAs may be required before a reduction in expression is observed. Different miRNAs can affect the regulation of a single transcript by co-operative binding to the 3' UTR and binding of multiple identical miRNAs can also enhance down-regulation (257). Each of the targets investigated were chosen according to complementarity between the 3' UTR and miRNA seed region. All targets were found to contain only one seed apart from *Scly* which contained two. The greater the number of seed regions in the 3' UTR that miRNA can bind to, the greater the miRNA activity (258;259). Another factor contributing to miRNA ability to down-regulate expression is the distance between miRNA seed sites in 3' UTR. It has been suggested that optimal activity of miRNAs occurs when 2 seed sites are separated between 13 and 35 nt (260). Our data shows a lack of seed sites in the 3' UTR of each predicted target and when more than one seed site was detected, the distance between sites was much larger than suggested for optimal activity. MicroRNA specificity may also be affected by the nucleotide present in the A1 position of the seed site. This corresponds to the first nucleotide of the miRNA, which is usually a uracil (this is the case for miR-9-1) such that an adenine in the position next to the seed site (3') may improve specificity (261). However, Table 5.1 shows the nucleotide present at the A1 position for each predicted target; none contained an adenine at this position. This may have contributed to reduced miRNA binding specificity. The target identification method used here relied solely on complementarity between the 3' UTR and the miRNA seed region. However, it has been suggested that complementarity to the seed region is not the only factor important for target recognition (230).

Various computational approaches have been used to identify miRNA targets. These approaches also use seed binding as an indicator of potential targets. TargetScan requires perfect complementary base pairing with the miRNA seed (261) but other resources, such as MiRanda, consider seed binding as important but do not require perfect complementarity (234;262). However, as a second criterion for target prediction, these programs also require cross species conservation. Both TargetScan and PicTar require that the portion of the 3' UTR

that interacts with the miRNA seed be conserved between at least five species. MiRanda also requires cross species conservation but only between human and rodent (234). In order to improve miRNA target prediction in future experiments, it may be better to assess cross species conservation and to also consider genes that have multiple predicted sites even if complementarity to the seed is not perfect. Target sites could also be 3' compensatory so the ability to detect targets may be reduced by focusing solely on the seed region (5' dominant sites).

MicroRNA mediated down-regulation of gene expression can result from either translational repression or mRNA degradation (262). Potentially, the lack of target validation at mRNA observed in the present study may be a reflection of translational repression occurring further downstream. It has been suggested that if the miRNA is sufficiently complementary to the mRNA target then mRNA cleavage would be the outcome; otherwise the miRNA would induce translational repression (263;264). It may have been more appropriate to try and validate each target at the protein level, as it could be the case that target mRNA expression was unaffected by miR-9-1 over-expression and that miRNA activity was mediated through repression of translation.

A recent study demonstrated successful identification and validation of hsa-miR-193b and its target urokinase-type plasminogen activator (uPA). Using anti-miR-193b in human breast cancer cells lines resulted in increased uPA protein expression and increased cell invasion. However, over-expression of miR-193b reduced protein expression and also reduced cell invasion (265). The work performed here highlights the difficulties involved when trying to identify and validate predicted miRNA/mRNA target pairs. The approach used in the present study attempted to increase the likelihood of identifying a valid miRNA/mRNA target pair by combining target identification methods with gene expression data from microarray analysis. By looking at genes that were down-regulated in kidney tissue at time-points when miRNA expression was up-regulated and vice versa, it was hoped that a valid target would be found. This was not the case in this study but the same strategy could be applied to miRNAs of interest in the future. The application of proteomics could further enhance miRNA studies. Strategies such as pulsed SILAC (stable isotope labelling with amino acids in cell

culture) labelling of proteins allow for genome wide quantification of protein synthesis (258;266). This method was utilised by Selbach and colleagues to measure changes in protein production in HeLa cells following modulation of miRNA expression. By pulse labelling miRNA transfected cells and control transfected cells with different heavy stable isotopes it was possible to measure differences in protein production between the two samples. This study found that a single miRNA could down-regulate production of hundreds of proteins (258). By combining such methods for analysis of protein expression with mRNA expression analysis, the ability to detect and validate miRNA targets could be vastly improved.

Chapter 6: General Discussion

A combination of congenic breeding and microarray analysis to assess changes in gene expression led to the identification of *Gstm1* as a positional and functional candidate gene for hypertension in the SHRSP (69). As *Gstm1* is part of a large family of antioxidant enzymes, it was proposed that depleted renal *Gstm1* levels in the SHRSP may contribute to the development of hypertension by increasing the susceptibility of kidney tubular cells to the damaging effects of oxidative stress. This in turn could impair the ability of the kidney to regulate the sodium and fluid balance and subsequently alter blood pressure. This study has aimed to investigate the role of *Gstm1* using an RNAi mediated approach and to develop molecular tools that could be used for targeted modulation of gene expression *in vivo*. In addition to this, two microRNAs that mapped to the congenic region were investigated to assess their potential contribution to differences in gene expression observed between the SHRSP, WKY and congenic rat strains.

The findings from chapter 3 indicate that expression of *Gstm1* can be effectively and reproducibly knocked down in response to siRNA and can be quantified at both mRNA and protein level. It has also been shown that by modulating the concentration of siRNA used any non-specific effects on the expression of other *Gstm* family members can be prevented and interferon response gene activation can be avoided. To be able to take investigation of the function of *Gstm1* into an *in vivo* setting the possibility of using local delivery to the kidney for *in vivo* gene knock-down was assessed but was found to be inappropriate as it resulted in significant renal damage. However, successful targeting of renal tubules in SHRSP following systemic delivery was demonstrated using a previously identified kidney targeting modified adenoviral vector (185). Furthermore, over-expression and RNAi sequences could be incorporated into these targeted adenoviral vectors allowing both approaches to be delivered to specific cells of interest. Short-hairpin RNA expressing vectors have been generated and were evaluated in NRK-52E cells, however knock-down of *Gstm1* was not confirmed in this cell line. The integration of targeted vectors and modulation of *Gstm1* expression would allow the role of *Gstm1* to be investigated more fully *in vivo*.

Following on from the optimisation of *Gstm1* knock-down performed in chapter 3, the experiments carried out in chapter 4 sought to investigate the

contribution of reduced *Gstm1* expression to oxidative stress. Reduced *Gstm1* expression was not sufficient to cause a change in glutathione levels and reduced activity could not be detected using a total GST activity kit. Lipid peroxidation (as determined by 8-isoprostane level) and DNA damage (as determined by 8-OH-2OG level) were unaffected by reducing *Gstm1* expression. However, when DNA damage was assessed by comet assay, a small but significant increase in tail length was observed in cells with reduced *Gstm1* expression, suggesting increased damage in these cells. The results generated tend to suggest that *Gstm1* alone is not responsible for cellular protection against products of oxidative stress such as lipid radicals, as suggested in the hypothesis of this study. Rather *Gstm1* may function as part of a larger pathway in the protection against oxidative stress.

Two miRNAs (miR-9-1 and miR-137) were identified that map to the chromosome 2 congenic region. It was proposed that miRNA within this region may target genes expressed in the kidney and contribute to differential gene expression in parental and congenic strains. Expression analysis of miR-9-1 and miR-137 found expression of miR-9-1 was lower in 16 week old congenic and WKY strains than in 5 week animals of the same strain but was unchanged in SHRSP and that expression of miR-137 was unchanged across all time-points in congenic and WKY strains but was significantly higher in 21 week old, salt-loaded SHRSP than in 21 week old SHRSP without salt. By combining previously generated microarray data with predicted miRNA targets using IPA, 7 predicted targets for miR-9-1 were identified. However, none of the predicted targets were validated by qRT-PCR in kidney tissue or in NRK-52E cells transfected with pre-miR-9. Although no targets were validated in this instance, miR-9-1 may still have a role in contributing to the changes in gene expression observed in kidney from congenic and WKY strains.

The combined congenic breeding and microarray strategy used to identify *Gstm1* has been used previously and led to the identification and confirmation of *Cd36* as a candidate gene for insulin resistance in the SHR (65;267). This strategy was also used to identify *Vcam1* and *Edg1* as candidate genes for salt sensitivity in the SHRSP (237). This study utilised IPA to generate a molecular network linking each gene and demonstrated how *Edg1* could regulate *Vcam1* expression.

Following on from identification of *Gstm1* as a candidate gene for hypertension in SHRSP, this study sought to further investigate its function and role in oxidative stress. Increased renal oxidative stress was identified in SHRSP (77). However, using RNAi to knock-down *Gstm1* expression in a rat kidney cell line did not lead to identification of a specific role for *Gstm1* in protection against products of oxidative stress. This would suggest that the decreased expression of *Gstm1* alone, as observed in SHRSP, is not responsible for reduced oxidative stress protection but instead may act as part of an oxidative stress pathway. As described previously, *Gstm1* is part of a large, highly homologous family of antioxidant enzymes. A recent study observed a small reduction (less than 2-fold) in expression of other *Gstm* isoforms in kidney from the SHRSP (268) but it may be that many small changes in the expression of genes participating in oxidative stress defence contribute to the overall phenotype observed. Indeed it would seem that for analysis of complex traits, instead of investigating singular candidate genes, it would be more informative to assess candidate pathways encompassing such genes (269).

This study has investigated the effects of reduced *Gstm1* expression; conversely, a transgenic SHRSP expressing *Gstm1* may provide greater information regarding a direct link between *Gstm1* and blood pressure. Our group has recently completed the generation of a *Gstm1* transgenic rat and studies are underway to investigate the effect of *Gstm1* over-expression on blood pressure. If *Gstm1* does indeed have a significant contribution to blood pressure regulation then it would be expected that over-expression in the SHRSP would cause a reduction in blood pressure.

RNA interference is now a commonly used method for knock-down of gene expression allowing for subsequent functional analysis and, as described in section 1.5.5, is a potential therapeutic for various human disorders. Various routes of administration have been evaluated for *in vivo* delivery of siRNA (270;271). Delivery vectors have also been used to drive expression of shRNA *in vivo,* such as adenoviral vectors (272), lentiviral vectors (273) and adeno-associated viral vectors (AAV) (162;274). However, *in vivo* expression of siRNA or shRNA can be problematic due to immune system activation (275;276). Not only can immune system activation be detrimental but a study that used AAV

mediated shRNA expression in mice found that shRNA expression caused liver damage and in some cases was fatal. They then discovered that this was due to saturation of the endogenous miRNA pathway machinery. However, after careful optimisation of AAV vector dose and selection of shRNA with lower expression, the study was able to demonstrate efficient and persistent silencing of hepatitis B virus in mice (277;278). Due to technical difficulties encountered by colleagues working on virus development it was not possible to generate the *Gstm1* shRNA expressing targeted adenoviral vectors. Given more time and optimisation, the completion of these vectors would provide an excellent tool for thorough *in vivo* investigation of *Gstm1* function. This system could also be applied to evaluate future renal expressed candidate genes in hypertension and oxidative stress.

MicroRNAs are an endogenous class of short RNA that regulate gene expression by binding the 3' UTR of target genes resulting in mRNA degradation (like siRNA) or translational repression. MicroRNAs represent another level of complexity in the control of gene expression, as one miRNA can target many genes and one gene can be targeted by many miRNAs (279). Genome wide profiling of miRNA expression in human heart disease found that in specific types of heart disease there was a distinct miRNA expression profile (280). This also supports the idea that a single miRNA is not responsible for gene expression changes contributing to phenotype, instead many miRNAs together regulate gene expression. This may account for the lack of significant change in predicted target gene expression following over-expression of miR-9-1 and also why targets for miR-137 were not identified in this study. As hypertension is a complex trait, it may be that many miRNAs regulate the expression of many genes, with each gene imparting a small effect and contributing to overall phenotype. Our group is currently analysing data generated from miRNA microarrays performed on kidney from SHRSP, WKY and congenic strains at the various time-points described in chapter 5. It is hoped that this in combination with IPA and molecular techniques to assess predicted targets will further elucidate the potential role of miRNAs in hypertension in the rat. In chapter 5, IPA was employed to interrogate microarray data and combined with miRNA target prediction. Although the targets identified were not validated in this study, the combination of miRNA and microarray analysis of congenic and parental strains may further

contribute to identification of candidate genes and also provide important information on how such genes are regulated. Ingenuity pathway analysis has been used to probe miRNA target lists and compare to genes known to have a role in cancer. This allowed a large list of targets to be stratified according to a reported role in a specific type of cancer (281). More recently, IPA has been used to build signalling networks using the predicted targets of 8 miRNAs found to be differentially expressed in heart failure (282).

It is hoped that by combining strategies to identify candidate genes with *in vitro* and *in vivo* functional analysis using techniques such as RNAi will lead to a better understanding of genes involved in oxidative stress and hypertension. Although the experiments performed here have not identified a specific role for *Gstm1,* the same approach could be used to evaluate future candidates. MicroRNA expression profiling adds another level of complexity and may provide important information regarding the differential expression of genes. The utilisation of microarray analysis of mRNA and miRNA expression may lead to identification of candidate miRNA that contribute to regulation of functionally important genes. The integration of such data using Ingenuity Pathway Analysis would allow for specific targets to be identified depending on whether they are part of a pathway of interest. Using such technologies may lead to the identification of pathways that directly contribute to oxidative stress or blood pressure regulation in the rat. It may then be possible to find similar regulatory mechanisms in human that could be translated to generate therapeutic measures for the treatment of essential hypertension.

Appendix

RefSeq	Gene ID	RefSeq	Gene ID	RefSeq	Gene ID	RefSeq	Gene ID
NM_001001508	Prg1	NM_001017376	Phyhip	NM_017162	Gif	NM_053584	Gosr1
NM_001002016	Lmna	NM_001017377	Paqr4	NM_017164	Capza3	NM_053598	Nudt4
NM_001003401	Enc1	NM_001017382	Frs3	NM_017214	Rgs4	NM_053603	Clic5
NM_001003404	Il22ra2	NM_001017386	Tmem10	NM_017224	Slc22a6	NM_053605	Smpd3
NM_001003957	Dnmt3a	NM_001017445	Ubxd8	NM_017226	Padi2	NM_053610	Prdx5
NM_001004084	RT1-Bb	NM_001017446	RGD1310199	NM_017230	Padi3	NM_053621	Magi2
NM_001004090	Tspan5	NM_001017451	RGD1309228	NM_017238	Vipr2	NM_053622	Pom121
NM_001004107	Tacc1	NM_001017453	RGD1311203	NM_017244	Crabp2	NM_053623	Acsl4
NM_001004210	Xbp1	NM_001017454	RGD1307799	NM_017249	Mbc2	NM_053624	Pitx1
NM_001004222	Arfip2	NM_001017482	LOC498033	NM_017255	P2ry2	NM_053635	St14
NM_001004266	RGD1303144	NM_001017499	LOC498353	NM_017259	Btg2	NM_053638	Idh3a
NM_001004269	Jam3	NM_001017504	LOC498425	NM_017261	Gria2	NM_053667	Lepre1
NM_001004271	Ugt2b4	NM_001017508	LOC498664	NM_017265	Hsd3b6	NM_053670	Crcp
NM_001004274	Igfbp4	NM_001017988	LOC303566	NM_017289	Gabrd	NM_053679	Dffa
NM_001004444	Zbtb1	NM_001024262	RGD1305424	NM_017291	Gabrr1	NM_053690	Dnajc14
NM_001004445	Znf183	NM_001024275	Rassf4	NM_017302	Slc16a7	NM_053693	Dmtf1
NM_001005547	Tspan3	NM_001024292	LOC499330	NM_017303	Kcnab1	NM_053700	Ccl28
NM_001005560	Pla2g6	NM_001024298	LOC499516	NM_017309	Ppp3r1	NM_053714	Ank
NM_001005872	Htatip	NM_001024303	LOC499677	NM_017313	Rab3ip	NM_053733	Bcl2l10
NM_001005886	Nsddr	NM_001024305	LOC499691	NM_017317	Rab27a	NM_053734	Ncf1
NM_001005889	Rdx	NM_001024307	LOC499732	NM_017321	Aco1	NM_053742	Pitpnb
NM_001006963	Itm2b	NM_001024313	LOC499900	NM_017325	Runx1	NM_053743	Cdc37
NM_001006973	mrpl11	NM_001024327	LOC500110	NM_017355	Rab4b	NM_053754	Abcg5
NM_001006981	Dlst	NM_001024338	LOC500348	NM_017356	Hpcal1	NM_053756	Atp5g3
NM_001006990	LOC304000	NM_001024343	LOC500445	NM_017361	Nup54	NM_053756	Atp5g3
NM_001006993	Sgcg	NM_001024344	LOC500449	NM_019123	St6galnac3	NM_053758	Plce1

Table A1 continued overleaf

RefSeq	Gene ID	RefSeq	Gene ID	RefSeq	Gene ID	RefSeq	Gene ID
NM_001007005	Arhgdia	NM_001024349	LOC500598	NM_019124	Rabep1	NM_053765	Gne
NM_001007009	MGC94915	NM_001024741	Chaf1b	NM_019126	Cgm3	NM_053778	Ipo13
NM_001007607	Pigq	NM_001024763	Nif3l1	NM_019135	Tnfrsf8	NM_053779	Serpini1
NM_001007609	Mfap3	NM_001024779	Cyp2u1	NM_019146	Bsn	NM_053788	Stx1a
NM_001007611	F101B_RAT	NM_001024780	Prkra	NM_019152	Capn1	NM_053798	Sacm1l
NM_001007626	Ggps1	NM_001024795	Rnf44	NM_019158	Aqp8	NM_053801	Sec14l2
NM_001007628	Cxxc5	NM_001024799	RGD1306302	NM_019172	Galr2	NM_053810	Snap29
NM_001007629	NTF2	NM_001024865	LOC684557	NM_019187	Coq3	NM_053812	Bak1
NM_001007636	S100a1	NM_001024991	Fahd1	NM_019191	Smad2	NM_053818	Slc6a9
NM_001007637	mrpl24	NM_001024992	LOC303332	NM_019202	Pla2g2c	NM_053837	Ap2m1
NM_001007641	Rnd3	NM_001025008	LOC314996	NM_019214	Slc26a4	NM_053843	FCGR3_RAT
NM_001007645	MGC95152	NM_001025009	Josd1	NM_019219	Rbbp9	NM_053847	Map3k8
NM_001007653	Mrps15	NM_001025014	Tmem50b	NM_019225	Slc1a3	NM_053848	Opcml
NM_001007662	Arcn1	NM_001025016	RGD1309120	NM_019230	Slc22a3	NM_053851	Cacnb2
NM_001007667	Sat	NM_001025019	RGD1306582	NM_019232	Sgk	NM_053878	Cplx2
NM_001007669	Zfp672	NM_001025020	RGD1310753	NM_019238	Fdft1	NM_053879	Cntn4
NM_001007679	RGD1359339	NM_001025022	RGD1308059	NM_019243	Ptgfrn	NM_053883	Dusp6
NM_001007682	Thtpa	NM_001025025	LOC363267	NM_019250	Ralgds	NM_053893	Sdc3
NM_001007688	RGD1359600	NM_001025027	Fundc1	NM_019256	P2rx7	NM_053912	Pscd3
NM_001007689	Ciapin1	NM_001025033	LOC498154	NM_019261	Klrc2	NM_053921	Pex12
NM_001007701	Tram1	NM_001025034	LOC498796	NM_019262	C1qb	NM_053923	Pik3c2g
NM_001007705	RGD1359144	NM_001025051	LOC500638	NM_019272	Sema4f	NM_053929	Slc7a9
NM_001007706	RGD1359191	NM_001025142	Trim35	NM_019280	Gja5	NM_053931	Gp1bb
NM_001007713	Tmbim1	NM_001025143	LOC498606	NM_019289	Arpc1b	NM_053936	Edg2
NM_001007714	Morf4l2	NM_001025151	LOC500625	NM_019304	Dgkb	NM_053945	Rims2
NM_001007727	Lypd1	NM_001025271	Sfpq	NM_019306	Flt1	NM_053959	Bin1

Table A1 continued overleaf

RefSeq	Gene ID	RefSeq	Gene ID	RefSeq	Gene ID	RefSeq	Gene ID
NM_001007730	Cabp7	NM_001025402	Umps	NM_019326	Neurod2	NM_053965	Slc25a20
NM_001007732	MGC94010	NM_001025412	RGD1305651	NM_019329	Cntn3	NM_053967	Spam
NM_001007737	RGD1359158	NM_001025418	Ppp2r1b	NM_019331	Pcsk3	NM_053972	RragB
NM_001007738	RGD1359349	NM_001025419	Tax1bp3	NM_019344	Rgs8	NM_053974	Eif4e
NM_001007742	Ubadc1	NM_001025635	Nars	NM_019345	Slc12a3	NM_053988	Calb2
NM_001007747	Pomgnt1	NM_001025648	Snapap	NM_019347	Slc14a2_v1	NM_053997	Kcnc3
NM_001007751	MGC94207	NM_001025684	Pex11b	NM_019351	Timm17a	NM_053998	Rab8a
NM_001007754	Rassf1	NM_001025688	Palmd	NM_019358	Pdpn	NM_057097	Vamp3
NM_001007755	Scly	NM_001025693	Cdca7	NM_019365	Rassf5	NM_057122	Psmc4
NM_001007759	Mar-03	NM_001025711	Atg4b	NM_019371	Egln3	NM_057124	P2ry6
NM_001008278	RGD1308696	NM_001025721	Colec12	NM_019378	Snip	NM_057133	Nr0b2
NM_001008279	Fliih	NM_001025726	Srpk1	NM_019623	Cyp4f1	NM_057148	Sep-02
NM_001008280	Lrrc59	NM_001025739	Rpl11	NM_019630	Gip	NM_057155	Xpnpep2
NM_001008287	Donson	NM_001025752	Ccrk	NM_019905	Anxa2	NM_057185	Folh1
NM_001008292	Diablo	NM_001025760	MGC116363	NM_020075	Eif5	NM_057192	Waspip
NM_001008307	RGD1311257	NM_001025769	C20orf165	NM_020076	Haao	NM_078620	Slc8a3
NM_001008319	Maea	NM_001029909	CPG2	NM_021266	Fzd1	NM_080477	Pfkfb2
NM_001008320	Rhoj	NM_001029920	RGD1310423	NM_021579	Nxf1	NM_080480	Pip5k2c
NM_001008334	Tmem97	NM_001029927	LOC502774	NM_021583	Ptges	NM_080576	Apoa5
NM_001008336	LOC682784	NM_001031646	Stoml2	NM_021587	Ltbp1	NM_080580	Rab3d
NM_001008339	Whsc2	NM_001031647	Dnali1	NM_021594	Slc9a3r1	NM_080581	Abcc3
NM_001008353	Mkks	NM_001031652	St6galnac2	NM_021653	Dio1	NM_080582	Abcb6
NM_001008354	Mrrf	NM_001031655	Manba	NM_021676	Shank3	NM_080583	Ap2b1
NM_001008356	Slc39a3	NM_001033683	Vat1	NM_021698	F13a1	NM_080585	Napa
NM_001008363	Zfand2a	NM_001033693	Slc31a2	NM_021702	Atxn3	NM_080688	Plcd4
NM_001008370	MGC105830	NM_001033704	Xylb	NM_021740	Ptma	NM_080689	Dnm1

Table A1 continued overleaf

RefSeq	Gene ID	RefSeq	Gene ID	RefSeq	Gene ID	RefSeq	Gene ID
NM_001008376	Trappc3	NM_001033862	Ceacam1	NM_021744	Cd14	NM_080780	P2rx5
NM_001008378	Tspan31	NM_001033864	Cflar	NM_021766	Pgrmc1	NM_080782	Cdkn1a
NM_001008384	Rac2	NM_001033866	Surf2	NM_021776	Ecel1	NM_080783	Gale
NM_001008386	LOC493574	NM_001033870	Csnk1g2	NM_021850	Bcl2l2	NM_080786	Slco2b1
NM_001008517	RGD1310553	NM_001033883	Cxcl12	NM_021868	Cttn	NM_080906	Ddit4
NM_001008518	MGC105649	NM_001033890	RGD1311072	NM_021997	Cyln2	NM_080907	Ppp4r1
NM_001008521	Ptk9	NM_001033891	LOC690779	NM_022179	Hk3	NM_130403	Ppp1r14a
NM_001008557	Mip1	NM_001033951	Npuk68	NM_022198	Clcn4-2	NM_130426	Tnfrsf1b
NM_001008560	Prss35	NM_001033998	Itgal	NM_022215	Gpd1	NM_130779	Adcy3
NM_001008561	Rnase9	NM_001034006	Centb2	NM_022218	Cmklr1	NM_130812	Cdkn2b
NM_001008767	Txnip	NM_001034032	Dnajc12	NM_022224	Pter	NM_133290	Zfp36
NM_001008768	Prim1	NM_001034079	Thrap4	NM_022240	A4galt	NM_133296	Xtrp3
NM_001008771	Wdr77	NM_001034112	Mlx	NM_022254	Gpr85	NM_133306	Oldlr1
NM_001008861	Usp11	NM_001034149	RGD1311815	NM_022257	Masp1	NM_133310	Icmt
NM_001008880	Scn4b	NM_001034163	Blmh	NM_022280	Lrat	NM_133380	Il4ra
NM_001008891	Ssr1	NM_001034835	RGD1309220	NM_022281	LOC688339	NM_133393	Lfng
NM_001009176	Trim10	NM_001034932	C1qtnf6	NM_022289	Snx16	NM_133394	Zdhhc7
NM_001009264	RGD1306635_predicted	NM_001034934	Arid5a	NM_022294	Eltd1	NM_133395	Tpo1
NM_001009357	Rqcd1	NM_001037158	Pcdhga9	NM_022388	Fxyd4	NM_133396	Tesk2
NM_001009424	Eps15	NM_001037187	LOC302680	NM_022392	Insig1	NM_133397	Erg
NM_001009478	Saa4	NM_001037191	RGD1306873	NM_022396	Gng11	NM_133402	Nap1l3
NM_001009490	Oas1f	NM_001037209	Mterfd2	NM_022400	Bcat2	NM_133406	Agpat4
NM_001009494	NP_001009494.1	NM_001037556	Nmnat1	NM_022404	Gbl	NM_133542	Igsf6
NM_001009540	Tacstd2	NM_001037649	RGD1306676	NM_022441	Acvrl1	NM_133553	B3galt4
NM_001009599	RGD1307679	NM_001037654	Dixdc1	NM_022498	Ppp1cc	NM_133560	Trak2
NM_001009600	Arhgdib	NM_001037774	Cldn8	NM_022513	Sult1b1	NM_133567	Centa1

Table A1 continued overleaf

RefSeq	Gene ID	RefSeq	Gene ID	RefSeq	Gene ID	RefSeq	Gene ID
NM_001009605	Brms1	NM_001037797	LOC500354	NM_022516	Ptbp1	NM_133568	Rasd2
NM_001009674	Itm2c	NM_001039002	RGD1304790	NM_022523	Cd151	NM_133571	Cdc25a
NM_001009675	Tceal1	NM_001039003	Mtrr	NM_022525	Gpx3	NM_133580	Rab26
NM_001009677	Plekhm1	NM_001039005	Mcoln2	NM_022534	Tcn2	NM_133583	Ndrg2
NM_001009683	Tor3a	NM_001039016	Zdhhc9	NM_022548	Wig1	NM_133593	Ap3m1
NM_001009687	Riok2	NM_001039017	RGD1309718	NM_022589	Tspan2	NM_133597	Chrnb3
NM_001009691	Dclk2_predicted	NM_001039021	Zdhhc8	NM_022596	Golga2	NM_133601	Cblb
NM_001009701	ITFG3_RAT	NM_001039044	Cdc42se1	NM_022597	Ctsb	NM_133610	Kcnh5
NM_001009705	MGC109149	NM_001039196	Slc39a13	NM_022598	Cnbp1	NM_133620	Zhx1
NM_001009708	Lmo4	NM_001039207	Narf	NM_022599	Synj2bp	NM_133651	Cav1
NM_001009713	Slc17a5	NM_001039455	RGD1309570	NM_022600	Adcy5	NM_134327	Cd69
NM_001009825	Ppp1r7	NM_001039505	Irx2	NM_022614	Inhbc	NM_134329	Adh7
NM_001009965	Eiih	NM_001040156	Aste1	NM_022639	Chrna10	NM_134334	Ctsd
NM_001010945	RGD1311474	NM_001042619	Hsd3b1	NM_022643	Hist1h2ba	NM_134363	Slc12a5
NM_001011557	RGD1305677	NM_001042621	Pip5k1a_predicted	NM_022671	Onecut1	NM_134371	Trpm8
NM_001011665	Trim26	NM_001044228	LOC289740	NM_022676	Ppp1r1a	NM_134373	Avpi1
NM_001011890	Rnps1	NM_001044237	LOC689500	NM_022697	Rpl28	NM_134379	UST4r
NM_001011893	Sep-04	NM_001044246	Mageb18_predicted	NM_022700	Arl3	NM_134413	Btbd14b
NM_001011893	Sep-04	NM_001044251	MGC112790	NM_022710	Pde1b	NM_134414	Exoc2
NM_001011902	Rabl5	NM_001044255	Coq2	NM_022853	Slc30a1	NM_134459	Mic2l1
NM_001011906	Acbd6	NM_001044267	MGC112775	NM_022860	B4galnt1	NM_138505	Adra2b
NM_001011914	Dr1	NM_001044274	Apin	NM_022864	Cplx1	NM_138530	Mawbp
NM_001011918	Anxa11	NM_001044297	LOC689907	NM_022936	Ephx2	NM_138613	Zfp179
NM_001011919	Gtpbp3	NM_001047110	LOC499770	NM_022944	Inppl1	NM_138833	Snrk
NM_001011923	Prpf4b	NM_001047743	MGC112883	NM_022953	Slit1	NM_138836	Prss8
NM_001011924	Mbd1	NM_001048184	Rragc_predicted	NM_022962	Lphn1	NM_138840	Tgoln2

Table A1 continued overleaf

RefSeq	Gene ID	RefSeq	Gene ID	RefSeq	Gene ID	RefSeq	Gene ID
NM_001011942	Cnnm2	NM_001048215	Kirrel3_predicted	NM_023023	Dpysl5	NM_138842	Sftpb
NM_001011947	Rai14	NM_001077641	Plcb1	NM_023092	Myo1c	NM_138848	Podxl
NM_001011952	Slc39a8	NM_001077648	Prdm2	NM_023969	Edg7	NM_138849	Bk
NM_001011954	Cybrd1	NM_001079700	Cdc42ep1_predicted	NM_023977	Golph3	NM_138858	Slc9a5
NM_001011961	Srms	NM_001080783	RGD1311552_predicted	NM_024000	Camkv	NM_138864	Ccdc5
NM_001011962	Ceecam1	NM_001080789	Arhgap9	NM_024002	Secisbp2	NM_138866	Eif2b5
NM_001011963	Asb6	NM_012498	Akr1b4	NM_024132	Faah	NM_138873	Nbn
NM_001011965	LOC652927	NM_012505	Atp1a2	NM_024133	Hap1	NM_138879	Sele
NM_001011969	Strap	NM_012517	Cacna1c	NM_024134	Ddit3	NM_138884	Akr1d1
NM_001011974	Akap2	NM_012521	S100g	NM_024135	Limk2	NM_138889	Cdh13
NM_001011983	Coq6	NM_012523	Cd53	NM_024138	Gng7	NM_138891	Gpr149
NM_001011985	Mknk2	NM_012526	Chgb	NM_024144	Pigm	NM_138893	Myo16
NM_001011999	LOC366923	NM_012527	Chrm3	NM_024155	Anxa4	NM_138894	Grasp
NM_001012012	Snx11	NM_012531	Comt	NM_024162	Fabp3	NM_138896	Pja2
NM_001012013	Acbd4	NM_012538	Cyp11b2	NM_024163	Begain	NM_138908	Slc22a9
NM_001012015	Lamp3	NM_012545	Ddc	NM_024379	Grid2	NM_138909	Foxe1
NM_001012032	Arhgap24	NM_012547	Drd2	NM_024385	Hhex	NM_138915	Drd1ip
NM_001012038	Mtmr3	NM_012548	Edn1	NM_024396	Abca2	NM_139036	Lhx5
NM_001012039	Efemp1	NM_012550	Ednra	NM_024400	Adamts1	NM_139040	RGD621098
NM_001012041	Isgf3g	NM_012555	Ets1	NM_024483	Adra1d	NM_139060	Csnk1d
NM_001012044	Lcp1	NM_012557	Fancc	NM_030586	Cyb5b	NM_139084	Magi3
NM_001012051	Zfp367	NM_012571	Got1	NM_030830	Luzp1	NM_139090	Acvr1c
NM_001012055	Cdh16	NM_012574	Grin2b	NM_030834	Slc16a3	NM_139094	Rbm16
NM_001012061	Cnksr3	NM_012576	Nr3c1	NM_030836	Arts1	NM_139097	Scn3b
NM_001012062	Map3k7ip2	NM_012579	Hist1h1t	NM_030838	Slco1a5	NM_139183	Crhbp
NM_001012064	Pvrl2	NM_012588	Igfbp3	NM_030841	Nptxr	NM_139188	Otos

Table A1 continued overleaf

RefSeq	Gene ID	RefSeq	Gene ID	RefSeq	Gene ID	RefSeq	Gene ID
NM_001012065	ADCK4_RAT	NM_012591	Irf1	NM_030842	Itga7	NM_139190	Calcoco1
NM_001012066	Sphk2	NM_012599	Mbl1	NM_030854	Lect1	NM_139192	Scd1
NM_001012067	Grwd1	NM_012607	Nefh	NM_030861	Mgat1	NM_139194	Fas
NM_001012079	Arhgef2	NM_012608	Mme	NM_030864	Mtr	NM_139252	Ppap2c
NM_001012080	Hfe2	NM_012610	Ngfr	NM_030990	Plp	NM_139255	LOC246120
NM_001012083	Snx7	NM_012615	Odc1	NM_030991	Snap25	NM_139324	Ehd4
NM_001012092	Xkr7	NM_012620	Serpine1	NM_030992	Pld1	NM_139331	Lrrc21
NM_001012119	Nptxr	NM_012631	Prnp	NM_030993	Ddn	NM_144730	Gata4
NM_001012120	Naga	NM_012634	Prps2	NM_030995	Mtap1a	NM_144747	Slc45a1
NM_001012122	Ecgf1	NM_012642	Ren1	NM_030996	Oprs1	NM_144748	LOC246263
NM_001012139	Plscr3	NM_012643	Ret	NM_031012	Anpep	NM_144752	Oas1b
NM_001012140	Rab34	NM_012648	Scnn1b	NM_031022	Cspg4	NM_144757	Zfp180
NM_001012147	Pxn	NM_012651	Slc4a1	NM_031026	Dncli2	NM_145081	Optn
NM_001012148	Ankrd13	NM_012652	Slc9a1	NM_031035	Gnai2	NM_145085	Pcyox1
NM_001012166	Abcb10	NM_012653	Slc9a2	NM_031047	Jup	NM_145088	Rmt1
NM_001012167	Pld3	NM_012654	Slc9a3	NM_031050	Lum	NM_145093	Aard
NM_001012169	Zfp143	NM_012655	Sp1	NM_031062	Mvd	NM_145677	Slc25a25
NM_001012170	Nap1l4	NM_012663	Vamp2	NM_031069	Nell1	NM_145682	Filip1
NM_001012174	Fkbp5	NM_012664	Syp	NM_031083	Pik4cb	NM_145723	Stx17
NM_001012188	Creb3l2	NM_012665	Syt2	NM_031094	Rbl2	NM_145724	ZN394_RAT
NM_001012189	Mboat5	NM_012666	Tac1	NM_031123	Stc1	NM_145767	Prrxl1
NM_001012195	Rnf41	NM_012681	Ttr	NM_031127	Suox	NM_145774	Rab38
NM_001012195	Rnf41	NM_012682	Ucp1	NM_031132	Tgfbr2	NM_145785	Hdgfrp3
NM_001012206	Phlda3	NM_012693	Cyp2a2	NM_031153	Sharpin	NM_145877	Kif1c
NM_001012213	Sfxn1	NM_012700	Stx1b2	NM_031241	Cyp8b1	NM_147205	St6gal1
NM_001012218	Rnf29	NM_012706	Grpr	NM_031320	Celsr3	NM_147211	Cr16

Table A1 continued overleaf

RefSeq	Gene ID	RefSeq	Gene ID	RefSeq	Gene ID	RefSeq	Gene ID
NM_001012469	Il21r	NM_012715	Adm	NM_031322	Lrp4	NM_152242	Gpr56
NM_001012476	Rnase11	NM_012719	Sstr1	NM_031332	Slc22a8	NM_152847	Snx27
NM_001012740	Cbln2	NM_012721	P2rxl1	NM_031334	Cdh1	NM_152935	Tomm20
NM_001013043	Sectm1a	NM_012725	Klkb1	NM_031337	St3gal5	NM_152938	Slc4a9
NM_001013066	Sipa1l3	NM_012728	Glp1r	NM_031339	Parg	NM_153311	Tmprss5
NM_001013070	Tspan4	NM_012732	Lip1	NM_031351	Atrn	NM_153467	Gsbs
NM_001013072	Sfxn2	NM_012735	Hk2	NM_031355	Vdac3	NM_153470	Lzts1
NM_001013077	Plekha3	NM_012740	Th	NM_001034942	Btbd15	NM_153722	Mrgprf
NM_001013079	Osbpl2	NM_012743	Foxa2	NM_001034998	Ctps2	NM_153724	Dscr1
NM_001013099	Slc38a6	NM_012747	Stat3	NM_031503	Ascl2	NM_153725	Slc17a8
NM_001013101	Moap1	NM_012756	Igf2r	NM_031511	Igf2	NM_153735	Nptx1
NM_001013103	Cdc34_predicted	NM_012758	Syk	NM_031525	Pdgfrb	NM_153740	Sap1
NM_001013120	Igsf11	NM_012761	Sp4	NM_031544	Ampd3	NM_170789	Cd3z
NM_001013124	Ung	NM_012764	Gata1	NM_031548	Scnn1a	NM_171992	Ccnd1
NM_001013135	Sdccag3	NM_012775	Tgfbr1	NM_031559	Cpt1a	NM_172008	Canx
NM_001013149	Mesdc1	NM_012778	Aqp1	NM_031568	Clcn7	NM_172021	Tbkbp1
NM_001013154	Pcgf6	NM_012779	Aqp5	NM_031588	Nrg1	NM_172066	Slc30a4
NM_001013156	Zcchc9	NM_012781	Arnt2	NM_031590	Wisp2	NM_172067	Spon1
NM_001013165	Lrrc23	NM_012789	Dpp4	NM_031597	Kcnq3	NM_172157	Arid1b
NM_001013171	Gulp1	NM_012798	Mal	NM_031600	Ptprn2	NM_172243	Ppif
NM_001013174	Laptm4b	NM_012800	P2ry1	NM_031612	Apln	NM_172327	Aip
NM_001013182	RGD1305117	NM_012813	St8sia1	NM_031614	Txnrd1	NM_172333	Cthrc1
NM_001013191	Cbfb	NM_012818	Aanat	NM_031639	Dlgh3	NM_172335	Gm2a
NM_001013211	Prp2_predicted	NM_012820	Acsl1	NM_031642	Klf6	NM_173105	Aqp11
NM_001013231	Pea15	NM_012821	Adcy6	NM_031658	Msln	NM_173126	Nid67
NM_001013238	Pttg1ip	NM_012828	Cacnb3	NM_031662	Camkk1	NM_173147	Vps54

Table A1 continued overleaf

RefSeq	Gene ID	RefSeq	Gene ID	RefSeq	Gene ID	RefSeq	Gene ID
NM_001013241	Lzic	NM_012843	Emp1	NM_031664	LOC691960	NM_173309	Elavl2
NM_001013243	Slc30a3	NM_012845	Ms4a2	NM_031675	Actn4	NM_173324	RGD708449
NM_001013250	Mageh1	NM_012863	Bhlhb8	NM_031678	Per2	NM_173337	Camk2n1
NM_001013429	Cldn14	NM_012869	Npy5r	NM_031693	Syt4	NM_175578	Dscr1l1
NM_001013434	Rras2	NM_012874	Ros1	NM_031696	Gpr88	NM_175579	Wnk4
NM_001013860	RGD1306819	NM_012879	Slc2a2	NM_031699	Cldn1	NM_175597	Ssx2ip
NM_001013869	RGD1306108	NM_012884	Cntn2	NM_031711	Arl2	NM_175755	Ppm1f
NM_001013878	RGD1359592	NM_012888	Tshr	NM_031713	Pirb	NM_175869	Plod2
NM_001013880	LOC290651	NM_012894	Adarb1	NM_031716	Wisp1	NM_176076	S100vp
NM_001013894	Gp49b	NM_012896	Adora3	NM_031727	Limk1	NM_176077	G6pc3
NM_001013898	RGD1311703	NM_012900	Ambn	NM_031735	Stk3	NM_176080	Naglt1
NM_001013905	RGD1307648	NM_012916	Bcan	NM_031740	B4galt6	NM_176856	Sep-09
NM_001013906	Lhfpl5	NM_012923	Ccng1	NM_031743	Slc24a2	NM_177421	Slc22a17
NM_001013907	LOC294513	NM_012924	Cd44	NM_031753	Alcam	NM_178092	Slc4a10
NM_001013911	Ift80	NM_012928	Cnga2	NM_031781	Apba3	NM_178093	Mtus1
NM_001013914	RGD1305808	NM_012929	Col2a1	NM_031784	Pias3	NM_178094	Itpkc
NM_001013919	Galk2	NM_012953	Fosl1	NM_031789	Nfe2l2	NM_178097	Sla
NM_001013922	RGD1307752	NM_012971	Kcna4	NM_031793	Ppig	NM_178102	Mapkapk2
NM_001013927	RGD1308734	NM_012980	Mmp11	NM_031802	Gabbr2	NM_178106	Entpd3
NM_001013930	LOC298139	NM_012981	Mras	NM_031803	Gmeb2	NM_181081	Myst2
NM_001013931	RGD1311249	NM_012983	Myo1d	NM_031816	Rbbp7	NM_181090	Slc38a2
NM_001013938	Vwa1	NM_012991	Npap60	NM_031819	Fath	NM_181377	Rtn4rl1
NM_001013939	Raver1h	NM_012999	Pcsk6	NM_031820	Dvl1	NM_181386	Tmem23
NM_001013954	RGD1308555	NM_013001	Pax6	NM_031976	Prkab1	NM_181474	Tfb1m
NM_001013976	RGD1305007	NM_013015	Ptgds	NM_031977	Src	NM_181637	Cdc91l1
NM_001013979	LOC304131	NM_013016	Ptpns1	NM_031979	Csda	NM_181687	Nnat

Table A1 continued overleaf

RefSeq	Gene ID	RefSeq	Gene ID	RefSeq	Gene ID	RefSeq	Gene ID
NM_001013980	LOC304138	NM_013026	Sdc1	NM_031983	Smarcd2	NM_182667	Myocd
NM_001013981	LOC304396	NM_013031	Slc18a2	NM_032061	Cntnap1	NM_182814	Cct4
NM_001013984	LOC304860	NM_013045	Tnr	NM_032066	Hsd17b12	NM_182816	Amigo2
NM_001013986	LOC305076	NM_013055	Map3k12	NM_032073	Kcnq1	NM_182824	Cd276
NM_001013997	RGD1309522	NM_013059	Alpl	NM_032074	Irs3	NM_182950	Tnfaip1
NM_001013999	RGD1311738	NM_013064	Hcrtr1	NM_032416	Aldh2	NM_182952	Cxcl11
NM_001014010	RGD1308147	NM_013068	Fabp2	NM_032613	Lasp1	NM_183052	Ube2v2
NM_001014011	Gramd3	NM_013070	Utrn	NM_033021	Sec31l1	NM_183054	Rhbg
NM_001014012	Zmat2	NM_013075	Hoxa1	NM_033352	Abcd2	NM_183326	Gabra1
NM_001014015	Rbm34	NM_013082	Sdc2	NM_033376	Kcnk3	NM_183329	Sra1
NM_001014018	RGD1309326	NM_013090	Vamp1	NM_052798	Zfp354a	NM_183332	Myadm
NM_001014022	Btbd10	NM_013095	Smad3	NM_052804	Fmr1	NM_198731	Chdh
NM_001014023	RGD1304579	NM_013100	Ptger1	NM_052983	Slc5a5	NM_198739	Ly6g5c
NM_001014030	RGD1309313	NM_013111	Slc7a1	NM_053301	Hfe	NM_198744	Tpd52l2
NM_001014041	LOC310721	NM_013113	Atp1b1	NM_053302	Admr	NM_198746	Klra5
NM_001014043	RGD1305778	NM_013114	Selp	NM_053323	Degs1	NM_198749	Rab15
NM_001014047	NP_001014069.1	NM_013121	Cd28	NM_053328	Bhlhb2	NM_198755	LHR2A_RAT
NM_001014051	LOC311548	NM_013125	Scn5a	NM_053329	Igfals	NM_198757	Srr
NM_001014064	Pars2	NM_013132	Anxa5	NM_053343	Dclk1	NM_198758	Rap2ip
NM_001014069	Snip1	NM_013136	Mak	NM_053355	Ikbkb	NM_198770	Zmynd19
NM_001014070	LOC313672	NM_013141	Ppard	NM_053360	Sh3kbp1	NM_198771	Fam3c
NM_001014072	RGD1311517	NM_013143	Mep1a	NM_053362	Dffb	NM_198777	MGC73003
NM_001014076	Nol10	NM_013151	Plat	NM_053380	Slc34a2	NM_198778	C11orf8h
NM_001014077	Clec14a	NM_013152	Slc18a1	NM_053381	Atp1b4	NM_198790	Rgsl2h
NM_001014087	Ccdc67	NM_013153	Has2	NM_053385	Prelp	NM_198791	NP_942086.1
NM_001014091	LOC315712	NM_013159	Ide	NM_053390	Il12a	NM_199096	Necap2

Table A1 continued overleaf

RefSeq	Gene ID	RefSeq	Gene ID	RefSeq	Gene ID	RefSeq	Gene ID
NM_001014093	Parp16	NM_013168	Hmbs	NM_053394	Klf5	NM_199110	Mfng
NM_001014095	Dzip1l	NM_013174	Tgfb3	NM_053403	Grb7	NM_199113	Popdc2
NM_001014100	LOC316326	NM_013187	Plcg1	NM_053427	Slc17a6	NM_199208	Rdh2
NM_001014130	RGD1309106	NM_013192	Kcnj6	NM_053429	Fgfr3	NM_199253	Pcsk9
NM_001014133	LOC360910	NM_013214	Acot7	NM_053437	Dgat1	NM_199267	Rela
NM_001014147	RGD1310571	NM_013222	Gfer	NM_053442	Slc7a8	NM_199269	Mamdc1
NM_001014162	RGD1309578	NM_016987	Acly	NM_053445	Fads1	NM_199391	RGD735112
NM_001014164	Cybasc3	NM_016993	Bcl2	NM_053455	Fgl2	NM_199407	Unc5c
NM_001014166	RGD1311155	NM_017006	G6pdx	NM_053457	Cldn11	NM_199463	Ripk5
NM_001014176	RGD1312003	NM_017007	Gad1	NM_053463	Nucb1	NM_199491	Fut7
NM_001014182	Mall	NM_017009	Gfap	NM_053484	Gas7	NM_199493	RGD735029
NM_001014202	RGD1311835	NM_017011	Grm1	NM_053491	Plg	NM_199495	Ndufa10
NM_001014209	LOC363060	NM_017020	Il6ra	NM_053502	Abcg1	NM_199501	Cdk2
NM_001014211	LOC363091	NM_017023	Kcnj1	NM_053503	Jub	NM_199502	Chrdl1
NM_001014216	RGD1306658	NM_017027	Mpz	NM_053511	Fbxo2	NM_201988	Pgpep1
NM_001014219	RGD1359242	NM_017037	Pmp22	NM_053516	Nol3	NM_203336	Esrrg
NM_001014232	RGD1308373	NM_017052	Sord	NM_053517	Shc1	NM_207610	Ube4a
NM_001014247	Lzts2	NM_017058	Vdr	NM_053520	Elf1	NM_207617	Iqsec3
NM_001014248	RGD1308127	NM_017061	Lox	NM_053521	Slc5a7	NM_212490	Atp6v1g2
NM_001014256	LOC365972	NM_017064	Stat5a	NM_053522	Rhoq	NM_212498	RGD1303066
NM_001014269	Lrrfip1	NM_017065	Gabrb3	NM_053524	Nox4	NM_212499	G7c
NM_001015009	Zadh1	NM_017070	Srd5a1	NM_053536	Klf15	NM_212505	Ier3
NM_001015010	Cib2	NM_017076	PVR	NM_053550	Pip5k2b	NM_212508	Nrm
NM_001015013	Mtvr2	NM_017079	Cd1d1	NM_053558	Trpc1	NM_212549	Ring1
NM_001015014	Surf6_predicted	NM_017107	Ogt	NM_053560	Chi3l1	NM_213562	Trim39
NM_001015026	Tm4sf12	NM_017110	Cart	NM_053561	Nap1l1	NM_213629	Arhgap20

Table A1 continued overleaf

RefSeq	Gene ID	RefSeq	Gene ID	RefSeq	Gene ID	RefSeq	Gene ID
NM_001015027	Crebl2	NM_017115	Myog	NM_053563	Ddx39	NM_001015034	Tnfrsf14
NM_001015028	Anks6	NM_017130	Neu2	NM_053568	Pcyt2	NM_017161	Adora2b
NM_001015032	Galnt3	NM_017156	CP2BC_RAT	NM_053569	Mbtps1	NM_053582	Lcn7

Table A1: Predicted miR-9-1 targets

RefSeq	Gene ID	RefSeq	Gene ID	RefSeq	Gene ID	RefSeq	Gene ID
NM_001001508	Prg1	NM_001024795	Rnf44	NM_019232	Sgk	NM_053811	Slc9a3r2
NM_001001510	Klhl10	NM_001024865	LOC684557	NM_019243	Ptgfrn	NM_053818	Slc6a9
NM_001002279	Rnf166	NM_001024874	Rhox9	NM_019250	Ralgds	NM_053851	Cacnb2
NM_001002798	Top1mt	NM_001024876	RGD1305156	NM_019253	Ptpn5	NM_053880	Dncic2
NM_001002819	Gfpt2	NM_001024885	RGD1308637	NM_019261	Klrc2	NM_053883	Dusp6
NM_001003957	Dnmt3a	NM_001024890	MGC114520	NM_019282	Grem1	NM_053896	Aldh1a2
NM_001003975	G4	NM_001024965	RGD1306925	NM_019331	Pcsk3	NM_053917	Inpp4b
NM_001003978	Gspt1	NM_001024968	RGD1307594	NM_019336	Rgs1	NM_053923	Pik3c2g
NM_001004228	Emcn	NM_001025000	RGD1309288	NM_019344	Rgs8	NM_053947	Mark1
NM_001004244	RGD1303127	NM_001025009	Josd1	NM_019362	Stk39	NM_053949	Kcnh2
NM_001004253	Syap1	NM_001025020	RGD1310753	NM_020089	LOC56764	NM_053978	Rab28
NM_001004255	Dek	NM_001025022	RGD1308059	NM_021653	Dio1	NM_053981	Kcnj12
NM_001004260	Slc22a18	NM_001025027	Fundc1	NM_021671	Tmem33	NM_053985	H3f3b
NM_001004277	Lypla3	NM_001025035	Thnsl1	NM_021682	Negr1	NM_053997	Kcnc3
NM_001004418	Tacc2	NM_001025685	Cd5l	NM_021693	Snf1lk	NM_053998	Rab8a
NM_001005538	MGC94288	NM_001025701	MGC116373	NM_021702	Atxn3	NM_054000	Kcnb2
NM_001005539	Smpdl3a	NM_001025756	MGC114379	NM_021766	Pgrmc1	NM_054002	Zbtb7a
NM_001005544	Morn1	NM_001029909	CPG2	NM_021776	Ecel1	NM_054011	Sh3bp5
NM_001005902	Abtb1	NM_001029914	LOC291823	NM_021835	Jun	NM_057139	Hnrpu
NM_001006991	Nudt9	NM_001029919	RGD1306053	NM_022198	Clcn4-2	NM_057141	Hnrpk
NM_001006993	Sgcg	NM_001030025	Upp1	NM_022224	Pter	NM_057148	Sep-02
NM_001006994	MGC94555	NM_001031663	LOC500419	NM_022254	Gpr85	NM_057210	Sv2a
NM_001007020	Hmgn3	NM_001033653	Akap12	NM_022257	Masp1	NM_080394	Reln
NM_001007145	Catna1	NM_001033680	Syt1	NM_022280	Lrat	NM_080397	Chst10

Table A2 continued overleaf

RefSeq	Gene ID	RefSeq	Gene ID	RefSeq	Gene ID	RefSeq	Gene ID
NM_001007235	Itpr1	NM_001033693	Slc31a2	NM_022296	Xylt2	NM_080411	Gpr83
NM_001007606	Sars1	NM_001033715	Cast	NM_022392	Insig1	NM_080480	Pip5k2c
NM_001007629	NTF2	NM_001033867	Crkrs	NM_022400	Bcat2	NM_080775	Smgb
NM_001007646	Fkbp9	NM_001033896	RGD1309886	NM_022403	Tdo2	NM_080888	Bnip3l
NM_001007660	MGC94183	NM_001033958	Obp3	NM_022407	Aldh1a1	NM_080902	Higd1a
NM_001007669	Zfp672	NM_001034006	Centb2	NM_022498	Ppp1cc	NM_080906	Ddit4
NM_001007681	Zfp219	NM_001034010	RGD1310827	NM_022585	Azin1	NM_130739	Acsl6
NM_001007688	RGD1359600	NM_001034110	Ctsf	NM_022589	Tspan2	NM_130749	Mark3
NM_001007694	Ifit3	NM_001034830	Zfp384	NM_022631	Wnt5a	NM_130779	Adcy3
NM_001007698	RGD1560806_predicted	NM_001034918	Iws1	NM_022690	Ube2g1	NM_130813	Kcnk15
NM_001007706	RGD1359191	NM_001034950	Rup2	NM_022697	Rpl28	NM_133306	Oldlr1
NM_001007720	Gorasp2	NM_001034994	Rwdd4a	NM_022698	Bad_v2	NM_133317	Tob1
NM_001007721	Emp2	NM_001035007	Mbtps2	NM_022853	Slc30a1	NM_133396	Tesk2
NM_001007730	Cabp7	NM_001037184	RGD1307100	NM_022864	Cplx1	NM_133397	Erg
NM_001007731	Golga7	NM_001037191	RGD1306873	NM_022939	Stx12	NM_133398	Mtdh
NM_001007737	RGD1359158	NM_001037214	Cdca4	NM_022946	Dlgap1	NM_133423	Yt521
NM_001007746	MGC94199	NM_001037336	Lrrc4	NM_022957	Serpina5	NM_133425	Ppp1r14c
NM_001008287	Donson	NM_001037772	LOC300963	NM_023025	Cyp2j3	NM_133427	Cyb5r4
NM_001008305	RGD1304686	NM_001037774	Cldn8	NM_023092	Myo1c	NM_133551	Pla2g4a
NM_001008325	RGD1311364	NM_001039005	Mcoln2	NM_023955	Scamp2	NM_133560	Trak2
NM_001008373	RGD1305356	NM_001039009	Zdhhc21	NM_023979	Apaf1	NM_133561	Brp44l
NM_001008511	Esrra	NM_001039010	Ppcs	NM_023991	Prkaa2	NM_133578	Dusp5
NM_001008521	Ptk9	NM_001039099	LOC291967	NM_024001	Mrs2l	NM_133611	Slc2a13
NM_001008557	Mip1	NM_001039196	Slc39a13	NM_024127	Gadd45a	NM_134327	Cd69
NM_001008694	LOC361571	NM_001039455	RGD1309570	NM_024151	Arf4	NM_134363	Slc12a5
NM_001008802	Kb1	NM_001039686	RGD1311934_predicted	NM_024361	Ndst1	NM_134371	Trpm8

Table A2 continued overleaf

RefSeq	Gene ID	RefSeq	Gene ID	RefSeq	Gene ID	RefSeq	Gene ID
NM_001008891	Ssr1	NM_001042619	Hsd3b1	NM_024371	Slc6a1	NM_134373	Avpi1
NM_001009264	RGD1306635_predicted	NM_001047110	LOC499770	NM_024379	Grid2	NM_134392	Spata6
NM_001009413	RGD1306495	NM_001077641	Plcb1	NM_024398	Aco2	NM_138504	Okl38
NM_001009622	Sar1b	NM_001079884	Galntl4_predicted	NM_024405	Axin1	NM_138515	Cyp2d4v1
NM_001009636	RGD1308082	NM_001080149	Ptpn20_predicted	NM_030829	Gprk5	NM_138519	Dkk3
NM_001009665	Ebag9	NM_001080150	RGD1309969	NM_030830	Luzp1	NM_138535	Grip2_v3
NM_001009677	Plekhm1	NM_012491	Add2	NM_030835	RAMP4	NM_138710	Dab2ip
NM_001009691	Dclk2_predicted	NM_012517	Cacna1c	NM_030849	Bmpr1a	NM_138710	Dab2ip
NM_001009704	Sipa1l2	NM_012527	Chrm3	NM_030990	Plp	NM_138833	Snrk
NM_001009825	Ppp1r7	NM_012537	C11B1_RAT	NM_031007	Adcy2	NM_138855	Spdy1
NM_001009967	Pip5k1c	NM_012538	Cyp11b2	NM_031011	Amd1	NM_138861	Prl2b1
NM_001011557	RGD1305677	NM_012545	Ddc	NM_031022	Cspg4	NM_138871	Tdrd7
NM_001011900	Tssk1	NM_012587	Ibsp	NM_031024	Dbn1	NM_138879	Sele
NM_001011914	Dr1	NM_012588	Igfbp3	NM_031123	Stc1	NM_138886	Ick
NM_001011941	Cdc37l1	NM_012589	Il6	NM_031139	Usf2	NM_138891	Gpr149
NM_001011944	Slc37a1	NM_012604	Myh3	NM_031351	Atrn	NM_139040	RGD621098
NM_001011947	Rai14	NM_012607	Nefh	NM_031541	Scarb1	NM_139097	Scn3b
NM_001011971	XRG4	NM_012619	Pah	NM_031561	LOC685953	NM_139190	Calcoco1
NM_001011974	Akap2	NM_012651	Slc4a1	NM_031563	Ybx1	NM_139256	Man2c1
NM_001011985	Mknk2	NM_012652	Slc9a1	NM_031597	Kcnq3	NM_139324	Ehd4
NM_001012000	Plscr4	NM_012655	Sp1	NM_031601	Cacna1g	NM_144748	LOC246263
NM_001012010	Rhot1_predicted	NM_012663	Vamp2	NM_031633	Foxm1	NM_144754	Cant1
NM_001012015	Lamp3	NM_012699	Dnajb9	NM_031656	Stx8	NM_145767	Prrxl1
NM_001012066	Sphk2	NM_012700	Stx1b2	NM_031657	Gprk6	NM_145774	Rab38
NM_001012092	Xkr7	NM_012708	Psmb9	NM_031659	Tgm1	NM_145782	Cyp3a18
NM_001012116	Spag1	NM_012724	Fcer1a	NM_031665	Stx6	NM_147135	Sbk1

Table A2 continued overleaf

ResSeq	Gene ID	RefSeq	Gene ID	RefSeq	Gene ID	RefSeq	Gene ID
NM_001012147	Pxn	NM_012765	Htr2c	NM_031678	Per2	NM_147205	St6gal1
NM_001012148	Ankrd13	NM_012781	Arnt2	NM_031685	Gosr2	NM_147215	Obp3
NM_001012169	Zfp143	NM_012812	Cox6a2	NM_031696	Gpr88	NM_153297	Cops2
NM_001012238	RGD1311980	NM_012815	Gclc	NM_031705	Dpys	NM_153310	St18
NM_001012464	Terf1	NM_012843	Emp1	NM_031722	Tmed2	NM_153467	Gsbs
NM_001012473	Polr2c	NM_012864	Mmp7	NM_031729	Ppp5c	NM_153629	Hspa4
NM_001013033	Tspyl	NM_012866	Nfyc	NM_031730	Kcnd2	NM_153728	Soat2
NM_001013040	Ptpn9	NM_012887	Tmpo	NM_031743	Slc24a2	NM_153735	Nptx1
NM_001013066	Sipa1l3	NM_012909	Aqp2	NM_031772	Rpo1-4	NM_153814	Cacna1h
NM_001013082	Pon2	NM_012922	Casp3	NM_031785	Atp6ap1	NM_172019	Ifi47
NM_001013084	Akr1b10	NM_012941	Cyp51	NM_031786	Trim3	NM_172045	Ppp1r14b
NM_001013094	Ccnl2	NM_012942	Cyp7a1	NM_031795	Ugcg	NM_172047	Eaf2
NM_001013161	Cstf1	NM_012950	F2r	NM_031798	Slc12a2	NM_172066	Slc30a4
NM_001013171	Gulp1	NM_012983	Myo1d	NM_031802	Gabbr2	NM_172157	Arid1b
NM_001013172	Fhl4	NM_013026	Sdc1	NM_031821	Plk2	NM_172223	Pxmp4
NM_001013192	Olfml1	NM_013037	Il1rl1	NM_031976	Prkab1	NM_172243	Ppif
NM_001013196	Dnajc4	NM_013045	Tnr	NM_031979	Csda	NM_172321	Slc6a15
NM_001013209	Dnajb6	NM_013049	Tnfrsf4	NM_032061	Cntnap1	NM_172328	Tac4
NM_001013218	Reep6	NM_013051	Scgb1a1	NM_032067	Ralbp1	NM_173096	Mx1
NM_001013224	Nmnat3	NM_013065	Ppp1cb	NM_032077	Pon1	NM_173098	Slc9a4
NM_001013228	Tcte1l	NM_013081	Ptk2	NM_032614	Txnl2	NM_173130	LOC286914
NM_001013907	LOC294513	NM_013102	Fkbp1a	NM_032617	Rab11b	NM_173141	Tfpi2
NM_001013933	Ube2a	NM_013113	Atp1b1	NM_033096	Ppm1b	NM_173300	Olr1271
NM_001013956	RGD1309049	NM_013127	Cd38	NM_033442	Gata2	NM_173328	Lgr4
NM_001013980	LOC304138	NM_013131	Nr3c2	NM_052804	Fmr1	NM_173339	Ceacam10
NM_001013992	LOC305691	NM_013133	Glra1	NM_053293	Gstt1	NM_175578	Dscr1l1

Table A2 continued overleaf

RefSeq	Gene ID	RefSeq	Gene ID	RefSeq	Gene ID	RefSeq	Gene ID
NM_001013994	Rcor2	NM_013159	Ide	NM_053297	Pkm2	NM_175758	Slc1a5
NM_001014011	Gramd3	NM_013179	Hcrt	NM_053301	Hfe	NM_177927	Serpinf1
NM_001014045	RGD1311463	NM_013192	Kcnj6	NM_053343	Dclk1	NM_178093	Mtus1
NM_001014064	Pars2	NM_017006	G6pdx	NM_053356	Col1a2	NM_178102	Mapkapk2
NM_001014073	RGD1305486	NM_017011	Grm1	NM_053358	Ssbp3	NM_178106	Entpd3
NM_001014075	RGD1311648	NM_017025	Ldha	NM_053394	Klf5	NM_178866	Igf1
NM_001014082	Ncln	NM_017029	Nef3	NM_053421	Arid4b	NM_178866	Igf1
NM_001014094	LOC315883	NM_017031	Pde4b	NM_053427	Slc17a6	NM_181090	Slc38a2
NM_001014109	LOC317379	NM_017044	Pth	NM_053429	Fgfr3	NM_181626	Hbld2
NM_001014122	Mif4gd	NM_017066	Ptn	NM_053455	Fgl2	NM_181631	Fbxo11
NM_001014126	RGD1306410	NM_017067	Chm	NM_053457	Cldn11	NM_181633	Gpr151
NM_001014130	RGD1309106	NM_017097	Ctsc	NM_053458	Rab9	NM_181636	Col23a1
NM_001014133	LOC360910	NM_017116	Capn2	NM_053502	Abcg1	NM_182817	Smagp
NM_001014149	RGD1305276	NM_017127	Chka	NM_053503	Jub	NM_183056	Lyk4
NM_001014172	Rsrc1	NM_017131	Casq2	NM_053521	Slc5a7	NM_183326	Gabra1
NM_001014175	LOC500378	NM_017156	CP2BC_RAT	NM_053530	Twist1	NM_184051	Prkag2
NM_001014177	LOC362056	NM_017159	Hal	NM_053536	Klf15	NM_198735	Art2b
NM_001014185	LOC362264	NM_017226	Padi2	NM_053549	Dnajc4	NM_198760	Slc16a6
NM_001014190	RGD1307218	NM_017238	Vipr2	NM_053557	Hrmt1l3	NM_198771	Fam3c
NM_001014231	RGD1308513	NM_017259	Btg2	NM_053577	SPP24_RAT	NM_198779	RGD735140
NM_001014245	RGD1305441	NM_017261	Gria2	NM_053591	Dpep1	NM_198783	Hrpap20
NM_001014275	Tceal8	NM_017263	Gria4	NM_053603	Clic5	NM_198972	Gkn1
NM_001015020	Tgif	NM_017288	Scn1b	NM_053610	Prdx5	NM_199237	Fshr
NM_001015025	Stk38	NM_017290	Atp2a2	NM_053633	Egr2	NM_199267	Rela
NM_001017485	LOC498145	NM_017298	Cacna1d_v3	NM_053650	Pdlim3	NM_199407	Unc5c
NM_001017498	LOC498350	NM_017305	Gclm	NM_053722	Clasp2	NM_199409	Panx2

Table A2 continued overleaf

RefSeq	Gene ID	RefSeq	Gene ID	RefSeq	Gene ID	RefSeq	Gene ID
NM_001024252	Pcaf	NM_017336	Ptpro	NM_053733	Bcl2l10	NM_199502	Chrdl1
NM_001024252	Pcaf	NM_017348	Slc6a8	NM_053736	Casp4	NM_201560	RGD1303142
NM_001024252	Pcaf	NM_019146	Bsn	NM_053738	Wif1	NM_203334	Slc6a5
NM_001024262	RGD1305424	NM_019147	Jag1	NM_053750	Nppc	NM_203336	Esrrg
NM_001024275	Rassf4	NM_019155	Cav3	NM_053769	Dusp1	NM_207586	Chia
NM_001024278	LOC367171	NM_019157	Aqp7	NM_053779	Serpini1	NM_207595	Ankra2
NM_001024296	LOC499418	NM_019194	Tef	NM_053801	Sec14l2	NM_207603	Fcgr3a
NM_001024305	LOC499691	NM_019207	Neurod3	NM_053805	Snai1	NM_207610	Ube4a
NM_001024316	LOC499951	NM_019218	Neurod1	NM_053806	Kcnk6	NM_212498	RGD1303066
NM_001024349	LOC500598	NM_019219	Rbbp9	NM_019221	Trp63	NM_212504	Hspa1b
NM_001024355	LOC500909						

Table A2 Predicted miR-137 targets

Reference List

(1) World Health Organisation: Global Burden of Disease 2004 Update. http://www.who.int/healthinfo/global_burden_disease/2004_report_update/en/print.html. 2004.

(2) British Heart Foundation Statistics Website. http://www.heartstats.org/homepage.asp. 2009.

(3) Yusuf S, Hawken S, Ounpuu S, Dans T, Avezum A, Lanas F et al. Effect of potentially modifiable risk factors associated with myocardial infarction in 52 countries (the INTERHEART study): case-control study. Lancet 2004; 364(9438):937-952.

(4) Sowers JR. Obesity as a cardiovascular risk factor. Am J Med 2003; 115 Suppl 8A:37S-41S.

(5) International Diabetes Federation: Diabetes Facts and Figures. http://www.idf.org/Facts_and_Figures. 2009.

(6) Levy D, Larson MG, Vasan RS, Kannel WB, Ho KK. The progression from hypertension to congestive heart failure. JAMA 1996; 275(20):1557-1562.

(7) Vasan RS, Beiser A, Seshadri S, Larson MG, Kannel WB, D'Agostino RB et al. Residual lifetime risk for developing hypertension in middle-aged women and men: The Framingham Heart Study. JAMA 2002; 287(8):1003-1010.

(8) Lewington S, Clarke R, Qizilbash N, Peto R, Collins R. Age-specific relevance of usual blood pressure to vascular mortality: a meta-analysis of individual data for one million adults in 61 prospective studies. Lancet 2002; 360(9349):1903-1913.

(9) Kannel WB, Dawber TR, Sorlie P, Wolf PA. Components of blood pressure and risk of atherothrombotic brain infarction: the Framingham study. Stroke 1976; 7(4):327-331.

(10) Klag MJ, Whelton PK, Randall BL, Neaton JD, Brancati FL, Ford CE et al. Blood pressure and end-stage renal disease in men. N Engl J Med 1996; 334(1):13-18.

(11) Chobanian AV, Bakris GL, Black HR, Cushman WC, Green LA, Izzo JL, Jr. et al. Seventh report of the Joint National Committee on Prevention, Detection, Evaluation, and Treatment of High Blood Pressure. Hypertension 2003; 42(6):1206-1252.

(12) Vasan RS, Larson MG, Leip EP, Evans JC, O'Donnell CJ, Kannel WB et al. Impact of high-normal blood pressure on the risk of cardiovascular disease. N Engl J Med 2001; 345(18):1291-1297.

(13) Neal B, MacMahon S, Chapman N. Effects of ACE inhibitors, calcium antagonists, and other blood-pressure-lowering drugs: results of prospectively designed overviews of randomised trials. Blood Pressure Lowering Treatment Trialists' Collaboration. Lancet 2000; 356(9246):1955-1964.

(14) Eckel RH, Grundy SM, Zimmet PZ. The metabolic syndrome. Lancet 2005; 365(9468):1415-1428.

(15) Kannel WB. Blood pressure as a cardiovascular risk factor: prevention and treatment. JAMA 1996; 275(20):1571-1576.

(16) Bianchi G, Fox U, Di Francesco GF, Giovanetti AM, Pagetti D. Blood pressure changes produced by kidney cross-transplantation between spontaneously hypertensive rats and normotensive rats. Clin Sci Mol Med 1974; 47(5):435-448.

(17) Meneton P, Jeunemaitre X, de Wardener HE, MacGregor GA. Links between dietary salt intake, renal salt handling, blood pressure, and cardiovascular diseases. Physiol Rev 2005; 85(2):679-715.

(18) Lavoie JL, Sigmund CD. Minireview: overview of the renin-angiotensin system--an endocrine and paracrine system. Endocrinology 2003; 144(6):2179-2183.

(19) Cowley AW, Jr. The genetic dissection of essential hypertension. Nat Rev Genet 2006; 7(11):829-840.

(20) Unger T. The role of the renin-angiotensin system in the development of cardiovascular disease. Am J Cardiol 2002; 89(2A):3A-9A.

(21) Donoghue M, Hsieh F, Baronas E, Godbout K, Gosselin M, Stagliano N et al. A novel angiotensin-converting enzyme-related carboxypeptidase (ACE2) converts angiotensin I to angiotensin 1-9. Circ Res 2000; 87(5):E1-E9.

(22) Santos RA, Simoes e Silva AC, Maric C, Silva DM, Machado RP, de B, I et al. Angiotensin-(1-7) is an endogenous ligand for the G protein-coupled receptor Mas. Proc Natl Acad Sci U S A 2003; 100(14):8258-8263.

(23) Kearney PM, Whelton M, Reynolds K, Muntner P, Whelton PK, He J. Global burden of hypertension: analysis of worldwide data. Lancet 2005; 365(9455):217-223.

(24) Franklin SS, Larson MG, Khan SA, Wong ND, Leip EP, Kannel WB et al. Does the relation of blood pressure to coronary heart disease risk change with aging? The Framingham Heart Study. Circulation 2001; 103(9):1245-1249.

(25) Appel LJ, Moore TJ, Obarzanek E, Vollmer WM, Svetkey LP, Sacks FM et al. A clinical trial of the effects of dietary patterns on blood pressure. DASH Collaborative Research Group. N Engl J Med 1997; 336(16):1117-1124.

(26) Vollmer WM, Sacks FM, Ard J, Appel LJ, Bray GA, Simons-Morton DG et al. Effects of diet and sodium intake on blood pressure: subgroup analysis of the DASH-sodium trial. Ann Intern Med 2001; 135(12):1019-1028.

(27) He J, Whelton PK, Appel LJ, Charleston J, Klag MJ. Long-term effects of weight loss and dietary sodium reduction on incidence of hypertension. Hypertension 2000; 35(2):544-549.

(28) Slama M, Susic D, Frohlich ED. Prevention of hypertension. Curr Opin Cardiol 2002; 17(5):531-536.

(29) Xin X, He J, Frontini MG, Ogden LG, Motsamai OI, Whelton PK. Effects of alcohol reduction on blood pressure: a meta-analysis of randomized controlled trials. Hypertension 2001; 38(5):1112-1117.

(30) He J, Bazzano LA. Effects of lifestyle modification on treatment and prevention of hypertension. Curr Opin Nephrol Hypertens 2000; 9(3):267-271.

(31) Longini IM, Jr., Higgins MW, Hinton PC, Moll PP, Keller JB. Environmental and genetic sources of familial aggregation of blood pressure in Tecumseh, Michigan. Am J Epidemiol 1984; 120(1):131-144.

(32) Feinleib M, Garrison RJ, Fabsitz R, Christian JC, Hrubec Z, Borhani NO et al. The NHLBI twin study of cardiovascular disease risk factors: methodology and summary of results. Am J Epidemiol 1977; 106(4):284-285.

(33) Sutherland DJ, Ruse JL, Laidlaw JC. Hypertension, increased aldosterone secretion and low plasma renin activity relieved by dexamethasone. Can Med Assoc J 1966; 95(22):1109-1119.

(34) Hansson JH, Nelson-Williams C, Suzuki H, Schild L, Shimkets R, Lu Y et al. Hypertension caused by a truncated epithelial sodium channel gamma subunit: genetic heterogeneity of Liddle syndrome. Nat Genet 1995; 11(1):76-82.

(35) Wilson FH, Disse-Nicodeme S, Choate KA, Ishikawa K, Nelson-Williams C, Desitter I et al. Human hypertension caused by mutations in WNK kinases. Science 2001; 293(5532):1107-1112.

(36) New MI, Levine LS, Biglieri EG, Pareira J, Ulick S. Evidence for an unidentified steroid in a child with apparent mineralocorticoid hypertension. J Clin Endocrinol Metab 1977; 44(5):924-933.

(37) Jeunemaitre X, Soubrier F, Kotelevtsev YV, Lifton RP, Williams CS, Charru A et al. Molecular basis of human hypertension: role of angiotensinogen. Cell 1992; 71(1):169-180.

(38) Corvol P, Persu A, Gimenez-Roqueplo AP, Jeunemaitre X. Seven lessons from two candidate genes in human essential hypertension: angiotensinogen and epithelial sodium channel. Hypertension 1999; 33(6):1324-1331.

(39) Caulfield M, Lavender P, Farrall M, Munroe P, Lawson M, Turner P et al. Linkage of the angiotensinogen gene to essential hypertension. N Engl J Med 1994; 330(23):1629-1633.

(40) Staessen JA, Kuznetsova T, Wang JG, Emelianov D, Vlietinck R, Fagard R. M235T angiotensinogen gene polymorphism and cardiovascular renal risk. J Hypertens 1999; 17(1):9-17.

(41) Jeunemaitre X, Lifton RP, Hunt SC, Williams RR, Lalouel JM. Absence of linkage between the angiotensin converting enzyme locus and human essential hypertension. Nat Genet 1992; 1(1):72-75.

(42) O'Donnell CJ, Lindpaintner K, Larson MG, Rao VS, Ordovas JM, Schaefer EJ et al. Evidence for association and genetic linkage of the angiotensin-converting enzyme locus with hypertension and blood pressure in men but not women in the Framingham Heart Study. Circulation 1998; 97(18):1766-1772.

(43) Fornage M, Amos CI, Kardia S, Sing CF, Turner ST, Boerwinkle E. Variation in the region of the angiotensin-converting enzyme gene influences interindividual differences in blood pressure levels in young white males. Circulation 1998; 97(18):1773-1779.

(44) Knight J, Munroe PB, Pembroke JC, Caulfield MJ. Human chromosome 17 in essential hypertension. Ann Hum Genet 2003; 67(Pt 2):193-206.

(45) Bianchi G, Ferrari P, Staessen JA. Adducin polymorphism: detection and impact on hypertension and related disorders. Hypertension 2005; 45(3):331-340.

(46) Bianchi G, Tripodi G, Casari G, Salardi S, Barber BR, Garcia R et al. Two point mutations within the adducin genes are involved in blood pressure variation. Proc Natl Acad Sci U S A 1994; 91(9):3999-4003.

(47) Tripodi G, Florio M, Ferrandi M, Modica R, Zimdahl H, Hubner N et al. Effect of Add1 gene transfer on blood pressure in reciprocal congenic strains of Milan rats. Biochem Biophys Res Commun 2004; 324(2):562-568.

(48) Casari G, Barlassina C, Cusi D, Zagato L, Muirhead R, Righetti M et al. Association of the alpha-adducin locus with essential hypertension. Hypertension 1995; 25(3):320-326.

(49) Cusi D, Barlassina C, Azzani T, Casari G, Citterio L, Devoto M et al. Polymorphisms of alpha-adducin and salt sensitivity in patients with essential hypertension. Lancet 1997; 349(9062):1353-1357.

(50) Clark CJ, Davies E, Anderson NH, Farmer R, Friel EC, Fraser R et al. alpha-adducin and angiotensin I-converting enzyme polymorphisms in essential hypertension. Hypertension 2000; 36(6):990-994.

(51) Tikhonoff V, Kuznetsova T, Stolarz K, Bianchi G, Casiglia E, Kawecka-Jaszcz K et al. beta-Adducin polymorphisms, blood pressure, and sodium

excretion in three European populations. Am J Hypertens 2003; 16(10):840-846.

(52) Padmanabhan S, Melander O, Hastie C, Menni C, Delles C, Connell JM et al. Hypertension and genome-wide association studies: combining high fidelity phenotyping and hypercontrols. J Hypertens 2008; 26(7):1275-1281.

(53) Caulfield M, Munroe P, Pembroke J, Samani N, Dominiczak A, Brown M et al. Genome-wide mapping of human loci for essential hypertension. Lancet 2003; 361(9375):2118-2123.

(54) Munroe PB, Wallace C, Xue MZ, Marcano AC, Dobson RJ, Onipinla AK et al. Increased support for linkage of a novel locus on chromosome 5q13 for essential hypertension in the British Genetics of Hypertension Study. Hypertension 2006; 48(1):105-111.

(55) Harrap SB. Where are all the blood-pressure genes? Lancet 2003; 361(9375):2149-2151.

(56) Province MA, Kardia SL, Ranade K, Rao DC, Thiel BA, Cooper RS et al. A meta-analysis of genome-wide linkage scans for hypertension: the National Heart, Lung and Blood Institute Family Blood Pressure Program. Am J Hypertens 2003; 16(2):144-147.

(57) Hirschhorn JN, Daly MJ. Genome-wide association studies for common diseases and complex traits. Nat Rev Genet 2005; 6(2):95-108.

(58) Genome-wide association study of 14,000 cases of seven common diseases and 3,000 shared controls. Nature 2007; 447(7145):661-678.

(59) OKAMOTO K, AOKI K. Development of a strain of spontaneously hypertensive rats. Jpn Circ J 1963; 27:282-293.

(60) McBride MW, Charchar FJ, Graham D, Miller WH, Strahorn P, Carr FJ et al. Functional genomics in rodent models of hypertension. J Physiol 2004; 554(Pt 1):56-63.

(61) Pinto YM, Paul M, Ganten D. Lessons from rat models of hypertension: from Goldblatt to genetic engineering. Cardiovasc Res 1998; 39(1):77-88.

(62) Nagaoka A, Iwatsuka H, Suzuoki Z, OKAMOTO K. Genetic predisposition to stroke in spontaneously hypertensive rats. Am J Physiol 1976; 230(5):1354-1359.

(63) Rapp JP. Genetic analysis of inherited hypertension in the rat. Physiol Rev 2000; 80(1):135-172.

(64) Aitman TJ, Gotoda T, Evans AL, Imrie H, Heath KE, Trembling PM et al. Quantitative trait loci for cellular defects in glucose and fatty acid metabolism in hypertensive rats. Nat Genet 1997; 16(2):197-201.

(65) Aitman TJ, Glazier AM, Wallace CA, Cooper LD, Norsworthy PJ, Wahid FN et al. Identification of Cd36 (Fat) as an insulin-resistance gene

causing defective fatty acid and glucose metabolism in hypertensive rats. Nat Genet 1999; 21(1):76-83.

(66) Pravenec M, Landa V, Zidek V, Musilova A, Kazdova L, Qi N et al. Transgenic expression of CD36 in the spontaneously hypertensive rat is associated with amelioration of metabolic disturbances but has no effect on hypertension. Physiol Res 2003; 52(6):681-688.

(67) Pravenec M, Churchill PC, Churchill MC, Viklicky O, Kazdova L, Aitman TJ et al. Identification of renal Cd36 as a determinant of blood pressure and risk for hypertension. Nat Genet 2008; 40(8):952-954.

(68) Clark JS, Jeffs B, Davidson AO, Lee WK, Anderson NH, Bihoreau MT et al. Quantitative trait loci in genetically hypertensive rats. Possible sex specificity. Hypertension 1996; 28(5):898-906.

(69) McBride MW, Carr FJ, Graham D, Anderson NH, Clark JS, Lee WK et al. Microarray analysis of rat chromosome 2 congenic strains. Hypertension 2003; 41(3 Pt 2):847-853.

(70) Jeffs B, Negrin CD, Graham D, Clark JS, Anderson NH, Gauguier D et al. Applicability of a "speed" congenic strategy to dissect blood pressure quantitative trait loci on rat chromosome 2. Hypertension 2000; 35(1 Pt 2):179-187.

(71) Rettig R, Schmitt B, Pelzl B, Speck T. The kidney and primary hypertension: contributions from renal transplantation studies in animals and humans. J Hypertens 1993; 11(9):883-891.

(72) Cowley AW, Jr., Roman RJ. The role of the kidney in hypertension. JAMA 1996; 275(20):1581-1589.

(73) Guyton AC. Blood pressure control--special role of the kidneys and body fluids. Science 1991; 252(5014):1813-1816.

(74) Crowley SD, Gurley SB, Oliverio MI, Pazmino AK, Griffiths R, Flannery PJ et al. Distinct roles for the kidney and systemic tissues in blood pressure regulation by the renin-angiotensin system. J Clin Invest 2005; 115(4):1092-1099.

(75) Masilamani S, Kim GH, Mitchell C, Wade JB, Knepper MA. Aldosterone-mediated regulation of ENaC alpha, beta, and gamma subunit proteins in rat kidney. J Clin Invest 1999; 104(7):R19-R23.

(76) Garvin JL, Ortiz PA. The role of reactive oxygen species in the regulation of tubular function. Acta Physiol Scand 2003; 179(3):225-232.

(77) McBride MW, Brosnan MJ, Mathers J, McLellan LI, Miller WH, Graham D et al. Reduction of Gstm1 expression in the stroke-prone spontaneously hypertension rat contributes to increased oxidative stress. Hypertension 2005; 45(4):786-792.

(78) Le TH, Fogo AB, Salzler HR, Vinogradova T, Oliverio MI, Marchuk DA et al. Modifier locus on mouse chromosome 3 for renal vascular pathology in AT1A receptor-deficiency. Hypertension 2004; 43(2):445-451.

(79) Yang Y, Parsons KK, Chi L, Malakauskas SM, Le TH. Glutathione S-transferase-micro1 regulates vascular smooth muscle cell proliferation, migration, and oxidative stress. Hypertension 2009; 54(6):1360-1368.

(80) Touyz RM. Reactive oxygen species, vascular oxidative stress, and redox signaling in hypertension: what is the clinical significance? Hypertension 2004; 44(3):248-252.

(81) Fortuno A, Jose GS, Moreno MU, Diez J, Zalba G. Oxidative stress and vascular remodelling. Exp Physiol 2005; 90(4):457-462.

(82) Vaziri ND, Wang XQ, Oveisi F, Rad B. Induction of oxidative stress by glutathione depletion causes severe hypertension in normal rats. Hypertension 2000; 36(1):142-146.

(83) Nabha L, Garbern JC, Buller CL, Charpie JR. Vascular oxidative stress precedes high blood pressure in spontaneously hypertensive rats. Clin Exp Hypertens 2005; 27(1):71-82.

(84) Cai H, Harrison DG. Endothelial dysfunction in cardiovascular diseases: the role of oxidant stress. Circ Res 2000; 87(10):840-844.

(85) Ushio-Fukai M, Zafari AM, Fukui T, Ishizaka N, Griendling KK. p22phox is a critical component of the superoxide-generating NADH/NADPH oxidase system and regulates angiotensin II-induced hypertrophy in vascular smooth muscle cells. J Biol Chem 1996; 271(38):23317-23321.

(86) Cave AC, Brewer AC, Narayanapanicker A, Ray R, Grieve DJ, Walker S et al. NADPH oxidases in cardiovascular health and disease. Antioxid Redox Signal 2006; 8(5-6):691-728.

(87) Griendling KK, Sorescu D, Ushio-Fukai M. NAD(P)H oxidase: role in cardiovascular biology and disease. Circ Res 2000; 86(5):494-501.

(88) Paravicini TM, Touyz RM. Redox signaling in hypertension. Cardiovasc Res 2006; 71(2):247-258.

(89) Chabrashvili T, Tojo A, Onozato ML, Kitiyakara C, Quinn MT, Fujita T et al. Expression and cellular localization of classic NADPH oxidase subunits in the spontaneously hypertensive rat kidney. Hypertension 2002; 39(2):269-274.

(90) Rajagopalan S, Laursen JB, Borthayre A, Kurz S, Keiser J, Haleen S et al. Role for endothelin-1 in angiotensin II-mediated hypertension. Hypertension 1997; 30(1 Pt 1):29-34.

(91) Rey FE, Cifuentes ME, Kiarash A, Quinn MT, Pagano PJ. Novel competitive inhibitor of NAD(P)H oxidase assembly attenuates vascular O(2)(-) and systolic blood pressure in mice. Circ Res 2001; 89(5):408-414.

(92) Ray R, Shah AM. NADPH oxidase and endothelial cell function. Clin Sci (Lond) 2005; 109(3):217-226.

(93) Blatter LA, Wier WG. Nitric oxide decreases [Ca2+]i in vascular smooth muscle by inhibition of the calcium current. Cell Calcium 1994; 15(2):122-131.

(94) Waldron GJ, Cole WC. Activation of vascular smooth muscle K+ channels by endothelium-derived relaxing factors. Clin Exp Pharmacol Physiol 1999; 26(2):180-184.

(95) Kerr S, Brosnan MJ, McIntyre M, Reid JL, Dominiczak AF, Hamilton CA. Superoxide anion production is increased in a model of genetic hypertension: role of the endothelium. Hypertension 1999; 33(6):1353-1358.

(96) Schachinger V, Britten MB, Zeiher AM. Prognostic impact of coronary vasodilator dysfunction on adverse long-term outcome of coronary heart disease. Circulation 2000; 101(16):1899-1906.

(97) Lockette W, Otsuka Y, Carretero O. The loss of endothelium-dependent vascular relaxation in hypertension. Hypertension 1986; 8(6 Pt 2):II61-II66.

(98) Higashi Y, Oshima T, Ozono R, Watanabe M, Matsuura H, Kajiyama G. Effects of L-arginine infusion on renal hemodynamics in patients with mild essential hypertension. Hypertension 1995; 25(4 Pt 2):898-902.

(99) Touyz RM, Schiffrin EL. Reactive oxygen species in vascular biology: implications in hypertension. Histochem Cell Biol 2004; 122(4):339-352.

(100) Forstermann U. Oxidative stress in vascular disease: causes, defense mechanisms and potential therapies. Nat Clin Pract Cardiovasc Med 2008; 5(6):338-349.

(101) Diaz MN, Frei B, Vita JA, Keaney JF, Jr. Antioxidants and atherosclerotic heart disease. N Engl J Med 1997; 337(6):408-416.

(102) Yusuf S, Dagenais G, Pogue J, Bosch J, Sleight P. Vitamin E supplementation and cardiovascular events in high-risk patients. The Heart Outcomes Prevention Evaluation Study Investigators. N Engl J Med 2000; 342(3):154-160.

(103) Lonn E, Bosch J, Yusuf S, Sheridan P, Pogue J, Arnold JM et al. Effects of long-term vitamin E supplementation on cardiovascular events and cancer: a randomized controlled trial. JAMA 2005; 293(11):1338-1347.

(104) May JM. How does ascorbic acid prevent endothelial dysfunction? Free Radic Biol Med 2000; 28(9):1421-1429.

(105) Heitzer T, Schlinzig T, Krohn K, Meinertz T, Munzel T. Endothelial dysfunction, oxidative stress, and risk of cardiovascular events in patients with coronary artery disease. Circulation 2001; 104(22):2673-2678.

(106) Gokce N, Keaney JF, Jr., Frei B, Holbrook M, Olesiak M, Zachariah BJ et al. Long-term ascorbic acid administration reverses endothelial vasomotor dysfunction in patients with coronary artery disease. Circulation 1999; 99(25):3234-3240.

(107) Taddei S, Virdis A, Ghiadoni L, Magagna A, Salvetti A. Vitamin C improves endothelium-dependent vasodilation by restoring nitric oxide activity in essential hypertension. Circulation 1998; 97(22):2222-2229.

(108) Heller R, Munscher-Paulig F, Grabner R, Till U. L-Ascorbic acid potentiates nitric oxide synthesis in endothelial cells. J Biol Chem 1999; 274(12):8254-8260.

(109) Heller R, Unbehaun A, Schellenberg B, Mayer B, Werner-Felmayer G, Werner ER. L-ascorbic acid potentiates endothelial nitric oxide synthesis via a chemical stabilization of tetrahydrobiopterin. J Biol Chem 2001; 276(1):40-47.

(110) Schnackenberg CG, Wilcox CS. The SOD mimetic tempol restores vasodilation in afferent arterioles of experimental diabetes. Kidney Int 2001; 59(5):1859-1864.

(111) Chu Y, Iida S, Lund DD, Weiss RM, DiBona GF, Watanabe Y et al. Gene transfer of extracellular superoxide dismutase reduces arterial pressure in spontaneously hypertensive rats: role of heparin-binding domain. Circ Res 2003; 92(4):461-468.

(112) Nishio E, Watanabe Y. The involvement of reactive oxygen species and arachidonic acid in alpha 1-adrenoceptor-induced smooth muscle cell proliferation and migration. Br J Pharmacol 1997; 121(4):665-670.

(113) Hamilton CA, Miller WH, Al Benna S, Brosnan MJ, Drummond RD, McBride MW et al. Strategies to reduce oxidative stress in cardiovascular disease. Clin Sci (Lond) 2004; 106(3):219-234.

(114) Zhang Y, Griendling KK, Dikalova A, Owens GK, Taylor WR. Vascular hypertrophy in angiotensin II-induced hypertension is mediated by vascular smooth muscle cell-derived H2O2. Hypertension 2005; 46(4):732-737.

(115) Yang H, Roberts LJ, Shi MJ, Zhou LC, Ballard BR, Richardson A et al. Retardation of atherosclerosis by overexpression of catalase or both Cu/Zn-superoxide dismutase and catalase in mice lacking apolipoprotein E. Circ Res 2004; 95(11):1075-1081.

(116) Zhang Y, Handy DE, Loscalzo J. Adenosine-dependent induction of glutathione peroxidase 1 in human primary endothelial cells and protection against oxidative stress. Circ Res 2005; 96(8):831-837.

(117) Forgione MA, Cap A, Liao R, Moldovan NI, Eberhardt RT, Lim CC et al. Heterozygous cellular glutathione peroxidase deficiency in the mouse: abnormalities in vascular and cardiac function and structure. Circulation 2002; 106(9):1154-1158.

(118) Hayes JD, Flanagan JU, Jowsey IR. Glutathione transferases. Annu Rev Pharmacol Toxicol 2005; 45:51-88.

(119) Jedlitschky G, Leier I, Buchholz U, Center M, Keppler D. ATP-dependent transport of glutathione S-conjugates by the multidrug resistance-associated protein. Cancer Res 1994; 54(18):4833-4836.

(120) Ishikawa T. The ATP-dependent glutathione S-conjugate export pump. Trends Biochem Sci 1992; 17(11):463-468.

(121) Wilce MC, Parker MW. Structure and function of glutathione S-transferases. Biochim Biophys Acta 1994; 1205(1):1-18.

(122) Berhane K, Widersten M, Engstrom A, Kozarich JW, Mannervik B. Detoxication of base propenals and other alpha, beta-unsaturated aldehyde products of radical reactions and lipid peroxidation by human glutathione transferases. Proc Natl Acad Sci U S A 1994; 91(4):1480-1484.

(123) Kuo WN, Kocis JM, Mewar M. Protein denitration/modification by glutathione-S-transferase and glutathione peroxidase. J Biochem Mol Biol Biophys 2002; 6(2):143-146.

(124) Pearson WR, Vorachek WR, Xu SJ, Berger R, Hart I, Vannais D et al. Identification of class-mu glutathione transferase genes GSTM1-GSTM5 on human chromosome 1p13. Am J Hum Genet 1993; 53(1):220-233.

(125) McIlwain CC, Townsend DM, Tew KD. Glutathione S-transferase polymorphisms: cancer incidence and therapy. Oncogene 2006; 25(11):1639-1648.

(126) Schneider J, Bernges U, Philipp M, Woitowitz HJ. GSTM1, GSTT1, and GSTP1 polymorphism and lung cancer risk in relation to tobacco smoking. Cancer Lett 2004; 208(1):65-74.

(127) Delles C, Padmanabhan S, Lee WK, Miller WH, McBride MW, McClure JD et al. Glutathione S-transferase variants and hypertension. J Hypertens 2008; 26(7):1343-1352.

(128) Makino A, Skelton MM, Zou AP, Roman RJ, Cowley AW, Jr. Increased renal medullary oxidative stress produces hypertension. Hypertension 2002; 39(2 Pt 2):667-672.

(129) Makino A, Skelton MM, Zou AP, Cowley AW, Jr. Increased renal medullary H2O2 leads to hypertension. Hypertension 2003; 42(1):25-30.

(130) Meng S, Roberts LJ, Cason GW, Curry TS, Manning RD, Jr. Superoxide dismutase and oxidative stress in Dahl salt-sensitive and -resistant rats. Am J Physiol Regul Integr Comp Physiol 2002; 283(3):R732-R738.

(131) Napoli C, Lemieux C, Jorgensen R. Introduction of a Chimeric Chalcone Synthase Gene into Petunia Results in Reversible Co-Suppression of Homologous Genes in trans. Plant Cell 1990; 2(4):279-289.

(132) Van der Krol AR, Mur LA, Beld M, Mol JN, Stuitje AR. Flavonoid genes in petunia: addition of a limited number of gene copies may lead to a suppression of gene expression. Plant Cell 1990; 2(4):291-299.

(133) Romano N, Macino G. Quelling: transient inactivation of gene expression in Neurospora crassa by transformation with homologous sequences. Mol Microbiol 1992; 6(22):3343-3353.

(134) Fulci V, Macino G. Quelling: post-transcriptional gene silencing guided by small RNAs in Neurospora crassa. Curr Opin Microbiol 2007; 10(2):199-203.

(135) Fire A, Xu S, Montgomery MK, Kostas SA, Driver SE, Mello CC. Potent and specific genetic interference by double-stranded RNA in Caenorhabditis elegans. Nature 1998; 391(6669):806-811.

(136) Tuschl T, Zamore PD, Lehmann R, Bartel DP, Sharp PA. Targeted mRNA degradation by double-stranded RNA in vitro. Genes Dev 1999; 13(24):3191-3197.

(137) Hannon GJ. RNA interference. Nature 2002; 418(6894):244-251.

(138) Elbashir SM, Lendeckel W, Tuschl T. RNA interference is mediated by 21- and 22-nucleotide RNAs. Genes Dev 2001; 15(2):188-200.

(139) Bernstein E, Caudy AA, Hammond SM, Hannon GJ. Role for a bidentate ribonuclease in the initiation step of RNA interference. Nature 2001; 409(6818):363-366.

(140) Liu Q, Rand TA, Kalidas S, Du F, Kim HE, Smith DP et al. R2D2, a bridge between the initiation and effector steps of the Drosophila RNAi pathway. Science 2003; 301(5641):1921-1925.

(141) Liu X, Jiang F, Kalidas S, Smith D, Liu Q. Dicer-2 and R2D2 coordinately bind siRNA to promote assembly of the siRISC complexes. RNA 2006; 12(8):1514-1520.

(142) Hammond SM, Bernstein E, Beach D, Hannon GJ. An RNA-directed nuclease mediates post-transcriptional gene silencing in Drosophila cells. Nature 2000; 404(6775):293-296.

(143) Tomari Y, Matranga C, Haley B, Martinez N, Zamore PD. A protein sensor for siRNA asymmetry. Science 2004; 306(5700):1377-1380.

(144) Hutvagner G, Simard MJ. Argonaute proteins: key players in RNA silencing. Nat Rev Mol Cell Biol 2008; 9(1):22-32.

(145) Matranga C, Tomari Y, Shin C, Bartel DP, Zamore PD. Passenger-strand cleavage facilitates assembly of siRNA into Ago2-containing RNAi enzyme complexes. Cell 2005; 123(4):607-620.

(146) Zamore PD, Tuschl T, Sharp PA, Bartel DP. RNAi: double-stranded RNA directs the ATP-dependent cleavage of mRNA at 21 to 23 nucleotide intervals. Cell 2000; 101(1):25-33.

(147) He L, Hannon GJ. MicroRNAs: small RNAs with a big role in gene regulation. Nat Rev Genet 2004; 5(7):522-531.

(148) Lee Y, Jeon K, Lee JT, Kim S, Kim VN. MicroRNA maturation: stepwise processing and subcellular localization. EMBO J 2002; 21(17):4663-4670.

(149) Lee Y, Ahn C, Han J, Choi H, Kim J, Yim J et al. The nuclear RNase III Drosha initiates microRNA processing. Nature 2003; 425(6956):415-419.

(150) Ketting RF, Fischer SE, Bernstein E, Sijen T, Hannon GJ, Plasterk RH. Dicer functions in RNA interference and in synthesis of small RNA involved in developmental timing in C. elegans. Genes Dev 2001; 15(20):2654-2659.

(151) Jinek M, Doudna JA. A three-dimensional view of the molecular machinery of RNA interference. Nature 2009; 457(7228):405-412.

(152) Elbashir SM, Harborth J, Lendeckel W, Yalcin A, Weber K, Tuschl T. Duplexes of 21-nucleotide RNAs mediate RNA interference in cultured mammalian cells. Nature 2001; 411(6836):494-498.

(153) Ovcharenko D, Jarvis R, Hunicke-Smith S, Kelnar K, Brown D. High-throughput RNAi screening in vitro: from cell lines to primary cells. RNA 2005; 11(6):985-993.

(154) McCaffrey AP, Meuse L, Pham TT, Conklin DS, Hannon GJ, Kay MA. RNA interference in adult mice. Nature 2002; 418(6893):38-39.

(155) Liu F, Song Y, Liu D. Hydrodynamics-based transfection in animals by systemic administration of plasmid DNA. Gene Ther 1999; 6(7):1258-1266.

(156) Davidson BL, Paulson HL. Molecular medicine for the brain: silencing of disease genes with RNA interference. Lancet Neurol 2004; 3(3):145-149.

(157) Xie FY, Woodle MC, Lu PY. Harnessing in vivo siRNA delivery for drug discovery and therapeutic development. Drug Discov Today 2006; 11(1-2):67-73.

(158) Jackson AL, Bartz SR, Schelter J, Kobayashi SV, Burchard J, Mao M et al. Expression profiling reveals off-target gene regulation by RNAi. Nat Biotechnol 2003; 21(6):635-637.

(159) Sorensen DR, Leirdal M, Sioud M. Gene silencing by systemic delivery of synthetic siRNAs in adult mice. J Mol Biol 2003; 327(4):761-766.

(160) Santel A, Aleku M, Keil O, Endruschat J, Esche V, Fisch G et al. A novel siRNA-lipoplex technology for RNA interference in the mouse vascular endothelium. Gene Ther 2006; 13(16):1222-1234.

(161) Zimmermann TS, Lee AC, Akinc A, Bramlage B, Bumcrot D, Fedoruk MN et al. RNAi-mediated gene silencing in non-human primates. Nature 2006; 441(7089):111-114.

(162) Wang X, Skelley L, Cade R, Sun Z. AAV delivery of mineralocorticoid receptor shRNA prevents progression of cold-induced hypertension and attenuates renal damage. Gene Ther 2006; 13(14):1097-1103.

(163) Chevalier C, Saulnier A, Benureau Y, Flechet D, Delgrange D, Colbere-Garapin F et al. Inhibition of hepatitis C virus infection in cell culture by small interfering RNAs. Mol Ther 2007; 15(8):1452-1462.

(164) Song E, Lee SK, Wang J, Ince N, Ouyang N, Min J et al. RNA interference targeting Fas protects mice from fulminant hepatitis. Nat Med 2003; 9(3):347-351.

(165) Bitko V, Musiyenko A, Shulyayeva O, Barik S. Inhibition of respiratory viruses by nasally administered siRNA. Nat Med 2005; 11(1):50-55.

(166) DeVincenzo J, Cehelsky JE, Alvarez R, Elbashir S, Harborth J, Toudjarska I et al. Evaluation of the safety, tolerability and pharmacokinetics of ALN-RSV01, a novel RNAi antiviral therapeutic directed against respiratory syncytial virus (RSV). Antiviral Res 2008; 77(3):225-231.

(167) Reich SJ, Fosnot J, Kuroki A, Tang W, Yang X, Maguire AM et al. Small interfering RNA (siRNA) targeting VEGF effectively inhibits ocular neovascularization in a mouse model. Mol Vis 2003; 9:210-216.

(168) Shen J, Samul R, Silva RL, Akiyama H, Liu H, Saishin Y et al. Suppression of ocular neovascularization with siRNA targeting VEGF receptor 1. Gene Ther 2006; 13(3):225-234.

(169) Bumcrot D, Manoharan M, Koteliansky V, Sah DW. RNAi therapeutics: a potential new class of pharmaceutical drugs. Nat Chem Biol 2006; 2(12):711-719.

(170) A phase I trial of a single intravitreal injection of REDD14NP to patients with CNV secondary to wet AMD. 2009.

(171) Livak KJ, Schmittgen TD. Analysis of relative gene expression data using real-time quantitative PCR and the 2(-Delta Delta C(T)) Method. Methods 2001; 25(4):402-408.

(172) AdEasy Adenoviral Vector System Instruction Manual. http://www.stratagene.com/manuals/240009.pdf. 2009.

(173) Yoo JY, Kim JH, Kim J, Huang JH, Zhang SN, Kang YA et al. Short hairpin RNA-expressing oncolytic adenovirus-mediated inhibition of IL-8: effects on antiangiogenesis and tumor growth inhibition. Gene Ther 2008; 15(9):635-651.

(174) Fechner H, Haack A, Wang H, Wang X, Eizema K, Pauschinger M et al. Expression of coxsackie adenovirus receptor and alphav-integrin does not correlate with adenovector targeting in vivo indicating anatomical vector barriers. Gene Ther 1999; 6(9):1520-1535.

(175) Herz J, Gerard RD. Adenovirus-mediated transfer of low density lipoprotein receptor gene acutely accelerates cholesterol clearance in normal mice. Proc Natl Acad Sci U S A 1993; 90(7):2812-2816.

(176) Nicklin SA, Wu E, Nemerow GR, Baker AH. The influence of adenovirus fiber structure and function on vector development for gene therapy. Mol Ther 2005; 12(3):384-393.

(177) Alemany R, Curiel DT. CAR-binding ablation does not change biodistribution and toxicity of adenoviral vectors. Gene Ther 2001; 8(17):1347-1353.

(178) Shayakhmetov DM, Gaggar A, Ni S, Li ZY, Lieber A. Adenovirus binding to blood factors results in liver cell infection and hepatotoxicity. J Virol 2005; 79(12):7478-7491.

(179) Parker AL, Waddington SN, Nicol CG, Shayakhmetov DM, Buckley SM, Denby L et al. Multiple vitamin K-dependent coagulation zymogens promote adenovirus-mediated gene delivery to hepatocytes. Blood 2006; 108(8):2554-2561.

(180) Waddington SN, Parker AL, Havenga M, Nicklin SA, Buckley SM, McVey JH et al. Targeting of adenovirus serotype 5 (Ad5) and 5/47 pseudotyped vectors in vivo: fundamental involvement of coagulation factors and redundancy of CAR binding by Ad5. J Virol 2007; 81(17):9568-9571.

(181) Waddington SN, McVey JH, Bhella D, Parker AL, Barker K, Atoda H et al. Adenovirus serotype 5 hexon mediates liver gene transfer. Cell 2008; 132(3):397-409.

(182) von Seggern DJ, Chiu CY, Fleck SK, Stewart PL, Nemerow GR. A helper-independent adenovirus vector with E1, E3, and fiber deleted: structure and infectivity of fiberless particles. J Virol 1999; 73(2):1601-1608.

(183) von Seggern DJ, Huang S, Fleck SK, Stevenson SC, Nemerow GR. Adenovirus vector pseudotyping in fiber-expressing cell lines: improved transduction of Epstein-Barr virus-transformed B cells. J Virol 2000; 74(1):354-362.

(184) Denby L, Work LM, Graham D, Hsu C, von Seggern DJ, Nicklin SA et al. Adenoviral serotype 5 vectors pseudotyped with fibers from subgroup D show modified tropism in vitro and in vivo. Hum Gene Ther 2004; 15(11):1054-1064.

(185) Denby L, Work LM, Seggern DJ, Wu E, McVey JH, Nicklin SA et al. Development of renal-targeted vectors through combined in vivo phage display and capsid engineering of adenoviral fibers from serotype 19p. Mol Ther 2007; 15(9):1647-1654.

(186) Gantier MP, Williams BR. The response of mammalian cells to double-stranded RNA. Cytokine Growth Factor Rev 2007; 18(5-6):363-371.

(187) Rebouillat D, Hovanessian AG. The human 2',5'-oligoadenylate synthetase family: interferon-induced proteins with unique enzymatic properties. J Interferon Cytokine Res 1999; 19(4):295-308.

(188) Hartmann R, Justesen J, Sarkar SN, Sen GC, Yee VC. Crystal structure of the 2'-specific and double-stranded RNA-activated interferon-induced antiviral protein 2'-5'-oligoadenylate synthetase. Mol Cell 2003; 12(5):1173-1185.

(189) Silverman RH. A scientific journey through the 2-5A/RNase L system. Cytokine Growth Factor Rev 2007; 18(5-6):381-388.

(190) Williams BR, Gilbert CS, Kerr IM. The respective roles of the protein kinase and pppA2' p5' A2' p5 A-activated endonuclease in the inhibition of protein synthesis by double stranded RNA in rabbit reticulocyte lysates. Nucleic Acids Res 1979; 6(4):1335-1350.

(191) Minks MA, West DK, Benvin S, Baglioni C. Structural requirements of double-stranded RNA for the activation of 2',5'-oligo(A) polymerase and protein kinase of interferon-treated HeLa cells. J Biol Chem 1979; 254(20):10180-10183.

(192) Danthinne X, Imperiale MJ. Production of first generation adenovirus vectors: a review. Gene Ther 2000; 7(20):1707-1714.

(193) Minks MA, Benvin S, Maroney PA, Baglioni C. Synthesis of 2'5'-oligo(A) in extracts of interferon-treated HeLa cells. J Biol Chem 1979; 254(12):5058-5064.

(194) Kohan DE. Progress in gene targeting: using mutant mice to study renal function and disease. Kidney Int 2008; 74(4):427-437.

(195) Hassan A, Tian Y, Zheng W, Ji H, Sandberg K, Verbalis JG. Small interfering RNA-mediated functional silencing of vasopressin V2 receptors in the mouse kidney. Physiol Genomics 2005; 21(3):382-388.

(196) Hwang M, Kim HJ, Noh HJ, Chang YC, Chae YM, Kim KH et al. TGF-beta1 siRNA suppresses the tubulointerstitial fibrosis in the kidney of ureteral obstruction. Exp Mol Pathol 2006; 81(1):48-54.

(197) Tsujie M, Isaka Y, Nakamura H, Imai E, Hori M. Electroporation-mediated gene transfer that targets glomeruli. J Am Soc Nephrol 2001; 12(5):949-954.

(198) Takabatake Y, Isaka Y, Mizui M, Kawachi H, Shimizu F, Ito T et al. Exploring RNA interference as a therapeutic strategy for renal disease. Gene Ther 2005; 12(12):965-973.

(199) Siolas D, Lerner C, Burchard J, Ge W, Linsley PS, Paddison PJ et al. Synthetic shRNAs as potent RNAi triggers. Nat Biotechnol 2005; 23(2):227-231.

(200) Li L, Lin X, Khvorova A, Fesik SW, Shen Y. Defining the optimal parameters for hairpin-based knockdown constructs. RNA 2007; 13(10):1765-1774.

(201) Li F, Mahato RI. Bipartite vectors for co-expression of a growth factor cDNA and short hairpin RNA against an apoptotic gene. J Gene Med 2009.

(202) Catala A. Lipid peroxidation of membrane phospholipids generates hydroxy-alkenals and oxidized phospholipids active in physiological and/or pathological conditions. Chem Phys Lipids 2009; 157(1):1-11.

(203) Harrison D, Griendling KK, Landmesser U, Hornig B, Drexler H. Role of oxidative stress in atherosclerosis. Am J Cardiol 2003; 91(3A):7A-11A.

(204) Minuz P, Fava C, Lechi A. Lipid peroxidation, isoprostanes and vascular damage. Pharmacol Rep 2006; 58 Suppl:57-68.

(205) Morrow JD, Hill KE, Burk RF, Nammour TM, Badr KF, Roberts LJ. A series of prostaglandin F2-like compounds are produced in vivo in humans by a non-cyclooxygenase, free radical-catalyzed mechanism. Proc Natl Acad Sci U S A 1990; 87(23):9383-9387.

(206) Davi G, Falco A, Patrono C. Determinants of F2-isoprostane biosynthesis and inhibition in man. Chem Phys Lipids 2004; 128(1-2):149-163.

(207) Morrow JD, Frei B, Longmire AW, Gaziano JM, Lynch SM, Shyr Y et al. Increase in circulating products of lipid peroxidation (F2-isoprostanes) in smokers. Smoking as a cause of oxidative damage. N Engl J Med 1995; 332(18):1198-1203.

(208) Laffer CL, Bolterman RJ, Romero JC, Elijovich F. Effect of salt on isoprostanes in salt-sensitive essential hypertension. Hypertension 2006; 47(3):434-440.

(209) Murphey LJ, Morrow JD, Sawathiparnich P, Williams GH, Vaughan DE, Brown NJ. Acute angiotensin II increases plasma F2-isoprostanes in salt-replete human hypertensives. Free Radic Biol Med 2003; 35(7):711-718.

(210) Morrow JD. Quantification of isoprostanes as indices of oxidant stress and the risk of atherosclerosis in humans. Arterioscler Thromb Vasc Biol 2005; 25(2):279-286.

(211) Umekawa T, Byer K, Uemura H, Khan SR. Diphenyleneiodium (DPI) reduces oxalate ion- and calcium oxalate monohydrate and brushite crystal-induced upregulation of MCP-1 in NRK 52E cells. Nephrol Dial Transplant 2005; 20(5):870-878.

(212) Evans MD, Dizdaroglu M, Cooke MS. Oxidative DNA damage and disease: induction, repair and significance. Mutat Res 2004; 567(1):1-61.

(213) Halliwell B, Whiteman M. Measuring reactive species and oxidative damage in vivo and in cell culture: how should you do it and what do the results mean? Br J Pharmacol 2004; 142(2):231-255.

(214) Shin CS, Moon BS, Park KS, Kim SY, Park SJ, Chung MH et al. Serum 8-hydroxy-guanine levels are increased in diabetic patients. Diabetes Care 2001; 24(4):733-737.

(215) Lee J, Lee M, Kim JU, Song KI, Choi YS, Cheong SS. Carvedilol reduces plasma 8-hydroxy-2'-deoxyguanosine in mild to moderate hypertension: a pilot study. Hypertension 2005; 45(5):986-990.

(216) Collins AR. Investigating oxidative DNA damage and its repair using the comet assay. Mutat Res 2009; 681(1):24-32.

(217) Tice RR, Agurell E, Anderson D, Burlinson B, Hartmann A, Kobayashi H et al. Single cell gel/comet assay: guidelines for in vitro and in vivo genetic toxicology testing. Environ Mol Mutagen 2000; 35(3):206-221.

(218) Singh NP, McCoy MT, Tice RR, Schneider EL. A simple technique for quantitation of low levels of DNA damage in individual cells. Exp Cell Res 1988; 175(1):184-191.

(219) Cemeli E, Baumgartner A, Anderson D. Antioxidants and the Comet assay. Mutat Res 2009; 681(1):51-67.

(220) Polke JM. Functional genomics in the stroke-prone spontaneously hypertensive rat: Genome wide and candidate gene analysis. 2008.

(221) Kand'ar R, Zakova P, Lotkova H, Kucera O, Cervinkova Z. Determination of reduced and oxidized glutathione in biological samples using liquid chromatography with fluorimetric detection. J Pharm Biomed Anal 2007; 43(4):1382-1387.

(222) Wang JF, Azzam JE, Young LT. Valproate inhibits oxidative damage to lipid and protein in primary cultured rat cerebrocortical cells. Neuroscience 2003; 116(2):485-489.

(223) Wang JF, Shao L, Sun X, Young LT. Glutathione S-transferase is a novel target for mood stabilizing drugs in primary cultured neurons. J Neurochem 2004; 88(6):1477-1484.

(224) Yang Y, Sharma R, Zimniak P, Awasthi YC. Role of alpha class glutathione S-transferases as antioxidant enzymes in rodent tissues. Toxicol Appl Pharmacol 2002; 182(2):105-115.

(225) Lawson JA, Rokach J, FitzGerald GA. Isoprostanes: formation, analysis and use as indices of lipid peroxidation in vivo. J Biol Chem 1999; 274(35):24441-24444.

(226) Schmid U, Stopper H, Schweda F, Queisser N, Schupp N. Angiotensin II induces DNA damage in the kidney. Cancer Res 2008; 68(22):9239-9246.

(227) Dizdaroglu M, Jaruga P, Birincioglu M, Rodriguez H. Free radical-induced damage to DNA: mechanisms and measurement. Free Radic Biol Med 2002; 32(11):1102-1115.

(228) Lee RC, Feinbaum RL, Ambros V. The C. elegans heterochronic gene lin-4 encodes small RNAs with antisense complementarity to lin-14. Cell 1993; 75(5):843-854.

(229) Reinhart BJ, Slack FJ, Basson M, Pasquinelli AE, Bettinger JC, Rougvie AE et al. The 21-nucleotide let-7 RNA regulates developmental timing in Caenorhabditis elegans. Nature 2000; 403(6772):901-906.

(230) Brodersen P, Voinnet O. Revisiting the principles of microRNA target recognition and mode of action. Nat Rev Mol Cell Biol 2009; 10(2):141-148.

(231) Eulalio A, Huntzinger E, Izaurralde E. Getting to the root of miRNA-mediated gene silencing. Cell 2008; 132(1):9-14.

(232) Lewis BP, Shih IH, Jones-Rhoades MW, Bartel DP, Burge CB. Prediction of mammalian microRNA targets. Cell 2003; 115(7):787-798.

(233) Bartel DP. MicroRNAs: target recognition and regulatory functions. Cell 2009; 136(2):215-233.

(234) Sethupathy P, Megraw M, Hatzigeorgiou AG. A guide through present computational approaches for the identification of mammalian microRNA targets. Nat Methods 2006; 3(11):881-886.

(235) Brennecke J, Stark A, Russell RB, Cohen SM. Principles of microRNA-target recognition. PLoS Biol 2005; 3(3):e85.

(236) Kuhn DE, Martin MM, Feldman DS, Terry AV, Jr., Nuovo GJ, Elton TS. Experimental validation of miRNA targets. Methods 2008; 44(1):47-54.

(237) Graham D, McBride MW, Gaasenbeek M, Gilday K, Beattie E, Miller WH et al. Candidate genes that determine response to salt in the stroke-prone spontaneously hypertensive rat: congenic analysis. Hypertension 2007; 50(6):1134-1141.

(238) Vazquez F, Hastings G, Ortega MA, Lane TF, Oikemus S, Lombardo M et al. METH-1, a human ortholog of ADAMTS-1, and METH-2 are members of a new family of proteins with angio-inhibitory activity. J Biol Chem 1999; 274(33):23349-23357.

(239) Luque A, Carpizo DR, Iruela-Arispe ML. ADAMTS1/METH1 inhibits endothelial cell proliferation by direct binding and sequestration of VEGF165. J Biol Chem 2003; 278(26):23656-23665.

(240) Iruela-Arispe ML, Carpizo D, Luque A. ADAMTS1: a matrix metalloprotease with angioinhibitory properties. Ann N Y Acad Sci 2003; 995:183-190.

(241) Okuda T, Sumiya T, Iwai N, Miyata T. Pyridoxine 5'-phosphate oxidase is a candidate gene responsible for hypertension in Dahl-S rats. Biochem Biophys Res Commun 2004; 313(3):647-653.

(242) Masuda M, Tsunoda M, Imai K. Low catechol-O-methyltransferase activity in the brain and blood pressure regulation. Biol Pharm Bull 2006; 29(2):202-205.

(243) Kanasaki K, Palmsten K, Sugimoto H, Ahmad S, Hamano Y, Xie L et al. Deficiency in catechol-O-methyltransferase and 2-methoxyoestradiol is associated with pre-eclampsia. Nature 2008; 453(7198):1117-1121.

(244) Mohamed MM, Sloane BF. Cysteine cathepsins: multifunctional enzymes in cancer. Nat Rev Cancer 2006; 6(10):764-775.

(245) Vasiljeva O, Korovin M, Gajda M, Brodoefel H, Bojic L, Kruger A et al. Reduced tumour cell proliferation and delayed development of high-grade mammary carcinomas in cathepsin B-deficient mice. Oncogene 2008; 27(30):4191-4199.

(246) Burger AM, Leyland-Jones B, Banerjee K, Spyropoulos DD, Seth AK. Essential roles of IGFBP-3 and IGFBP-rP1 in breast cancer. Eur J Cancer 2005; 41(11):1515-1527.

(247) Watanabe T, Suda T, Tsunoda T, Uchida N, Ura K, Kato T et al. Identification of immunoglobulin superfamily 11 (IGSF11) as a novel target for cancer immunotherapy of gastrointestinal and hepatocellular carcinomas. Cancer Sci 2005; 96(8):498-506.

(248) Suzu S, Hayashi Y, Harumi T, Nomaguchi K, Yamada M, Hayasawa H et al. Molecular cloning of a novel immunoglobulin superfamily gene preferentially expressed by brain and testis. Biochem Biophys Res Commun 2002; 296(5):1215-1221.

(249) Esaki N, Nakamura T, Tanaka H, Soda K. Selenocysteine lyase, a novel enzyme that specifically acts on selenocysteine. Mammalian distribution and purification and properties of pig liver enzyme. J Biol Chem 1982; 257(8):4386-4391.

(250) Kimura F, Suzu S, Nakamura Y, Nakata Y, Yamada M, Kuwada N et al. Cloning and characterization of a novel RING-B-box-coiled-coil protein with apoptotic function. J Biol Chem 2003; 278(27):25046-25054.

(251) Meroni G, Diez-Roux G. TRIM/RBCC, a novel class of 'single protein RING finger' E3 ubiquitin ligases. Bioessays 2005; 27(11):1147-1157.

(252) Schmittgen TD, Lee EJ, Jiang J, Sarkar A, Yang L, Elton TS et al. Real-time PCR quantification of precursor and mature microRNA. Methods 2008; 44(1):31-38.

(253) Esau CC. Inhibition of microRNA with antisense oligonucleotides. Methods 2008; 44(1):55-60.

(254) Cheng AM, Byrom MW, Shelton J, Ford LP. Antisense inhibition of human miRNAs and indications for an involvement of miRNA in cell growth and apoptosis. Nucleic Acids Res 2005; 33(4):1290-1297.

(255) Davis S, Lollo B, Freier S, Esau C. Improved targeting of miRNA with antisense oligonucleotides. Nucleic Acids Res 2006; 34(8):2294-2304.

(256) Meister G, Landthaler M, Dorsett Y, Tuschl T. Sequence-specific inhibition of microRNA- and siRNA-induced RNA silencing. RNA 2004; 10(3):544-550.

(257) Krek A, Grun D, Poy MN, Wolf R, Rosenberg L, Epstein EJ et al. Combinatorial microRNA target predictions. Nat Genet 2005; 37(5):495-500.

(258) Selbach M, Schwanhausser B, Thierfelder N, Fang Z, Khanin R, Rajewsky N. Widespread changes in protein synthesis induced by microRNAs. Nature 2008; 455(7209):58-63.

(259) Doench JG, Petersen CP, Sharp PA. siRNAs can function as miRNAs. Genes Dev 2003; 17(4):438-442.

(260) Saetrom P, Heale BS, Snove O, Jr., Aagaard L, Alluin J, Rossi JJ. Distance constraints between microRNA target sites dictate efficacy and cooperativity. Nucleic Acids Res 2007; 35(7):2333-2342.

(261) Lewis BP, Burge CB, Bartel DP. Conserved seed pairing, often flanked by adenosines, indicates that thousands of human genes are microRNA targets. Cell 2005; 120(1):15-20.

(262) John B, Enright AJ, Aravin A, Tuschl T, Sander C, Marks DS. Human MicroRNA targets. PLoS Biol 2004; 2(11):e363.

(263) Hutvagner G, Zamore PD. A microRNA in a multiple-turnover RNAi enzyme complex. Science 2002; 297(5589):2056-2060.

(264) Bartel DP. MicroRNAs: genomics, biogenesis, mechanism, and function. Cell 2004; 116(2):281-297.

(265) Li XF, Yan PJ, Shao ZM. Downregulation of miR-193b contributes to enhance urokinase-type plasminogen activator (uPA) expression and tumor progression and invasion in human breast cancer. Oncogene 2009.

(266) Schwanhausser B, Gossen M, Dittmar G, Selbach M. Global analysis of cellular protein translation by pulsed SILAC. Proteomics 2009; 9(1):205-209.

(267) Pravenec M, Landa V, Zidek V, Musilova A, Kren V, Kazdova L et al. Transgenic rescue of defective Cd36 ameliorates insulin resistance in spontaneously hypertensive rats. Nat Genet 2001; 27(2):156-158.

(268) Koh-Tan HH, Graham D, Hamilton CA, Nicoll G, Fields L, McBride MW et al. Renal and vascular glutathione S-transferase mu is not affected by pharmacological intervention to reduce systolic blood pressure. J Hypertens 2009; 27(8):1575-1584.

(269) Dominiczak AF, Graham D, McBride MW, Brain NJ, Lee WK, Charchar FJ et al. Corcoran Lecture. Cardiovascular genomics and oxidative stress. Hypertension 2005; 45(4):636-642.

(270) Behlke MA. Progress towards in vivo use of siRNAs. Mol Ther 2006; 13(4):644-670.

(271) Whitehead KA, Langer R, Anderson DG. Knocking down barriers: advances in siRNA delivery. Nat Rev Drug Discov 2009; 8(2):129-138.

(272) Fechner H, Suckau L, Kurreck J, Sipo I, Wang X, Pinkert S et al. Highly efficient and specific modulation of cardiac calcium homeostasis by adenovector-derived short hairpin RNA targeting phospholamban. Gene Ther 2007; 14(3):211-218.

(273) Tiscornia G, Singer O, Verma IM. Design and cloning of lentiviral vectors expressing small interfering RNAs. Nat Protoc 2006; 1(1):234-240.

(274) Xia H, Mao Q, Eliason SL, Harper SQ, Martins IH, Orr HT et al. RNAi suppresses polyglutamine-induced neurodegeneration in a model of spinocerebellar ataxia. Nat Med 2004; 10(8):816-820.

(275) Sledz CA, Holko M, de Veer MJ, Silverman RH, Williams BR. Activation of the interferon system by short-interfering RNAs. Nat Cell Biol 2003; 5(9):834-839.

(276) Schlee M, Hornung V, Hartmann G. siRNA and isRNA: two edges of one sword. Mol Ther 2006; 14(4):463-470.

(277) Grimm D, Streetz KL, Jopling CL, Storm TA, Pandey K, Davis CR et al. Fatality in mice due to oversaturation of cellular microRNA/short hairpin RNA pathways. Nature 2006; 441(7092):537-541.

(278) Grimm D. Small silencing RNAs: state-of-the-art. Adv Drug Deliv Rev 2009; 61(9):672-703.

(279) Meltzer PS. Cancer genomics: small RNAs with big impacts. Nature 2005; 435(7043):745-746.

(280) Ikeda S, Kong SW, Lu J, Bisping E, Zhang H, Allen PD et al. Altered microRNA expression in human heart disease. Physiol Genomics 2007; 31(3):367-373.

(281) Gusev Y. Computational methods for analysis of cellular functions and pathways collectively targeted by differentially expressed microRNA. Methods 2008; 44(1):61-72.

(282) Naga Prasad SV, Duan ZH, Gupta MK, Surampudi VS, Volinia S, Calin GA et al. A unique microRNA profile in end-stage heart failure indicates alterations in specific cardiovascular signaling networks. J Biol Chem 2009.